Universidade de Aveiro

Departamento de Biologia

2018

Ana Raquel de Azevedo e Costa

Intertidal seagrass modelling in a mesotidal coastal lagoon
Modelação de pradarias marinhas intertidais numa laguna costeira mesotidal

Universidade de Aveiro

Departamento de Biologia

2018

Ana Raquel de Azevedo e Costa

Intertidal seagrass modelling in a mesotidal coastal lagoon
Modelação de pradarias marinhas intertidais numa laguna costeira mesotidal

Dissertação apresentada à Universidade de Aveiro para cumprimento dos requisitos necessários à obtenção do grau de Doutor em Biologia, realizada sob a orientação científica do Doutor João Miguel Sequeira Silva Dias, Professor Associado com Agregação do Departamento de Física da Universidade de Aveiro, da Doutora Ana Isabel Lillebø, Investigadora Principal do Departamento de Biologia da Universidade de Aveiro e do Doutor João Lencart e Silva, Investigador Sénior na Longline Environment no Reino Unido

A autora foi financiada pela Fundação para a Ciência e Tecnológica (FCT), através da bolsa de Doutoramento com a referência SFRH/BD/84613/2012, no âmbito do Quadro de Referência Estratégico Nacional (QREN) e do Programa Operacional de Potencial Humano (POPH), comparticipado pelo Fundo Europeu e por fundos nacionais do Ministério da Educação e Ciência (MEC). Este trabalho foi desenvolvido no âmbito do Projecto LAGOONS financiado pelo 7º Programa Quadro – FP7/2007-2013 (contracto Nº. 283157); e Projecto AquiMap (MAR-02.01.01-FEAMP-0022), co-financiado pelo Programa MAR2020, Portugal 2020 e União Europeia através do Fundo Europeu dos Assuntos Marítimos e das Pescas.

o júri/ jury

Presidente/Chairman	**Doutor Vitor José Babau Torres** Professor Catedrático do Departamento de Física da Universidade de Aveiro
Vogais/Examiners committee	**Doutor Mogens René Flindt** Professor Associado do Departamento de Biologia da Syddansk Universitet (Dinamarca)
	Doutor Ramiro Joaquim de Jesus Neves Professor Associado do Departamento de Engenharia Mecânica do Instituto Superior Técnico da Universidade de Lisboa
	Doutor João Miguel Magalhães Neto Investigador Auxiliar da Escola Superior de Turismo e Tecnologia do Mar do Instituto Politécnico de Leiria
	Doutor Alexandre Firmino Vaz Professor Auxiliar Convidado do Departamento de Física da Universidade de Aveiro
	Doutor João Miguel Sequeira Silva Dias (Orientador/Supervisor) Professor Associado com Agregação do Departamento de Física da Universidade de Aveiro

acknowledgments

This work was only possible thanks to the active support and encouragement of a great number of people. Thank you all for the patience, friendship and help.

To my three supervisors, I would like to express my appreciation for the amazing opportunity it was working with you all. To Professor João Miguel Dias for his availability for brainstorming, tireless encouragement and valuable advice. Thank you so much for always providing me the best possible working conditions, for your guidance and patience. To Doutora Ana Lillebø, the first supervisor of my academic journey, it was very grateful to me to be able to work with you again. For your outstanding help in the "biological part" of this work, guidance in some field surveys and kind encouragements, thank you so much. To Doutor João Lencart for introducing me to water quality modelling. Thank you for your extraordinary patience in explaining to me the "basic" concepts, appreciated suggestions and technical support to solve diverse problems. Thank you all for never giving up on me.

To the NMEC (Estuarine and Coastal Modelling Group) working group, for sharing solutions and ideas for modelling implementation and results. To Renato Mendes for helping on the climatological analysis and Carina Lopes for helping on Matlab. To Leandro Vaz for valuable suggestions in the analysis of model performance. To Nuno Vaz for kindly providing data for validation of salt and heat transport. A special acknowledgement is given to Magda Sousa and Américo Ribeiro for their massive and crucial help in Delft3D problem-solving.

To Ana I. Sousa, thank you for your fellowship, help in field surveys and lab work. Thank you so much for making available the data on the spatial distribution of seagrass meadows in Ria de Aveiro lagoon and permanent accessibility to clarify any doubts. To Bruna Marques for guidance in grain-size determinations. To Professor João Serôdio for kindly allowing us to use his lab for sampling processing.

To those who are not specifically mentioned here, but in one way or another, always show your care, friendship and companionship. Thank you very much.

To my long-time friends, always present for the best and the worst. Your kindness, help, sharing, patience and understanding turn me into a better person every single day. We still have a long way ahead but thank you for sharing our defeats but, most importantly, our conquests.

To the most important and supportive people of my life, my family. To my parents and brother, for your unconditional love and support in all moments of my life. To Tiago Luna for your love, permanent encouragement, outstanding patience and for sharing with me the best and exceptional "gift" from the universe: my Martinha, my everything. Thank you so much.

Thank you all.

palavras-chave

Hidrodinâmica, qualidade da água, DPSIR, modelação numérica, pradarias marinhas, Laguna de Aveiro, dessecação, recuperação, alterações climáticas

resumo

As pradarias marinhas constituem importantes habitats de plantas superiores, adaptadas à colonização de ambientes costeiros e estuarinos, que desempenham importantes funções nestes ecossistemas. O seu declínio acentuado verificado a escalas regionais/locais (Ria de Aveiro) e globais tem, no entanto, apresentado implicações nefastas para a sustentabilidade dos ecossistemas onde estão inseridas. Neste contexto, o objectivo principal deste trabalho consistiu em aprofundar o conhecimento presente da dinâmica das pradarias marinhas na Ria de Aveiro, sob o ponto de vista multidisciplinar (colheita e tratamento de dados experimentais e modelação numérica), bem como prever as potenciais alterações ao nível do sistema nestas comunidades. Desta forma, pretende-se contribuir para a promoção de estratégias de conservação adequadas para minimizar o seu declínio e potenciar a sua recuperação. Partindo da aplicação de um modelo conceptual DPSIR (Drivers-Pressures-State-Impacts-Responses), concluiu-se que as alterações graduais nas características hidrodinâmicas estão na base do declínio local destas comunidades, presentemente colonizadas por pradarias monoespecíficas intertidais de *Zostera noltei*. A escassez de modelos numéricos de pradaria é acentuada, sendo ainda mais proeminente quando se tratam de comunidades intertidais, sujeitas a períodos alternados de exposição ao ar e submersão. Desta forma, as particularidades inerentes às comunidades de pradarias intertidais foram investigadas, mostrando maior influência das características sedimentares no teor relativo de água da planta, em detrimento do tempo de exposição ao ar. Posteriormente, foi desenvolvido um modelo biológico de pradaria, juntamente com um modelo de dessecação da planta, com vista a suprimir a lacuna previamente identificada, sendo ambos posteriormente acoplados ao modelo de qualidade da água (Delft3D-WAQ). Utilizando os dados experimentais colhidos na área de estudo (Canal de Mira) calibrou-se o modelo numérico, tendo-se verificado uma reprodução fiável das variáveis-estado descritas pela biomassa aérea e subterrânea. Porém, a presente configuração requer melhorias adicionais, nomeadamente no que respeita à interface sedimento-planta e dinâmica interna de nutrientes, previamente a ser passível de ser aplicado a outros sistemas com desafios semelhantes. O desempenho do modelo numérico foi analisado por diferentes metodologias que apresentaram resultados divergentes, o que sugere a necessidade de desenvolvimento e aplicação de metodologias adicionais para uma conclusão robusta. Foi realizada uma análise de sensibilidade, que permitiu aferir que os parâmetros usados para descrever a dependência da temperatura ambiente (água e ar) são os mais sensíveis. Deste modo, salienta-se a sua potencial importância e sugere-se a sua consideração em planeamentos experimentais futuros com maior frequência de amostragem nas medições *in situ*. Numa abordagem exploratória, simularam-se dois eventos extremos, caudal fluvial extremo e onda de calor, tendo os resultados apresentado, respectivamente, uma diminuição das condições favoráveis para a presença de pradarias em termos de velocidade da corrente e salinidade, e um claro decréscimo no crescimento da planta.

Seguindo uma abordagem prospectiva, estabeleceram-se diferentes cenários evolutivos para o futuro, resultantes das expectáveis alterações climáticas, de acordo com a projecção mais e menos pessimista (RCP 4.5 e RCP 8.5). As previsões numéricas obtidas indicam uma perda acentuada de áreas colonizadas por pradarias marinhas (entre aproximadamente 30 e 70%, respectivamente) comparativamente à situação presente. As áreas colonizadas por pradarias que mostraram uma maior resiliência, nos dois cenários de alterações climáticas, situam-se na zona sul e noroeste da laguna central. Na análise espacial da anomalia entre o cenário de referência e de alterações climáticas, não se verificou um padrão uniforme, havendo áreas que apresentam um decréscimo nas condições favoráveis para a presença de pradarias marinhas, simultaneamente à ocorrência de áreas que apontam para um melhoramento das mesmas condições. Para uma abordagem mais efectiva e holística da evolução natural e modelação destes sistemas, deve considerar-se uma maior cobertura espacial e temporal dos descritores bióticos e abióticos destas comunidades. Deve ser ainda incluído o levantamento das actividades antropogénicas decorrentes e previstas no contexto do desenvolvimento socio-económico da região (escala temporal até meio do século), e ainda, deve ser feito o enquadramento nos cenários futuros no contexto das alterações climáticas (escala temporal até final do século), para que medidas de gestão possam ser implementadas no sentido de promover a resiliência destes habitats, de forma a garantir os serviços prestados.

keywords

Hydrodynamics, water quality, numerical modelling, DPSIR, seagrass meadows, Aveiro Lagoon, desiccation, seagrass recovery, climate change

abstract

Seagrass meadows are important habitats of marine plants, adapted to the colonization of coastal and estuarine environments, which provide important functions within the ecosystem. The remarkable decline of seagrass meadows at regional/local (Ria de Aveiro) and global scales has presented however negative implications for the sustainability of the ecosystems where they follow this trend. In this context, the main objective of this work was to improve the present knowledge about seagrass dynamics in the Ria de Aveiro, from a multidisciplinary viewpoint (experimental data collection and treatment and numerical modelling), as well as to anticipate potential changes at the system level in these communities. Therefore, it is intended to contribute to the promotion of adequate management and conservation strategies to minimize its decline and enhance its recovery. From the application of a conceptual DSPIR framework (Drivers-Pressures-State-Impacts-Responses), the results pointed that gradual changes in hydrodynamic characteristics are the basis of the local decline of these communities, presently colonized by monospecific intertidal meadows of *Zostera noltei*. The scarce availability of seagrass models is even more prominent when dealing with intertidal communities, subject to alternating periods of exposure to air and submergence. As so, the inherent peculiarities of intertidal seagrass *Z. noltei* communities were investigated, showing a greater influence of the sedimentary characteristics on the relative water content of the plant, rather than the air exposure time. Afterwards, it was developed a seagrass biological model together with a desiccation model of the plant, in order to suppress the previously identified gap, both of which were later coupled to the water quality model (Delft3D-WAQ). The numerical model was calibrated using experimental data collected in the study area (Mira Channel), showing a reliable reproduction of the state variables described by means of above and belowground biomass. However, the present set up needs to be improved, namely in what regards sediment-plant interface and internal nutrient dynamics, before it can be applied to other systems with similar challenges. The performance of the numerical model was analysed through different methodologies that presented divergent results, which suggests the application of further approaches for a robust conclusion. A sensitivity analysis was computed, showing that the parameters used to describe the dependence of the ambient temperature (water and air) are the most sensitive, suggesting that these should be particularly addressed in future experimental surveys, by increasing the frequency of the *in situ* measurements. Two exploratory simulations of extreme event, extreme river flow and heat-wave, respectively showed a decrease in the favourable conditions for seagrass presence, according to the water velocity and salinity; and clear negative impacts on seagrass growth. Following a prospective viewpoint, different evolutionary scenarios to the future, resulting from the foreseen climate change, were set according to the more and less pessimistic projection (RCP 4.5 and RCP 8.5). The numerical model projections pointed out for a noticeable loss of colonised areas by seagrass (between around 30 and 70%, respectively) compared to the present situation.

The multiple stressors analysed generally showed a synergistic effect on the loss of the relative area of seagrass, compared to the isolated sum of each of the factors, which highlights the complex and intrinsic relations established between them. The areas colonized by seagrass meadows that showed greater resilience, to the two simulated climate change scenarios, are located in the south and northwest areas of the central lagoon. The spatial distribution of the anomalies between the reference and the climate change scenarios, showed no uniform pattern of variation, occurring areas with descreased favourable conditions for seagrass presence, but also some areas that verified an improvement of these conditions. For a more effective and holistic approach to the natural evolution and modelling of these systems, a wider spatial and temporal coverage of biotic and abiotic descriptors of these communities should be performed. Moreover, the overview of the ongoing and forthcoming anthropogenic actions must also be included, in the context of the socio-economic development of the region, as well as the framework of the future scenarios in the scope of climate change (temporal scale referred to the end of the century). As so, the management actions can be implemented to promote the resilience of these habitats and assure the services provided by the ecosystem.

PUBLICATIONS AND COMMUNICATIONS IN THE CONTEXT OF THIS DISSERTATION

A number of publications in peer reviewed journals and presentations at international and national conferences resulted from the research developed in the scope of this thesis. The publications were used as basis for several chapters of this thesis (marked in bold in the list below).

Papers in international journals indexed in Web of Science:

- Azevedo, A., Lencart e Silva J.D., Lillebø A.I., Ribeiro, A.S., Sousa, A.I., Sousa, M.C., Dias J.M (*in prep*). Coupled hydrodynamic-biological model to set potential areas for seagrass thriving under a climate change context. **(Chapters 7, 8)**

- Sousa, A.I., Silva, J.F., Azevedo, A., Lillebø, A.I., (*submitted to Journal of Applied Ecology*). Variability of seagrass meadows spatial extent and Blue Carbon over a decade in a coastal lagoon: Ria de Aveiro (Portugal).

- Azevedo, A., Lillebø, A.I., Silva, J.L.E., Dias, J.M. (2017). Intertidal seagrass models: Insights towards the development and implementation of a desiccation module. Ecological Modelling. 354, 20-25. **(Chapter 5)**

- Azevedo A., Dias J.M., Lillebø A.I. (2016). Thriving of *Zostera noltei* under intertidal conditions: implications for the modelling of seagrass populations. Marine Biology. 163, 1-8. **(Chapter 5)**

- Azevedo A., Sousa A.I., Lencart e Silva J.D., Dias J.M., Lillebø A.I. (2013). Application of the generic DPSIR framework to seagrass communities of Ria de Aveiro: a better understanding of this coastal lagoon. Journal of Coastal Research. SI65, 19-24. **(Chapter 2)**

- Lencart e Silva J. D., Azevedo A., Lillebø A.I., Dias J.M. (2013) Turbidity under changing physical forcing over two contrasting locations of seagrass meadows. Journal of Coastal Research. SI65, 2023-2028.

Conference abstracts, proceedings and communications:

- Azevedo, A., Lillebø, A.I., Lencart e Silva, J.D., Dias, J.M., 2017. Modelling intertidal seagrass meadows: physical influence on biological processes. Encontro Ciência '17, 03-05 Julho 2017, Lisboa, Portugal.

- Azevedo, A., Lillebø, A.I., Lencart e Silva, J.D., Dias, J.M., 2015. Intertidal Seagrass Models: Development and Implementation of a Desiccation Module. ECSA55, 06-09 September 2015, London, United Kingdom.

- Azevedo, A., Lillebø, A.I., Dias, J.M., 2015. Numerical Models of Seasonal Dynamics of Seagrasses: A Review. ECSA55, 06-09 September 2015, London, United Kingdom.

- Azevedo, A., Dias, J.M., Lillebø, A.I., 2015. Thriving of Intertidal Seagrass *Zostera noltei*: Influence of Sediment Type and Intertidal Height. 4th Mediterranean Seagrass Workshop, 18-22 May 2015, Sardinia, Italy.

- Azevedo A., Lencart e Silva J.D., Lillebø A.I., Dias J.M., 2014. Towards the Improvement of Currently Available *Zostera noltii* seagrass models. ECSA54, 12-16 May 2014, Sesimbra, Portugal.

- Azevedo, A., Lencart e Silva, J.D., Lillebø, A.I., Dias, J.M., 2014. Evolução Hidrodinâmica e Impacto nas Pradarias Marinhas da Ria de Aveiro. Encontro de Oceanografia, 21-22 May 2014, Aveiro, Portugal.

- Lencart e Silva J. D., Azevedo A., Lillebø A.I., Dias J.M., 2013. Turbidity and seagrass meadows under changing physical forcing. International Costal Symposium, 08-12 April 2013, Plymouth, United Kingdom.

- Azevedo, A., Sousa, A.I., Lencart e Silva, J.D., Dias, J.M., Lillebø, A.I., 2013. Application of the generic DPSIR framework to seagrass communities of Ria de Aveiro: a better understanding of this coastal lagoon. International Costal Symposium, 08-12 April 2013, Plymouth, United Kingdom.

- Azevedo, A., Lillebø, A.I, Lencart e Silva, J.D., Dias, J.M., 2013. Zosteraceae seagrasses modelling: state of the art and milestones. 48th European Marine Biology Symposium International Costal Symposium, 19-23 August 2013, Galway, Ireland.

- Azevedo, A., Lencart e Silva, J.D., Lillebø, A.I., Dias, J.M., 2013. Morphodynamics of Portuguese Seagrass Meadows: Dependence on *Zostera noltii* Decline and Related Physical Factors. 2ª Conferência sobre Morfodinâmica Estuarina e Costeira, 09-10 Maio de 2013, Aveiro, Portugal.

Oral communications by invitation:

- Azevedo, A. and Lillebø, A.I., 2018. LAGOONS EU Project - Modelling the processes associated with intertidal seagrass communities in Ria de Aveiro. Life SeResto final conference, 11 April 2018, Rome, Italy.

- Azevedo, A., 2017. Interacções de Processos Físicos e Biológicos na Ria de Aveiro Utilizando Modelos Matemáticos, Jornadas do Mar e da Atmosfera, 25 May 2017, Aveiro, Portugal.

x

CONTENTS

LIST OF FIGURES

LIST OF TABLES

LIST OF SYMBOLS

AB	Aboveground biomass
A_{M2}	Amplitude of M_2 tidal constituent
A_{S2}	Amplitude of S_2 tidal constituent
BB	Belowground biomass
Bias	Percentage model bias
CN	Central-north area of Ria de Aveiro lagoon
CS	Central-south area of Ria de Aveiro lagoon
CV	Current velocity, tide
D/Depth	Depth of the water column
df	Degrees of freedom
Eh	Redox potential
EP	Epiphytes
f_5 (T)	Mortality limitation due to ambient temperature
F(I)	Limiting function light
F(S)	Limiting function space
F(T)	Limiting function ambient temperature
G	Seagrass growth
g_{max}	Maximum seagrass growth rate
h_c	Height of the canopy
HSL	Half-saturation constant for light

I_c	Light available at the top of the seagrass canopy height
I	Light at the water surface
K	Desiccation rate
K_0	Function value at T=T0
K_L	Extinction coefficient of aboveground biomass
K_m	Function value at T=Tm
K_{shad}	Light attenuation factor
K_w	Extinction coefficient of water
L	Light
LM	Aboveground mortality
LMR_{20}	Maximum aboveground mortality rate at 20ºC
MD	Mechanical damage; natural mortality
MS	Mean square
NS	Nitrogen from sediment
NW	Nitrogen from water
O2diss	Dissolved oxygen
OSF	Other Seagrass Features
p	Significance level
R	Respiration
RM	Belowground mortality
RMR_{20}	Maximum belowground mortality rate at 20ºC
RN	Precipitation (rain)
$RWC_{seagrass}$	Relative water content of seagrass leaves

$RWC_{sediment}$	Relative water content of sediment
PS	Phosphorous from sediment
PW	Phosphorous from water
SL	Space limiting function
SS	Sum of squares; (in Table 1.2 self shading)
stt	Controls the shape of the function
Time/t	Time
T	Ambient (air/water) temperature
T_{M2}	Period of M_2 tidal constituent
T_{S2}	Period of S_2 tidal constituent
T_{opt}	Optimal temperature for seagrass growth
TA	Translocation rhizomes-shoots
TIN	Total internal nitrogen
TIP	Total internal phosphorous
TR	Translocation shoots-rhizomes
$trns_{AB\_BB}$	Carbon translocation coefficient from aboveground to belowground organs
T_{sed}	Sediment temperature
T_{wat}	Water temperature
u,v or w	Velocity points
WH	Water height
WS	Wind speed
Y	Effective quantum yield of photosystem II
δ	Threshold depth

ζ	Water level
θ	Mortality increasing rate with ambient temperature
ρ	Water density
σ	Maximum aboveground biomass
φ_{M2}	Phase of M_2 tidal constituent
φ_{S2}	Phase of S_2 tidal constituent

LIST OF ACRONYMS

ADI	Alternating Direction Implicit
BOD	Biochemical Oxygen Demand
CF	Cost Function
CMEMS	Copernicus Marine Environment Monitoring System
CMIP5	Coupled Model Intercomparison Project Phase 5
CORDEX	Coordinated regional climate Downscaling Experiment
CSIRO	Commonwealth Scientific and Industrial Research Organisation
DO	Dissolved Oxygen
DOC	Dissolved Organic Carbon
DOM	Dissolved Organic Matter
DPSIR	Drivers-Pressures-State-Impacts-Responses Framework
DW	Dry Weight
ECMWF	European Centre for Medium-Range Weather Forecasts
EMS	Environmental Modelling Suite
ERSEM	European Regional Seas Ecosystem Model
ETR	Electron Transfer Rate
GCM	Global Circulation Models
GSA	Global Sensitivity Analysis
GUI	Graphical User Interface
HSP	Heat Shock Proteins

HWDI	Heat Wave Duration Index
IFS	Integrated Forecasting System
IPCC	Intergovernmental Panel on Climate Change
LOI	Loss On Ignition
LSA	Local Sensitivity Analysis
ME	Model Efficiency – Nash Sutcliffe Model Efficiency
N	Nitrogen
NA	Not Available/Not Applicable
NW	Northwest
ODE	Ordinary Differential Equation
P	Phosphorous
PAR	Photosynthetic Active Radiation
PLCT	Open Process Library Tool (Delft3D)
POM	Particulate Organic Matter
RCM	Regional Circulation Models
RCP	Representative Concentration Pathway
RWC	Relative Water Content
RMSE	Root Mean Squared Error
SAV	Submerged Aquatic Vegetation
SCI	Sites of Community Importance
SLR	Sea Level Rise
SPA	Special Protection Area
SSE	Sea Surface Elevation

SSS	Sea Surface Salinity
SST	Sea Surface Temperature
SWIM	Soil and Water Integrated Model
TOM	Total Organic Matter
WFD	Water Framework Directive

Chapter 1

GENERAL INTRODUCTION

This chapter presents a brief inspection of the research scope to contextualise the problem under study, followed by the literature review of basic concepts related with seagrass meadows and numerical models. Different viewpoints of numerical modelling are presented, such as the general aspects, specificities of numerical models applied to seagrass meadows and panoply of numerical models applied to the study of Ria de Aveiro system (study area). This chapter culminates with a systematisation of the major motivations and aims that drove this work, as well as a synthesis of the structure of this thesis.

1.1 INTRODUCTION

The coastal areas worldwide have been extensive preferred sites of human population settlement, due to its unique characteristics and location (Newton et al., 2016). Within these areas, estuarine systems represent important ecotones, setting dynamic and complex transition links between the land and sea. As one of the most productive ecosystems, these systems present distinct natural features that support high biodiversity and provide valuable environmental goods and services, backing up many economic and social activities (e.g. harbour facilities, shipping, tourism, recreational and commercial coastal fisheries, industrial and urban development) (Costanza et al., 1997; Duarte, 2000; Lillebø et al., 2011). The resulting effects of these demographic pressures, exacerbated by global climate changes, increase the demands on resources and therein degradation of natural systems, requiring active management actions, long-term monitoring and conservation plans of coastal and estuarine areas (McLusky and Elliott, 2004).

Structural and ecological dynamics of estuarine systems, particularly its biogeochemistry and primary production, highly depend on the interaction between physical processes, driven by tidal currents, river discharge, wind and local topography (Bianchi, 2007). The hydrodynamic environment critically influence the transport and variability of organisms (Cloern et al., 2014;

Morais et al., 2012), pollutants (Pato et al., 2008; Xu and Chua, 2017), organic matter (Jiang et al., 2017) and other major water quality features of the coastal systems (Lillebø et al., 2005; Mateus et al., 2008; Park et al., 2014; Wild-Allen and Andrewartha, 2016). The resulting dynamic feedbacks between biotic and physical processes set complex interactions, usually addressed by means of coupled hydrodynamic-ecological numerical models, as resourceful tools to simulate the response to different scenarios of estuarine processes and interactions (Ganju et al., 2016).

The aforementioned characteristics of estuarine areas provide a wide range of suitable habitats for several types of biological communities, each of them with an important role to its overall functioning. As key ecosystem components, primary producers have a major role in both pelagic and benthic communities, representing the base of trophic webs, by using inorganic nutrients as building blocks to synthetise through photosynthesis readily consumable organic matter (photosynthesis). Although the importance of primary producers is widely recognised and included in estuarine ecological models, most only consider phytoplankton and/or macroalgae (e.g. Longo et al., 2016; Lopes et al., 2010; Lopes et al., 2009; Rodrigues et al., 2015). The wider applicability of these ecological models becomes limited though when dealing with estuarine benthic communities, such as seagrasses, and practically null if studying those colonizing tidal flats periodically exposed to low tide.

Within the estuarine benthic communities, seagrasses are macrophytes fully adapted to the marine environment, forming dense and highly productive meadows. As the only true marine angiosperms, seagrasses are reliable bioindicators of ecosystem change and health due to their sensibility to human-induced disturbances (Martínez-Crego et al., 2008; Montefalcone, 2009) and one of the “biological quality elements” to be used in defining the ecological status of transitional and coastal waters (Annex V - WFD, European Commission, 2000; Lillebø et al., 2007; OSPAR Commission, 2005). Conservation and restoration of these habitats have become a priority addressed in coastal management, conservation and planning (Lillebø et al., 2011; Short et al., 2011).

The direct and/or indirect pressures of human activities, such as eutrophication, climate change, increase water turbidity, pollutants, coastal development, and new species introduced, result in a generalized seagrass decline and habitat fragmentation (Duarte, 2000; Duarte, 2002; Leston et al., 2008; Orth et al., 2006). These pressures lead to a significant loss of biodiversity and related contributions to ecosystems’ health and quality, as sediment stabilizer, reducer of water currents minimizing coastal erosion and provider of habitat and shelter for ecological and economic valuable species of invertebrates and fishes (e.g. Lillebø et al., 2011 and references therein; Orth et al., 2006).

In Ria de Aveiro (NW Portugal), a coastal lagoon that comprises most of the previous referred physical (Dias et al., 1996a, b) and biotic (Bueno-Pardo et al., 2018; Rodrigues et al., 2012) features, the indirect impact of anthropogenic activities is effectively pointed out as the most important driver of seagrass decline in the lagoon. Seagrasses were formerly abundant and diverse (Silva et al., 2004; Silva et al., 2005b), though currently occur as monospecific

Zostera noltei (dwarf eelgrass) meadows restricted to intertidal areas (Azevedo et al., 2013). Due to the complex impacts of anthropogenic activity on biological, chemical and geological processes affecting water and ecological quality, recent applications of numerical models have shown to be most useful to better understand its local dynamics, namely at low trophic levels (e.g. Lopes et al., 2015; Rodrigues et al., 2015). In spite of the important efforts from Kenov et al. (2013) to model the dynamics of seagrass meadows in Ria de Aveiro lagoon, it remains a gap on the importance of low tide periods, which seagrass leaves are air exposed, and on the potential impacts of climate change, that may modify its natural variability.

Therefore, the integration of a seagrass biological model into a water quality-hydrodynamic coupled model will provide an integrated approach to study the dynamics and the current state of seagrass meadows and predict its evolution based on climate change projections. Considering the importance of multiple stressor scenarios in the planning and implementation of proposed management policies, these results may support the estimation of potential areas for seagrass restoring according to hydrodynamics, water quality and sediment matrices. This study contributes to improve the previous knowledge on seagrass numerical models, namely concerning the understanding and simulation of dynamic processes occurring in intertidal meadows under multiple stressors scenarios, and additionally to the overall holistic management of Ria de Aveiro lagoon.

1.2 OBJECTIVES

The main goal of this study is to develop a biological model considering the seasonal dynamics of intertidal seagrass *Zostera noltei* and integrate it into a water quality model suite (Delft3D). This model will be developed and validated for the Ria de Aveiro coastal lagoon and structured for further developments to be applied to other similar systems. More specifically, the present work aims to:

i) Contribute towards a better representation of the processes of intertidal seagrass modelling, through a review of the available models and adaption to function accordingly to the sediment type and tide;

ii) Include in the model the most important processes occurring on a daily basis, according to the comparison between the tidal cycle (low *vs* high tide) and circadian cycles (night *vs* day);

iii) Improve the already existent seagrass models to respond to tidal cycle (low *vs* high tide) and sediment type, through the development and testing of a desiccation model of intertidal seagrass meadows;

iv) Plan and execute field surveys to collect observational data to model testing and performance, for both seagrass seasonal dynamic cycle and desiccation experiments;

v) Apply a hydrodynamic and water quality models out to explore this results to ultimately identify and characterize the potential most favourable areas for seagrass meadows establishment;

vi) Apply a hydrodynamic and water quality model results to assess the restoring potential of seagrass meadows in Ria de Aveiro lagoon, through mapping of seagrass distribution in the context of different prospective scenarios, considering multiple stressors, including climate change.

The approach used to accomplish the above-listed aims involves the implementation of numerical models and analysis of data collected at field survey, to investigate the dynamics of intertidal seagrass meadows, at the particular case of Ria de Aveiro lagoon. Results are discussed considering two time-scales:

i) Present and near future focusing on the repercussions of changes in the water column compartment in the production and decline trend of intertidal seagrass meadows of Ria de Aveiro;
ii) End of the century in the context of climate change scenarios.

1.3 LITERATURE REVIEW

1.3.1 Seagrass meadows

The most extensive seagrass meadows are subtidal, although some species are also able to thrive in the physically challenging environment of intertidal areas (Figure 1.1) (den Hartog, 1970). Alternate states of air-exposure and immersion imply remarkable adaptation strategies to cope with desiccation (Sandoval-Gil et al., 2014), different light environments (Novak and Short, 2011), abruptly ambient temperature and salinity changes (Table 1.1) (Massa et al., 2009). Even though, the main structural features and functions of seagrass meadows are essentially uniform, independently of growing at subtidal or intertidal environments (Duarte, 1991).

Seagrass plants present a rhizomatous growth pattern, with a horizontal rhizome extending in sediment and forming a vertical rhizome at discrete intervals, which develops leaves from a basal meristem. This vertical unit, comprising aboveground leaves and belowground roots,

constitutes a ramet, the modular unit of seagrass growth. The horizontal rhizome assures the continuity between ramets (Borum and Greve, 2004; Hogarth, 2007).

Extension and branching of the horizontal rhizome through genetically identical shoots result in a plant expansion, as a clone, that may occupy large areas dominated by a single species (Arnaud-Haond et al., 2012; Reusch et al., 1999b; Reusch et al., 1999a).

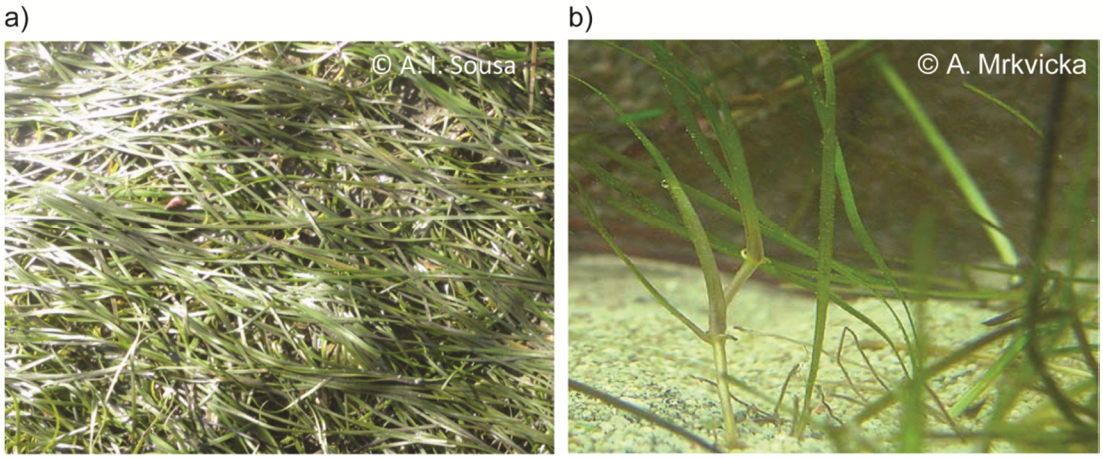

Figure 1.1 *Zostera noltei* meadows at a) intertidal and b) subtidal environments.

Table 1.1 Main differences between the subtidal and intertidal environment of seagrass meadows. Note that during the emersion periods, intertidal seagrass behave like subtidal congeners (NA - Not Applicable)

	Subtidal	Intertidal
Desiccation	N.A.	• Strategies/adaptations to cope with desiccation (e.g. leaves lying flat on the sediment surface and reduce surface area for evaporation)
CO_2 diffusion	• Gas diffusion slower in the water • Facilitated by water movement	• Gas diffusion faster in air
Light	• Efficient photosynthesis more difficult to achieve as the depth of water increases (light attenuation with depth; depth-limited)	• Availability of light is not a limiting factor • Higher UV-B radiation may damage sensitive cell organelles, depressing photosynthesis
Salinity Water temperature	• Salinity and water temperature does not fluctuate greatly	• Cope with high salinity ranges: depends on the evaporation and flow evaporation of freshwater from land

A flexible modular seagrass pattern of growth reflects the availability of resources in the surrounding environment, through variable patterns of biomass allocation to the different plant components (Hogarth, 2007). Besides rhizomatous growth, seagrass plants may also present sexual reproduction, propagating by dispersal of rhizome fragments or aboveground components that retain the ability to form roots (Hall et al., 2006).

As seagrass mostly grows at soft sediments, such as mud or sandy ones, this pattern of horizontally branching rhizomes with roots provides a suitable anchorage mechanism to thrive in these intrinsically unstable sediments, effectively holding sediment together and reducing its mobility (Hemminga and Duarte, 2000). These modifications of the surrounding sediment environment and the reduction of local flow velocity through seagrass canopy show that not only physical characteristics affect seagrass growth and survival, but the reverse is valid too. In fact, seagrass plants are ecosystem engineers, dynamically changing the vicinity abiotic environment through positive or negative feedbacks (van der Heide et al., 2012).

Photosynthetic activity requires visible light radiation between 350-700 nm, which attenuates rapidly with increasing depth (absorption by water and scattering by suspended particles). A network of gas-filled lacunae drives gas exchange with the environment, getting carbon dioxide and releasing oxygen, and provides buoyancy, which upright seagrass leaves to optimise light capture. This system of air-filled channels also supply the belowground parts, to compensate low oxygen concentrations usually presented in often organic-rich estuarine sediments, producing an oxygenated microzone (rhizosediment) around them and increasing the penetration of oxygen into the sediment (Borum and Greve, 2004). The sources of inorganic carbon are the water column and the atmosphere, for intertidal seagrass. The dissolved inorganic nutrients required for seagrass growth, namely nitrogen (N) in the form of nitrate (NO_3^-) and ammonium (NH_4^+), and phosphorous (P) in the form of phosphate (PO_4^{3-}), are uptake from sediment interstitial water through rhizome apparatus and water column through leaves (Flindt et al., 1999; Nayar and Bott, 2015; Pérez-Lloréns and Niell, 1993a).

Seagrass can stand high concentrations and ranges of salinity, although their tolerance mechanisms are complex and not straightforward, differing from species to species and in their responses to changing salinities. Generally, seagrass is euryhaline, showing tolerance between hyposaline (<10 ‰) or hypersaline (>45 ‰) conditions (Hemminga and Duarte, 2000).

The productivity and diversity of these habitats are remarkable, though seagrass diversity is surprisingly low. In fact, of about 60 seagrass species known, only four native seagrass species are found at European waters, *Zostera marina*, *Zostera noltei*, *Cymodocea nodosa* and *Posidonia oceanica*, and only the first three occur at Portuguese mainland (Cunha et al., 2013). As the only seagrass species currently presented in the study area (Ria de Aveiro lagoon), *Zostera noltei* (Hornemann) shows a spatial distributional range from temperate areas of Norwegian southern coast to the Mediterranean Sea, Black Sea, Canary Islands and far south at Mauritanian coast (Borum and Greve, 2004; Short et al., 2007). According to Cunha et al. (2013), Portuguese mainland comprises the central distributional range of *Zostera noltei*.

The *Z. noltei* seagrass is a small, fast-growing seagrass species usually with narrow, ribbon-shaped leaves with 6-22 cm in length and 0.5-1.5 mm wide. It forms dense monospecific stands, found at coastal and estuarine areas with soft sedimentation, presenting a vertical distribution ranging to both intertidal and subtidal areas, between <0 m and about 10 m depth (den Hartog, 1970; Short et al., 2010).

New leaves appear in spring, where an increase in shoot density result from continuous branching of the rhizome and stops around September/October (Vermaat and Verhagen, 1996). The rhizomes of *Z. noltei* are thin, rapidly growing and appear to be short-lived (<1 year) in nature, taking advantage of seasonal increases in light and nutrients rather than metabolites stored in the rhizome (Marbà et al., 1996). It presents low toleration to a critical level of burial and erosion (4-8 cm) mainly due to the small size and lack of vertical rhizomes (Cabaço and Santos, 2007).

As the other seagrass plants, *Z. noltei* present both types of reproduction: vegetative (or clonal growth) and/or sexual reproduction (Alexandre et al., 2006). The low expression of *Z. noltei* seedling in the wild, has suggested however that vegetative reproduction may be more important than sexual reproduction (Davison and Hughes, 1998), although more recent genetic studies suggest that sexual reproduction might be important (Alexandre et al., 2006 and references therein).

Similar to other seagrass meadows, the declines reported for *Z. noltei* are mainly resulted of indirect human pressures at coastal areas. Increased nutrient load from runoff reduce the water quality of the system, usually resulting in a eutrophic state of the system through intense macroalgae growth, which causes higher turbidity water and shading of benthic communities (Flindt et al., 1999; Silva et al., 2004; van Lent et al., 1991). Seagrass beds of *Z. noltei* may successfully recover from the stress of eutrophication when implementing adequate and integrated management actions to improve the system ecological quality (e.g. improvement of the hydrodynamics of the system), such as those reported for Mondego estuary (Leston et al., 2008; Lillebø et al., 2005). Other drivers of substantial seagrass decline may be due to natural causes, such as the wasting disease (Sullivan et al., 2013).

1.3.2 Numerical models

Numerical models are simplified descriptions of a complex real system and usually build up over several assumptions, which reflect model limitations. Since one model does not include all the properties of a real system, a useful one may represent a fair trade-off between the simulation of fundamental processes and the assumptions.

The emergent efforts on developing numerical models to be applied to more realistic representations, namely to dynamic estuarine systems, expand the geographical and knowledge areas of model application. Moreover, these advances follow increments on the

capacity of computational calculus, better knowledge of natural systems and the need of new tools to address multidisciplinary problems, within a holistic viewpoint.

The study of physical processes at coastal marine environments is generally based on the use of the well-established and described shallow water equations, derived from the Navier-Stokes equations (e.g. Lencart e Silva et al., 2013; Sousa and Dias, 2007; Wang, 1994). The formulation of biological state variables though is much more complex. As no model offers a full description of all estuarine ecological processes, they are mainly empirical and formulated to solve specific problems. The higher complexity and limited knowledge of marine processes are challenging when establishing the core state variables to describe the system of interest and the links between model components (Williams, 2006). Moreover, the parameterizations of ecological systems may overlook important processes on a small-scale and some parameter values may be site-specific. In spite of these constraints, numerical models applied to abiotic and biotic systems are most useful to understand complex dynamics of marine ecosystems (Moll, 2000) and as additional tools to support management actions (LAGOONS, 2014; Lillebø et al., 2015).

1.3.2.1 Numerical modelling applied to seagrass meadows

There are many types (e.g. stress evaluation, habitat mapping, sexual reproduction, hydrodynamics-plant interaction) and scales of application (from plastochrone intervals to seagrass seasonal dynamics) of seagrass numerical models. The most important ones, however, in the scope of this work, are those aiming to simulate the dynamics of seasonal biomass cycle (Table 1.2). Table 1.2 synthetises the seagrass species that have been modelled showing the main state variables considered, the forcing functions and other considered variables. It can be seen that the main state variables considered are the above and belowground biomass and that the main forcing functions are light and water temperature.

The photosynthetic activity in seagrass is highly dependent on light availability, namely Photosynthetically Active Radiation (PAR). Critical for seagrass growth, it is widely accepted as one of the primary limiting variables, indispensable as forcing function in seagrass production models (Burd and Dunton, 2001; Zimmerman et al., 1994). Simple model frameworks of seagrass may be particularly useful to study its response to stormy events that may reduce the overall water quality, as reported by Buzzelli et al. (2012). Moreover, changes in light availability may be as important as driven by shifts in primary production, as simulated for *Z. marina* by Zaldívar et al. (2009).

Besides light availability, water temperature and the concentration of dissolved inorganic nutrients, mainly nitrogen and phosphorous, are suitable to be limiting variables of seagrass growth. Water temperature controls several rates of physiological processes of organisms and therefore are often included within seagrass model formulae (Short, 1980; Wetzel and Neckles, 1986). In fact, modelling studies applied to Venice Lagoon, conducted for *Z. marina* (Zharova et

al., 2001) and *Cymodocea nodosa* (Zharova et al., 2008) showed that high temperatures result in noticeable inhibition of production and recruitment of new seagrass shoots. Nutrient limitation however is not widely included in seagrass models, particularly in systems with reportedly high concentrations of nutrients in the water column or in sediment interstitial water (Verhagen and Nienhuis, 1983; Zharova et al., 2008; Zharova et al., 2001).

High loads of nutrients trigger extraordinary macroalgae production, which may conduce to a eutrophic state of the system, increasing the vertical light attenuation, scattering on water column and shading of the bottom communities. As so, several modelling studies investigate growth responses of multiple submersed vascular plants to eutrophication and habitat degradation, as reported at the Chesapeake Bay for *Z. marina* (Cerco and Moore, 2001; Madden and Kemp, 1996) and *Potamogeton perfoliatus* (Bartleson et al., 2005).

Generalised seagrass models have evolved from simple growth and production models (Bocci, 2000), to more complex ones considering space limiting functions and internal nutrient dynamics for nitrogen (Bocci et al., 1997; Elkalay et al., 2003) and phosphorous (Baird et al., 2016; Kenov et al., 2013).

Explicit seagrass processes have been included within biogeochemical or ecosystem models, to address hypothesis related with the relative contributions of each primary producer and overall ecosystem production, as well as biotic relationships between producers (e.g. competition for light, nutrients), as reported for *Z. noltei* and epiphytic community, in Thau lagoon (France), by Plus et al. (2003). Moreover, this wide viewpoint of the system may improve numerical modelling results, as showed by Aveytua-Alcázar et al. (2008) for seasonal and interannual trends in nutrient concentrations and different response to the various factors controlling their primary production, through coupling a seagrass model of *Z. marina* in ERSEM (European Regional Seas Ecosystem Model). A recent work, conducted by Baird et al. (2016) for seagrass of macrotidal estuary of Gladstone Harbour (Australia), developed a novel formulation, built around a nitrogen-specific leaf area parameter, to calculate photosynthetic rate and fraction of seafloor covered by seagrass and integrated in a biogeochemical environmental modelling suite (EMS - CSIRO Environmental Modelling Suite).

Physiological processes may be overlooked in ecosystem models, but in its turn provide valuable information on intrinsic control mechanisms of seagrass beds' dynamics and phenological stage. The study conducted by da Silva and Asmus (2001) is an example of numerical modelling of seasonal dynamics of vegetated beds of seagrass *Ruppia maritima* and epiphytes in Patos Lagoon (Brazil), focusing on dynamics at smaller scales, such as biomass of blades, stems, roots plus rhizomes, seeds and fruit and epiphytes biomass. As so, an approach using numerical seagrass modelling should compromise between physiological detail and manageable model complexity, according to the model purposes and study aims.

Table 1.2 Syntheses of seagrass seasonal dynamic models.

Reference Species (Location)	AB	BB	TIN	TIP	OSF	L	T	CV	WS	RN	NW	NS	PW	PS	R	MD	TR	TA	EP	SL	SS
Short (1980) *Z. marina* (USA)																					
Madden and Kemp (1996) Various (USA)																					
Bocci et al. (1997) *Z. marina* (Italy)																					
Bocci (2000) *Z. noltei* (Italy)																					
da Silva and Asmus (2001) *R. maritima* (Brazil)																					
Burd and Dunton (2001) *H. wrightii* (USA)																					
Zharova et al. (2001) *Z. marina* (Italy)																					
Elkalay et al. (2003) *P. oceanica* (France)																					
Plus et al. (2003) *Z. noltei* (France)																					
Bartleson et al. (2005) *P. perfoliatus* (USA)																					
Aveytua-Alcázar et al. (2008) *Z. marina* (Mexico)																					
Zharova et al. (2008) *C. nodosa* (Italy)																					
Zaldivar et al. (2009) *Z. marina* (Italy and France)																					
Buzzelli et al. (2012) *S. filiforme* (USA)																					
Kenov et al. (2013) *Z. noltei* (Portugal)																					
Baird et al. (2016) Various (Australia)																					

State variable

Additional parameter

Forcing function

AB Aboveground biomass

BB Belowground biomass

TIN Total internal nitrogen

TIP Total internal phosphorous

OSF Other seagrass features (shoots, blades, seeds, fruits)

L Light

T Water temperature

CV Current velocity, tide

WS Wind speed

RN Precipitation (rain)

NW Nitrogen from water (N-NH4 and N-NO3)

NS Nitrogen from sediment (N-NH4. Only Plus et al. (2003) considered N-NO3)

PW Phosphorous from water (P-PO4)

PS Phosphorous from sediment (P-PO4)

R Respiration

MD Mechanical damage; natural mortality

TR Translocation shoots-rhizomes

TA Translocation rhizomes-shoots

EP Epiphytes

SL Space limitation function

SS Self-shading

1.3.2.2 Numerical modelling applied to Ria de Aveiro

Regardless of the multi-disciplinary studies relying on surveyed data collection carried out over the last two decades, the literature research presented in this section focus on the hydrodynamic and water quality modelling aspects of Ria de Aveiro lagoon. In fact, numerical modelling studies, using diverse model suites, have provided major contributions to a deeper knowledge of lagoon hydrodynamics (e.g. Dias et al., 2001; Vaz et al., 2007b), as well as sediment dynamics (e.g. Abrantes et al., 2006; Lopes et al., 2006), morphodynamics (e.g. Plecha, 2011), ecological and water quality features (Lopes et al., 2008b; Rodrigues et al., 2009b; Trancoso et al., 2005). A synthesis of the main hydrodynamic models applied to Ria de Aveiro lagoon is presented in Appendix 1.

The first works on numerical modelling addressed the lagoon hydrodynamics from the tidal dynamics viewpoint, using the SYMSYS2D structured grid model (Dias et al., 1996a, b, 2000, 2001). This model, calibrated by Dias and Lopes (2006a) and Dias and Lopes (2006b), have been widely used therein to study pollutants and sediment transport, distribution and fluxes in Ria de Aveiro (e.g. Dias et al., 2007; Lopes et al., 2006; Pato et al., 2008). Moreover, also using structured grids, there are practical applications of DELFT3D-FLOW and MOHID with 2D, to study general hydrodynamic characteristics (LAGOONS, 2014; Lillebø et al., 2015; Vaz et al., 2007b), and 3D configurations of MOHID to evaluate stratification within the lagoon (Vaz et al., 2009).

Later applications used MORSYS2D, an unstructured grid model, aiming to investigate the main processes conditioning sediment dynamics at the inlet area (Plecha, 2011; Plecha et al., 2012) and the effects of potential mean sea level rise on inlet morphodynamics (Lopes et al., 2011a). Also, further applications with other unstructured grid models, such as SELFE and ELCIRC have been helpful to investigate numerous applications, including the mapping of potential inundation areas (Fortunato et al., 2013), determination of uncertainties in modelling of salinity fields (Tomás et al., 2014), risk assessment due to mean sea level rise (Lopes and Dias, 2014), climate change effects (Rodrigues, 2012) and impacts of morphological changes within the lagoon (e.g. Lopes et al., 2013b; Picado et al., 2009, 2010).

On the context of this work, special emphasis is given to hydrodynamic applications aiming to explain diverse biological patterns. They are the study of sedimentation processes and dynamics of saltmarshes (SIMSYS2D, Silva et al., 2009a; MOHID, e.g. Valentim et al., 2013), hydrodynamic conditions on microbiological estuarine dynamics (SIMSYS2D, e.g. Cerejo and Dias, 2007; Santos et al., 2014), salinity gradients on benthic macrofauna biodiversity (MOHID, Rodrigues et al., 2011) and changes in tidal and river forcing on physical controls of turbidity of two distinct seagrass meadows (Delft3D-FLOW, Lencart e Silva et al., 2013).

Most of the water quality models applied to Ria de Aveiro lagoon focus on the dynamics of lower trophic levels and its dependence on environmental drivers (Appendix 1). These models generally include phytoplankton as the main primary producer, under different tidal, atmosphere

and river discharge forcing (e.g. Lopes et al., 2010; Lopes et al., 2015; Rodrigues, 2012). Furthermore, and as a rising concern, the impact of extreme run-off events due to climate change have been studied with Mike3 model to evaluate potential changes on phytoplankton dynamics, through shifting of limiting factors (Lopes et al., 2015).

Recent studies have also been recognising the importance of benthic primary producers to the overall primary production of the system and therefore, including them as dynamic variables in numerical models. As so, Trancoso et al. (2005) used MOHID Water Modelling System to simulate the dynamics and productivity of macroalgae. More recently, Kenov et al. (2013) developed a newly benthic module integrated into MOHID, comprised in a coupled hydrodynamic and biogeochemical model, to simulate the dynamics of benthic biomass, composed by seagrass, microphytobenthos and benthic feeders. Vaz et al. (2016) adapted the last implementation to compute microphytobenthos production and assess the modelling response to different oceanic and river forcing.

Besides primary production, few works also contemplate primary consumption. Rodrigues et al. (2009a) and Rodrigues et al. (2009b) firstly applied an unstructured grid, fully coupled hydrodynamic SELFE model with ecological model EcoSim 2.0 to study the phytoplankton and zooplankton dynamics of the lagoon. This model was later revised to simulate oxygen cycle and validated along a salinity gradient (Mira channel), for different temporal and spatial scales (Rodrigues et al., 2012). Furthermore, it was applied to predict potential estuarine ecosystem changes due to anthropogenic activity (dredging) and climate change (sea level rise and different hydrological regimes) (Rodrigues et al., 2015).

As a good indicator of the overall water quality status, the dissolved oxygen concentration and distribution throughout the lagoon have also been included in a number of water quality models of the system (Lopes et al., 2005; Lopes and Silva, 2006; Lopes et al., 2008b), together with nutrient dynamics (Trancoso et al., 2005). The study of the spatial and temporal variability of these parameters, through a water quality numerical modelling approach, is most helpful to determine the origin and fate of nutrients within the lagoon, as well as the main vulnerable areas to dissolved oxygen depletion, according to seasonality, tidal cycle and river discharge regime.

Of the diverse application of aforementioned models to hydrodynamic and water quality environments of Ria de Aveiro lagoon, the numerical model suite Delft3D was a preferred choice, mainly due to its applications in the scope of LAGOONS Project to this system (LAGOONS, 2012; Lillebø et al., 2015) and to other estuarine systems worldwide (Chen et al., 2016; Hu et al., 2015; Huang et al., 2016). Moreover, the existence of an Open Process Library in Delft3D-WAQ provides the possibility to create additional substances, processes acting on new and existing substances, additional coefficients in formulae and further tools, pointed to meet the users' specific requirements. Therefore, as a versatile open-source model suite able to simulate multiple coastal systems with different features and resolutions, it shows high potential to study the hydrodynamics and water quality of coastal systems such as Ria de Aveiro lagoon, as well as the interactions with particular biological processes, such as seagrass seasonal dynamics.

1.4 STRUCTURE OF THIS WORK

This thesis is organised in 9 chapters. The current Chapter 1 presents a brief introduction to contextualize the problem under study, starting from a general background on the features and importance of estuarine systems, converging to seagrass meadows habitats. The general objectives and a short literature review concerning the modelling approaches to seagrass meadows and the diverse applications of numerical models to study the hydrodynamics and ecology of Ria de Aveiro lagoon are followed. Chapter 2 presents a description of the study area, from the hydrodynamic, geomorphological and ecological viewpoints, highlighting the evolution and present state of seagrass meadows in Ria de Aveiro. Chapter 3 presents the results and discussion of collected data from field surveys, later used to calibrate the model in Chapter 7. Chapter 4 presents the features and processes described by the seagrass model, as well as a preliminary model testing. Chapter 5 described the development of the desiccation module and the results from the collected data to support it. Chapter 6 is dedicated to the numerical model suite Delft3D, followed by Chapter 7, which presents the modifications to prior applications in Ria de Aveiro, as well as the validation of the hydrodynamic model and the calibration of seagrass biological model, coupled to the water quality model. Chapter 8 presents some of the applications of the model, such as the development of prospective scenarios to suggest potential favourable areas to seagrass restoring in Ria de Aveiro lagoon, according to the hydrodynamic and water quality features, and considering different hypothetical extreme events and climate change scenarios and the mapping. Chapter 9 presents the main conclusions of this dissertation and suggestions for further research.

This thesis also included appendixes, which complement the main chapters. Appendix 1 comprises a resume of the hydrodynamic and water quality models applied to Ria de Aveiro lagoon. Appendix 2 synthetises the evolution of tidal prism and seagrass covered area in Ovar channel. Appendix 3 summarised the temperature limiting function according to Kenov et al., (2003). Appendix 4 described the methodology to calculate evapotranspiration. Appendix 5 presents the climatology for river discharge parameters. Appendix 6 illustrates model inputs for climate change scenarios. Appendix 7 presents the maps showing the spatial distribution of the normalised anomaly for each descriptor and scenario.

Chapter 2

CHARACTERIZATION OF THE STUDY AREA

This chapter provides insights of the main characteristics of the study area, Ria de Aveiro lagoon (NW Portugal), under the viewpoints of hydro-morphological, ecological and quality features of the system. Afterwards, the evolution of seagrass meadows in the study area is reported and systematised by the application of a DPSIR framework.

2.1 HYDRO-MORPHOLOGICAL FEATURES

The Ria de Aveiro is a shallow coastal lagoon, with a very irregular geometry, located at the northwestern coast of Portugal and integrated into the Vouga river catchment area (Figure 2.1). Besides the four main channels (Mira, S. Jacinto-Ovar, Ílhavo and Espinheiro), it has a complex network of narrower ones, connected with the Atlantic Ocean through an artificial channel. This system is 45 km long and 10 km wide and has an average depth of about 1 m, except in navigation channels where dredging operations are carried out (Dias et al., 1996a).

Tide is the main circulation driver within the lagoon, which is predominantly semi-diurnal, presenting a respectively minimum and maximum tidal range of 0.6 m (neap tides) and 3.2 m (spring tides) (Dias et al., 1996a, 2000). This mean tidal range of about 2 m designates the Ria de Aveiro as a mesotidal lagoon (Dias et al., 2000). Moreover, non-tidal contributions to the circulation include wind-driven currents during small periods and gravitational flows as result of density gradients formed by freshwater runoff and seawater. The resulting flow is modified by both frictional drag due to bottom roughness and channels complex geometry (Dias et al., 1996a). Numerical modelling with the most recent bathymetric surveys showed a tidal prism at lagoon mouth of 65.8 Mm^3 and 139.7 Mm^3 (Lopes et al., 2013b) and a water covered area of 64.9 km^2 and 89.2 km^2, at neap and spring tides (Lopes et al., 2013a), respectively.

The residence time for lagoon central area, i.e. with strong marine influence, is about 2 days, whereas at the upper reaches it is higher than 2 weeks (Dias et al., 2001). As so, at the low residence time (i.e. central areas of the lagoon), particles flush out faster toward the lagoon

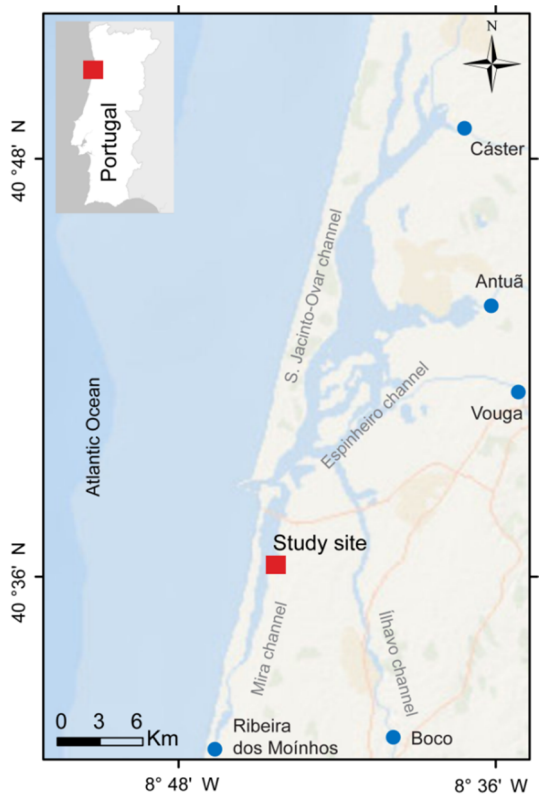

Figure 2.1 Location of Ria de Aveiro region, with lagoon main tributaries (blue dots: discharge position) and study site (red square).

mouth, while at the head of the main channels, the sediments are longer retained and likely deposited in the bottom (Lopes and Dias, 2007).

The Vouga and Antuã rivers inflow into Espinheiro channel and are considered the main sources of freshwater input into the lagoon (Dias et al., 1996a), with mean flows of 80 m^3/s and 20 m^3/s (Génio et al., 2008; Stefanova et al., 2015), respectively. Smaller contributions of freshwater sources are the drainage channels in Ribeira dos Moínhos (Mira channel, 10 m^3/s), Boco (Ílhavo channel, 5 m^3/s) and Cáster (S.Jacinto-Ovar channel, 5 m^3/s) (Génio et al., 2008). These mean rivers flows are not however widely consistent in the literature. For the two main tributaries (Vouga and Antuã), Dias et al. (2000) referred values of 29 and 2 m^3/s, Dias and Lopes (2006a) values of 50 and 5 m^3/s, 60 and 4.5 m^3/s (Vaz et al., 2016). For Ribeira dos Moínhos, Boco and Cáster the indicated values are 3.6, 1.6 and 1.0 m^3/s, respectively (Vaz et al., 2016).

This coastal system is usually considered well mixed and vertically homogeneous, due to the ratio of tidal to freshwater volume flux (Dias et al., 1996b). However, episodic flood events (i.e. high freshwater inflows) induce significant differences on the surface and bottom salinity and water temperature, and so vertical stratification may occur (Dias et al., 1996b, 2000; Vaz et al., 2005; Vaz et al., 2009; Vaz et al., 2007a).

The influence of tides has a major effect on suspended material transport and distribution throughout the lagoon, sediments (Dias et al., 1996b; Lopes et al., 2001), organisms, such as

bacterioplankton (Cunha et al., 2003) and microalgae (Cerejo and Dias, 2007), pollutants (Pato et al., 2008) and organic matter (Lopes et al., 2008a). In fact, net sediment transport along the main channels and areas of the lagoon are attributed to tidal asymmetry, as well as wind stress and river runoff (Lopes and Dias, 2007; Lopes et al., 2006), contributing in general to increase the sediment export toward the ocean (Lopes and Dias, 2007). The sediment concentrations present a semi-diurnal and fortnightly periodicity (Lopes et al., 2001, 2006), shifting according to tides, spring-neap cycles and seasons (Abrantes et al., 2006). Furthermore, tidal flow was found to be the main driver of changes in turbidity, while river-borne plumes may become important during extreme events (Lencart e Silva et al., 2013; Lillebø et al., 2015).

Off the geomorphological point of view, the anthropogenic activity has been extensively affecting the natural evolution of Ria de Aveiro lagoon. The construction of a fixed inlet in 1808 deeply changed its hydrodynamics, shifting the flow circulation from river to tidal dominant (Silva and Duck, 2001). Over the last 30 years further interventions (e.g. extensions of inlet breakwaters in 1987 and 2012, regular dredging to assure the navigability safety of inlet and main channels and degradation of saltpans walls) contributed to some noteworthy geomorphological changes, such as the deepening of the main channels, though keeping its overall geometry (Lopes et al., 2013b).

The progressive evolution of inlet configuration throughout time and the resulting inlet channel deepening promoted changes in the lagoon hydrodynamics (Dias and Mariano, 2011) and also on the sediment dynamics. As result, some works evidenced the lagoon capacity to export sediments (Plecha, 2011), and the increase on tidal wave amplitude and propagation, verified by the increase of average amplitude and a decrease of the phase of M_2 constituent (Araújo et al., 2008). As so, there was a significant amplification of the lagoon flooded area (+16% between 1987/88-2012, spring tides), which affected tidal propagation through the increase of tidal currents, tidal prism (+6% at the inlet) and tidal asymmetry (Dias and Picado, 2011; Lopes et al., 2013b; Picado et al., 2009). Moreover, morphological changes influenced the sediment transport and distribution, shifting the preferential deposition zones to the flooding areas and increasing the erosion fluxes and settling times (Costa et al., 2011; Picado et al., 2011).

Besides the direct anthropogenic-driven changes in the lagoon, recent assessments aimed to study the lagoon evolution under a global climate change perspective. In fact, although the residual transport of sediments should remain mostly seaward, its magnitude is very sensitive to the sea level rise (Lopes et al., 2011b; Lopes et al., 2011a). Tidal prism is also highly sensitive to sea level rise and expected to increase (+28% at the inlet, spring tides), which enhances the risk of some marginal areas to become flood-prone, namely those located at low altitude and nearby the margins of deeper channels (Lopes, 2016; Lopes and Dias, 2015; Lopes et al., 2011b). This consequence is boosted by storm surges, inducing higher current velocities, tidal prisms, the marginal risk of erosion and salinization of lagoon marginal lands (Lopes et al., 2013a; Lopes et al., 2013b).

2.2 ECOLOGICAL AND WATER QUALITY FEATURES

The geographical location of Ria de Aveiro and its natural resources, both natural capital and ecosystem services, contributes to its recognised value at national and international scales (LAGOONS, 2012; Lillebø et al., 2015; Sousa et al., 2017b; Sousa et al., *submitted;* Sousa et al., 2016). In fact, its unique characteristics from an ecological point of view highlight the need of conservation under several normative documents, namely as a Natura 2000 network classified area, the designation of Special Protection Area (SPA) under the wild birds conservation and the inclusion of several areas classified as Sites of Community Importance (SCI).

Specific hydro-morphological features like those aforementioned in the previous section (e.g. low depth and tidal amplitude) provide favourable conditions for the occurrence of high biodiversity habitats, such as large areas of mudflats (Figure 2.2a), saltmarshes (Figure 2.2b) and intertidal seagrass *Zostera noltei* (Figure 2.2c), which support many ecological and economic important species of invertebrates and fishes (Bueno-Pardo et al., 2018).

These key habitats to the overall ecosystem productivity provide a wide range of ecosystem services, which promotes and supports high biodiversity. The saltmarshes and seagrass meadows, colonized by halophytes and macrophytes respectively, have a significant role on primary production, nutrient cycling, protection against erosion through sediment stabilization and provide habitat, shelter and nursery areas for many fish species. Benthic microalgae (microphytobenthos) colonise the upper layers of bottom sediments of intertidal mudflats and are major contributors to high production rates, supporting high biomass and species richness of macroinvertebrates. However, these habitats are highly dependent on the hydrodynamic patterns of the lagoon. In fact, it influences the sedimentation processes of saltmarshes as reported by Silva et al. (2009a), the characteristics and stability of saltmarsh plants, considering changes on sea level rise scenarios (Duarte et al., 2014; Valentim et al., 2013) and tidal-driven differences in total suspended solids concentration (i.e. turbidity) characterise relevant physical mechanisms between two seagrass patches (Lencart e Silva et al., 2013).

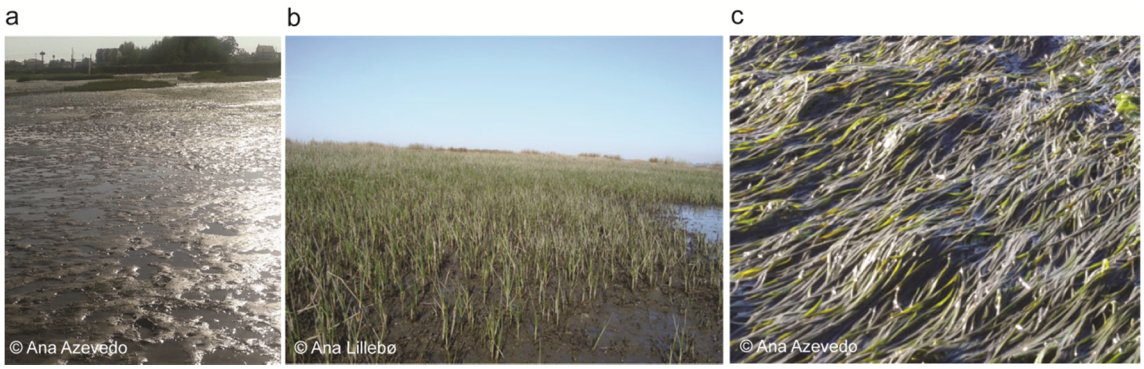

Figure 2.2 Illustration of a) intertidal mudflats; b), saltmarshes; and c) seagrass meadows of Ria de Aveiro lagoon.

Moreover, hydrodynamics also determines the distribution and activity of bacteria in surface microlayer through vertical mixing/stratification according to stronger/weaker current velocities (Santos et al., 2011; Santos et al., 2014) and the spatial distribution of benthic macrofauna (Rodrigues et al., 2011).

As important drivers of a healthy ecosystem state, the dynamics of primary producers and variation of the main environmental factors in Ria de Aveiro have been performed, through field surveys and numerical modelling approaches. Previous applications of numerical tools to this coastal system showed that the hydrodynamics highly influences primary production. As reported by Trancoso et al. (2005), the lagoon hydrodynamic conditions may condition the competition between phytoplankton and macroalgae, whereas Lopes et al. (2010) suggested that local morpho-hydrodynamic features influence the primary production, through tidal currents and system morphology (e.g. depth). Beyond the simulation of primary production, a hydrodynamic-ecological coupled model successfully simulated the diurnal and seasonal dynamics of zooplankton dynamics of the ecosystem (Rodrigues et al., 2009a; Rodrigues et al., 2012; Rodrigues et al., 2009b), under anthropogenic (e.g. dredging) and climate change scenarios (Rodrigues, 2012; Rodrigues et al., 2015).

Primary production and respiration are among the major factors conditioning the oxygen budget in the water column (Lopes et al., 2008b). Therefore, and as one of the main criteria for the assessment of water quality, dissolved oxygen (DO) concentration, has been estimated in Ria de Aveiro lagoon. A study performed with both experimental data and numerical modelling found that the far ends of main channels are the most vulnerable areas, showing low DO and high biochemical oxygen demand (BOD) concentrations (Lopes et al., 2005).

The low residence time of lagoon central areas and the strong dependence of tidal transport processes on DO distributional patterns assumed that a generalised eutrophication state of this coastal system is unlikely (Lopes et al., 2007; Lopes and Silva, 2006). Nevertheless, the nutrient distribution is variable within the lagoon, and so the water quality may also change spatially (Lopes et al., 2007; Lopes et al., 2017). The sources of dissolved inorganic nutrients support the productivity of Ria and so, chlorophyll-a and the main nutrient concentrations (i.e. nitrate, ammonium and phosphate) have been also included in the water quality assessments (e.g. Lopes et al., 2008a; Lopes et al., 2017; Rodrigues, 2012) and modelling (e.g. Lopes et al., 2010; Lopes and Silva, 2006). The spatial distribution of chlorophyll-a and nutrients (nitrate, ammonium and phosphate) shows that generally higher concentrations occur at the inner areas of the lagoon, during low tide, probably due to anthropogenic organic-rich point sources and therein mineralisation (Lopes et al., 2007; Lopes et al., 2010). Excluding nitrate, none of the other nutrients shows a clear seasonality nor is linearly depend with salinity patterns of the lagoon, indicating that only nitrate may precede from freshwater inputs, whereas the others (ammonium and phosphate) may be directly related to the biological activity and mineralisation of organic matter (Lopes et al., 2007). The ranges and peaks of nutrients concentrations for Ria de Aveiro lagoon are variable throughout the literature and appear to present wide spatial and temporal variability. However, specifically for Mira channel (location of the study site - Figure

2.1, red square) recent data on nutrient concentrations, collected by Rodrigues et al. (2012) showed a mean range of ammonium concentrations between 1 and 21 μM, while for nitrates, the variability appears to be higher, presenting mean concentration values between 4 and 347 μM and for phosphate, 1 to 33 μM.

The present low susceptibility of the lagoon to eutrophication should persist under a climate change perspective, since the available projections point out to a decrease in river discharge base flow. However, the increasing magnitude and return period of extreme events may induce changes in nutrient availability in the lagoon, including potential shifts onto a nutrient limitation condition (Lopes et al., 2015). In addition, intensification of these occurrences may also increase turbidity and reduce light penetration in the water column, reducing phytoplankton biomass and benthic primary production (Lopes et al., 2015; Vaz et al., 2016).

2.3 SEAGRASS MEADOWS IN RIA DE AVEIRO

As mentioned in the previous section, some areas of Ria de Aveiro lagoon present suitable conditions for the establishment and growth of seagrass meadows. Consistently with other coastal systems worldwide, these habitats present a remarkable ecological importance in this coastal lagoon (Bueno-Pardo et al., 2018), hosting nursery areas for many fishes (Vasconcelos et al., 2010) and invertebrates species (Rodrigues et al., 2011).

In Ria de Aveiro lagoon, seagrass meadows also had a social-economic importance. In fact, the harvesting of “moliço”, a mixture of seagrass plants (*Zostera marina* and *Zostera noltei*) with green (Ulva sp.) and red (Gracillaria sp.) macroalgae used as natural fertiliser for agricultural fields, was a high yield activity for the vicinity human populations (Santos and Duarte, 1991). The increasing pressure on harvesting conducted to the regulation of this activity, through licensing, establishment of harvest seasons and mandatory documentation of harvesting tools and selling prices (Santos and Duarte, 1991).

After the 1960s, the seagrass harvesting decreased, mainly due to changes in agricultural practices (i.e. increased use of chemical fertilizers), rather than due to seagrass depletion, resulting in a loss of its economic value (Silva et al., 2004). At the end of 1990s, the commercial harvesting of seagrass fully ceased (Silva et al., 2004).

Although its ecological and past social-economic importance, the abundance and species richness of seagrass in Ria de Aveiro lagoon have reportedly changed and followed the worldwide tendency of declining, especially in the last three decades (Silva et al., 2004). The changes in seagrass meadows throughout time were reviewed by Azevedo et al. (2013) and summed up in Table 2.1, including additional data from recent assessments. According to Silva et al. (2004), until the 1960s there was a dense coverage of Submerged Aquatic Vegetation (SAV), composed by *Stuckenia pectinata*, *Ruppia cirrhosa*, *Zostera noltei* and *Zostera marina*.

Table 2.1 Chronological changes of seagrass meadows in Ria de Aveiro lagoon.*(seagrass+macroalgae); ** aboveground; NA - Not Available (Adapted from Azevedo *et al.*, 2013).

Species	Period	Location	Cover distribution	Biomass data	Reference
Zostera noltei	1984	Ovar channel	8 km^2 (subtidal+intertidal)	300-600 $gDW.m^{-2}$ *	Silva et al. (2004)
Zostera noltei	1998 vs 2005	Ria de Aveiro	Large intertidal areas with unvegetated sediment, new areas colonised by *Z. noltei*	Aerial photographs (1998) vs field observations (2005)	Silva and Duck (2007)
Zostera noltei	2003	Ovar channel	1 km^2 (intertidal)	100-300 $gDW.m^{-2}$ *; Sept.2002-June 2003: 154±142 $gDW.m^{-2}$ (Zostera)	Silva et al. (2004)
Nano-zostera noltei	2002-2004	10 intertidal sampling points with *N. noltei* + adjacent areas with sparse macroalgae coverage	3 km^2 (2004) (intertidal)	110±50 g m^{-2} (AFDW)	Silva et al. (2009b)
Zostera noltei & Zostera marina	2008	Mira channel	Z. marina: 10 patches (<2m); Z. noltii: 0.130 km^2 (intertidal)	N.A.	Cunha et al. (2013)
Zostera noltei	2010	Ovar channel	0.431 km^2 (intertidal)	N.A.	Cunha et al. (2013)
Zostera noltei	2013-2014	Ria de Aveiro	2.3 km^2 (intertidal)	N.A.	Sousa, AI (personnal communication)
Zostera noltei	2013	Mira channel (Intertidal)	N.A (Intertidal)	44-255** $gDW\ m^{-2}$	This work

The same authors also confirmed the subtidal presence of the abovementioned species and intertidal *Zostera noltei* in a survey conducted at the 1980s. Nevertheless, the seagrass decline in Ria de Aveiro have been noticeable throughout the last decades of the 20th century, both in terms of extension and biodiversity. In the beginning of the 21st century, at Ovar channel, *Zostera noltei* (dominant species) was restricted to the intertidal zone, and mixed with macroalgae species, namely *Ulva sp*. and *Gracilariopsis longissima* (Silva et al., 2004). In fact, according to Table 2.1, from 1984 to 2003 at Ovar channel, the seagrass extension decreased about 88%, while from 2003 to 2010 it decreased 57%.

Recent assessments reinforce that currently, the seagrass status of Ria de Aveiro lagoon, is mainly expressed by monospecific stands of *Zostera noltei* restricted to intertidal flats, pointing out a fully subtidal disappearance (e.g. Cunha et al., 2013; Silva et al., 2009b; Sousa et al., *submitted*). The overall area presently occupied by seagrass in Ria de Aveiro is about 2.3 km^2, distributed along Mira channel and in the northern (CN) and southern (CS) areas of central lagoon (Figure 2.3).

The distribution of seagrass meadows in Ria de Aveiro lagoon seems to be mostly represented by small patches that contributes to about ¾ of the total area (Figure 2.4a). More than 50% of these patches are located in the entrance of Ílhavo channel, at the southern area of central lagoon (CS), while the remaining percentage appears to be similarly distributed along Mira channel and the northern area of central lagoon (CN) (Figure 2.4b). The northern areas of central lagoon (CN) present the lower number of patches, though the most extensive ones (Figure 2.4c).

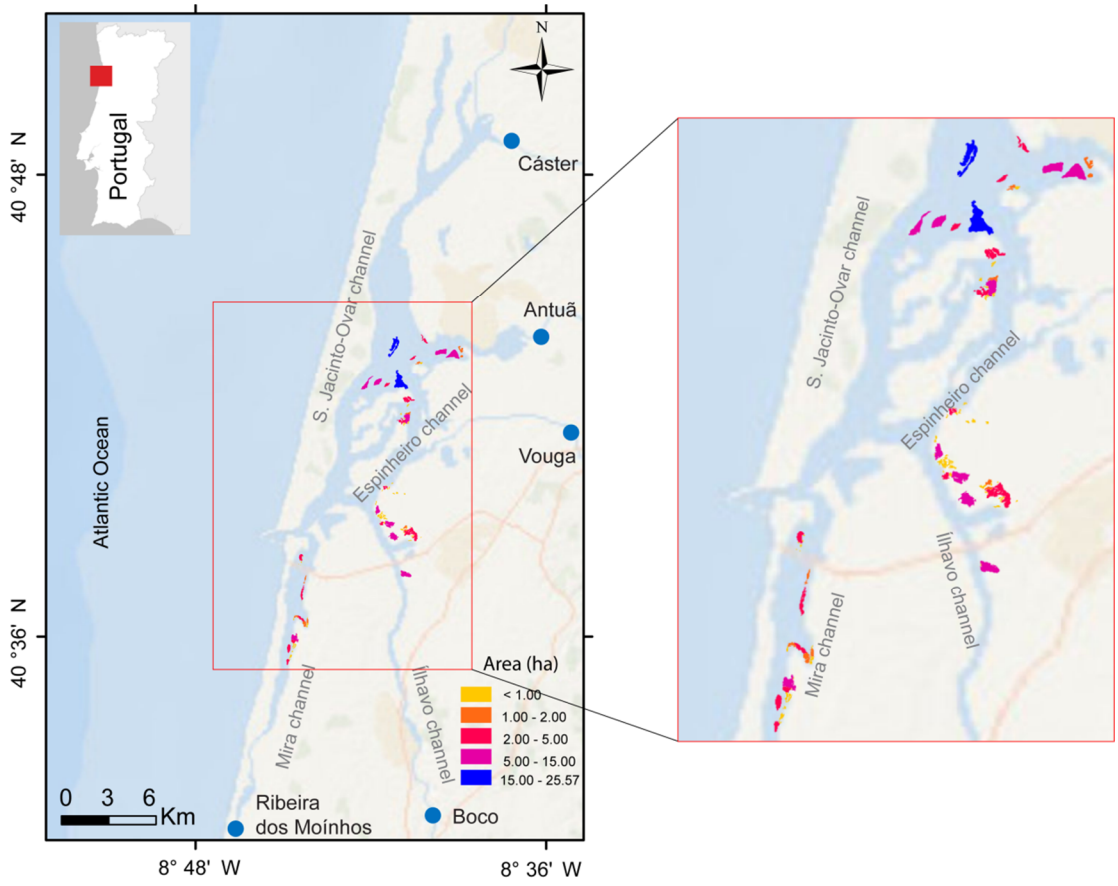

Figure 2.3 Spatial distribution of *Zostera noltei* in Ria de Aveiro, classified according to patch area and with the detail of the area with seagrass meadows (Sousa et al., *submitted*).

a

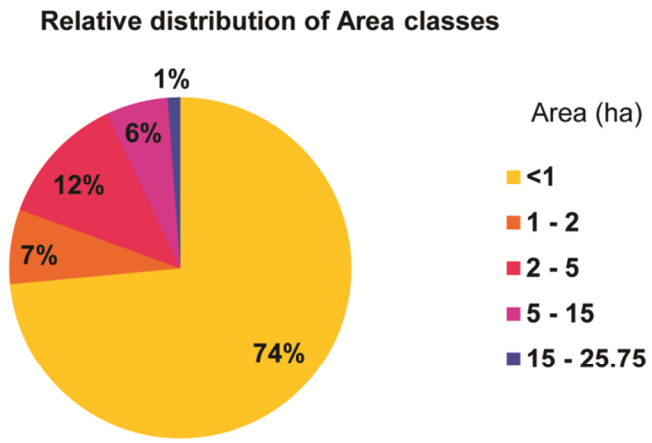

b

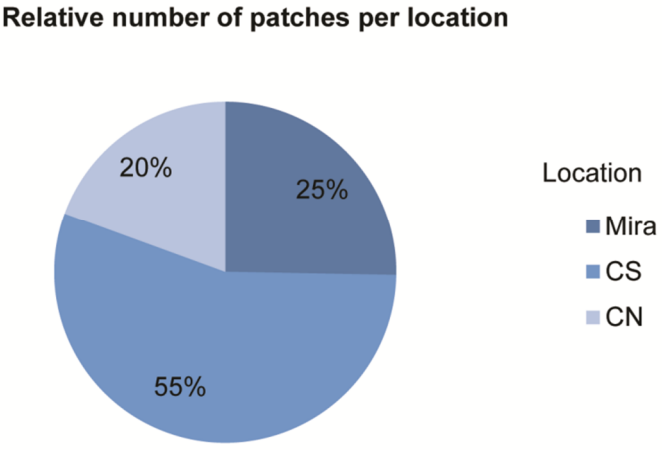

c

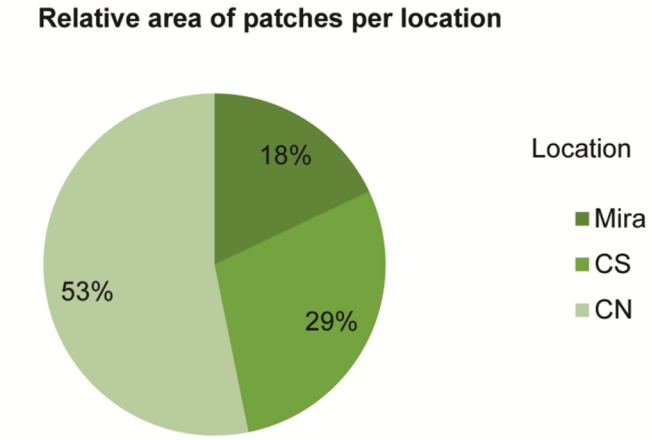

Figure 2.4 Relative distribution of seagrass meadows in Ria de Aveiro, according to the a) area classes of Figure 2.3; b) a number of patches per location c) and area per location. Mira - Mira channel, CS - Central-South lagoon and CN - Central-North lagoon.

Considering the current state of seagrass meadows in Ria de Aveiro lagoon, it is crucial to understand the drivers that conducted to its decline. To propose some potential actions foreseeing the ecosystem ecological quality status, Azevedo et al. (2013) applied a DPSIR framework (Drivers-Pressures-State-Impacts-Responses) to the Zosteraceae communities of Ria de Aveiro lagoon, from the viewpoint of combined pressures that potentially led to an extended decline of seagrass biodiversity (Figure 2.5). Summing up, the authors pointed out that previously mentioned changes in hydrodynamic patterns of the lagoon are in the origin of seagrass decline in this coastal system.

In fact, through deepening of the major channels (dredging operations) and construction of inlet piers (Silva and Duck, 2001; Silva et al., 2004; Silva et al., 2009b), the tidal prism (Appendix 2), water velocity, turbidity and sediment resuspension increased, besides the loss of fine sediments and nutrients (Silva et al., 2004). As so, there was less light available that reached the seagrass canopy, that together with the sedimentation in seagrass covered areas, lead to a decrease in seagrass productivity and therein to a full loss of subtidal meadows and reduction of the extension and biodiversity of intertidal ones (Silva et al., 2004).

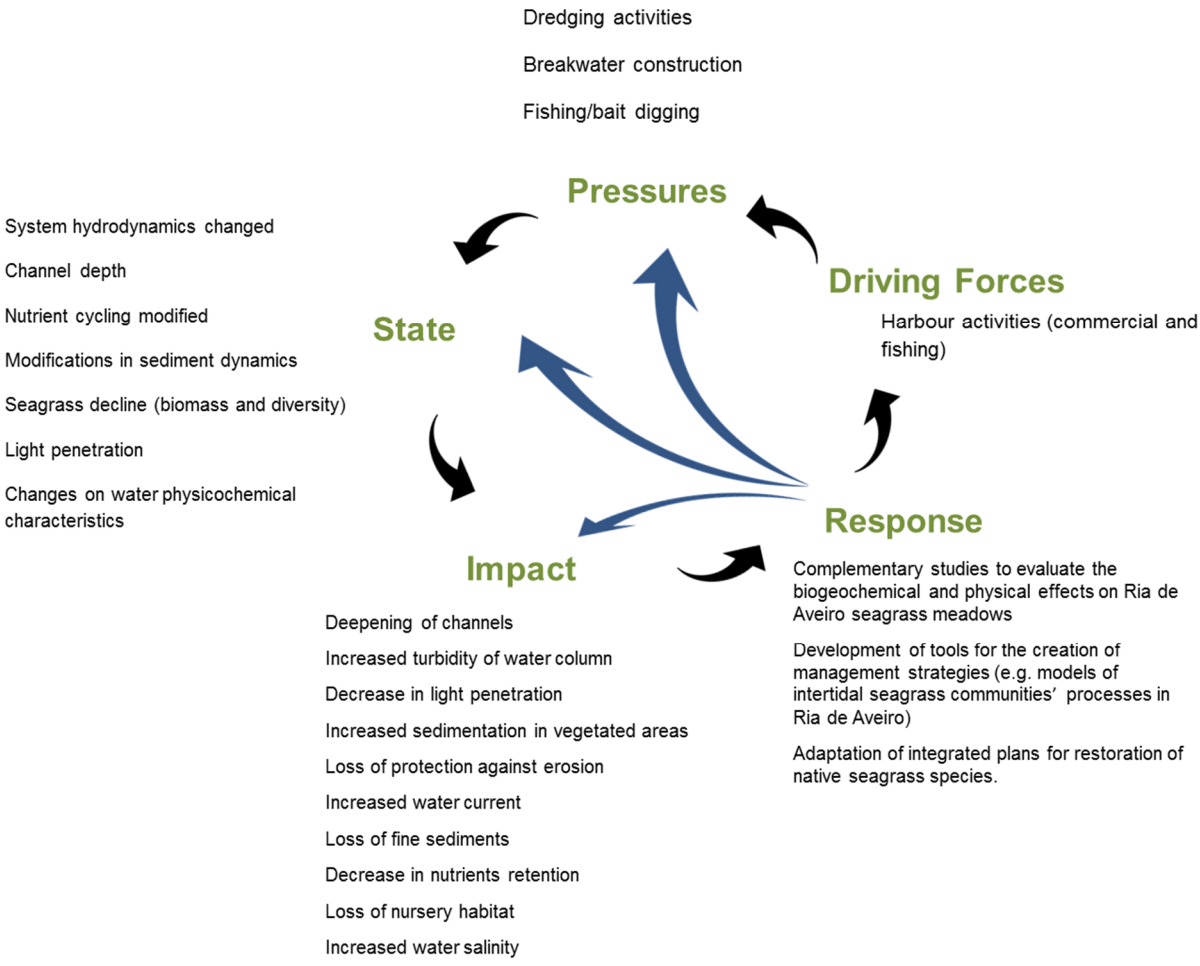

Figure 2.5 Application of DPSIR framework to the Zosteraceae seagrass communities of Ria de Aveiro (from Azevedo et al., 2013).

The seagrass decline in Ria de Aveiro lagoon is thus suggested to be mainly due to indirectly human-induced disturbances, as illustrated by Figure 2.6, although other factors should not be neglected, such as the potential natural decline due to the abandon of “moliço” harvesting activity.

As responses to seagrass decline, from the scientific and academic point of view, it was suggested the development of a model of intertidal *Zostera noltei* processes in Ria de Aveiro lagoon (this work). With this, comprehensive information is intended to be produced as supportive of management actions, recognizing the importance of sustainability of inherent ecosystems services and functions, and the assessment of potential effects of climate change context, considering future prospective scenarios. Therefore, the present work wills to provide a better understanding of the dynamics and possible evolution of these habitats, to help in their preservation and recovery.

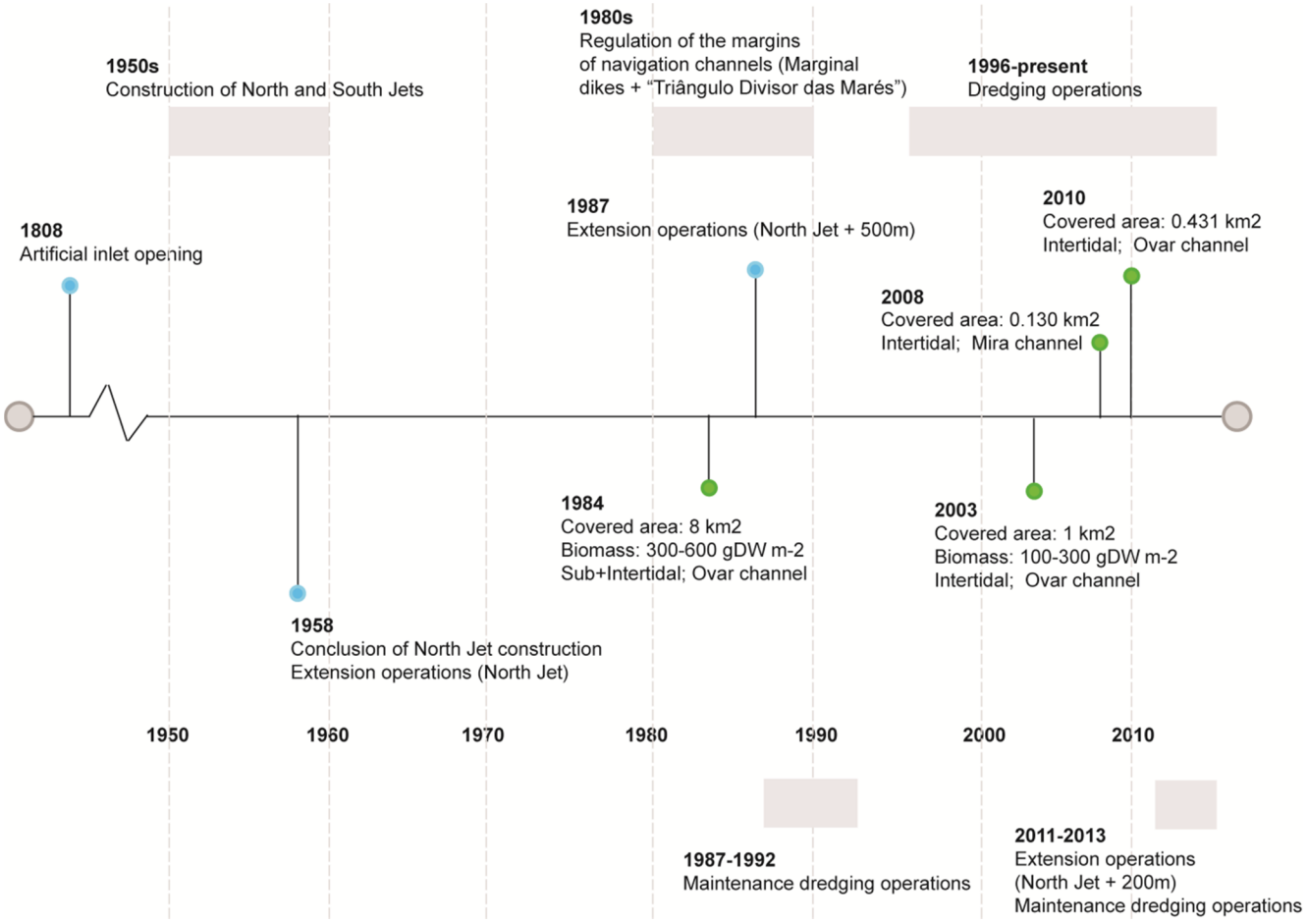

Figure 2.6 Timeline of major historical anthropogenic operations (blue dots and grey rectangles) in Ria de Aveiro and changes in seagrass covered area and/or biomass (green dots).

2.4 SUMMARY OF THE CHAPTER

The current chapter summarised the importance of both hydrodynamic and water quality features, namely turbidity/light availability to seagrass dynamics in Ria de Aveiro lagoon. However, from the best information available, the most noticeable changes in both seagrass covered area and biomasses throughout the last decades seems to be majorly related to alterations in the hydrodynamic regime of the study area, as result of anthropogenic activities.

As so, it suggested that potential management plans for seagrass restoration and recuperation in Ria de Aveiro lagoon, must inevitable contemplate the evolution of hydrodynamic characteristics of the lagoon.

Chapter 3

SEAGRASS SEASONAL DYNAMICS

This chapter presents the methodology used in this work to collect and analyse experimental data, during monthly field surveys, performed from November 2012 to November 2013 at a representative intertidal mudflat colonized by *Zostera noltei*, in Ria de Aveiro lagoon. The resulting dataset will be later used in forthcoming chapters for calibration of the model. The results are presented and discussed, foreseeing the dynamics of seagrass seasonality.

3.1 RATIONALE

As seagrass dynamics is expected to markedly change throughout the year, assessing indicators of seagrass abundance is most useful to monitor the seasonal patterns of these communities. Therefore, above and belowground biomasses and shoot density were ground surveyed at a monthly periodicity, together with general abiotic parameters from water and sediment environments.

The biomass of seagrass reported in the present work relates to the dry weight of seagrass per m^2 and distinguishes the above from belowground organs. The shoot density reports to the number of seagrass shoots per m^2.

Data analysis for both biotic and abiotic parameters followed two different methodologies: a simplistic one, resulting from the raw analysis of the sampling data, and a more complex one that required data manipulation and null hypothesis testing. Furthermore, the relationship between biotic and abiotic parameters intended to understand the isolated and/or combined effect of the variability of abiotic parameters in the seasonal patterns of intertidal seagrass meadows.

3.2 MATERIALS AND METHODS

3.2.1 Experimental design

The study site is located at Mira Channel (Figure 3.1a), previously described and characterised in Chapter 2. For each month during a year, seagrass plants were randomly sampled at five sites with cylindrical corers, and abiotic parameters, such as pH, sediment temperature and redox potential of the sediment, have been measured *in situ* with a multiparameter probe (WTW-pH 330i set equipped with SenTix® 41). Furthermore, the measurement of dissolved oxygen, water temperature and salinity (WTW Conductivity meter 330i set equipped with Tetracon® 325 probe) of the closest water channel remaining at low tide, as well as at two or three nearby tidal pools also took place, whenever it was possible.

The material collected at each corer was gently washed through a 500 µm mesh screen to save the benthic macrofauna (used in another research project) and avoid breaking the leaves. Afterwards, off all the shoots counted, it was measured the leaf length and width of 25 randomly selected complete leaves per replicate.

The washing of biological material with distilled water followed the separation of above and belowground organs of each shoot. After the removal of water excess with absorbent paper, it was determined the fresh weight of above and belowground parts. After samples dried at 60ºC for at least 48h, they were weighted (dry weight) and stored in plastic bags at room temperature.

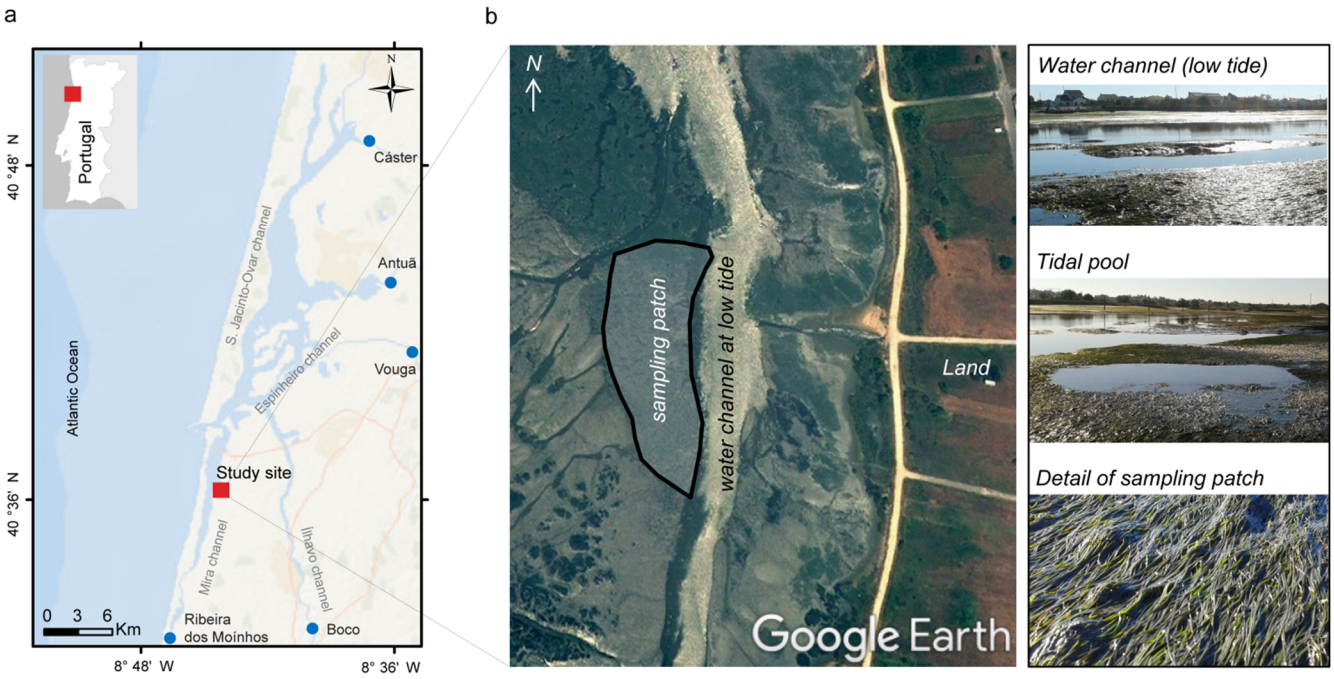

Figure 3.1 a) Location of study site in Ria de Aveiro lagoon, with b) detail of study site location and main features.

3.2.2 Data analysis

Data analysis comprised the raw analysis of experimental data, as a preliminary exploratory approach, followed by a more complex methodology, which required the calculation of a resemblance matrix by the Euclidean distance method, and further hypothesis testing, under the null hypothesis of no significant differences among *seasons*, using permutation multivariate analysis of variance with the PERMANOVA+ add-on in PRIMER v6 (Anderson et al., 2008). *Seasons* factor comprise the four seasons of the year: spring (March, April, May), summer (June, July, August), autumn (September, October, November) and winter (December, January, February).

In the case of biotic data, the analysis followed a two-way hierarchical design, with *months* nested in *seasons*, as the main fixed factor. For the abiotic data, the normalization of data preceded the calculation of the resemblance matrix (Clarke and Gorley, 2006). Abiotic data followed a one-way hierarchical design, with *seasons* as a fixed factor.

For both biotic and abiotic data, the *pseudo-F* values in the PERMANOVA main tests were evaluated in terms of significance among different seasons and, when the main test revealed statistical differences ($p<0.05$), the *t*-statistic was calculated for pair-wise comparisons.

An exploratory approach over the environmental variables used the BIOENV routine (Clarke and Gorley, 2006) to determine the best correlation with the biotic data, and therefore, inspect on what abiotic variables best describe the biotic patterns.

3.3 RESULTS

3.3.1 Leaf length and width

Morphometric data presented high spatial variability, which remained similar throughout the year, but showed no remarkable temporal variation. The leaf length (Figure 3.2a) and leaf width (Figure 3.2b) present no clear seasonal patterns. Lowest leaf length occurs during the early spring, while the highest values predominate at late autumn and winter (Figure 3.2a). The results on hypothesis testing show significant differences of leaf length among seasons ($p<0.05$), rejecting the null hypothesis (Table 3.1 and Table 3.2).

The average of leaf width remains analogous throughout the year (~0.08 cm) with a slight increase of average value at late spring (Figure 3.2b). Hypothesis testing reveals no significant differences of seagrass leaf width among seasons ($p>0.05$), failing to reject the null hypothesis (cf. Table 3.1).

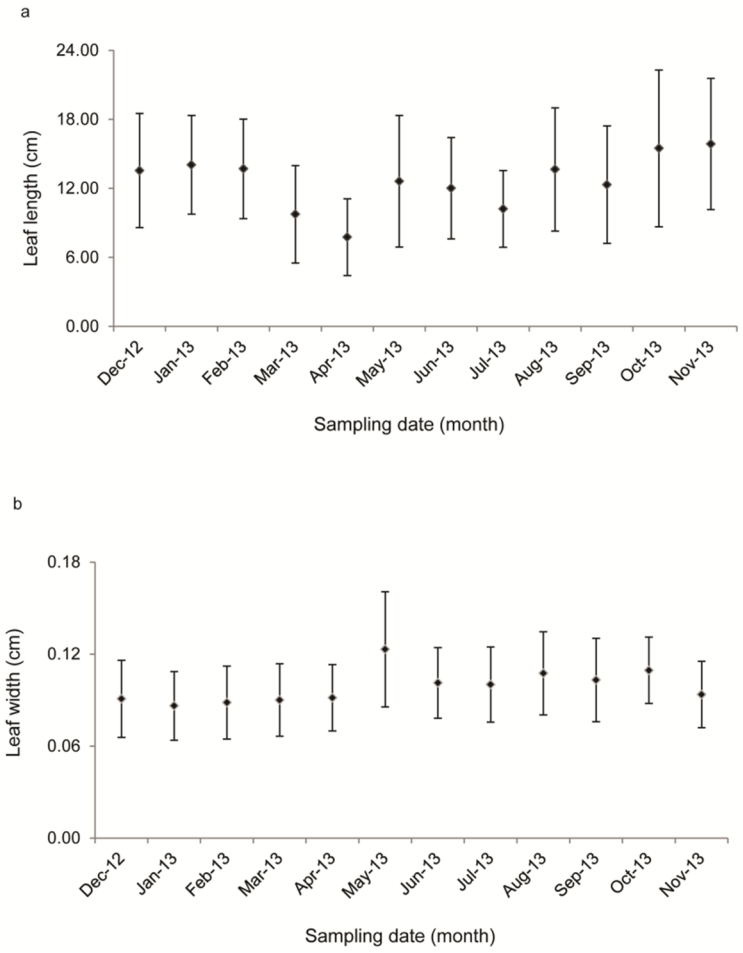

Figure 3.2 Seasonal cycle of seagrass (a) leaf length and b) width (*n=5*).

3.3.2 Shoots density and biomass

Data from shoot density and above and belowground biomass also showed high spatial variability and was highly heterogenic. Temporal variation is more notorious for shoot density and aboveground biomass. The shoot density presents a clear seasonal pattern, with higher values at spring and ranging between 2260-20600 shoots m^{-2} (Figure 3.3a). The variability within months is remarkably heterogenic throughout the year and hypothesis testing points out to significant differences on seagrass shoot density among seasons ($p<0.05$), rejecting the null hypothesis (Table 3.1 and Table 3.2).

Table 3.1 PERMANOVA main-test results for the biotic descriptors of seagrass (df - degrees of freedom, SS - sum of squares, MS - mean square, *p* - significance level)

Test	df	SS	MS	*Pseudo-F*	*p*
Leaf Length					
Season	3	193.04	64.346	4.3358	0.0478 *
Months (Season)	8	118.73	14.841	2.3651	0.0311
Residuals	48	301.19	6.2747		
Total	59	612.95			
Leaf Width					
Season	3	2.0605×10^{-3}	6.8683×10^{-4}	1.4583	0.2959 (ns)
Months (Season)	8	3.7678×10^{-3}	4.7097×10^{-4}	2.4057	0.0273
Residuals	48	9.3971×10^{-3}	1.9577×10^{-3}		
Total	59	1.5225×10^{-2}			
Shoot Density					
Season	3	2.9712×10^{8}	9.9039×10^{7}	4.9603	0.0475 *
Months (Season)	8	1.5973×10^{8}	1.9967×10^{7}	2.804	0.0132
Residuals	48	3.4179×10^{8}	7.1206×10^{6}		
Total	59	7.9864×10^{8}			
Aboveground Biomass					
Season	3	12408	4135.9	3.3187	0.0742 (ns)
Months (Season)	8	9969.7	1246.2	1.0058	0.4459
Residuals	48	59473	1239		
Total	59	81850			
Belowground Biomass					
Season	3	2320.6	773.53	1.0795	0.4107 (ns)
Months (Season)	8	5732.3	716.54	3.3488	0.0037
Residuals	48	10271	231.97		
Total	59	18324			

Significance level: (ns) – non significant, * $p<0.05$, ** $p<0.01$

Table 3.2 Values for *t*-statistic and associated significance in the pairwise comparisons for biotic descriptors.

Season	Leaf Length	Shoot Density
Winter vs Spring	2.9013 **	3.2898 **
Winter vs Summer	1.9462 **	-
Spring vs Autumn	-	2.8206 **

Significance level: (ns) – non significant, * $p<0.05$, ** $p<0.01$

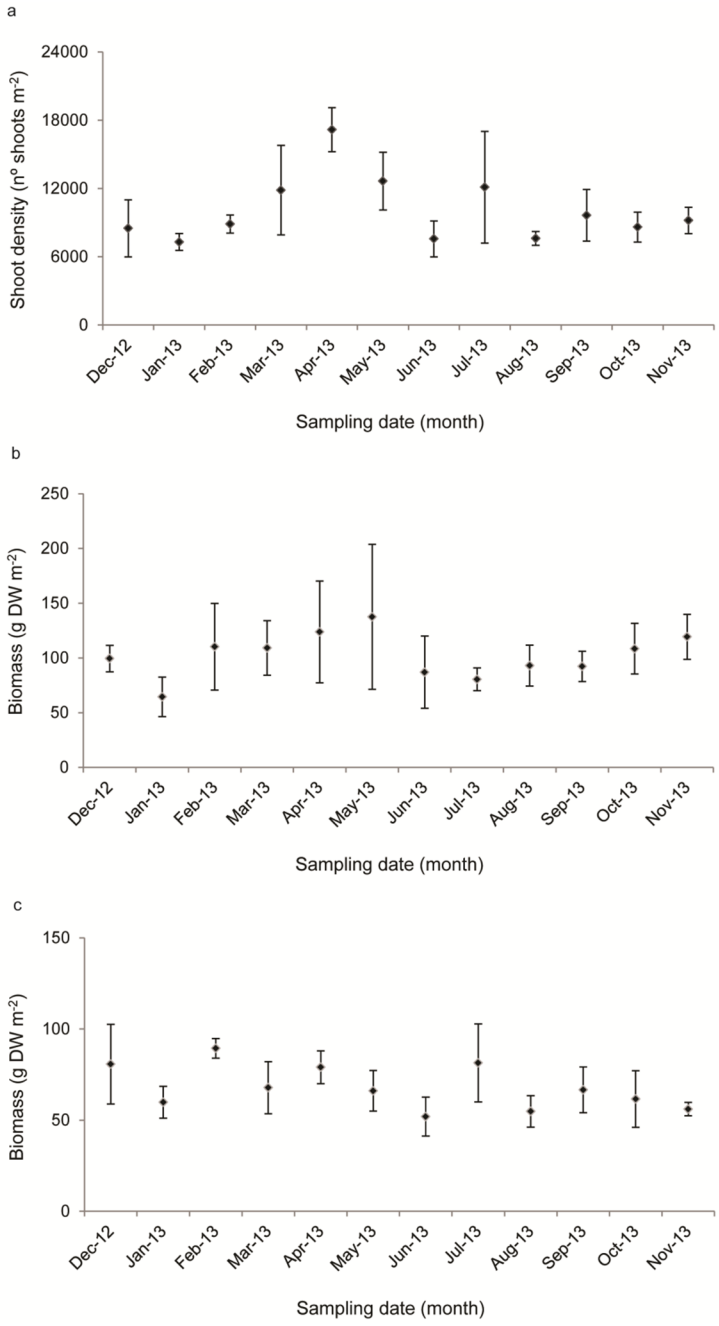

Figure 3.3 Seasonal cycle of seagrass shoot density (a), above (b) and belowground biomass (c) (*n*=*5*).

Aboveground biomass shows a visible seasonal pattern, presenting minimum values at mid-winter and maximum at late spring of 44 and 255 g DW m^{-2}, respectively (Figure 3.3b). Similar to shoot density, the variability of aboveground biomass within months is heterogenic throughout the year, but in this case, there are no significant differences among seasons (p>0.05), failing to reject the null hypothesis (Table 3.1).

Belowground biomass presented no clear seasonal pattern (Figure 3.3c), ranging from 37 to 112 g DW m^{-2}. Similar to the aboveground biomass, hypothesis testing on belowground biomass failed to reject the null hypothesis (p>0.05) (Table 3.1).

The relative contribution of aboveground material presented higher values in spring and autumn (range: 61-68% and 58-68%, respectively; average 63%), comparing with those found for winter (range: 52-55%; average: 54%) and summer (range: 50-63%; average: 58%). Furthermore, the relative contribution of belowground material to the total biomass was generally higher in winter (range: 45-48%; average: 46%), followed by summer season (range: 37-50%; average 42%). For both spring and summer seasons, this relative contribution was in average 37% (range: 32-39% and 32-42%, respectively).

Figure 3.4 illustrated the ratio of above/belowground biomass from this work, as well as in other work for *Z. noltei* in Thau lagoon (France) (Plus et al., 2003), for further discussion. The data shows high variability, partially coming from the high variability previously observed for the above and belowground biomass data (spatial), but also due to seasonality. The average ratio of above and belowground biomass was higher for autumn and spring (range: 1.1-2.8 and 0.9-3.4, respectively; average: ~1.8), followed by summer (range: 0.7-3.5; average: 1.5) and winter (range: 0.7-2.6; average: 1.2).

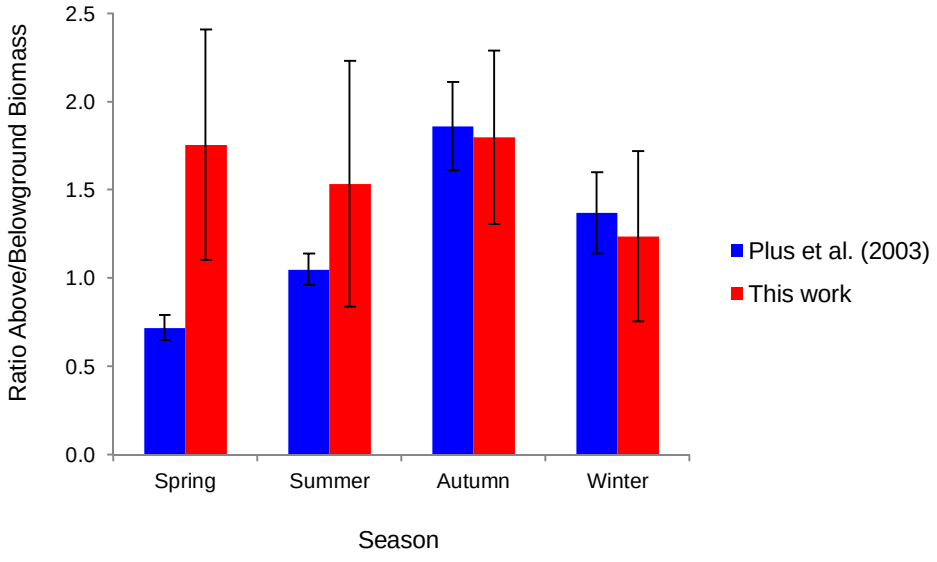

Figure 3.4 Comparison of above/belowground biomass ratios for different seasons for Ria de Aveiro lagoon and Thau Lagoon (Plus et al., 2003).

3.3.3 Abiotic parameters

To support and infer about the variability of biotic data, the measurement of abiotic parameters took place, whenever possible, at the remaining water channel during low tide, nearby water pools and sediment of collection sites.

The dissolved oxygen measured at the water channel presents higher values during winter months (maximum in December, 11.3 mg L^{-1}), and lower ones during summer (minimum of 7.1 mg L^{-1}) (Figure 3.5a). For tidal pools (Figure 3.6a), the range of variation of this parameter is higher than the occurring at the water channel, though it is not possible to discuss its seasonality, as the recording of data has not been possible every month.

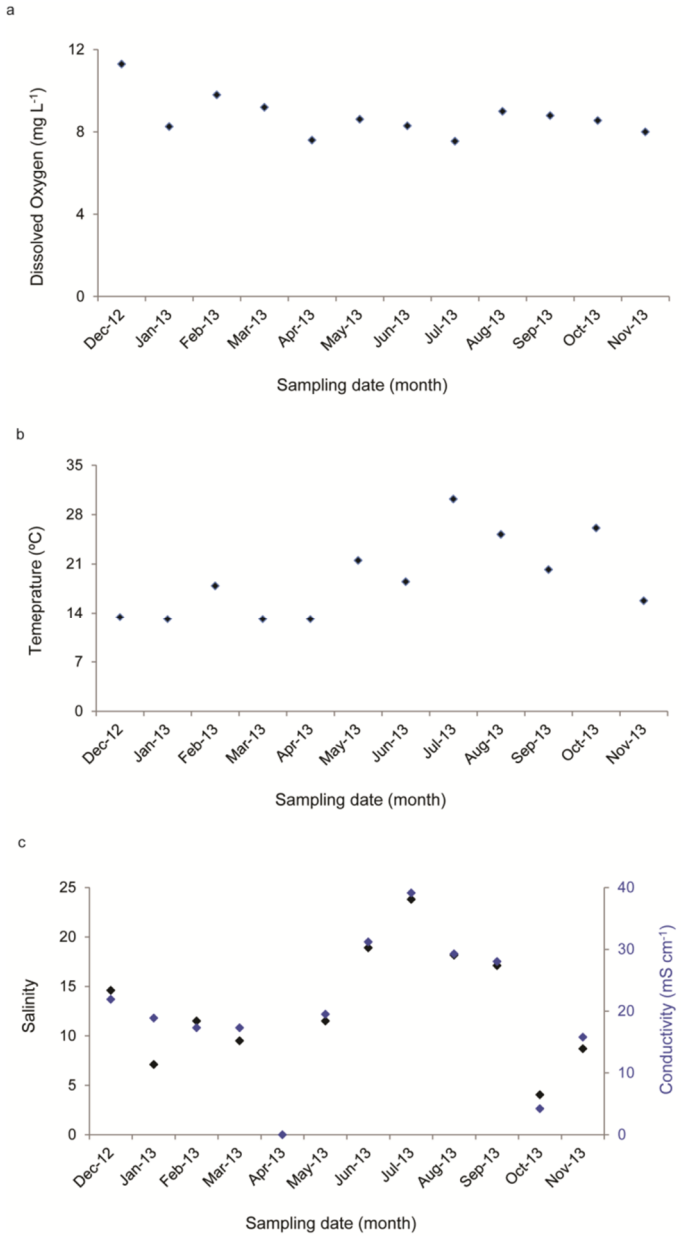

Figure 3.5 Abiotic parameters measured at the low tide water channel: a) dissolved oxygen, b) water temperature and c) water salinity and conductivity.

Water temperature in the water channel presents no clear seasonal trend and no significant differences between seasons (Table 3.3). It shows generally lower values in winter and early spring (~13 ºC) and higher ones during the summer (maximum 30 ºC) and early autumn months (Figure 3.5b). Moreover, this parameter showed a similar pattern for the tidal pools, registering higher values during the summer and lower during late autumn (no data available for winter months) (Figure 3.6b).

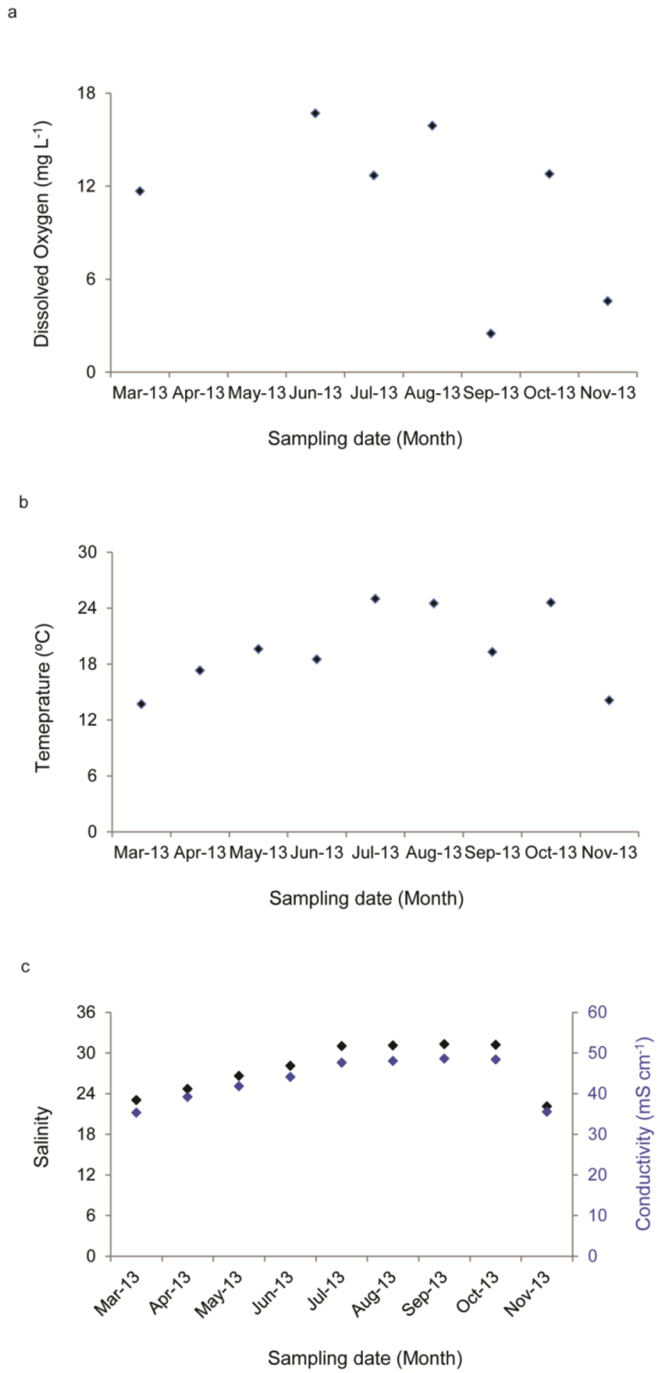

Figure 3.6 Abiotic parameters measured at the low tide water pools: a) dissolved oxygen, b) water temperature and c) water salinity and conductivity.

Table 3.3 PERMANOVA main-test results for the abiotic descriptors of seagrass (df - degrees of freedom, SS - sum of squares, MS - mean square, p - significance level)

Test	df	SS	MS	*Pseudo-F*	*p*
Redox potential (Eh)					
Season	3	8.7876	2.9292	0.95795	0.5298 (ns)
Sites (Season)	8	24.462	3.0578	5.6999	0.0001
Residuals	48	25.75	0.53646		
Total	59	59			
pH					
Season	3	15.958	5.3194	2.9513	0.1082 (ns)
Sites (Season)	8	14.419	1.8024	3.0226	0.0057
Residuals	48	28.623	0.59631		
Total	59	59			
Sediment temperature (Tsed)					
Season	3	39.812	13.271	5.6957	0.0284 *
Sites (Season)	8	18.64	2.33	204.06	0.0001
Residuals	48	0.54807	1.1418×10^{-2}		
Total	59	59			
Dissolved oxygen (O2diss)					
Season	3	3.0934	1.0311	1.0433	0.4262 (ns)
Residuals	8	7.9066	0.9883		
Total	11	11			
Water temperature (Twater)					
Season	3	5.5264	1.8421	2.6924	0.1079 (ns)
Residuals	8	5.4736	0.6842		
Total	11	11			
Salinity					
Season	3	6.7731	2.2577	4.273	0.0541 (ns)
Residuals	8	4.2269	0.52836		
Total	11	11			

Significance level: (ns) – non significant, * $p<0.05$, ** $p<0.01$

The results of salinity and water conductivity for the water channel (Figure 3.5c) and tidal pools (Figure 3.6c) clearly show they are co-variables, as so null hypothesis testing is only applied to salinity. Hypothesis testing over salinity data shows no significant differences (p>0.05) (Table 3.3). Summer months generally present the highest values of salinity (~25) and conductivity (~38 mS cm^{-1}) in the water channel, while the late autumn and winter months (rainy season) present lower values (minimum of 4.0 for salinity and 4.2 mS cm^{-1} for conductivity) (Figure 3.5c). For tidal pools (Figure 3.6c), salinity and conductivity reveal a lower range of variation, comparing with the same parameters for water channel (cf. Figure 3.5c). There is no data available on salinity and conductivity of water pools for the winter months.

Concerning the abiotic parameters measured in the sediment, the average potential redox is higher during mid-spring (maximum: -24.64 mv) and late summer/early autumn and lower during midsummer and late winter (minimum: -163.86 mV) (Figure 3.7a). Hypothesis testing points out to no significant differences of redox potential among seasons (p>0.05), failing to reject the null hypothesis (Table 3.3).

The pH in the sediment presents higher values during the winter (average maxima: 7.53) and remains practically invariable during the rest of the year, with marginal increases during late spring/early summer and early autumn (Figure 3.7b). Hypothesis testing applied to sediment pH, similar to sediment redox potential, showed no significant differences among seasons (p>0.05) (Table 3.3).

The temperature of the sediment reveals higher values during mid and late summer and mid-autumn, with lower spatial variability (Figure 3.7c). Hypothesis testing points out to significant differences in sediment temperature among seasons (p<0.05), rejecting the null hypothesis (Table 3.3 and Table 3.4).

Table 3.4 Values for *t*-statistic and associated significance in the pairwise comparisons for abiotic descriptors.

Season	Sediment Temperature
Winter vs Spring	16.704 **
Winter vs Summer	41.911 **
Winter vs Autumn	52.256 **
Spring vs Summer	35.473 **
Spring vs Autumn	40.466 **
Summer vs Autumn	11.735 **

Significance level: (ns) – non significant, * p<0.05, ** p<0.01

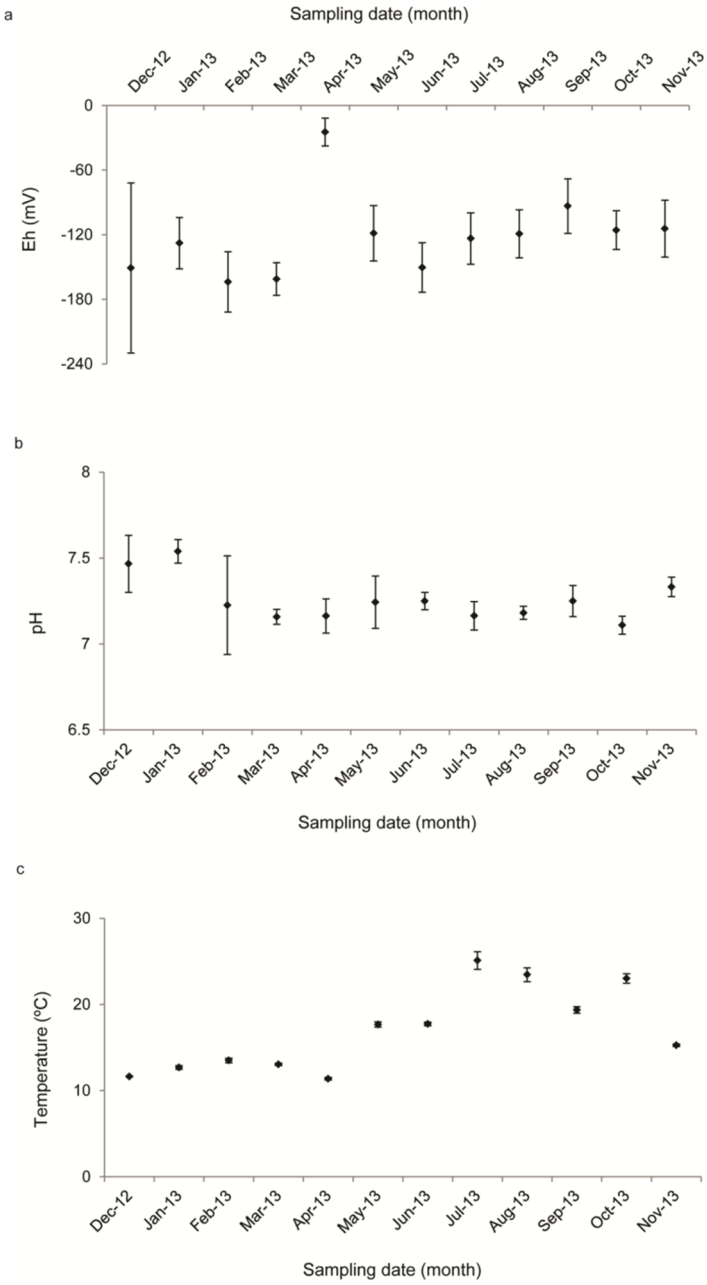

Figure 3.7 Abiotic parameter measured in sediment during low tide, throughout the annual cycle (n=5): a) redox potential, b) pH and c) temperature.

3.3.4 Relationship between biotic and abiotic parameters

The application of BIOENV routine calculates the best correlation between the abiotic (Eh, pH, sediment temperature, dissolved oxygen, water temperature, salinity and conductivity) and biotic datasets (only for aboveground and belowground biomass, as they comprise the biotic features used in the model), indicating the respective selection of variables (Table 3.5).

The variability of belowground biomass was best described by solely one abiotic variable (dissolved oxygen), though the Spearman rank correlation was low (0.310).

In the case of aboveground biomass, the best correlation comprised a selection of two abiotic variables, namely pH and salinity (Spearman correlation: 0.358).

Table 3.5 Results of BIOENV routine: best Spearman correlation and respective selection of variables.

	Eh	pH	Tsed	O2diss	Twat	Salinity	Cond.	Spearman
AB								0.358
BB								0.310

AB – aboveground biomass, BB – belowground biomass, Eh – redox potential, Tsed – temperature of sediment, O2diss – dissolved oxygen, Twat – temperature of water, Cond. – Conductivity, Spearman – Spearman rank correlation

3.4 DISCUSSION OF RESULTS

3.4.1 Leaf morphometry

Concerning some foliar biometric parameters experimentally determined in this work, such as leaf length and leaf width, the results seem to be overall similar to those found in literature available for *Z. noltei* elsewhere.

In fact, and according to a study developed at two Mediterranean lagoons, the mean leaf length of *Z. noltei* leaves, in environments with low impacts of human activity, varied between 55.1 mm to 214.2 mm (Pergent-Martini et al., 2005), which is within the range of experimental variation from this work (about 40-260 mm). The same authors also mentioned mean leaf widths between 1.0-2.0 mm (vs 0.9 mm in this work), registering higher values in more pristine areas.

According to the same authors both leaf length and leaf width of *Z. noltei* present inter-annual and seasonal variation. Although in this work only leaf length showed seasonal variability, it verifies higher values during the winter season, as the cited authors have. The mean leaf width remained invariable throughout the year but also showed maximum mean values in late spring/early summer, as reported by Pergent-Martini et al. (2005).

Changes found between morphological traits of *Z. noltei* leaves may be due to differences on major factors not assessed in present work, such as waves and nutrient interactions, which can significantly reduce leaf length (La Nafie et al., 2012). Moreover, interactive effects of hydrodynamic and light stresses seem also to induce changes in plant morphometry, at leaf length level. Higher current velocities enhance water turbidity and subsequently reduce

available light to seagrass growth, resulting in a preferential allocation of biomass into belowground structures, bearing short leaves (de los Santos et al., 2010).

Sediment environment has a strong influence on seagrass dynamics, particularly in intertidal areas. However, experimental assessments on the effects of burial and erosion in intertidal *Z. noltei* showed no particular evidence of sediment level effects on leaf length, ruling out a major effect on leaf morphometry (Cabaço and Santos, 2007).

3.4.2 Shoot density and biomass

Regarding the other biotic data collected in this work, previous works also comprised the collection and determination of the number of shoots and above and belowground biomasses, to address the seasonal dynamics of seagrass.

In the present work, shoot density ranged from 2260-20600 shoots m^{-2}. This is consistent with some previous works studying vegetative shoots of well-established *Z. noltei* beds of Arcachon Bay (France, 4000-9000 shoots m^{-2} in winter and 11000-22000 shoots m^{-2} in summer) (Auby and Labourg, 1996), Zandkreek estuary (SW Netherlands, 1000-23000 shoots m^{-2}) (Vermaat and Verhagen, 1996) and Biguglia and Urbino Mediterranean lagoons (France, 1600-19600 shoots m^{-2}) (Pergent-Martini et al., 2005).

In further assessments of shoot density for *Z. noltei*, some works report substantial lower values than those found in the present work. Most of these, similar to leaf morphometric parameters, showed that induced exposures of intertidal seagrass to disturbances might result in lower shoot densities. For assessments performed in an intertidal *Z. noltei* meadow nearby an urban wastewater discharge in Ria Formosa (Portugal), Cabaço et al. (2008) showed that shoot density was higher at the most distant site from the discharge source, during summer (more than 13000 shoots m^{-2}), which is still considerably lower than the maxima found for the present work. In *Z. noltei* patchy meadows, strongly affected by wind-generated waves, boat waves and propellers of small recreational boats, as reported by Paul and Amos (2011) for Ryde Sand (UK), the shoot densities reach the maxima in summer (~4600 shoots m^{-2}) and minima in winter (600 shoots m^{-2}).

Besides impacted areas, in mixed meadows of *Zostera noltei* and *Zostera marina*, the shoot density maxima occurs in July, ranging from 2764–2944 shoots m^{-2} (Laugier et al., 1999) to 3593 shoots m^{-2} (Plus et al., 2001), which is still very low comparing with results from this work for intertidal monospecific meadows of *Z. noltei*.

Though the range of variation found for seagrass shoot density in this work is within the ones found for relatively undisturbed areas, as aforementioned, the general overall seasonal pattern with minima in winter and maxima in summer is not as clear here as shown in the previous works. In fact, this work registered the lowest shoot density values in autumn and winter seasons, with higher values reached during mid-spring.

Moreover, although the present work considered no variation of shoot density along the vertical intertidal gradient, this should be addressed in future works, as previous studies show that medium intertidal *Z. noltei* meadows present significant higher shoot density (4671-13004 shoots m^{-2}), compared with low and high intertidal (1433-10297 shoots m^{-2} and 2141-6989 shoots m^{-2}, respectively) (Cabaço et al., 2009). Nevertheless, in the peculiar case of the study area however, the slope along intertidal area is very low (Azevedo et al., 2016), pointing out that these ranges on shoot density may be more notorious between the seagrasses exposed during low tide and those presented in tidal pools, rather than the intertidal gradient itself.

The results of *Z. noltei* biomass were overall consistent with those found in the literature for other coastal lagoons (Auby and Labourg, 1996; Cardoso et al., 2004; Pérez-Lloréns and Niell, 1993a; Pergent-Martini et al., 2005; Plus et al., 2003; Plus et al., 2001; Vermaat et al., 1993). In terms of seasonal pattern, most of the aforementioned studies report a unimodal pattern with maxima in summer and minima in winter. For the present work, the aboveground biomass is actually maximum at late spring (255 g DW m^{-2}) and minimum at mid-winter (44 g DW m^{-2}), but also present an autumn peak which has already been previously reported for *Z. noltei* (Bocci, 2000) and *Z. marina* in Venice lagoon (Bocci, 2000; Zharova et al., 2001). The minimum values are within the range of variation of those found in the literature, even though the maximum ones are slightly higher. Typical minimum and maximum values of the aboveground biomass of *Z. noltei* lie between 30-50 g DW m^{-2} and 180-200 g DW m^{-2} (Pergent-Martini et al., 2005), respectively, while for vegetative shoots they range between 40-80 g DW m^{-2} and110-150 g DW m^{-2} (Auby and Labourg, 1996).

The belowground biomass in this work presents a minimum of 37 g DW m^{-2} and maximum of 112 g DW m^{-2} and does not follow a clear seasonal pattern, which is similar to the findings of a study conducted by Pergent-Martini et al. (2005), conducted for two different anthropogenic-impacted Mediterranean lagoons. Characteristic minimum and maximum values of belowground biomass are between 25-30 g DW m^{-2} and 70-75 g DW m^{-2} (Pergent-Martini et al., 2005), respectively, and for vegetative shoots 40-60 g DW m^{-2} and 140-200 g DW m^{-2} (Auby and Labourg, 1996).

These biological traits of *Z. noltei* presented high spatial heterogeneity within the sampling patch. This variability changed throughout the year without any particular trend, which appears to also occur elsewhere, as showed in the study of Plus et al. (2003). Although the authors do not point out any particular cause to explain that variability, in this work it is believed that local physical disturbances difficult to track, for example, caused by trampling of bait diggers (Silva et al., 2005b), may help to explain some of these differences. Moreover, the location of sampling sites in the context of the meadow geometry may also comprise one potential factor to support the higher spatial heterogeneity, as previously shown for seagrass *Cymodocea nodosa* (Duarte and Sandjensen, 1990).

Regarding the relative contribution of each biomass fraction to the total biomass, higher values for belowground organs occurred in winter, similar to those found by Sousa et al. (2017a), for *Z. noltei* in Ria de Aveiro lagoon. The average found in this work is slightly higher

comparing with the referred study, with 46% (this work) vs 37% (Sousa et al., 2017a) for winter, and 37% (this work) vs 33% (Sousa et al., 2017a) for spring. The range of variation was however lower than those found by the same authors.

In spite of the high variability, the results for above/belowground ratio are generally consistent with other studies (Figure 3.4) (Plus et al., 2003), pointing out for an equilibrated metabolic cost of plant maintenance and low allocation of biomass to non-photosynthetic organs of *Z. noltei* at the study area (Pergent-Martini et al., 2005). These results are however not as high as those found by a study conducted by Auby and Labourg (1996).

3.4.3 Abiotic parameters

The abiotic data determined in the remaining water channel at low tide, such as dissolved oxygen, water temperature and salinity, overall followed the existing recorded patterns for the system. Dissolved oxygen does not present such clear seasonal pattern as water temperature and salinity, but these were distinctively higher in late spring and summer seasons than in winter. This is expected, as major freshwater inputs are heavier during winter, while during summer, salinity normally rises, reaching closer values to those found for seawater. Data from physical factors measured in tidal pools are not highly explored and discussed in this work, as it is not available for the whole year and no information on pool shape and depth is currently available, which fluctuates abiotic parameters (e.g. water temperature, salinity, shading, among others).

Furthermore, abiotic data from sediment are substantial important, as seagrasses are marine rooted plants and ecosystem engineers, actively interacting with the surrounding environment (Bos et al., 2007). Overall, the parameters measured at sediment, such as temperature, pH and Eh also followed existing recorded patterns. Sediment temperature revealed very low spatial variability within the meadow, with higher values naturally occurring in late spring and summer seasons. The ranges of sediment temperature and pH are within those found in the literature for seagrass meadows of the same geographical area (Sousa et al., 2017a). Sediment redox potential was also expectedly less negative in months with higher seagrass biomass, as chemical changes in the rhizosphere of several plants are widely reported, namely at level of redox potential, oxygen and nutrient profiles (Lillebø et al., 2006).

3.4.4 Relationship between biotic and abiotic parameters

Regarding the exploratory approach using BIOENV routine, the low Spearman correlation between the overall biotic data and abiotic descriptors assessed in this work reveals that the later were not enough to explain the seagrass shoot density and biomass seasonality. As seagrass growth is widely accepted to depend on physical, chemical and biological factors, intrinsic and complex interactions between them, may however be unable to isolate single or

low number combination of abiotic factors, foreseeing the predictability of seagrass seasonal cycle (Greve and Binzer, 2004).

Off the measured abiotic parameters, the combination of pH and salinity was the best achieved to explain the variability of aboveground biomass of *Z. noltei*, even though it presented a low correlation coefficient. These findings may be partially explained by those presented by Sousa et al. (2017a), also for *Z. noltei* in Ria de Aveiro lagoon, showing that salinity had no significant relationship with aboveground biomass for both winter and late spring seasons, although pH presented significant relationship with aboveground biomass for late spring. Also according to Sousa et al. (2017a), for above and belowground biomass during winter seasons, ambient temperature had a significant relationship with these seagrass traits, which have not been clear in correlation coefficients found in the present work.

Moreover, some important physical requirements for seagrass growth, such as light and other substratum characteristics (e.g. grain size and organic matter content), not taken into account in the correlation, may be relevant sources of variability and further considered (Philippart, 1995a).

3.5 CONCLUSION

As one of the most common approaches to address the seasonality of seagrass meadows, experimental data have been collected and analysed, from an intertidal monospecific meadow of *Zostera noltei* in Ria de Aveiro lagoon.

Morphometric data presented high spatial variability, which remained similar throughout the year, but not a remarkable temporal variation. Data from shoot density and above and belowground biomasses also showed high spatial variability, which was highly heterogenic along the year. Patterns of temporal and seasonal variation were more notorious for shoot density and aboveground biomass, and not so much for belowground biomass. Abiotic data collected was not able to describe the major variability of biotic data. The main shortcomings arise from a solely one-year sampling, which does not consider the inter-annual natural variability of the seagrass community, and limited abiotic data collected. Unlike other systems (e.g. Bertelli et al., 2017; Plus et al., 2010), there are not a long-time series datasets regarding seagrass habitats of the Ria de Aveiro lagoon.

The dataset of experimental data presents limitations and restrictions that may limit the comprehension and representability of the seagrass dynamics of the meadow under study, nevertheless, it comprises the best information available and the results showed to be consistent with those found in other works developed for comparable systems. As so, these data will be used later on in the present work for the assessment of model performance.

Chapter 4

SEAGRASS BIOLOGICAL MODEL

The present chapter comprises the conceptualisation of the seagrass biological model and the definition of the formulations adopted, in terms of state variables, forcing functions, processes, parameters and the links between them, providing a comprehensive description on how the biological model effectively works.

This chapter also comprises a preliminary model testing, aiming to verify its coherence in terms of units and links between model features, which is mandatory to check and assure a valid mass balance.

4.1 CONCEPTUALISATION OF THE BIOLOGICAL MODEL

Many of the models developed for *Z. marina* have been used as references for the development of *Z. noltei* models (e.g. Kenov et al., 2013; Plus et al., 2003). In the present work however, the formulations developed for other seagrass species were also considered, which will be timely referred and justified, whenever no parameter data was available specifically for *Z. noltei*, data on *Z. marina* was preferred.

The conceptual diagram of the model, presented in Figure 4.1, represents *Z. noltei* dynamics using two state variables: the aboveground biomass (*AB*) and belowground biomass (*BB*), both expressed in *gDW* m^{-2} units. Whereas the aboveground biomass comprises the shoots and leaves, the belowground biomass designates to the roots-rhizomes system.

The rate of change of each state variable is given by two major processes: the gross seagrass growth (*G*), which was computed for above and belowground organs, and seagrass mortality, distinct for the above (*LM*) and belowground organs (*RM*). Light[1] (*L)*, ambient temperature (*T*) and space availability (*S*) fundamentally control the gross production rate, while seagrass mortality is solely given by a temperature-depend process, resulting from the normal

[1] Throughout this work *Light* refers specifically to PAR (photosynthetic active radiation), the spectral range of solar radiation between the wavelengths of 400-700 nm, and that is mainly used by photosynthetic organisms to perform photsynthesis.

tissue senescence. The belowground growth depends on the carbon fixed by the leaves and translocated to the belowground parts.

In the scope of this work, neither nitrogen nor phosphorous were considered limiting factors, therefore nutrients were not primarily dealt with in the biological model, as a seagrass growth limiting function. This assumption is supported by both historical data on nutrient dynamics in Ria de Aveiro lagoon, that classifies it as a non-oligotrophic-like system, and by the widely reported adaptation of seagrass to overcome deficits of dissolved nutrients in the water column, using the rhizosphere apparatus to uptake these supplies from interstitial water of sediment environment.

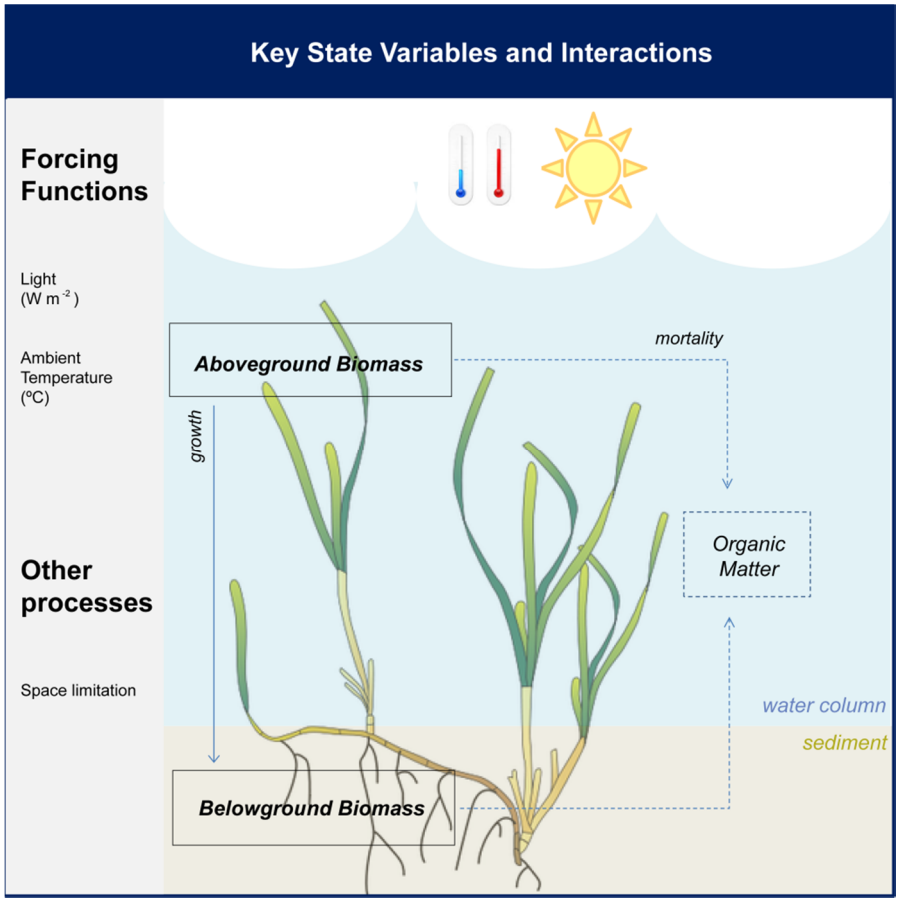

Figure 4.1 Conceptual diagram of the seagrass model. Black rectangles represent the state variables, forcing variables are illustrated at the top of the diagram) and blue arrows represent fluxes between state variables. To keep the diagram simple, a collective box for the dead organic matter was used (dashed rectangle).

4.2 BIOLOGICAL MODEL EQUATIONS

The formulation of the system of ordinary differential equations (*ODEs*) dedicated to above and belowground biomasses was preliminary numerically solved by running a licensed version of Powersim Studio (Powersim Studio 9 Express, Student License), based on the Runge-Kutta 4th-order integration method. For model forcing, typical values of water temperature and surface radiation for temperate zones have been used.

The differential equations used in this work were adapted from previous ones developed for *Zostera noltei*, where the dynamics of above and belowground organs, are expressed as:

$$\frac{dAB}{dt} = (1 - trns_{AB\_BB}) \cdot G \cdot AB - LM \cdot AB \tag{4.1}$$

and

$$\frac{dBB}{dt} = trns_{AB\_BB} \cdot G \cdot AB - RM \cdot BB \tag{4.2}$$

Where, $trns_{AB\_BB}$ is carbon translocation coefficient from aboveground to belowground organs, G is growth rate, AB is aboveground biomass, LM is aboveground mortality, RM is belowground mortality and BB is belowground biomass.

4.2.1 Growth function, *G*

The *Z. noltei* growth (*G*, day^{-1}) have been expressed as a multiplicative formulation between the maximum seagrass growth rate (g_{max}, day^{-1}) and dimensionless limiting functions, which range from 0 (i.e. total limitation) to 1 (no limitation) Eq. (4.3).

$$G = g_{\max} \cdot F(T) \cdot F(I) \cdot F(S) \tag{4.3}$$

Where, *F(T)*, *F(I)* and *F(S)* are limiting functions of ambient temperature, light and space, respectively. The maximum seagrass growth rate was set differently for above (g_{maxAB}) and belowground biomass (g_{maxBB}), following the methodology of Elkalay et al. (2003).

4.2.2 Ambient temperature limitation function, *F(T)*

The modelling of ambient temperature limitation, generally represented by bell-shaped functions, mostly depends on three parameters. They are: the ambient temperature (*T*), which in intertidal seagrass models refers to air temperature when above the current water level (emersion) and water temperature when below the current water level (immersion); optimal growth temperature (T_{opt}) and a temperature range parameter that represents the sigmoid curve width. This type of function represents a growth rate, increasing up to a temperature optimum and then decreasing for higher temperatures. When the water depth was nil, the ambient temperature addresses to air temperature.

$$F(T) = \begin{cases} K_0^{((T_{opt}-T)/T_{opt})^{stt}}, T \le T_{opt} \\ K_m^{((T-T_{opt})/(T_{\max}-T_{opt})^{stt}}, T > T_{opt} \end{cases} \quad (4.4)$$

Where, T is ambient temperature, T_{opt} is optimal temperature for seagrass growth, K_0 is function value at $T=T_0$ (considering T_0=0 ºC), K_m is function value at $T=T_{max}$ and *stt* controls the shape of the function.

In the present formulation of the ambient temperature limitation function, it has not been considered the complex process inherent to the shading mechanisms and therein variations in ambient temperature of beneath bended leaves and wet sediment.

4.2.3 Light limitation function, *F(L)*

The light limiting factor sets the relationship between ambient light and the photosynthetic rate of seagrass. In this model, the formulation adopted followed the one presented by Kenov (2014) for *Z. noltei* with a modification from Zharova et al. (2008), describing the light limiting function with a Michaelis-Menten type kinetics – Eq. (4.5).

$$F(L) = \frac{I_c}{I_c + HSL} \quad (4.5)$$

Where, I_c is light available at the top of the seagrass canopy height and HSL is half-saturation constant for light.

As the formulation of the biological model intents to simulate the intertidal dynamics of *Z. noltei*, the light limitation function should take into account alternate periods of submersion and air-exposure. As so, summarily, under submersion periods, light availability decreases as the water deepens (Figure 4.2a). At ebb tide, leaves bend closer to the water surface, and therefore light availability is expected to increase (Figure 4.2b).

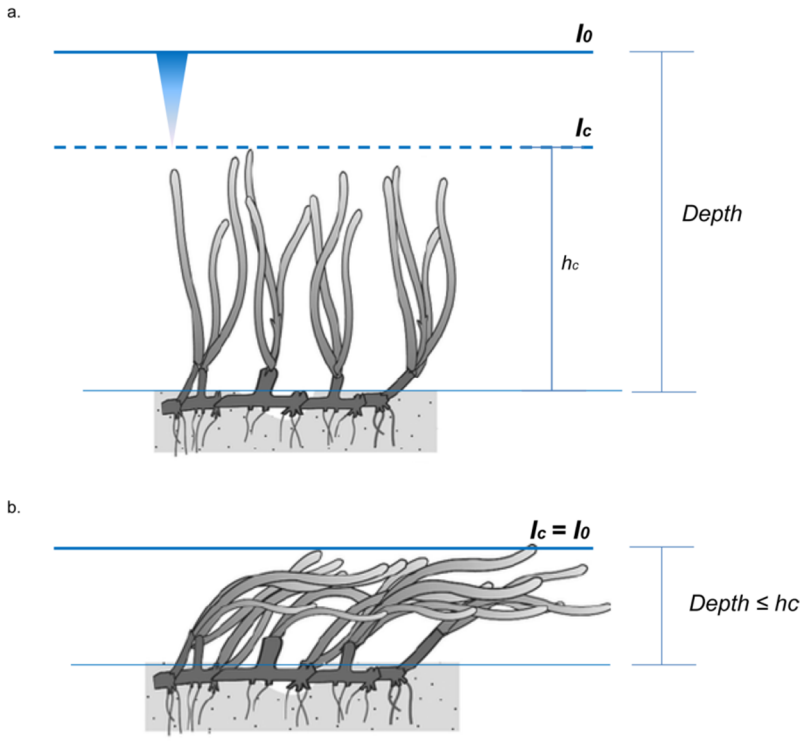

Figure 4.2 Schematic representation of light extinction with depth and light at the top of the canopy, for (a) submerged periods and (b) emerged periods, where I_c - light at the top of the canopy, I_0 - light at the water surface; h_c - height of the canopy, *Depth* - depth of the water column (Adapted from Koch et al., 2006).

The formulation used in the present model to describe the light available for seagrass growth, considered the ones used by Kenov (2014) and Zharova et al. (2008), to differentiate between the distinct light regimes of intertidal seagrass meadows, according to the height of the canopy and the depth of water column – Eq. (4.6).

$$I_c = \begin{cases} I_0 \cdot e^{(-K_{shad} \cdot Depth_{10})}, h_c < Depth \\ I_0, h_c \geq Depth \end{cases} \quad (4.6)$$

Where, I_0 is light at the sea surface, K_{shad} is light attenuation factor, h_c is height of the canopy, $Depth$ is depth of the water column and

$$Depth_{10} = \frac{Depth}{10} \tag{4.7}$$

$$K_{shad} = K_w + K_L \cdot \frac{AB}{Depth} \tag{4.8}$$

Where, K_w is extinction coefficient of water and K_L is extinction coefficient of aboveground biomass.

4.2.4 Space limitation function

Space limitation function of seagrass growth has been proposed in diverse seagrass models. All formulae present some similarities, depending on the aboveground biomass and a factor to set a threshold for maximum aboveground biomass (σ) – Eq. (4.9). In the models available in the literature, this parameter usually ranges between 297-500 gDW m^{-2}.

$$F(S) = \max\left(0{,}1 - \frac{AB}{\sigma}\right) \tag{4.9}$$

Where, σ is the maximum aboveground biomass.

In ecological models, the formulation of the space limitation function is further completed to take into account the competition for space, by including the dependence on macroalgae biomass (Kenov, 2014).

4.2.5 Above and Belowground mortality

The seagrass above and belowground decay is expressed in different ways according to different works. Several authors address it as the respiration rate exponentially increasing with the ambient temperature (Bocci et al., 1997; Elkalay et al., 2003; Zaldívar et al., 2009), while few model it as a constant rate (Aveytua-Alcázar et al., 2008) or as a function of wind speed and water temperature (Plus et al., 2003). Although the aforementioned ones take into account

the effect of water temperature in the natural senescence of seagrass, further studies express the later as a function of photoperiodicity (Kenov, 2014).

As ambient temperature is a major factor in controlling the physiological processes of organisms, including mortality, the formulation adopted in this work followed the one developed for *Z. noltei* by Plus et al. (2003). For aboveground organs,

$$LM = LMR_{20} \times f_5(T) \tag{4.10}$$

and for belowground organs,

$$RM = RMR_{20} \times f_5(T) \tag{4.11}$$

Where,

$$f_5(T) = \theta^{T-20} \tag{4.12}$$

and LMR_{20} is maximum aboveground mortality rate at 20ºC, $f_5(T)$ is mortality limitation due to ambient temperature, RMR_{20} is maximum belowground mortality rate at 20ºC, θ is mortality increasing rate with temperature.

Foreseeing the simplicity of the model, a collective box with the general designation of "*Organic matter*" (cf. Figure 4.1) comprises both above and belowground dead organic matter.

Summing up the main features of the biological model, Table 4.1 presents the major state variables, forcing functions, limiting functions of seagrass growth and parameters considered to simulate the seasonal dynamics of an intertidal seagrass. Reference values and respective units, used for the preliminary testing analysis of the model, are also comprised in Table 4.1.

Table 4.1 Synthesis of model features, listing the parameters used in the model, as well as the reference values available in the literature.

State variables

Abbreviation	Short description	Units
AB	Aboveground biomass	gDW m^{-2}
BB	Belowground biomass	gDW m^{-2}

Forcing functions

Abbreviation	Short description	Units
I_0	Light	W m^{-2}
T	Ambient temperature*	ºC

Limiting functions of *Z. noltei* growth

Abbreviation	Short description	Units
$F(T)$	Temperature limitation function	adim.
$F(L)$	Light limitation function	adim.
$F(S)$	Space limitation function	adim.

Parameters

Abbreviation	Short description	Reference value (Units)	Reference
$trns_{AB\_BB}$	Translocation of aboveground to belowground biomass	0.25 (adim.) 0.2 (adim.)	Kenov (2014); Kenov et al., (2013); Zharova et al., (2008)
$g_{\max}$	Maximum growth rate	0.23 (d^{-1}) 0.043	Kenov, (2014); Kenov et al., (2013); Philippart, (1995b)
K_0	Function value at $T = T_0$ (T_0 = 0ºC)	0.01 (adim.)	Zharova et al., (2008)
K_m	Function value at $T = T_{\max}$	0.00001 (adim.)	Zharova et al., (2008)
T_{opt}	Optimal temperature for growth	29 (ºC) 20 (ºC)	Zharova et al., (2008); Zaldívar et al., (2009)
$T_{\max}$	Maximum temperature for growth	35 (ºC)	Zharova et al., (2008)
stt	Control the shape function on $F(T)$	1.8 (adim.) 2 (adim.)	Zharova et al., (2008); Zharova et al., (2001)
HSL	Half-saturation constant for light	24 (W m^{-2})	Bocci et al., (1997); Kenov, (2014); Zaldívar et al., (2009)
K_w	Extinction coefficient of water	0.4 (m^{-1}) 1.2 (m^{-1})	Chapelle et al., (2000); Plus et al., (2003); Zaldívar et al., (2009); Zharova et al., (2008)
K_L	Extinction coefficient of leaf biomass	0.0272 (gDW^{-1} m^2)	Zharova et al., (2008)
σ	Maximum aboveground biomass	500 (gDW m^{-2}) 297(gDW m^{-2})	Elkalay et al., (2003); Kenov, (2014); Kenov et al., (2013); Zharova et al., (2008)
LMR_{20}	Maximum aboveground mortality rate at 20 ºC	0.025 (d^{-1}) 0.02-0.06 (d^{-1})	Plus et al., (2003); Philippart, (1995b)
RMR_{20}	Maximum belowground mortality rate at 20 ºC	0.025 (d^{-1})	Plus et al., (2003)
θ	Mortality increasing rate with temperature	1.1 (adim.)	Plus et al. (2003)

adim. - Dimensionless

*if submerged, T = Twater (water temperature); else, T=Tair (air temperature)

4.3 PRELIMINARY MODEL TESTING

A preliminary model testing comprised the verification of conservation of mass balances in a 0-D configuration, followed by a brief analysis to assess how the main limitation functions of seagrass vary according to changes in the specific parameters of the formulation of each one of them (1D – time).

The software used to perform these tests was Powersim Studio (PowersimStudio 10 Academic, Student License). Light and water temperature functions varied with unimodal hypothetic curves (Eqs. (4.13) and (4.14)), respectively, representative for mid-latitude of the Northern Hemisphere; Figure 4.3, dark blue and green lines, respectively) and the ordinary differential equations were solved by a 4th order Runge-Kutta integration method, with a daily timestep and for two years. The light and water temperature used to force the model were repeated as the run was biennial.

$$Light(time) = 110 \cdot \cos\left(\frac{2\pi}{365} \cdot time - \frac{2\pi \cdot 188}{365}\right) + 150 \tag{4.13}$$

$$Water\_temperature(time) = 10 \cdot \cos\left(\frac{2\pi}{365} \cdot time - \frac{2\pi \cdot 200}{365}\right) + 18 \tag{4.14}$$

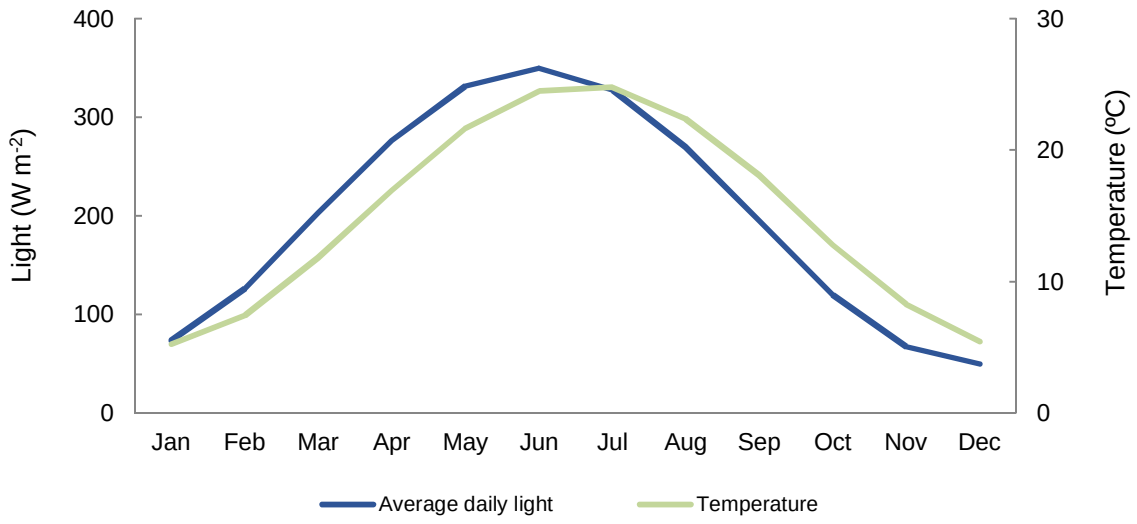

Figure 4.3 Light and water temperature used to force the model during the preliminary testing.

4.3.1 Limiting functions of growth

The ambient temperature limitation function, *F(T)* presents a unimodal pattern, as a function of the ambient temperature (Figure 4.4a). Variations of a 10-factor of the function parameter K_0, shows that an increase of K_0 turns out on lower temperature limitation for the same ambient temperature, particularly at the rising part of the curve (Figure 4.4b). Variations on K_m by the same factor show that higher values imply a less steep decrease in the limitation curve and therefore, for the same ambient temperature, an increasing of K_m turns out a lower temperature limitation for the decrescent part of the curve (Figure 4.4c).

Increasing the parameter that controls the shape of the temperature limiting function (*stt*), shows that higher *stt* values illustrate a wider range of ambient temperature with less limitation to seagrass growth, getting closer to a typical bell shape-like curve (Figure 4.4d). Changes in optimal temperature (T_{opt}) for seagrass growth express shifts at the ambient temperature that the non-limitation of seagrass growth by temperature occurs (Figure 4.4e). Increases of the maximum temperature considered for seagrass growth shows that the higher the maximum temperature values (T_{max}) are, the less is the growth limitation by ambient temperature (Figure 4.4f).

As the light limitation function, *F(L)*, follows a typical Michaelis-Menten function (saturation curve), higher values of half-constant saturation for light (*HSL*) requires less irradiance to reach the *plateau* or the carrying capacity of the system (Figure 4.5a). As expected, the light limitation function is closer to its minimum (i.e. zero) with increased depth (*Depth*) (Figure 4.5b).

For higher aboveground biomasses (*AB*), the values for the light limiting function also gets closer to zero (i.e. more limiting), representing a higher self-shading, i.e. higher interception of light due to optimal and geometrical properties of the canopy, with higher aboveground biomass (Figure 4.5c). Increasing the extinction coefficient of water (K_w) also reduces the light available for benthic environments and benthic primary producers, such as seagrass (Figure 4.5d).

The above (*LM*) and belowground mortality (*RM*) are described as exponential functions. The curves presented in Figure 4.6 are solely presented for aboveground mortality, as the literature band for maximum mortality rate at 20 ºC (LMR_{20} and RMR_{20}, for above and belowground, respectively) is similar (cf. Table 4.1). As so, the higher the maximum mortality rate at 20 ºC, the higher the above and/or belowground mortality at higher ambient temperatures (Figure 4.6a). Moreover, the base of the exponential function is the mortality increasing rate with ambient temperature (θ), which shows that slight increases of these parameter presents a notorious increase in above and/or belowground mortality, particularly at higher ambient temperatures (Figure 4.6b).

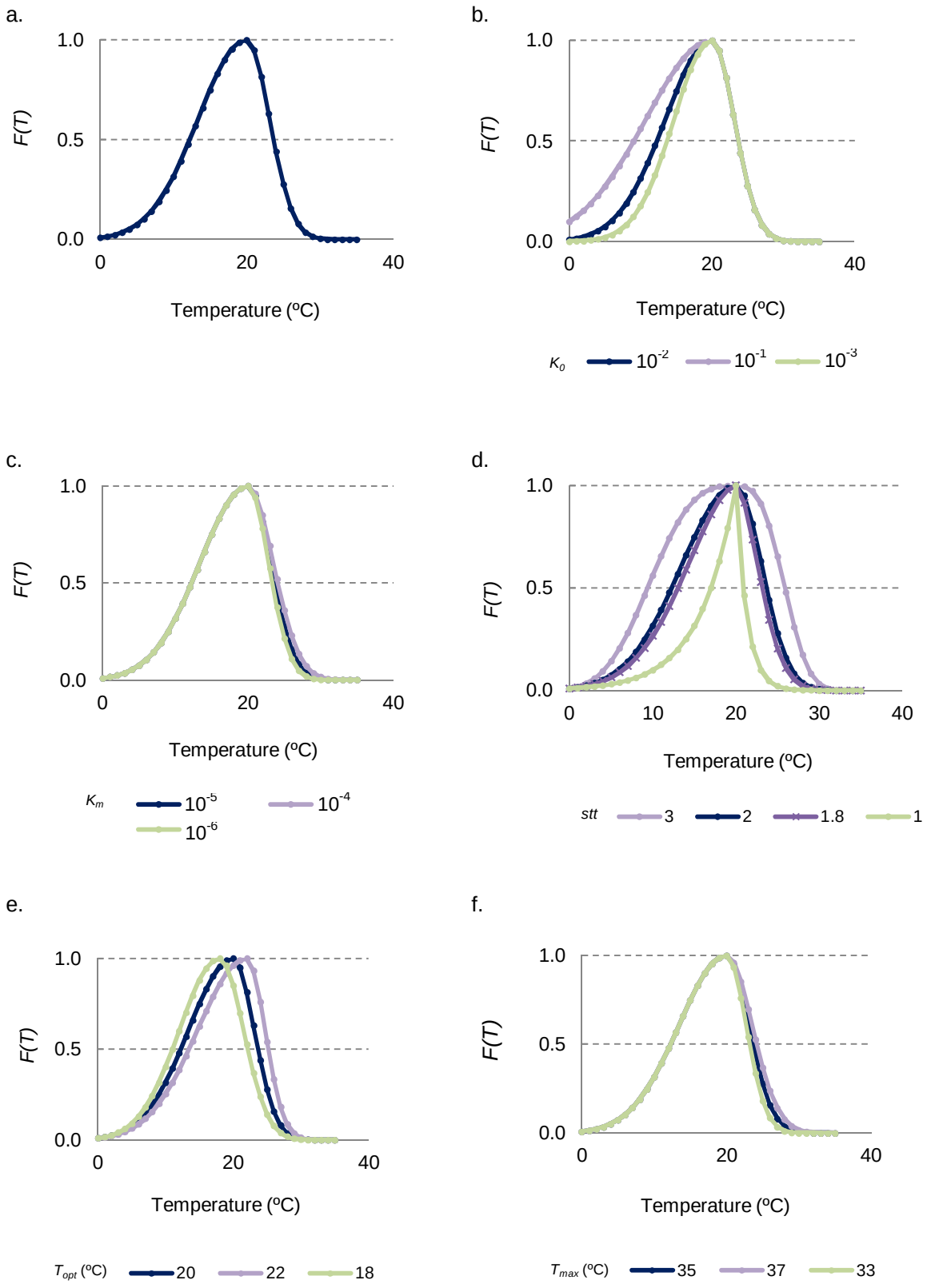

Figure 4.4 Temperature limitation function, *F(T)*, for seagrass growth according to a) the ambient temperature, and respective variations in formulation parameters of b) K_0, c) K_m, d) *stt*, e) T_{opt} and f) T_{max}.

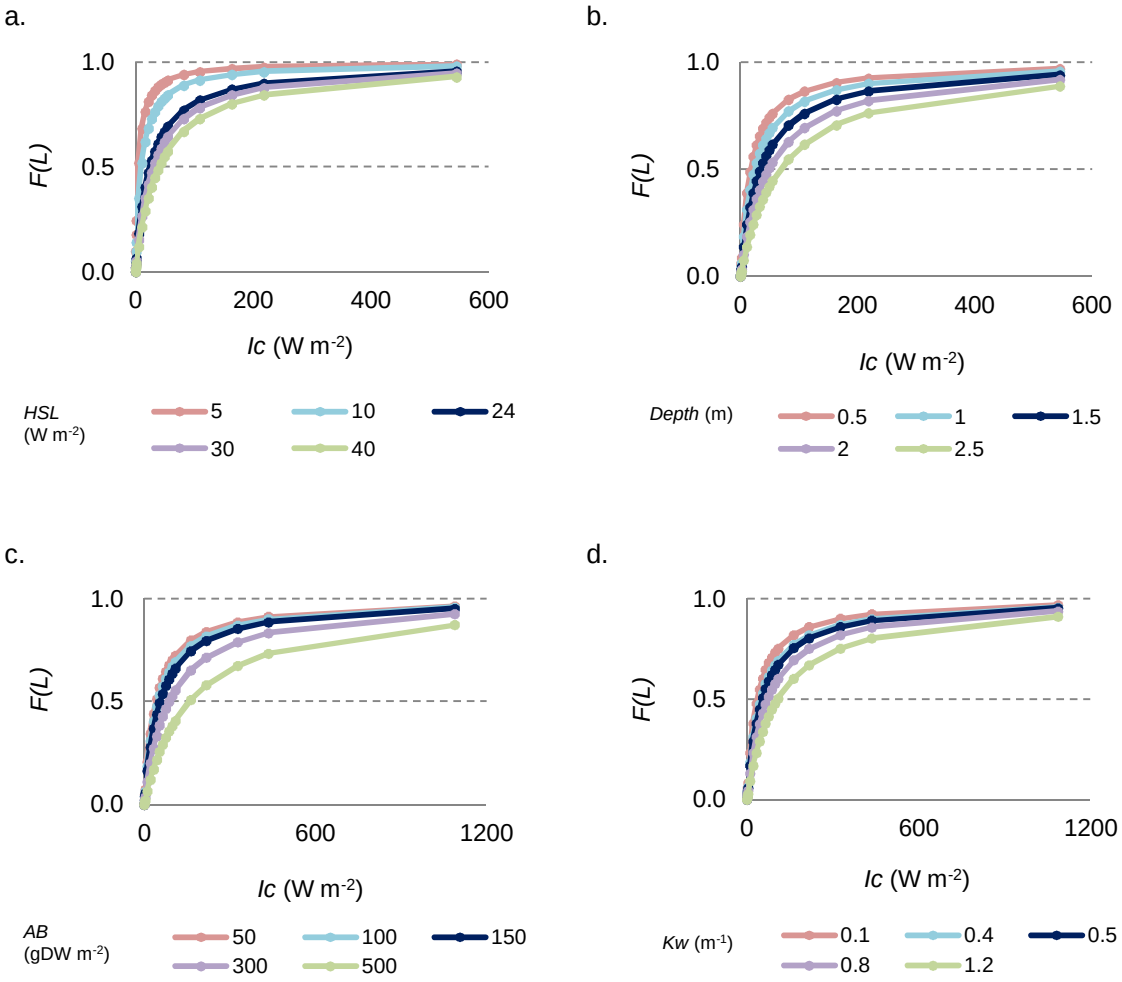

Figure 4.5 Light limitation function, *F(I)*, for seagrass growth as a function of the light on the top of the canopy, I_c, for variations in a) *HSL* and b) *Depth*, and as a function of the irradiance for variations in c) K_w and d) K_L.

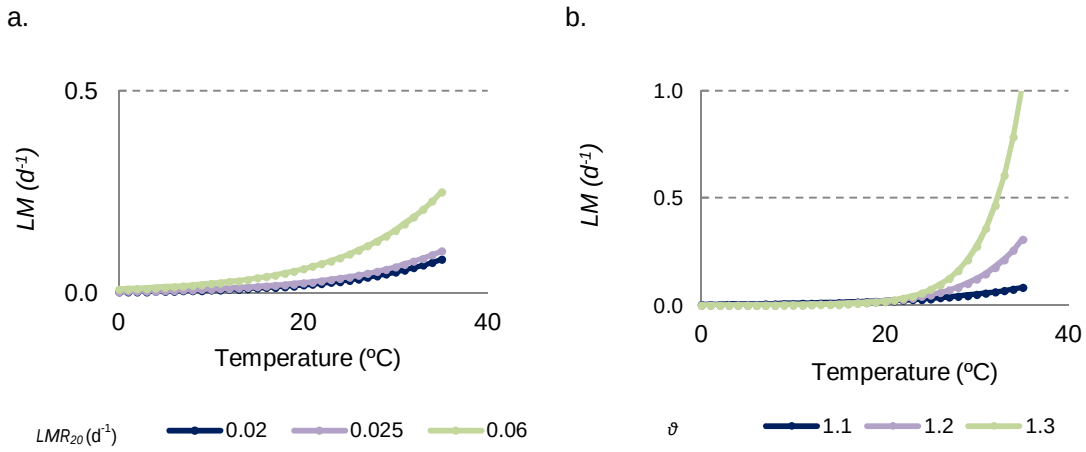

Figure 4.6 Dependence of leaf mortality (*LM*), according to variations of a) LMR_{20} and b) θ.

For the space limitation function, the formulation adopted in the present work solely depends on the aboveground biomass of seagrass. As so, the plot of the space limitation as a function of aboveground biomass shows that an increase of the carrying capacity of the system reflects a less limitation of seagrass growth by space, for the same aboveground biomass values (Figure 4.7).

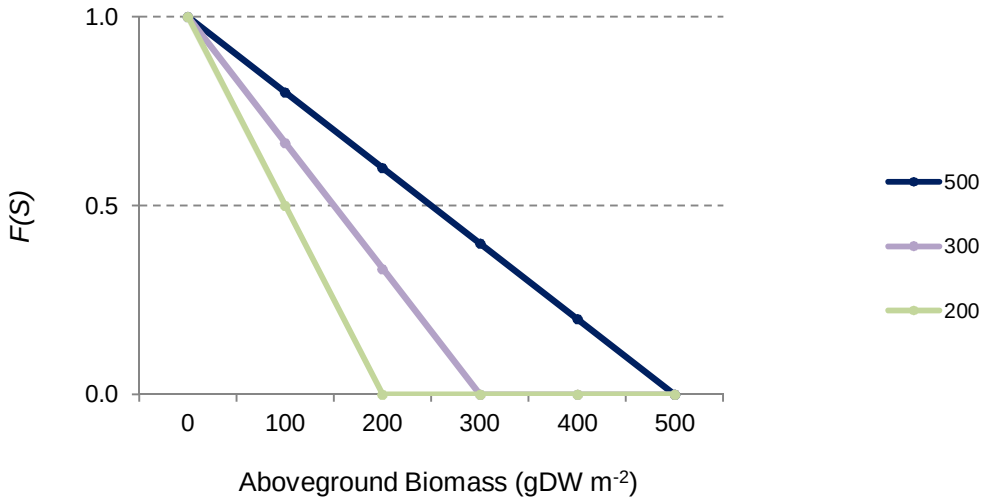

Figure 4.7 Space limitation function, *F(S)*, for different values of maximum aboveground biomass.

4.3.2 State variables

The main state variables used in this work to address seagrass seasonal dynamics were the aboveground biomass (*AB*) and the belowground biomass (*BB*).

Both preliminary results on the simulation of above (Figure 4.8a) and belowground biomasses (Figure 4.8b) followed a unimodal seasonal pattern, increasing in response to light and water temperature in spring, reaching maximum values during the summer season, and declining in autumn until the minimum reached in the winter, as light and water temperature decrease. The range of variation was higher for the aboveground biomass than for the belowground.

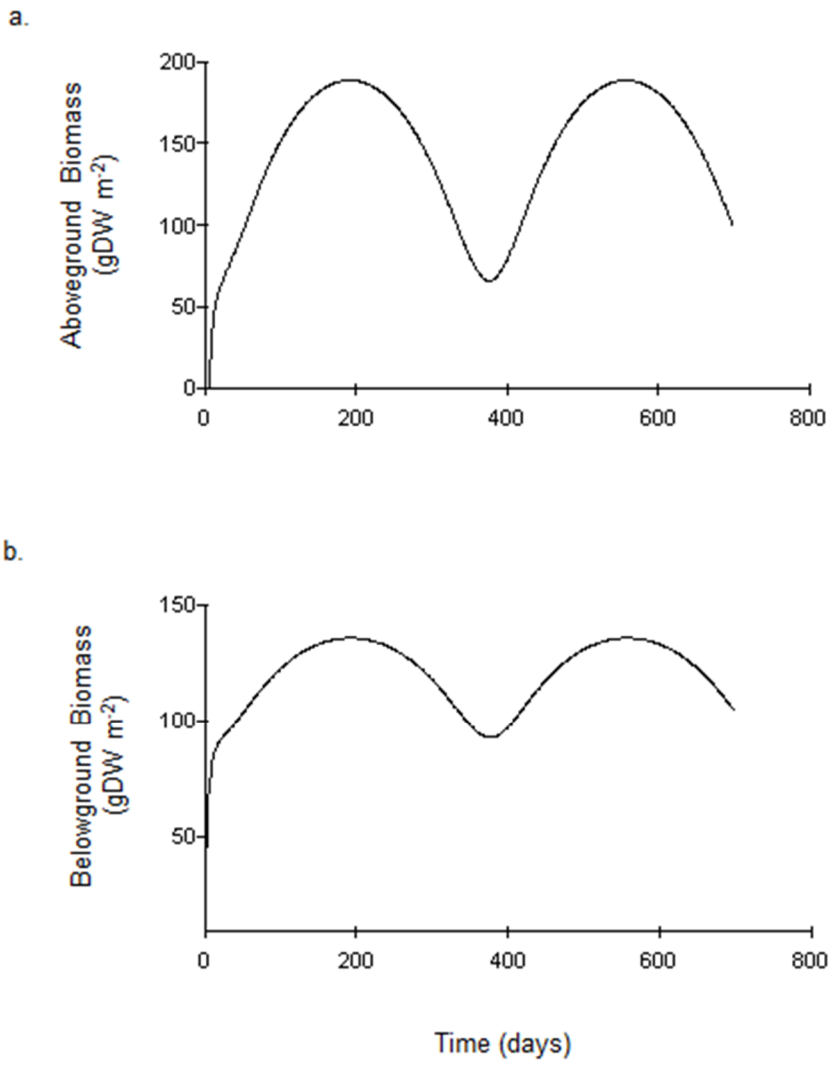

Figure 4.8 Results of the simulated a) above and b) belowground biomass, for preliminary model testing using Powersim.

4.4 DISCUSSION OF RESULTS AND CONCLUSION OF THE CHAPTER

The biological model used in the present work was built-up from previously formulations and model applications to seagrass meadows in coastal lagoons, under different forcing functions. Here, the seasonal growth of above and belowground biomass (state variables) are fundamentally controlled by the ambient temperature (*T*), light (*L)* and space availability (*S*). As this model mainly comprise the mutual processes to different seagrass species, different formulations have been considered, though the model parameters were set to those found in the literature for *Z. noltei*, whenever available.

The ambient temperature is a major factor in controlling the physiological processes of organisms, as it modulates a wide set of biological, physical and chemical rates. Moreover, since the current projections for the upcoming decades indicate an increase of the air and seawater temperatures through climate change, this factor was essential to address, particularly in intertidal seagrass that have to withstand emersion periods and physiological stresses therein, such as their tolerance survival to heat waves (Massa et al., 2009) and air-exposure effects on seagrass net photosynthesis (Pérez-Lloréns and Niell, 1993b).

Light also comprises an important requirement of seagrass growth, and one of most important ecological functions of seagrass meadows, due to the primary production driven by photosynthesis, which converts inorganic matter to readable consumable organic matter by other organisms. In fact, both in subtidal environments with favourable physical conditions or intertidal meadows with high turbidity, it is a most limiting function (Duarte, 1989). The response of seagrass growth to the light limitation presents a linear response at low light levels and a typical saturation curve above a determined photosynthetic photon flux, following a Michaelis-Menten type kinetics.

Space limitation addresses the carrying capacity of the system, as above a certain threshold the growth is no longer possible. Nevertheless, the growth of *Z. noltei* limited by space appears to be more important than light and temperature factors, when macroalgae are present (Kenov, 2014).

Although *Z. noltei* growth models also consider nutrient availability (nitrogen and phosphorous) as an important limiting function of growth (e.g. Plus et al., 2003), it was not taken into account throughout this work, as the population in Canal de Mira is not limited by nutrients. In addition, for the inclusion of nutrients, extra experimental work is required to evaluate the contribution of sediment interstitial water (high and low tide conditions) and water column (high tide condition) to the overall nutrient requests. Though in oligotrophic systems, with plenty available light, primary producers may compete for nutrients in the water column, seagrass may overcome this privation by additionally up taking nutrient supplies from the sediment (Passarge et al., 2006). Furthermore, in eutrophic systems, where nutrients are in excess, primary producers may compete for light. In spite of the moderate degree of eutrophication in Ria de Aveiro lagoon (Ferreira et al., 2003), the human contribution for this state seems to be overall low, when comparing to other Portuguese estuarine systems. As so, as historical data on nutrient dynamics in this coastal lagoon points out that this may not be the major limitation of seagrass growth, the pressure from nutrient loads is not expected to increase (Lopes et al., 2017) and seagrass meadows are adapted to alternative mechanisms of nutrient uptake by roots, neither nitrogen nor phosphorous were primarily dealt with in the biological model. This assumption has also been considered in previous works, but for other seagrass species, such as *Cymodocea nodosa* (Venice Lagoon (Italy), Zharova et al., 2008).

The unimodal patterns with maxima in summer and minima in winter obtained for the preliminary simulation of *Z. noltei* dynamics showed that the state variables (above and

belowground biomass) presented consistent patterns and overall ranges within those found in the literature, for both modelling and ground-surveyed approaches (Auby and Labourg, 1996; Cardoso et al., 2004; Pérez-Lloréns and Niell, 1993a; Pergent-Martini et al., 2005; Plus et al., 2003; Plus et al., 2001; Vermaat et al., 1993).

In this stage, the mass balance was tested and showed the consistency of the numerical formulation. Moreover, this chapter comprised the test of the boundaries of the model and checked the sensitivity of free parameters under simple conditions that allowed for a more comprehensive analysis of the results and sustained the choice of values. No preliminary calibration of the model has been carried out, as the model calibration and performance assessment through its comparison with ground-surveyed seagrass biomass data is addressed in the forthcoming Chapter 7.

Chapter 5

SEAGRASS BIOLOGICAL MODEL: DESICCATION ADD-ON

The current chapter presents the field surveyed investigation on *RWC* (relative water content) of *Z. noltei* leaves in Ria de Aveiro lagoon, considering the air exposure times and selected sediment descriptors. It also comprises the mathematical formulation of desiccation model, based on both literature revision and data analysis from the field experiment, the description and testing of the empirical desiccation model (to function according to the tide, air temperature and sediment type), and discussion of its limitations foreseeing future progress.

5.1 RATIONALE

As previously reported, most of the seagrass populations live permanently submerged due to desiccation constraints (Koch, 2001). Those able to withstand the steeper variations of environmental factors during air exposure periods comprise both temperate species of Zostera (Vermaat and Verhagen, 1996) and tropical species (Björk et al., 1999).

Wider ambient temperature ranges, solar irradiance and desiccation are therefore major limiting challenges for seagrass growth in intertidal areas. Furthermore, these stresses may be boosted under a globally changing environment (Helmuth et al., 2006), resulting in extensive impacts to seagrass species health and ecosystem functioning (Duarte, 2002). This issue is particularly important to highlight potential synergies between different sources of anthropogenic impacts, namely to seagrass populations restricted to intertidal areas and presenting a current decline status, as those of Ria de Aveiro lagoon (Azevedo et al., 2013; Cunha et al., 2013; Silva et al., 2004).

The research topic of intertidal seagrass desiccation generally comprises the effects of the relative water content of seagrass leaves ($RWC_{seagrass}$) on photosynthetic performance, as result of changes in air exposure and air temperature during emersion periods (e.g. Jiang et al., 2014; Kahn and Durako, 2009; Leuschner et al., 1998). However, as ecosystem engineers, seagrass

establish important interactions with the vicinity sedimentary compartment (Bos et al., 2007), but the role of sediment descriptors on the $RWC_{seagrass}$ has not been widely studied.

As so, the current section presents the field surveyed investigation on *RWC* of *Z. noltei* leaves, along two parallel intertidal transects in Ria de Aveiro lagoon, according to the air exposure times and sediment descriptors. These descriptors include the *RWC* of sediment ($RWC_{sediment}$), organic matter (measured as % *LOI* – loss on ignition) and grain size. Its assessment is most important to acquire missing descriptors to model the existent population, providing a deeper knowledge of inherent particularities of intertidal seagrass populations and plan suitable management actions to minimize further local loss.

The mathematical formulation of the desiccation model, based on both literature revision and data analysis from the aforementioned field experiment, defines the *RWC* as a dynamic variable, depending on hydration and desiccation of seagrass leaves. Therefore, this section also includes the description and testing of an empiric desiccation model, to function according to tide, air temperature and sediment type, and discussion of its limitations foreseeing future progress. Moreover, it then provides the first steps towards more complete formulae of current numerical dynamic seagrass models to address intertidal populations.

5.2 METHODOLOGY

5.2.1 Field survey experiment

5.2.1.1 Sampling procedure

The field survey experiment took place at a healthy intertidal seagrass meadow in Ria de Aveiro lagoon (cf. Figure 2.1), on the 13th August 2014, which corresponded to extreme spring tidal conditions and so with higher air exposure times, for the summer of 2014. The tidal range was about 3 m and the peak of the ebb tide was coincident with midday/noon.

Sampling took place simultaneously in two parallel transects, starting at high tide, then following ebbing and flooding, respectively, and finishing 12h later at high tide. The two transects were defined according to the sediment grain size and *Z. noltei* coverage. The two locations were chosen due to their similar *Z. noltei* coverage (shoots density and morphology) and proximity, meaning that both sites are exposed to similar desiccation factors, namely wind action, tidal cycle, irradiance and air temperature. Both transects took into account the Percent Cover Standards (Seagrass Watch, 2012). To be eligible for sampling, the sampling sites had a coverage of at least 65-75% according to these criteria (Figure 5.1a-b). Sampling sites were spaced by about 10 m: the one in sandy sediment was about 50 m long with 5 collection points (Transect S, cf. Figure 5.1c-d), while the one in fine sand/muddy sediment was about 80 m with

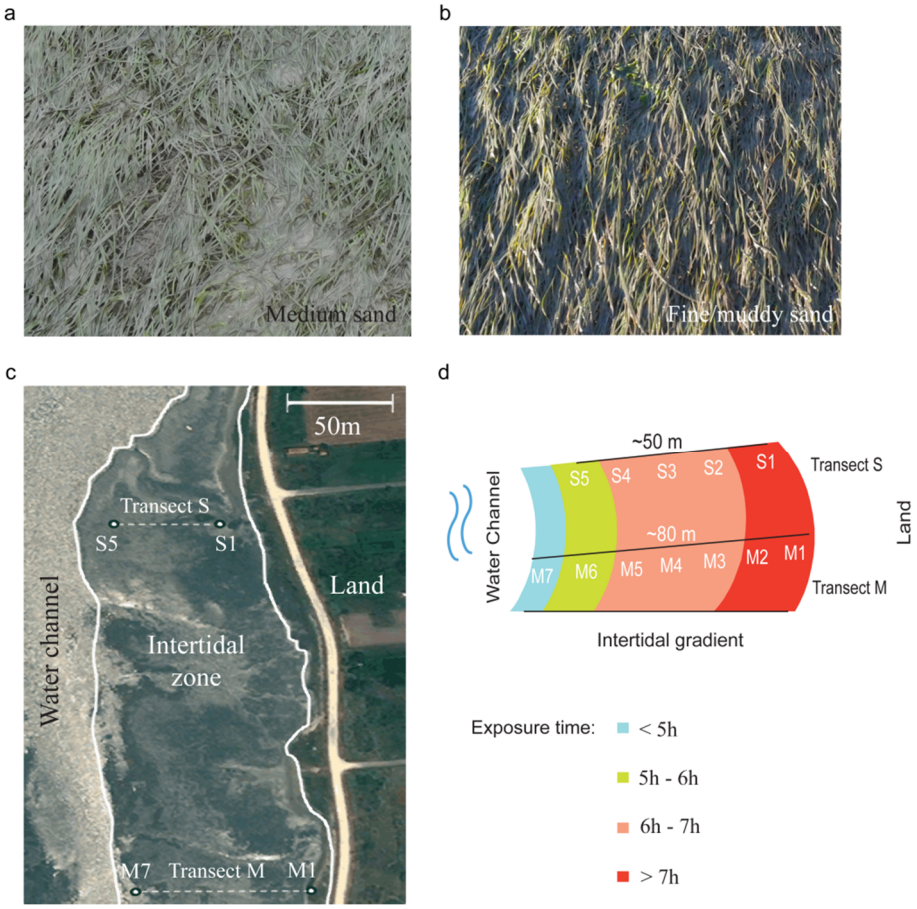

Figure 5.1 Detail of seagrass covered area in a) medium-sized sand and b) fine/muddy sandy sediments; c) Schematic representation of the defined transects (in sandy sediment - Transect S; and in fine sand/muddy sediments - Transect M) and d) air exposure periods.

7 collection sites (Transect M, cf. Figure 5.1c-d). The exposure times, as illustrated in Figure 5.1d, shows the relative position of each sampling point to the water channel and land.

The samples collected immediately after the ebb tide and right before the flood tide, comprised five seagrass shoots and two composite sediment samples from the top 5 cm per site, which corresponds to the maximum average depth of *Z. noltei* roots (Lillebø et al., 2006). This method improved spatial coverage and reduced the sediment spatial variability for the assessment of the relative water content of seagrass ($RWC_{seagrass}$), sediment ($RWC_{sediment}$) and sediment grain size.

Sediment samples, collected by hand cores, included a composite sample of 75 mL, kept in individual closed plastic containers and used to determine $RWC_{sediment}$, while another sample of circa 0.50 L was placed in a different closed plastic container to determine sediment grain size. The same sediment samples collected to study the $RWC_{sediment}$ were then used to determine the percentage of loss on ignition (%*LOI*).

During the sampling period, *Z. noltei* samples were kept individually in plastic bags sealed with a zip. All samples, plants and sediments, were reserved in the dark and with coolers. Note

that sampling started with high tide and followed ebbing, meaning that the samples that remained longer in the field in coolers were the ones expected to have been water saturated. This also means that the last samples to be collected were the ones that had been more exposed to desiccation and the ones that were processed first back in the lab. After the sampling cycle, all the collected samples were transported to the lab and immediately processed (maximum 20 min after the last sampling). In the laboratory, *Z. noltei* samples were immediately processed and sediment samples were kept in the closed plastic containers in the dark at a temperature of 4 ºC. The first samples to be processed were the *Z. noltei* samples exposed during low tide, i.e., collected during the flooding; and afterwards the ones of during the ebbing (in between, these samples were also kept at a temperature of 4ºC). The sediment processing followed the same order. The composite sample used for determining $RWC_{sediment}$ was homogenised inside the container, divided into three subsamples aliquots and immediately weighted for wet weight (3 analytical replicates from spatially composite samples).

5.2.1.2 Laboratory analysis

For seagrass samples, the above and belowground organs of each shoot were separated. The aboveground organs were gently cleaned with a soft brush to remove any possible attached sediment particles. Afterwards they were weighted (fresh weight) and dried at 60 ºC until the weight was stabilised (~48h). Then, the dry weight was determined. This last procedure was also applied to the sediment samples collected to determine the $RWC_{sediment}$.

For the remaining sediment samples, %*LOI* was determined by loss of weight on ignition at 500ºC for 6 hours and grain size fractions were obtained by sieving dried sediment following the same procedure used by Statton et al. (2013).

5.2.1.3 Data analysis

The difference between the fresh and dry weight, for both seagrass and sediment samples, was calculated and converted in the relative water content ($RWC_{seagrass}$ and $RWC_{sediment}$, respectively). Average *RWC* values for each site and respective standard deviation are presented and discussed between and within transects.

For each site, local elevation was estimated for the survey day through the analysis of a time series of sea surface elevation (*SSE*) from a nearby station. The time of emersion and immersion at each site was registered on the field survey and crossed with the *SSE* time series. The *SSE* data is referenced to the local mean sea level.

Further sediment descriptors included the total organic matter percentage and 7 grain-size fractions (>2 mm; 1-2; 0.5-1; 0.25-0.5; 0.125-0.25; 0.063-0.125; <0.063 mm). The median diameter was calculated and the sediment classified accordingly to the Wentworth scale (Wentworth, 1922).

After the preliminary analysis of raw data, the correlation between the $RWC_{seagrass}$ and the sediment descriptors was investigated, through the superimposition of each sediment descriptor to an ordination analysis of $RWC_{seagrass}$, performed with the software PRIMER v6. In order to evaluate what sediment descriptor was better in describing the pattern of the $RWC_{seagrass}$, the correlation between the matrices was calculated.

5.2.2 Desiccation model

5.2.2.1 Model description

The principle adopted to develop the desiccation module was the decline of relative water content of seagrass leaves ($RWC_{seagrass}$) at air-exposure periods during low tides. As so, the desiccation module was constructed by setting a system of stocks and flows and simulated changes on *RWC* over time. The performance of the module was assessed through a comparison between its predictions and field surveyed data.

A switch depending on the height of the local water column activates its functioning, i.e. during ebbing if the water column height is zero, an air-exposed period is detected, and the module is consequently activated. Once the height of the water column is larger than zero, the module is switched off and the hydration of the leaves occurs.

Set and calculation of *ODE*s (ordinary differential equations) system run with a licensed version of Powersim Studio (Powersim Studio 9 Express, student license), using the Euler Integration Method.

The atmosphere and seawater were the only sinks and sources of $RWC_{seagrass}$ considered. During air-exposure periods of leaves, the dehydration/desiccation process is dependent of air temperature, which controls the desiccation rate, empirically determined through testing simulations, by the best fitting of field survey data with module results for the *RWC*. This rate was set on 0.04 $(ºC\ d)^{-1}$ for the simulations of *RWC* at muddy-fine sand sediment and 0.07 $(ºC\ d)^{-1}$ for medium-sized sand sediment, due to the changes on water retention ability by different sediment types. The sensitivity analysis of desiccation parameter (*K*) for both sediment types was carried out by evaluating the effect of a ±10% variation on the model results for the *RWC* variable.

According to the results from Pérez-Lloréns et al. (1994), none of the different seagrass species considered in these authors' study had a constant rate of depletion in water content per

time of air exposure. As so, an exponential depletion of water content was preferred in this work, following the findings of Björk et al. (1999), rather than a linear constant dehydration.

As time recovery of relative water content after re-submersion was not mentioned elsewhere, hydration was set as a conditional pulse function depending on the height of the water column, assuming that it is instantaneously recovered after re-submersion. At a submersion period (water height > 0), a pulse is applied until the *RWC* reaches 100%. The diagram inherent to the conceptualization of the desiccation module is presented in Figure 5.2. It illustrates that the model considers in terms of ambient temperature ranges, light regimes and other model features, respectively during immersion and emersion periods. A synthesis of the module features is described in Table 5.1.

5.2.2.2 Simulation settings and scenarios

To test the functioning of the module, some scenarios were set for tide and air temperature. Each simulation was run with a time step of 15 minutes, during a period of 15 days to study both neap and spring tides, at a constant depth of 40 cm, since it corresponds to the average depth of upper limit of seagrass distribution in the study area. Different time steps (Δt = 1, 5, 15 and 30 minutes) were tested (results not shown) and the differences of modelled *RWC* never exceeded 2%. As so, choosing 15 minutes as time step resulted from a trade-off between simulation real-time and the desired resolution of *RWC*.

Only M_2 and S_2 tidal harmonic constituents were considered to characterize the tide since they account for more than 80% of the tidal energy at Aveiro lagoon (Dias et al., 2000). The considered phase and amplitude of these tidal harmonic constituents were those estimated by Lopes and Dias (2015) for a nearby station of the study site.

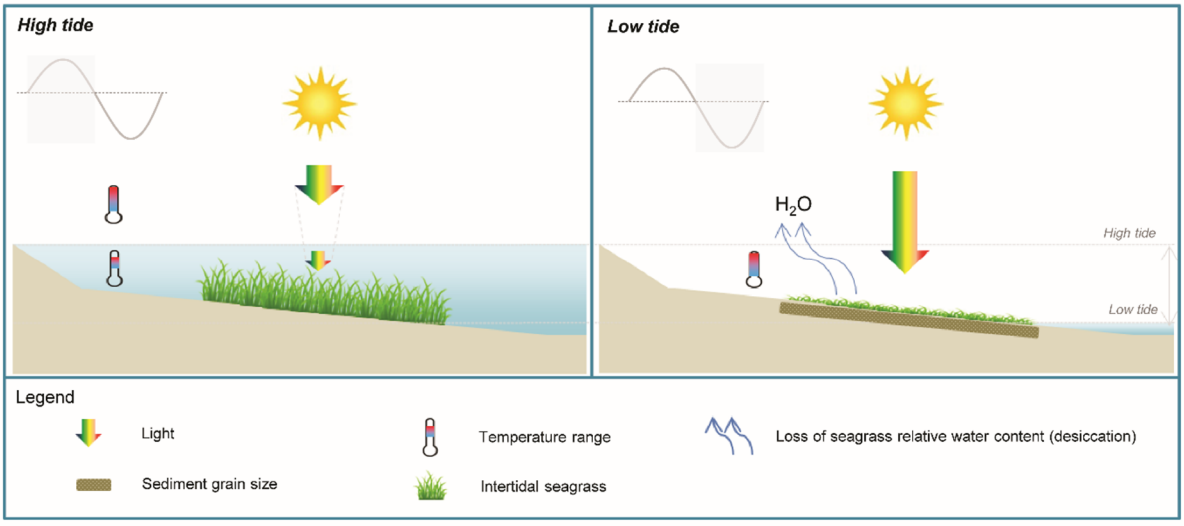

Figure 5.2 Conceptualization of the desiccation module.

Table 5.1 Features of Desiccation Model

	Features	Symbol	Equation/Value
State Variables	Relative Water Content (%)	*RWC*	$\frac{dRWC}{dt} = \begin{cases} 100, if\ WH > 0\ \wedge fully\ hydrated \\ PULSEIF(WH > 0, 100 - RWC), if\ WH > 0\ \wedge fully\ hydrated \\ RWC \times T \times K, if\ WH = 0 \end{cases}$
Forcing Functions	Air Temperature (ºC)	*T*	Described in Methodology (section 5.2.2.2)
	Sea Surface Elevation (m)	*SSE*	$SSE = A_{M_2} \times \cos\left(\frac{2\pi}{T_{M_2}} - \varphi_{M_2}\right) + A_{S_2} \times \cos\left(\frac{2\pi}{T_{S_2}} - \varphi_{S_2}\right)$
Parameters and Variables	Depth (m)	*D*	0.4
	Water Height (m)	*WH*	$WH = \begin{cases} SSE + D, if\ SSE + D > 0 \\ 0, if\ SSE + D \leq 0 \end{cases}$
	Amplitude of M_2 tidal constituent (m)	A_{M_2}	0.99
	Period of M2 tidal constituent (days)	T_{M_2}	0.5175
	Phase of M2 tidal constituent (rad)	φ_{M_2}	1.55
	Amplitude of S2 tidal constituent (m)	A_{S_2}	0.33
	Period of S2 tidal constituent (days)	T_{S_2}	0.5
	Phase of S2 tidal constituent (rad)	φ_{S_2}	2.34
	Time (days)	*t*	-
	Desiccation rate [(ºC day)$^{-1}$]	*K*	0.04, if muddy/fine sand sediments 0.07, if medium sized sand

Notes: - Phase and amplitude of tidal harmonic constituents M_2 and S_2 were estimated by Lopes and Dias (2015) for a nearby station of the study site.
- *PULSEIF* is a function of Powersim software. Summary, it gives a conditional pulse - PULSEIF (Condition, Volume) – according to a condition that determines if the pulse is going to occur (if condition is true) or not (if the condition is false). If the condition is true, a volume is pulsed until the maximum *RWC* value (i.e., 100%) is reached.

In the considered air temperature scenarios, daily maximum air temperature corresponded to the maximum recorded at the Meteorological Station of University of Aveiro for the day of field survey: 20.6 ºC. The annual maximum corresponded to the maximum air temperature registered during the whole year of 2014: 31.2 ºC. Following Massa et al. (2009), the sub-lethal air temperature considered was taken as thermal tolerance limits for natural populations of *Z. noltei* in Ria Formosa lagoon (Southern Portugal): 38 ºC. The modelled *RWC* value corresponding to this value of air temperature was designated as $RWC_{critical}$, addressing to the relative water content of leaves, below which the photosynthetic activity cannot be fully recovered.

Some well-accepted methods developed to determine the evapotranspiration of terrestrial crops were also applied, in order to assess its potential applicability on the estimation of seagrass water content loss under air exposure. The inputs required to calculate the potential evapotranspiration by Penman-Monteith method (Monteith, 1965) and Priestley-Taylor Method (Priestley and Taylor, 1972) (for formulation details please address to Appendix 4), are solar radiation, air temperature, wind speed and air relative humidity, which were recorded at the Meteorological Station of University of Aveiro for the day of field survey.

5.3 RESULTS

5.3.1 Field survey experiment

5.3.1.1 Relative water content of seagrasses ($RWC_{seagrasses}$)

The results for the relative water content of *Z. noltei* leaves ($RWC_{seagrass}$) are presented in Figure 5.3a – for the medium sandy sediments (Transect S) – and Figure 5.3b – for fine sand/mud sediments (Transect M) –, showing that no regular pattern was found between the *RWC* variation and the different intertidal heights (i.e. air exposure periods) for both transects. In Transect S, the water loss between the ebb and flooding tides ranged between 18-31%, with the lowest values being registered in the middle of the transect (medium intertidal), while the highest ones were obtained for the lower intertidal plants (cf. Figure 5.3a). For Transect M, the loss of water from seagrasses was lower, ranging from 8-16%, with minor values found in the lower-middle of the transect (medium intertidal, M5) and the highest loss being registered in the upper-middle of the transect (medium intertidal, M3) (cf. Figure 5.3b).

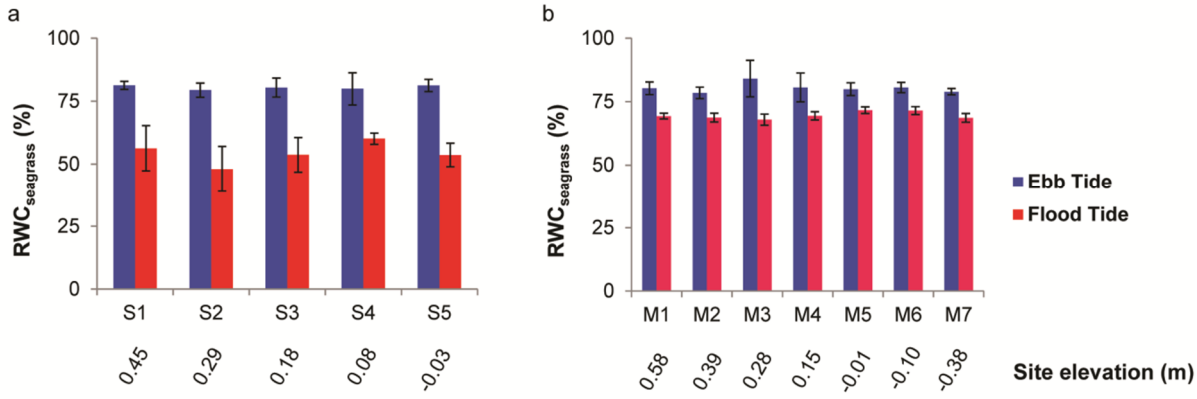

Figure 5.3 Relative Water Content for seagrasses ($RWC_{seagrass}$) during ebbing and flooding for a) Transect S and b) Transect M. Error bars (in black) corresponds to the standard deviation.

5.3.1.2 Sediment Descriptors

The sediment descriptors assessed were the relative water content of the sediment ($RWC_{sediment}$), the organic matter (%*LOI*) and the grain size.

The results of $RWC_{sediment}$ are illustrated in Figure 5.4, whereas the normalised ordination analysis for sediment descriptors is presented in Figure 5.5. The loss of $RWC_{sediment}$ between the ebbing and flooding tides was lower for Transect S, with values lower than about 2% of water content (Figure 5.4a). For Transect M, the loss of sediment water content was higher, with values between 3 and 7% (Figure 5.4b). However, the $RWC_{sediment}$ was clearly higher for the sediments of Transect M than for Transect S, which is confirmed by the normalized ordination analysis of this descriptor and where two main groups were identified: one composed by the samples of Transect S (Group A, Figure 5.5a), other composed by the samples of Transect M (Group B, Figure 5.5a), except the sites M5 and M6 (Figure 5.5b).

The normalized ordination analysis of organic matter content (%*LOI*) showed that the samples between transects are also distinct and separated into the same groups previously identified, except that site M5 has also been included in Group B (Figure 5.5b).

The grain size of sediment samples for Transect S was classified as clean medium sand (S1, S3 and S5) and silty medium sand (S2 and S4). The grain size classification for the sediment samples from Transect M was more heterogeneous. In fact, only the sediments of M6 can truly be classified as mud, presenting fine particle contents higher than 50%. Notwithstanding, the samples of the upper beach of Transect M are classified as silty (M1 and M3) and clean (M2) medium sand, the remaining samples were classified as very silty fine sand towards the lower intertidal (M4, M5 and M7). The results of the MDS (Multi-Dimensional

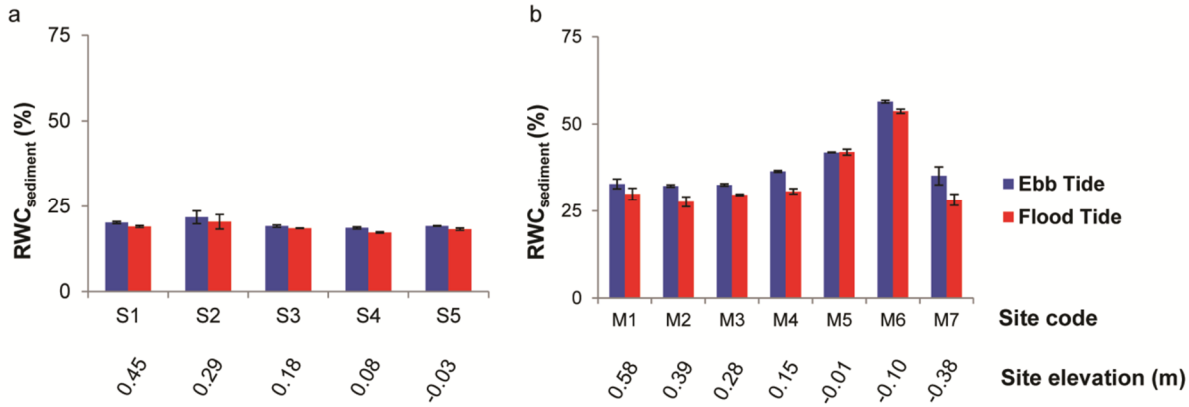

Figure 5.4 Relative Water Content for sediment ($RWC_{sediment}$) during ebbing and flooding for a) Transect S and b) Transect M.

Scaling) ordination analysis of the normalized dataset showed a clear separation between the samples of Transects S and M (Figure 5.5c).

The %*LOI* of the sediment is well correlated with the fraction of grain size <0.063 mm, the fines fraction of the sediment samples (r^2=0.8973). Sediment samples for Transect S – medium sand sediment – registered lower values of total organic matter, less than 10%, while the samples from Transect M – fine sand/mud sediment – registered higher values of fines fraction, higher than 15%, except for the site M2, presenting a lower value than the expected. This difference might be due to some spatial variability within the area, which is not immediately perceptible due to seagrass coverage. As previously mentioned, the grain size classification for Transect M sediment samples was more heterogeneous, and this is the reason why it was choose to collect composite sediment samples to follow the defined transect and to improve spatial coverage.

5.3.1.3 Integration of $RWC_{seagrasses}$ and Sedimentary Descriptors

The $RWC_{sediment}$, *TOM* and fines fraction of the sediment were overlapped to the ordination analysis of the $RWC_{seagrasses}$ to qualitatively assess the relative importance of sediment features on the $RWC_{seagrasses}$ (Figure 5.5d-f, with respective detail in g-i). All sedimentary descriptors were useful to explain the overall ordination distribution of $RWC_{seagrasses}$ data, showing a very clear separation between transects. The seagrass samples from Transect S presented higher *RWC* losses, which is associated to lower $RWC_{sediment}$ (Figure 5.5d), lower content of %*LOI* (Figure 5.5e) and lower content on fines fraction of the sediment (Figure 5.5f). The lower losses of $RWC_{seagrasses}$ were associated with sediments with higher *RWC* content (Figure 5.5d), as well

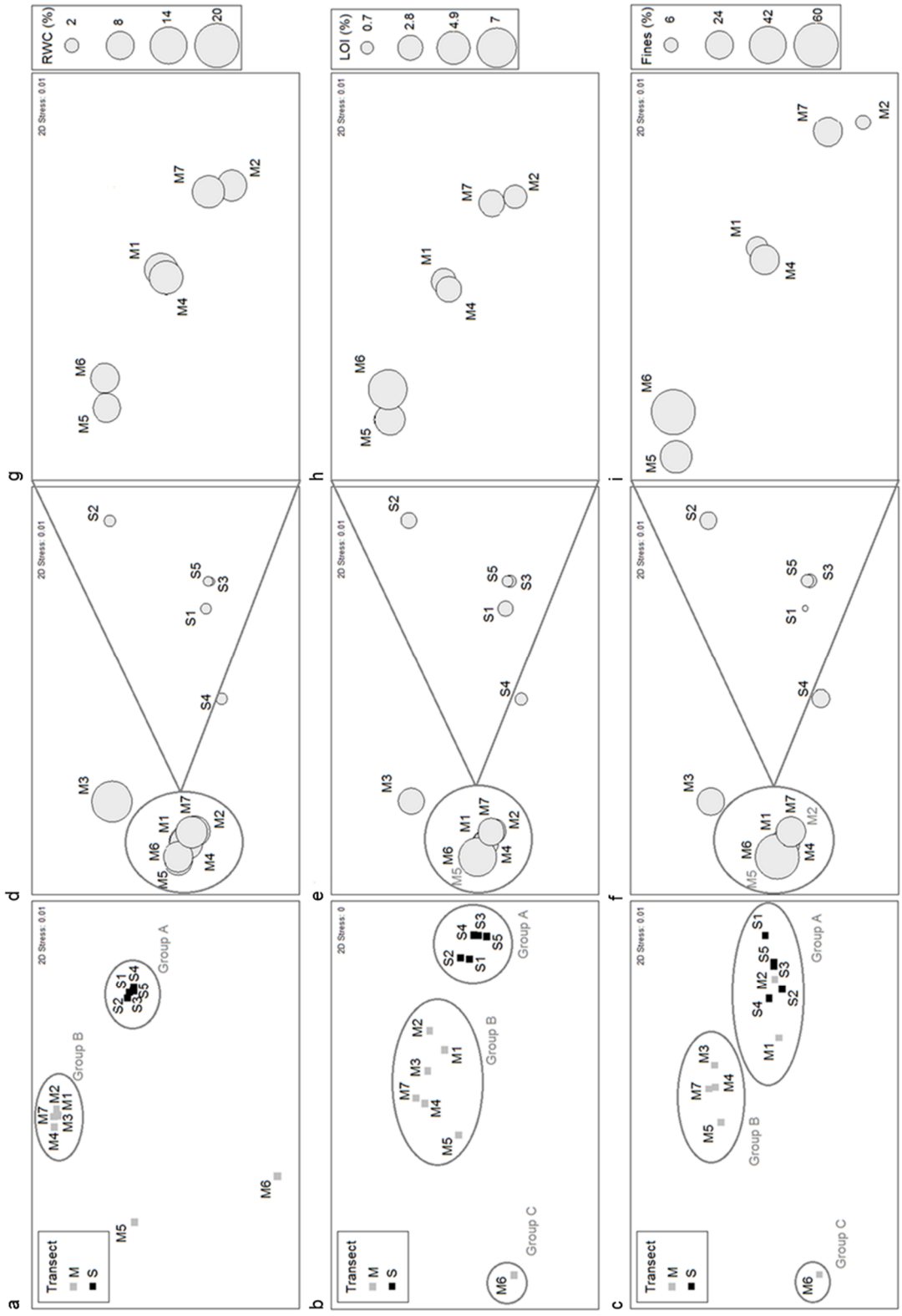

Figure 5.5 Normalized ordination analysis for sediment descriptors: a) $RWC_{sediment}$, b) Total Organic Matter (*TOM*) and c) fraction of fine sediment; and overlapping of respectively sediment descriptor to ordination analysis of $RWC_{seagrass}$ d), e), f), with detail g), h) and i).

as higher contents on %*LOI* (Figure 5.5e) and fines fraction (Figure 5.5f). No regular pattern was found for the $RWC_{seagrasses}$ within transects, which was consistent with the $RWC_{sediment}$ (Figure 5.5g), although some variability was found for the remaining descriptors: %*LOI* and fines fraction (Figure 5.5h-i, respectively).

Further analysis was performed to estimate what sediment descriptor contributes the most to explain the $RWC_{seagrasses}$. *TOM* was the best-correlated sediment descriptor (r^2=0.7594), followed by the $RWC_{sediment}$ (r^2=0.669). The fines fraction of the sediment presented the lowest correlation with the $RWC_{seagrasses}$ (r^2=0.5224).

5.3.2 Desiccation Model

The desiccation module was tested through its response to tidal cycle and air temperature for two different sediment types: muddy-fine sand and medium sand. In fact, for each simulation, the *RWC* loss of seagrass leaves varied according to the tidal cycle. In spring tides, *RWC* loss was higher when comparing to neap tides for the same air temperature and sediment type, with differences of about 4-10% of *RWC* between tides.

For the same air temperature, losses of the *RWC* in muddy-fine sand sediments were lower compared to the medium sand. Thus, for 20.6 ºC, *RWC* losses were only 11-15% for the muddy-fine sand sediments (Figure 5.6a) while for medium sand was about 19-25% (Figure 5.6d), for neap and spring tides respectively. Similar to the trend verified for the lower air temperature simulated, the intermediate value used (31.2 ºC) showed that *RWC* losses were about 17-22% for muddy-fine sand sediments (Figure 5.6b) and 28-36% for medium sand sediments (Figure 5.6e), for neap and spring tides respectively. For the annual maximum air temperature considered, the *RWC* losses were 20-27% to muddy-fine sand sediments (Figure 5.6c) and 32-42% (Figure 5.6f) to medium sand sediments.

For different air temperature scenarios, there is an average *RWC* loss of about 13 to 24% from the lower to the higher air temperature for the muddy-fine sand sediment, while for the medium sand, there is a higher average *RWC* loss between the lower and higher air temperatures, about 22 to 37%, respectively. Overall, the tests performed showed that *RWC* loss of seagrass leaves increases with air temperature. Furthermore, spring tides reflected higher air-exposure periods and consequently higher *RWC* loss of seagrass leaves than those occurring at neap tides, for both sediment types.

The simulation of *RWC* for sub-lethal air temperature estimated that $RWC_{critical}$ was about 65% (average between the *RWC* loss of both sediments types for spring tide, for 38 ºC).

The sensitivity analysis showed that the *RWC* modelling results to a variation of ±10% in desiccation parameter remained small (<1%), for both sediment types.

The hourly plant evapotranspiration using Priestley-Taylor method (1972) and Penman-Monteith method (1965) (cf. Annex 4, “Priestley-Taylor method (1972)” and “Penman-Monteith

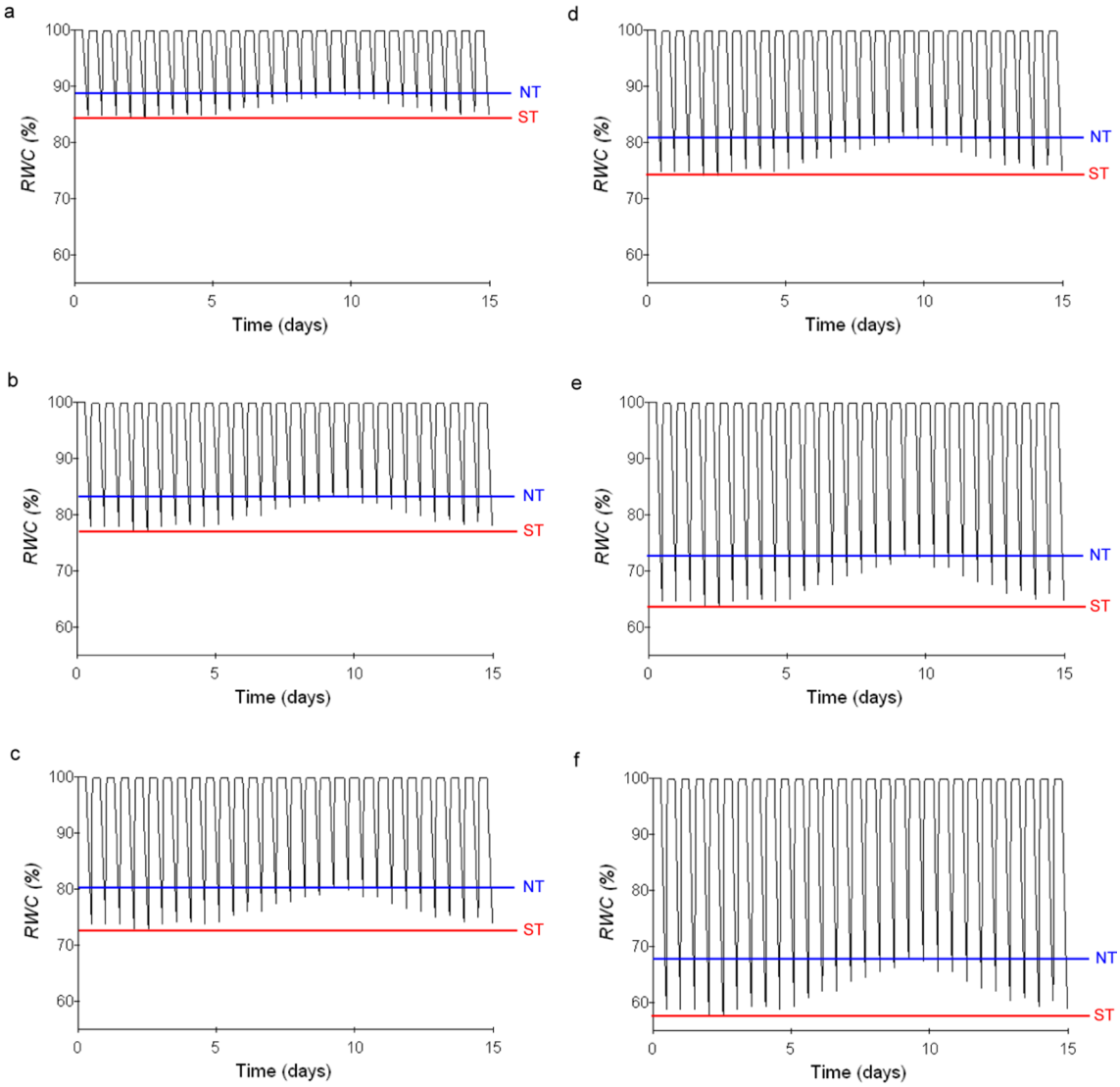

Figure 5.6 Modelled Relative Water Content (*RWC*) of seagrass leaves for different air temperature scenarios for a desiccation rate (*K*) of 0.04 and 0.07 [(ºC d)$^{-1}$] at respectively, a) and d) 20.6ºC; b) and e) 31.2ºC; and c) and f) 38ºC. The blue horizontal line marks the minimum calculated *RWC* at neap tide (*NT*) and the red one the minimum calculated *RWC* at spring tide (*ST*).

method (1965)") are presented in Figure 5.7. The results of the application of these evapotranspiration methods showed a large overestimation of field and model results.

As no clear pattern was found on *in situ* leaf water content according to intertidal height (Figure 5.8a-b), the averaged loss of water content of seagrass leaves for both sediment types was compared with the average rate of plant loss per hour for each method. The plant water loss computed with the Priestley-Taylor method was about 3 and 9 times higher than field data for medium sand sediment (0.08±0.04 mm hour^{-1}) and muddy sand sediments (0.03±0.02 mm hour^{-1}), respectively. For the Penman-Monteith method, the computed plant water loss was about 2 and 5 times higher than field data for medium sand sediment and muddy sand sediments, respectively.

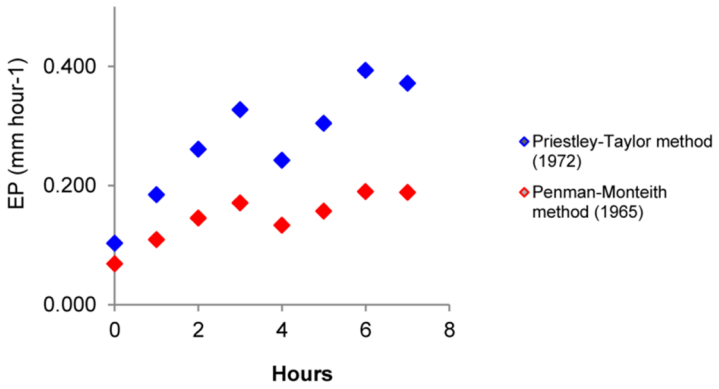

Figure 5.7 Hourly plant evapotranspiration using the methods of Priestley-Taylor (1972) and Penman-Monteith (1965).

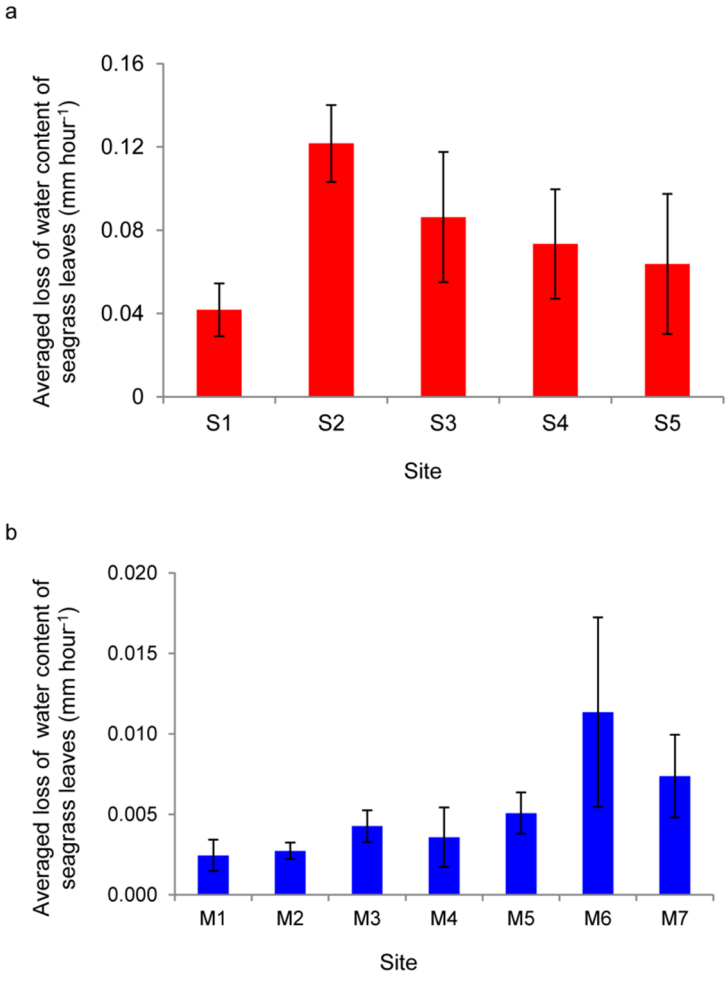

Figure 5.8 Average field surveyed leaf water content loss per hour, according to intertidal height and sediment type a) medium sand (red bars) and b) muddy fine sand (blue bars).

5.4 DISCUSSION OF RESULTS

5.4.1 Field Survey Experiment

The differences obtained for the $RWC_{seagrasses}$ between the ebbing and flooding tides were expected for each site in both transects, considering that seagrasses are exposed to a desiccating atmospheric condition, leading to *RWC* losses during the low tide periods of a tidal cycle. Thus, although desiccation tolerance has been hypothesized to explain intertidal vertical zonation in seagrasses (Koch, 2001) and the maximum irradiance and air temperature during this study coincided with the peak of the ebb tide, no regular pattern of variation was observed for $RWC_{seagrasses}$ within each transect. This result was not consistent with the findings of a work conducted by Leuschner et al. (1998) that showed that *Z. noltei* leaves lost up to 50% of its water content after 5h exposure during low tide, attesting that the degree of leaf water loss rapidly increased with the distance from the water line and thus was a function of the duration of exposure. However, the results of the present study are in agreement with other studies reported for several tropical and subtropical seagrass species, for which the variation in tolerance to desiccation did not directly correlate with its vertical distribution (Björk et al., 1999; Tanaka and Nakaoka, 2004), highlighting that the relationship between desiccation tolerance and zonation patterns of intertidal seagrasses remains unclear (Shafer et al., 2007).

The relative tolerance to desiccation relies on the high flexibility of leaves during air-exposure periods at low tides, through its deposition in a thin film of water on muddy sediments and self-shading (Azevedo et al., 2016; Björk et al., 1999). Moreover, it tolerates high light intensities comparing with congeners, showing a presumable adaptation to life upper in the shore and to turbid environments typical of intertidal mudflats (Vermaat et al., 1996).

The inability to find a trend of variation on $RWC_{seagrasses}$ across the intertidal zone in the study area, for both sediment types, suggests that the toleration and thriving of *Z. noltei* to periodic air exposure may rely on some intrinsic mechanisms of adaptation, such as the minimization of water loss. In fact, a study conducted by Björk et al. (1999) for *Halophila ovalis*, highlighted the importance of leaves' flexibility that bend down and lie flat in the sediment, protecting the underlying leaves from solar radiation and reducing the evaporation, so as to avoid water loss. Besides, further studies on seagrass features, such as different morphotypes of *Z. noltei*, characterised with longer and wider leaves at low intertidal to shorter and narrow leaves at high intertidal, showed distinct osmotic acclimations depending on its intertidal vertical distribution (Sandoval-Gil et al., 2014). Conversely, such morphological differences were not observed in *Z. noltei* leaves collected in the study area, even if the ranges of air exposure times were similar to those used in Cabaço et al. (2009) and Sandoval-Gil et al. (2014).

Regarding the sediment descriptors, $RWC_{sediment}$ was the most suitable to directly explain the $RWC_{seagrasses}$. Higher $RWC_{sediment}$ had been associated with the higher content of fine

particles and %*LOI*, which was expected since sediments with smaller grain size have reduced interstitial space and thus decreased permeability. Concerning $RWC_{seagrasses}$, it is suggested that intertidal *Z. noltei* in the study area thrives better in muddy/finer sediments than in medium sandy ones, as these types of sediment present different porosity and therefore different capability to water retention/loss. This is consistent with work conducted in Tauranga Harbour (New Zealand) with intertidal *Z. muelleri*, showing that high morphological plasticity allows it to grow efficiently under a wide range of environmental conditions and its growth is benefited by the high mud content of the sediment (Kohlmeier et al., 2014). This trend was also observed for *Z. noltei* in some Basque Country estuaries, where a higher occurrence tendency towards more fine-grained sediments was found (Valle et al., 2011). Still, contrary to the tendency observed, Folmer et al. (2012) disclosed that fine grain size in combination with the accumulation of organic matter has a negative impact on seagrass density, since it decreases pore water exchange and leads to hypoxic sediment conditions that slows down seagrass growth. Therefore, it is suggested that the threshold level of fine particles and %*LOI* is not reached in Ria de Aveiro lagoon, still providing favourable conditions for the growth of intertidal *Z. noltei*.

Although it was clear that sediment compartment performs a potentially more important role for intertidal *Z. noltei* thriving than the desiccation as result of air exposure itself, it is highlighted that other factors may be considered to assess suitable sites for intertidal seagrass prospective restoration, such as hydrodynamic exposure and water quality-related factors.

5.4.2 Desiccation model

The discussion of the desiccation model is presented in two parts: the first where the desiccation module predictions are compared with the expectations and previous works, as well as the main limitations found; the second aimed to discuss some potential guidelines for future module coupling with previously developed seagrass models.

5.4.2.1 Desiccation module and limitations

This work consisted in a preliminary approach to the development of a desiccation module for intertidal seagrasses. The patterns obtained from the desiccation module were expected, since it was found an increase of relative water content (*RWC*) loss with an increase in air temperature.

Field survey data collected for a spring tidal cycle showed a maximum *RWC* loss of about 15% for seagrass leaves in muddy-fine sand sediments and 31% for the ones in medium sized sand sediments (Azevedo et al., 2016). At the same maximum air temperature registered on the field survey day (20.6 ºC), module predictions showed that *RWC* loss was 13% and 24%, for the muddy-fine sand sediments and medium-sized sediments, respectively. Thus, the module is underestimating the *RWC* loss of seagrass leaves. Moreover, similar to seaweeds (Fernández

et al., 2015), seagrasses themselves are adapted to tolerate periodic air exposure mainly through the retention of ambient humidity and self-shading. The leaves of some species are flexible and able to bend down and lie flat in the sediment protecting underlying leaves from solar radiation and reducing the evaporation (Björk et al., 1999). Thus, together with the loss of water by seagrass leaves, also the evaporation of sediment water content should be considered as a future step in the desiccation module development. In this context, it is then suggested to include evapotranspiration in the module as future work.

As the sub-lethal air temperature for *Z. noltei* is 38º C (Massa et al., 2009), the $RWC_{critical}$ estimated in this work for this conditions was about 35%, i.e. a loss of leaf relative water content of 35% may already reflect a noticeable decreasing of photosynthetic performance, which over extended periods condition its full recovery and therefore plant thriving and survival. This result is consistent with the findings of Björk et al. (1999) for intertidal seagrass species *Halophila ovalis* and *Halodule wrightii*, for which, at a relative water content loss of ~30%, there is a decrease of electron quantum yields of photosystem II of about 87% and 69%, respectively, compared with fully hydrated leaves. These authors also showed that this loss of photosynthetic performance showed no recovery at least during the next twenty minutes after re-submersion. Moreover, for some intertidal macroalgae species, a study conducted by Beer and Eshel (1983) for different *Fucus* species showed that photosynthesis decreased about 50% upon halved initial water content, while for green macroalgae *Ulva* sp., Sven and Eshel (1983) showed a disruption of photosynthesis under a water loss of 35%.

Despite the model delivering expected results and the inclusion of the main drivers of the desiccation process, some limitations remain. First, the wind is recognised to have a strong effect on the desiccation of intertidal species, for both algae and seagrass. However, due to the lack of data available on the relationship between wind and desiccation of emerged seagrass leaves, it was impossible so far to include this complex forcing in the presented formulation. As for air temperature an empirical formulation was used, the same rationale for wind speed would significantly increase the model complexity and thus was not performed to keep a simple approach. In this context, and due to the documented importance of wind in desiccation of several types of intertidal organisms (Coelho et al., 2009; Gao et al., 1998; Lamote et al., 2012), further improvements to the module should be performed taking this into consideration. Moreover, considering the morphological differences between seagrasses and terrestrial vegetation, the estimation of a crop coefficient specific for seagrasses may be useful in the determination of seagrass meadow evapotranspiration, though requiring further adjustments to estimate the potential evapotranspiration calculated through the Penman-Monteith (Monteith, 1965) and Priestley-Taylor (Priestley and Taylor, 1972) methods. In fact, although other authors also used and compared these evapotranspiration models for intertidal mangrove forests (Edebeatu, 2015), the straightforward application of both evapotranspiration models failed to represent seagrass water content loss under air exposure (cf. Figure 5.7 and Figure 5.8).

Furthermore, the current work was developed only from the point of view of a temperate climate condition and mesotidal and semi-diurnal tides. However, intertidal seagrasses are

distributed in areas characterized by different air and water temperatures and tidal regimes (Björk et al., 1999; Collier and Waycott, 2014). Thus, a more complete assessment of the performance of the model should consider wider sets of air temperature, light and tidal scenarios in order to generalise its applicability.

Future work will include its integration with the biological modelling, which in its turn will be coupled with a water quality model. With this, it is expectable to get the “big picture” and provide reliable ideas and suggestions to the management of local areas, as well as an integrated approach with meteorological, hydrodynamic and water quality forcing.

5.4.2.2 Recommendations for module coupling with previously developed seagrass models

Due to the widespread inclusion of photosynthesis in seagrass models, a suggestion to prepare the desiccation module for coupling is through effective quantum yield of photosystem II (*Y*), which is widely used as a proxy to estimate the fluorescence of Chl-*a* (Silva et al., 2005a).

As previously reported, Massa et al. (2009) pointed out that both maximum quantum yield of photosystem II and survival of *Z. noltei* are dependent on the air temperature during the exposure periods. An increase of irradiance levels (*I*), that seagrass leaves may experiment at air-exposure periods, results in an increase of the electron transfer rate (*ETR*) (Silva et al., 2005a), through the relation expressed in Eq.(5.1) (Schreiber et al., 1995).

$$ETR = Y \times I \times Absorption\ factor \times 0.5 \tag{5.1}$$

The absorption factor for *Z. noltei* was set at 0.79 by Silva and Santos (2003).

However, photosynthetic rates and thus the ability of electron transfer in the leaves may be dependent on the *RWC* of the leaves. As reported by Leuschner et al. (1998) for intertidal *Z. marina* and *Z. noltei*, as long as leaf water contents are favourable, elevated photosynthetic rates are supported by both high irradiance and a readily available carbon source due to the rapid diffusion of CO_2 in the air. Therefore, the principle of coupling suggested in this work is that if *RWC* of seagrass leaves decreases and reaches a critical value ($RWC_{critical}$), then the photosynthetic activity should decrease at a rate depending on the increment of air temperature. This threshold would be reached at sub-lethal air temperatures, with a faster and steeper decrease of photosynthetic activity comparing with lower air temperatures.

Moreover, experimental data for both temperate (Massa et al., 2009) and tropical seagrass species (Collier and Waycott, 2014) showed a time lag between high air temperature (i.e. above sub-lethal temperature) exposure and mortality and between high air temperature exposure and effects on photosynthetic performance. As so, this time lag should also be taken into account in the future improvements of seagrass desiccation model formulae.

5.5 CONCLUSIONS

Seagrasses are key components of coastal ecosystems that mainly live in subtidal environments. Some species, however, may withstand periodic air exposure periods and highly variable abiotic factors, expanding their presence to intertidal areas.

In this section, the study of desiccation dynamics suggested that relative importance of sediment characteristic is more effective in conditioning the *RWC* of seagrasses over a tidal cycle than air exposure time. Seagrass leaves of colonised finer grain size sediments presented less relative water loss, suggesting a more suitable habitat for *Z. noltei* establishment.

The sediment compartment integrated the conceptualisation and formulation of desiccation model development, besides tidal cycle and air temperature. The model results simulate higher losses of *RWC* of seagrasses at high air temperatures and spring low tides in medium sized sand sediments, following the field-surveyed data patterns and expected results.

Coupling of desiccation and water quality models, performed throughout this study, opens potential improvements of the model, in both description and parameterization of processes, as future research perspectives. The adaptation of evapotranspiration estimations to seagrasses during air exposure periods, further study of wind effect on desiccation and the prospection to a wider application to other seagrass populations are additional guidelines to model improvement.

Chapter 6

NUMERICAL MODEL DELFT3D

This chapter presents a brief description of the numerical model suite (Delft3D) used therein, and particularly focus on the modules widely explored in the scope of this study: Delft3D-FLOW (hydrodynamic module) and Delft3D-WAQ (water quality module). The basic conceptual and numerical aspects of the model are also presented, as well as their main features that contributed to select this model suite to conduct this work.

6.1 INTRODUCTION

Delft3D is a fully integrated computer software suite for a multi-disciplinary approach, carrying out simulations of flows, sediment transports, waves, water quality, morphological developments and ecology, for coastal, river and estuarine areas. These different sets of applications, comprised in specific modules, are grouped around a mutual dynamic and interactive interface (GUI – Graphical User Interface). The modules widely used in this work were Delft3D-FLOW and Delft3D-WAQ.

Delft3D-FLOW is a multi-dimensional (2D or 3D) hydrodynamic simulation program, which calculates non-steady flow and transport phenomena that result from tidal and meteorological forcing on a rectilinear or a curvilinear fitted grid. Besides the standard features of numerical models for coastal and estuarine areas, it has the advantage of providing a robust simulation of drying and flooding of intertidal flats and domain decomposition for the optimisation of computational resources (Deltares, 2014b).

Delft3D-WAQ is the water quality module of Delft3D software. Analogous to other models for the same purpose, it computes the mass balance of selected substances (i.e. state variables), for each computational cell, assuring the mass conservation principle (Deltares, 2017). It considers mass-driven transport by advection and dispersion, as the last is derived from Delft3D-FLOW hydrodynamic model. Delft3D-WAQ is highly versatile, presenting the complex possibility to extend the substances and processes within the Open Process Library Tool (PLCT), but also a user-friendly interface, especially suitable for non-expert users (Deltares,

2014b). In the scope of this work, other modules of the Delft3D suite have been used, such as RGFGRID, for grid generation, QUICKIN for preparing and manipulating grid-oriented data (e.g. bathymetry and initial conditions), and QUICKPLOT, for auxiliary visualisation and animation of simulation results. As these modules have only been used punctually, for further information, please address to Delft3D Open Source Community (URL: oss.deltares.nl/web/delft3d).

6.2 HYDRODYNAMIC MODEL: DELFT3D-FLOW

The Ria de Aveiro model set-up is based on Delft3D-FLOW software suite (license Deltares – Delft Hydraulics, The Netherlands). This hydrodynamic model simulates two-dimensional (depth-averaged) or three dimensional (3D) unsteady flow and transport resulting from meteorological and tidal forcing, including the density distribution from non-uniform water temperature and salinity (density-driven flow) (Deltares, 2014b).

6.2.1 Numerical scheme

Regarding the physical processes, the system of equations consists of horizontal equations of motion, the continuity equation, and the transport equations for conservative constituents, formulated in orthogonal curvilinear or spherical co-ordinates (Deltares, 2014b).

The numerical method used by Delft3D-FLOW to solve the abovementioned equations is based on finite differences. As so, to solve partial differential equations, these are transformed from physical to the computational space (discretisation).

In the present application, the variables are therefore rearranged on a particular staggered grid, so-called Arakawa C-grid. Water level points (pressure points) are defined in the centre of a (continuity) cell, surrounded by four grid points, and the velocity components are perpendicular to the grid cell faces (Figure 6.1).

For shallow water solvers, the use of this staggered grid prevents spatial oscillations in the water levels (Deltares, 2014b).

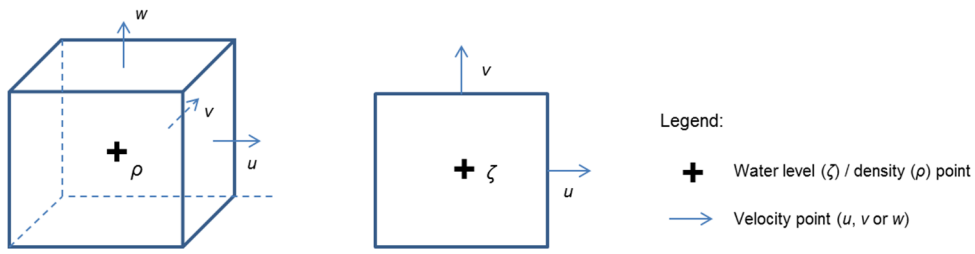

Figure 6.1 Representation of the numerical grid scheme, illustrating the points of calculation of different properties (Ribeiro, 2015).

In the vertical direction, a σ-grid was used, which follows the bottom topography and the free surface. As the σ-grid is boundary fitted to both bottom and moving free surface, a smooth representation of the topography is obtained.

An ADI (Alternating Direction Implicit) time integration method is used to solve the system of equations and it is based on the division of the time step in two, which consist of half time steps. Spatial discretization of the horizontal advection terms uses a dissipative reduced phase error scheme (Cyclic method).

6.2.2 Governing equations

The computation of physical phenomena in Delft3D-FLOW is based on several mathematical formulations. The depth-averaged continuity equation is a numerical statement of the conservation of mass, given by Eq. (6.1):

$$\frac{\partial \zeta}{\partial t} + \frac{1}{\sqrt{G_{\xi\xi}}\sqrt{G_{\eta\eta}}}\frac{\partial\left[(d+\zeta)U\sqrt{G_{\eta\eta}}\right]}{\partial \xi} + \frac{1}{\sqrt{G_{\xi\xi}}\sqrt{G_{\eta\eta}}}\frac{\partial\left[(d+\zeta)V\sqrt{G_{\eta\eta}}\right]}{\partial \eta} = Q \tag{6.1}$$

and the horizontal momentum equations in the x (Eq. (6.2)) and y (Eq. (6.3)) directions are defined as:

$$\frac{\partial u}{\partial t} + \frac{u}{\sqrt{G_{\xi\xi}}}\frac{\partial u}{\partial \xi} + \frac{v}{\sqrt{G_{\eta\eta}}}\frac{\partial u}{\partial \eta} + \frac{w}{d+\zeta}\frac{\partial u}{\partial \sigma} - \frac{v^2}{\sqrt{G_{\xi\xi}}\sqrt{G_{\eta\eta}}}\frac{\partial \sqrt{G_{\eta\eta}}}{\partial \xi} + \frac{uv}{\sqrt{G_{\xi\xi}}\sqrt{G_{\eta\eta}}}\frac{\partial \sqrt{G_{\xi\xi}}}{\partial \eta} - fv =$$
$$= -\frac{1}{\rho_0\sqrt{G_{\xi\xi}}}P_\xi + F_\xi + \frac{1}{(d+\zeta)^2}\frac{\partial}{\partial \sigma}\left(\nu_v\frac{\partial u}{\partial \sigma}\right) + M_\xi \tag{6.2}$$

And

$$\frac{\partial v}{\partial t} + \frac{u}{\sqrt{G_{\xi\xi}}}\frac{\partial v}{\partial \xi} + \frac{v}{\sqrt{G_{\eta\eta}}}\frac{\partial v}{\partial \eta} + \frac{w}{d+\zeta}\frac{\partial v}{\partial \sigma} - \frac{uv}{\sqrt{G_{\xi\xi}}\sqrt{G_{\eta\eta}}}\frac{\partial \sqrt{G_{\eta\eta}}}{\partial \xi} + \frac{u^2}{\sqrt{G_{\xi\xi}}\sqrt{G_{\eta\eta}}}\frac{\partial \sqrt{G_{\xi\xi}}}{\partial \eta} + fu =$$
$$= -\frac{1}{\rho_0\sqrt{G_{\eta\eta}}}P_\eta + F_\eta + \frac{1}{(d+\zeta)^2}\frac{\partial}{\partial \sigma}\left(\nu_v\frac{\partial v}{\partial \sigma}\right) + M_\eta \tag{6.3}$$

Where ζ is the free-surface water elevation; *t* is the time; $\sqrt{G_{\xi\xi}}$and $\sqrt{G_{\eta\eta}}$ are the coefficients used to transform curvilinear to rectangular co-ordinates; *d* is water depth; *U* and *V* are the depth-averaged velocities; *u*, *v* and *w* are the velocities in ξ, η and σ directions, respectively; *Q* is discharge per unit area; *f* is the Coriolis parameter, ρ_0 is the reference density of water; P_ξ and P_η are the gradient hydrostatic pressure; F_ξ and F_η represent the unbalance of horizontal Reynolds' stresses; M_ξ and M_η represent the contributions due to external sources of sinks of momentum.

Under the shallow water assumption, the vertical momentum equation is reduced to a hydrostatic pressure equation - Eq.(6.4) -, not considering vertical accelerations due to buoyancy effects and sudden variations in bottom topography.

$$\frac{\partial P}{\partial \sigma} = -g\rho H \tag{6.4}$$

After integration, the hydrostatic pressure is given by Eq.(6.5):

$$P = P_{atm} + gH\int_{\sigma}^{0}\rho(\xi,\eta,\sigma',t)d\sigma' \tag{6.5}$$

Where, $H$is the total water depth, given by $H = d + \zeta$; and $P_{atm}$is the atmospheric pressure. The formulations for the computation of the pressure gradient vary according to a constant density or a non-uniform density.

6.2.3 Drying and flooding criteria

The ability of Delft3D-FLOW model for robustly simulate drying and flooding succession of intertidal flats is already reported for Ria de Aveiro lagoon (Pinheiro, 2017). To evaluate if a grid cell is flooded or dried, a set of model input parameters, namely *threshold depth* should be carefully chosen, which is calculated by Eq. (6.6) (Deltares, 2014b), with *δ* as the threshold depth, *a* the characteristic amplitude and *N* the number of time steps per tidal period. Considering a maximum tidal amplitude of 2 m and a time step of 0.50 minutes (*N*=1440), the threshold should be higher than 0.009 m to avoid water depth becoming negative in just one time step.

$$\delta \geq \frac{2\pi|a|}{N} \tag{6.6}$$

The threshold depth assumed in this work was 0.10 m, therefore for water depths higher than this value the grid cell is wet, while if the water depth is lower than half of the threshold depth the grid cell is dry.

6.2.4 Heat flux

The selected heat flux model was the *Heat flux model 2*, as successfully used in previous works of numerical modelling for other Portuguese estuarine systems, using Delft3D-FLOW (Ribeiro, 2015). This heat model combines net solar (short-wave) and net atmospheric (long-wave) radiation. The terms related to heat losses due to evaporation, back radiation and convection are computed by the model (Deltares, 2014b).

6.3 ECOLOGICAL MODEL: DELFT3D-WAQ

6.3.1 Conceptual description

Similar to other water quality numerical models, the water quality module of Delft3D model (Delft3D-WAQ) computes the mass balance of selected substances (i.e. state variables), for each computational cell, assuring the mass conservation principle (Deltares, 2017). In fact, the mass transported by water flow from one cell to the next result in a negative and a positive term in the mass balance of respective first and second computational cells. Through the combination of computational cells in 1D, 2D or 3D, the substances can be transported throughout them and represent the overall water system. Changes in mass driven by transport include both advective and dispersive transport. The first reports to single transport by flowing water, which in the present setup is derived from Delft3D-FLOW hydrodynamic model, while the last is due to the transport resulting from a concentration gradient.

Within a computational cell, one substance may also undergo certain processes and be converted into other substances. Changes in mass driven by processes include physical processes, such as the rearation, as well as (bio) chemical (e.g. nitrification) and biological processes (e.g. primary production).

Moreover, mass originated from outside the modelled system may be added to a computational cell, through located sources (e.g. river discharges). Changes driven by sources include the addition of mass from water loads and the extraction of mass by intakes.

Considering these major mass-changing drivers, to proceed in one time step, Delft3D-WAQ solves Eq. (6.7) for each computational cell and for each state variable, which is a simplified representation of the advection-diffusion-reaction equation.

$$M_i^{t+\Delta t} = M_i^t + \Delta t \times \left(\frac{\Delta M}{\Delta t}\right)_{Tr} + \Delta t \times \left(\frac{\Delta M}{\Delta t}\right)_{P} + \Delta t \times \left(\frac{\Delta M}{\Delta t}\right)_{S} \quad (6.7)$$

Where, M_i^t is mass at the beginning of a time step, $M_i^{t+\Delta t}$ is mass at the end of a time step, $\left(\frac{\Delta M}{\Delta t}\right)_{Tr}$ is due to changes by transport, $\left(\frac{\Delta M}{\Delta t}\right)_{P}$ changes by physical, (bio)chemical or biological processes and $\left(\frac{\Delta M}{\Delta t}\right)_{S}$ changes by sources (e.g. waste loads, river discharges).

Therefore, running the water quality using Delft3D-WAQ model requires a previous run of hydrodynamic (Delft3D-FLOW) simulation and make it suitable for application in the water quality simulation in hand. Afterwards, this outcome and the creation or selection of substances and water quality processes (Open Processes Library Tool – PLCT) comprise the scenario of water quality simulation (Water Quality input), including the definition of initial conditions, boundary conditions, waste loads, simulation time and the output variables. The simulation is then run (DELWAQ), following the workflow summarised in Figure 6.2.

Delft3D-WAQ deal with the composition of water, but its features go far beyond the *stricto sensu*, including also the modelling of biological components up to the level of primary producers and consumption by grazers, as well as the composition of sediment in water quality modelling (Figure 6.3).

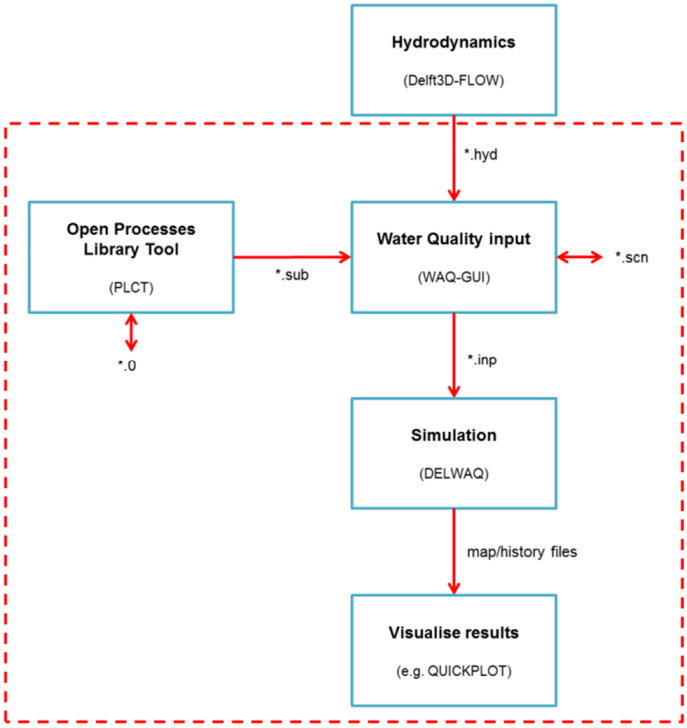

Figure 6.2 Simplified overview of the modules and data flow diagram in Delft3D-WAQ. Modules are represented in rectangles and the files they share are annotated on the arrows (adapted from Deltares, 2014a).

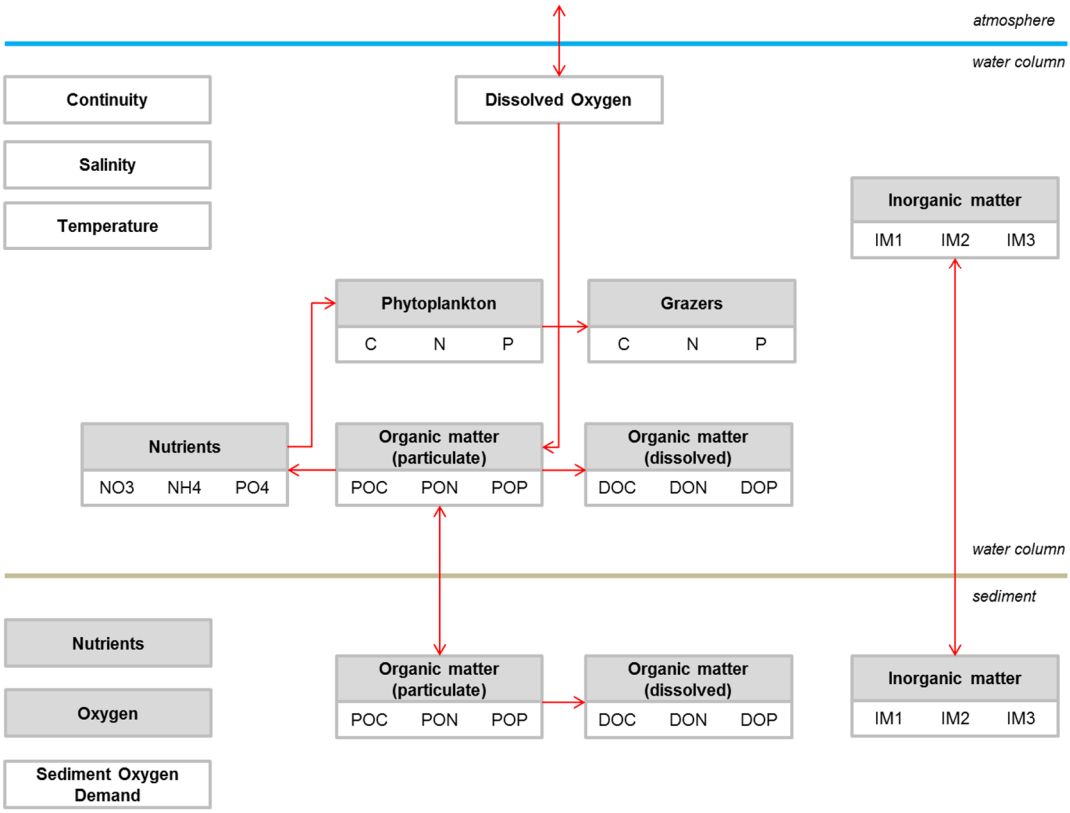

Figure 6.3 General overview of substances included in Delft3D-Water Quality. Substances are organised in functional groups (grey header), except some that form a group of their own. Major links between substances are represented (red arrows), although for visualisation purposes many are omitted.

The sediment is an important and complex compartment of a water system, providing suitable habitat for a wide range of fauna and flora, acting as a sink of particulate and dissolved matter, and establishing exchanges with the upper lying water column (Figure 6.3). Moreover, seagrasses, as benthic organisms, highly depend on the physical and chemical properties of the sediment, may change the sediment stability and erosion/deposition processes, by their potential effect on bed shear stress and shear strength of the sediment (Deltares, 2017).

The modelling framework in Delft3D-WAQ to address the interaction of sediment-water column may follow two distinct approaches: the so-called *S1-S2 approach* and the *layered sediment approach*. The first one, adopted in the configuration previously applied to Ria de Aveiro lagoon (LAGOONS, 2012; Lencart e Silva et al., 2013), has been chosen as it is a simplified alternative of sediment compartment modelling, involving the simulation of substances only subjected to conversion processes and no mass transport within the sediment (particulate substances) (Deltares, 2017). Moreover, it does not consider processes such as different consolidation or separate exchange/reaction rates of different strata.

6.3.2 Numerical aspects

As a multi-dimensional water quality model, Delft3D-WAQ, solves the advection-diffusion-reaction equation. The solution of this equation requires the use of discrete segments in space with finite mesh sizes (*Δx*, *Δy*, *Δz*) and finite time step (*Δt*). Diverse numerical discretisation schemes for discretising the partial differential equations in terms of space and time are available, according to its accuracy, robustness and efficiency. Space discretisation may take advantage of upwind discretisation of first or higher order, while time integration may follow explicit, semi-implicit or implicit methods. As numerical discretisation implies different strategies to solve the discretised system of equations, these solution methods are or iterative or direct solvers (Deltares, 2017).

In present work, the numerical integration scheme selected was an *Implicit upwind scheme with an iterative* solver, as it is a computationally efficient method for large time-steps, positive and without a specific stability criterion for *Δt* for transport (restricted by accuracy and stability criteria for processes).

6.3.2 Open process library tool

One of the main features of Delft3D-WAQ module is the Open Process Library Tool (PLCT). It is an extensible collection of subroutines used by the water quality module in Delft3D and has two main modes of operation: the simple selection of substances and water quality processes for a particular computation; and the possibility to extend the library itself with new *substances* and *processes* (Deltares, 2014a). The last feature provides the option of a sophisticated “user programmable water quality”, which one may create substances and processes additional to the already existing ones, to meet the specific requirements of water quality modelling processes of interest to the user. Newly created and described *substances* and *processes*, using the *GUI* (graphical user interface), are then connected by setting the program code of a generated Fortran90 subroutine, saving extra time in non-relevant computer programming and data structures. Afterwards, the compilation of this source file generates a *DLL* (Dynamic Link Library), which together with the process definition file saved from the *GUI*, incorporates the new process into the Delft3D library database.

The process library includes extensive water quality components, such as *substances*, *processes*, *items* and *fluxes*. The *substances* represent state variables of the system (e.g. concentrations, densities), that accumulate their value over the time of simulation and change according to flows running in and/or out of them. The concentration/density is computed by time-integrating the reaction equation together or without the Advection-Diffusion Equation (ADE), respectively for those *substances* carried with the water or fixed to the bottom substrate

(e.g. benthic organisms, such as seagrasses). The *processes* represent the water quality kinetics, i.e. the fluxes between the substances. As so, the *process* produces *fluxes*. The *items* comprise the input variables for the *processes* and the output variables that work as inputs of other *processes*. They can be constant in time or a time function homogeneous for the entire modelled area or spatially heterogeneous. It can also be a spatially heterogeneous factor constant in time.

6.4 SUMMARY OF THE CHAPTER

As the aim of the present work focus on intertidal seagrass meadows, a numerical model with a robust performance at intertidal areas would be mandatory.

Delft3D modelling suite has a clear advantage on this subject, but further has the possibility of developing and connecting new state variables and processes in the water quality model. This feature allows going beyond the default formulations of the model, by meeting the user-specific requirements, e.g. in the present work, the coupling of a dynamic intertidal seagrass model with an add-on to assess seagrass desiccation response). Furthermore, the user-friendly interface facilitates the whole process of modelling and setting-up different evaluation scenarios.

The present application will take advantage from previous knowledge and successfully application of Delft3D-FLOW and Delft3D-WAQ modules in Ria de Aveiro lagoon, developed in the scope of LAGOONS project (LAGOONS, 2012; Lillebø et al., 2015).

Chapter 7

MODEL IMPLEMENTATION

This chapter primarily presents a short description of the model configuration (Configuration #1), for both hydrodynamics (Delft3D-FLOW) and water quality (Delft3D-WAQ) models, developed in the LAGOONS project for Ria de Aveiro lagoon (Lencart e Silva et al., 2013; Lillebø et al., 2015). As the aforementioned configuration was the basis of this work, but required ponctual adaptations to meet the specific aims of the current study, the features of the model configuration (Configuration #2), for both hydrodynamics (Delft3D-FLOW) and water quality (Delft3D-WAQ) models are also presented. This methodology was followed by the model validation for Configuration #2 and description of model inputs used to force the models. Afterwards, this chapter also presents the coupling procedure and calibration of seagrass model, including the coupling with the water quality model (Delft3D-WAQ) and the inclusion of the desiccation model add-on.

7.1 INTRODUCTION

The Delft3D-FLOW model was firstly applied to Ria de Aveiro in the scope of project LAGOONS (Configuration #1). Its application was preferred to other model suites extensively used to study system's hydrodynamics, due to its ability to support curvilinear grids essential to achieve the project aims (LAGOONS, 2012). At this configuration, the hydrodynamic model solved the Navier-Stokes shallow water equations with hydrostatic, Boussinesq and *f*-plane approximations, using a horizontal Arakawa-C grid, with control volumes and for the most applications an Alternating Direction Implicit (ADI) integration method (Deltares, 2014b; LAGOONS, 2012; Lencart e Silva et al., 2013). The vertical configuration used a σ-grid and the turbulence closure model selected was the k-ε, as the transport equation must be solved for the turbulent kinetic energy k and the energy dissipation ε.

7.2 MODEL CONFIGURATION

7.2.1 Configuration #1

7.2.1.1 Delft3D-FLOW

A Cartesian, curvilinear orthogonal grid has been built to represent the main hydrodynamic features of the lagoon with the minimum number of calculation points (9828 points). The curvilinear properties of the grid allow a resolution between about 30-700 m at narrow channels and offshore open boundary, respectively (Lencart e Silva et al., 2013). As Ria de Aveiro lagoon is mostly a vertically well-mixed system (Dias et al., 2000, 2001), a 2D depth-averaged approximation was made.

The numerical bathymetry of Ria de Aveiro used in this work resulted from its interpolation to the numerical grid obtained from a set of topo-hydrographic surveys (1987-88, 2011, 2012), starting with the most recent one and moving to earlier surveys where later data was unavailable (LAGOONS, 2012).

Tidal propagation was modelled by imposing the main 19 astronomic constituents at the open boundary and calibrated through the adjustment of the bottom roughness, assuming the Manning formulation of the Chezy coefficient (LAGOONS, 2012).To accurately represent the tidal propagation within the lagoon, the model simulates wet and drying of intertidal areas for a water level threshold of 0.1m. The wind-driven circulation was prescribed by a spatially-constant wind momentum flux (Lencart e Silva et al., 2013).

To calibrate the model, a set of runs were performed to compare model predictions against 15 tide gauge stations (Figure 7.1a), where observed time series of *SSE* (sea surface elevation), measured between 2002-2004, were available for at least 30 days long. The calibration of bottom roughness followed the procedure of Picado et al. (2010).

The heat model uses air temperature, combined net solar (short-wave), net (long-wave) atmospheric radiation, relative humidity, and wind speed to calculate heat losses due to evaporation, back radiation and convection. Freshwater boundary conditions for water temperature, were imposed at five freshwater points, representing the outflows of Vouga, Antuã, Boco, Cáster and the system of discharging at the head of Mira channel, designated as Ribeira dos Moínhos (cf. Figure 2.1). The transport of salt considered the input of freshwater from the catchment and the salinity prescribed at the oceanic open boundary (LAGOONS, 2012, 2014; Lencart e Silva et al., 2013; Lillebø et al., 2015).

To assess the model performance for salt and heat flux, the model predictions were compared with the water temperature and salinity observations at 32 stations along 10 sections of Espinheiro channel, carried out by Vaz and Dias (2008) (Figure 7.1b).

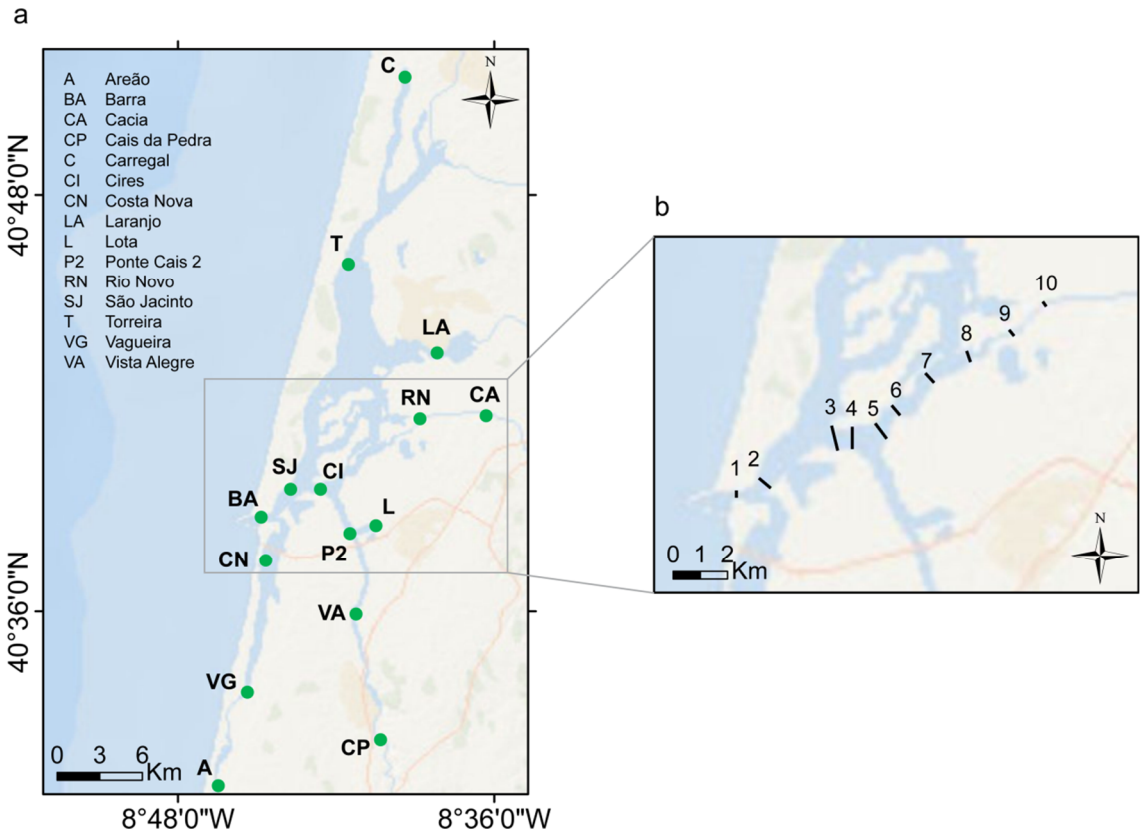

Figure 7.1 Representation of stations used for a) calibration and validation of the hydrodynamic model and b) calibration and validation of salt and heat model.

7.2.1.2 Delft3D-WAQ

The initial configuration included 23 *substances*, comprising a single group of primary producers (algae except diatoms), the dissolved and particulate organic forms of major nutrients, such as carbon, nitrogen and phosphorous, and suspended inorganic matter, considering the fraction already inside the lagoon and the fraction imported from the catchment (Table 7.1).

The processes include algae growth, settling and resuspension of particulate matter, mineralisation of particulate and dissolved matter, including nitrification, denitrification, oxidative processes for phosphorous and reaeration of oxygen.

Table 7.1 Selected substances in Delft3D-WAQ for Configuration #1.

Substance	Description	Unit
Green	Non-diatoms algae	gC/m^3
OXY	Dissolved oxygen concentration	g/m^3
Inorganic dissolved nutrients		
NO3	Nitrate	gN/m^3
NH4	Ammonium	gN/m^3
PO4	Ortho-phosphate	gP/m^3
Dissolved Organic Matter		
DOC	Dissolved Organic Carbon	gC/m^3
DON	Dissolved Organic Nitrogen	gN/m^3
DOP	Dissolved Organic Phosphorous	gP/m^3
Particulate Detrital Organic Matter		
POC1	Particulate Organic Carbon fraction 1	gC/m^3
POC2	Particulate Organic Carbon fraction 2	gC/m^3
PON1	Particulate Organic Nitrogen fraction 1	gN/m^3
PON2	Particulate Organic Nitrogen fraction 2	gN/m^3
POP1	Particulate Organic Phosphorous fraction 1	gP/m^3
POP2	Particulate Organic Phosphorous fraction 2	gP/m^3
Suspended Inorganic Matter		
IM1	Suspended inorganic matter fraction 1	g/m^3
IM2	Suspended inorganic matter fraction 2	g/m^3
Particulate Detrital Matter - Sediment		
DetCS1	Fast decomposing detrital carbon in layers S1 and S2	gC
DetNS1	Fast decomposing detrital nitrogen in layers S1 and S2	gN

Table 7.1 (cont.)

Substance	Description	Unit
DetPS1	Fast decomposing detrital phosphorous in layers S1 and S2	gP
OOCS1	Slow decomposing detrital carbon in layers S1 and S2	gC
OONS1	Slow decomposing detrital nitrogen in layers S1 and S2	gN
OOPS1	Slow decomposing detrital phosphorous in layers S1 and S2	gP
IM1S1	Inorganic matter fraction 1 in bed layer 1	g

7.2.2 New configuration: Configuration #2

As aforementioned, the aims of the present work required punctual modifications on the numerical grid of Configuration #1, which comprised its refining at Mira channel (detail of Figure 7.7a and b) and aggregation of decomposed domains with the improvement of grid orthogonality (Figure 7.2a and b). These modifications incremented the number of calculation cells (177x458 cells), therein calculated solution points (15733 points) and grid resolution (15-570 m). The increase in grid resolution provided a better delimitation of the existent areas of seagrasses. The conversion of 6 decomposed domains into a single one overcome the difficulties that arose from defining the initial conditions of above and belowground seagrass biomass, when seagrass patches were located in the interface of contiguous domains.

Similarly to the Configuration #1, the model simulates wet and drying of intertidal areas using a water level threshold of 0.1m.

7.2.2.1 Delft3D-FLOW

The final configuration for the hydrodynamic model is common to the Configuration #1, except for the numerical grid and domain composition. A synthesis of the model configuration used for all the production runs are therefore listed on Table 7.2.

The initial conditions of the water level, water temperature and salinity were set constant throughout the numerical domain, following the mean values found for the study region and also previously used in Configuration #1 (LAGOONS, 2012; Lencart e Silva et al., 2013; Lillebø et al., 2015).

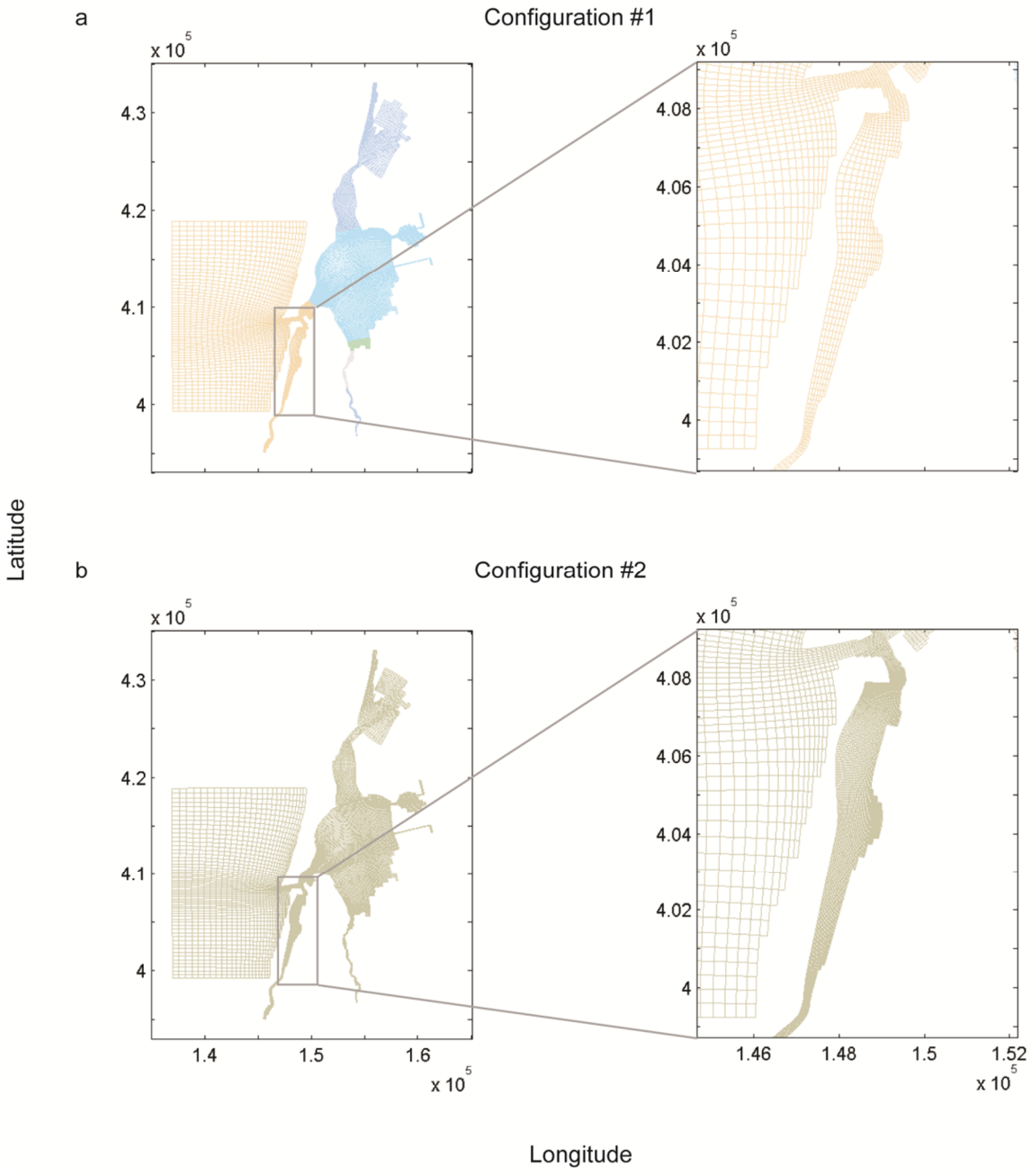

Figure 7.2 Numerical grids for a) Configuration #1 and b) Configuration #2, with respective detail for Mira channel. Latitude and Longitude presented in decimal degrees.

Table 7.2 Modelling configuration of Delft3D-FLOW for the study area.

Parameter	Specification
Time step	30 seconds
Duration	1 year
Constituents	Salinity and water temperature
Wind	Variable
Discharge	Variable
Waves	No
Tide	Warm start of 2 weeks
Initial conditions	Warm start of 2 weeks
Boundary forcing	Harmonic constituents
Bottom roughness method	Variable Manning coefficient
Wall slip condition	Free
Background horizontal eddy viscosity	0.5 $m^2 s^{-1}$
Background horizontal eddy diffusity	10 $m^2 s^{-1}$
Threshold depth	0.1 m
Water temperature	Heat flux model
Heat flux model	Absolute flux, net solar radiation

7.2.2.2 Delft3D-WAQ

The present application of Delft3D-WAQ is an extension of a previous calibrated and validated one to Ria de Aveiro lagoon, developed in the scope of LAGOONS project (LAGOONS, 2012; Lillebø et al., 2015).

The Delft3D-WAQ model uses hydrodynamic quantities calculated by Delft3D-FLOW to parameterise its advection-diffusion numerical scheme, besides water temperature and salinity. These properties, calculated by FLOW module and communicated to WAQ-module, using a spatial and time coupling algorithm, allow different time step and spatial resolution within WAQ, thus the computation time and load.

In the present application, the complementary state variables and fluxes created to address seagrass meadows (cf. Chapter 4), were added together to those of the previous configuration, described in section 7.2.1.2 (LAGOONS, 2012; Lencart e Silva et al., 2013; Lillebø et al., 2015). It adds the seasonal dynamics of seagrass meadows with the add-on to address intertidal communities to Delft3D-WAQ model, by taking advantage of the possibility of creation and setting of new substances and processes, through the Open Process Library Tools.

Comparing with the conceptual model presented in Chapter 4, the coupling of seagrass dynamics+desiccation module with Delft3D-WAQ allows to include the tide, in the biological seagrass model, as a key forcing function and the desiccation as an extra process of concern. The senescence of seagrasses contributes to the Particulate Organic Matter (POM) and Dissolved Organic Matter (DOM) pools, specifically to the Particulate Organic Carbon (POC) and Dissolved Organic Carbon (DOC). The mineralization of the organic matter is assured by the biogeochemical processes already implemented in the water quality model (Deltares, 2017).

A synthesis of the model configuration used for all the production runs is listed in Table 7.3. The initial conditions for the above and belowground biomasses were set constant throughout the numerical domain, with a value of 60 gDW m^{-2}.

Table 7.3 Modelling configuration of Delft3D-WAQ for the study area.

Parameter	Specification
Number of layers	1 (2D model)
Uniform dispersion (1st direction)	1 m^2 s^{-1}
Uniform dispersion (2nd direction)	1 m^2 s^{-1}
Numerical integration method	15 (iterative solver, backward differences)
Timestep	30 minutes

7.3 VALIDATION OF CONFIGURATION #2

As the calibration of the hydrodynamic model was beyond the aim of this study and the modifications were minor, a validation of the new model configuration was performed rather than a model re-calibration. It was assumed that if the comparison of model predictions for sea surface elevation and tidal amplitude and phases of mean tidal constituents, as well as water temperature and salinity, were similar to those observed and predicted with Configuration #1, then the model's ability to represent the tidal propagation and salt and heat patterns within the model domain was preserved. The initial conditions, model setup and inputs used to validate Configuration #2 are the same as those used in Configuration #1. The initial conditions for water level, water temperature and salinity, as well as boundary conditions, turbulence and heat flux model remained therefore unaltered, besides the same bathymetric data, tidal, meteorological and river discharge forcing.

The model predictions for water level were compared against observed sea surface elevation at 15 stations (cf. Figure 7.1a).

To test the model performance, a first visual comparison of both observed and predicted water level preceded the computing of two error parameters for each station, the root mean square error (*RMSE*, Eq.7.1) (Stow et al., 2009) and *Skill* (Willmott, 1981) (Eq. 7.2). The root mean square error calculates the absolute measure of the model deviation from data and is one of the most computed error parameters to assess model performance in terms of reproduction of tidal patterns (e.g. Dias and Lopes, 2006a; Lopes, 2016; Ribeiro, 2015; Rodrigues, 2015).

$$RMSE = \sqrt{\frac{1}{N}\sum_{i=1}^{N}\left[\zeta_0(t_i) - \zeta_m(t_i)\right]^2} \tag{7.1}$$

$$Skill = 1 - \frac{\sum\left|\zeta_m - \zeta_0\right|^2}{\sum\left[\left|\zeta_m - \overline{\zeta_0}\right| + \left|\zeta_0 - \overline{\zeta_0}\right|\right]^2} \tag{7.2}$$

N is the length of *SSE* datasets, $\zeta_0(t_i)$ and $\zeta_m(t_i)$ are observed and predicted *SSE* at time t_i, respectively. The closest *RMSE* is to zero, the better is the model performance. For local comparison of *SSE*, *RMSE* values <5% represents an excellent agreement between model and observations, while an *RMSE* between 5-10% indicates a very good agreement (Dias et al., 2009).

The predictive *Skill* overcomes the sensitivity of correlation statistics to differences in predicted mean variances. As so, *Skill* values of 1 correspond to a perfect adjustment between predictions and observations, though if it is higher than 0.95 the agreement is considered excellent (Dias et al., 2009). The *RMSE* and *Skill* values for Configuration #1, Configuration #2 and a recent application using unstructured grids with ELCIRC hydrodynamic model are in Table 7.4.

The station located near the lagoon mouth presented *RMSE* values of about 6 cm (Barra), with the best model results generally obtained for those located closer to the lagoon entrance. The highest discrepancies occurred at the northern and southernmost located stations (Carregal, with *RMSE* of 13 cm, Vista Alegre with 23 cm and Cais da Pedra 25 cm).

The model's ability in predicting the spring-neap for the inner stations is thus slightly smaller than the verified for the stations near the mouth, presenting a smaller *Skill* and higher *RMSE*. Even though the new model configuration (Configuration #2) generally predicts the water levels with good accuracy, showing better results than Configuration #1 in 9 out of 15 stations and ELCIRC implementation from Lopes (2016) in 11 out of 15 stations.

The harmonic analysis, performed through *T_Tide* package of MATLAB routines (Pawlowicz et al., 2002), allowed quantifying the main differences between model predictions and observed data, through comparison of amplitudes and phase of the main solar (K_1, O_1) and lunar (M_2, S_2)

tidal constituents. The harmonic analysis for model predictions and observed *SSE* time series for the major diurnal and semidiurnal tidal constituents is presented in Figure 7.3 for both Configuration #1 and Configuration #2.

The overall agreement between model predictions and observed data showed that both amplitude and phase are good for semidiurnal constituents M_2 and S_2, which account for more than 80% of tidal energy (Dias et al., 2000). The highest differences in amplitude and phase occurred mostly in the head of the channels (about 19 cm for M_2 in Areão and Cais da Pedra; and 10 cm for S_2 in Vista Alegre).

Table 7.4 *RMSE* and *Skill* for Configuration #1, Configuration #2 and a recent application using ELCIRC model with an unstructured grid (Lopes, 2016).

Station	Configuration #1		Configuration #2		Lopes (2016)	
	RMSE (m)	Skill	RMSE (m)	Skill	RMSE (m)	Skill
Areão	0.2185	0.9500	0.1555	0.9724	0.1838	0.9201
Barra	0.0649	0.9980	0.0599	0.9983	0.0745	0.9975
Cacia	0.1735	0.9498	0.1249	0.9885	0.2447	0.9335
Cais da Pedra	0.3121	0.8918	0.2493	0.9352	0.2319	0.9335
Carregal	0.2590	0.9021	0.2254	0.9160	0.2610	0.8640
Cires	0.1464	0.9949	0.1300	0.9925	0.1260	0.9930
Costa Nova	0.0999	0.9949	0.0967	0.9953	0.0882	0.9958
Laranjo	0.1390	0.9870	0.1571	0.9824	0.2693	0.9406
Lota	0.0807	0.9968	0.0809	0.9967	0.1086	0.9942
Ponte do Cais 2	0.0587	0.9985	0.0641	0.9981	0.0724	0.9975
Rio Novo	0.0987	0.9941	0.1295	0.9888	0.1949	0.9698
S. Jacinto	0.1309	0.9913	0.0904	0.9957	0.0876	0.9957
Torreira	0.0652	0.9962	0.0721	0.9950	0.0970	0.9910
Vagueira	0.1211	0.9894	0.1929	0.9706	0.2207	0.9559
Vista Alegre	0.3022	0.9312	0.2284	0.9570	0.2342	0.9211

The agreement for diurnal constituents (O_1 and K_1) is also generally good, with the highest differences computed at Cais da Pedra (about 1.5 cm for O_1) and Lota (about 2 cm for K_1).

Therefore, in general, the results of harmonic analysis showed that the circulation model reproduces well the tidal amplitude and phase.

The observed data used for the validation of salt and heat models are fortnightly CTD surveys at 10 stations along the Espinheiro channel (cf. Figure 7.1b), from November 2003 to September 2004, gathered by Vaz and Dias (2008).

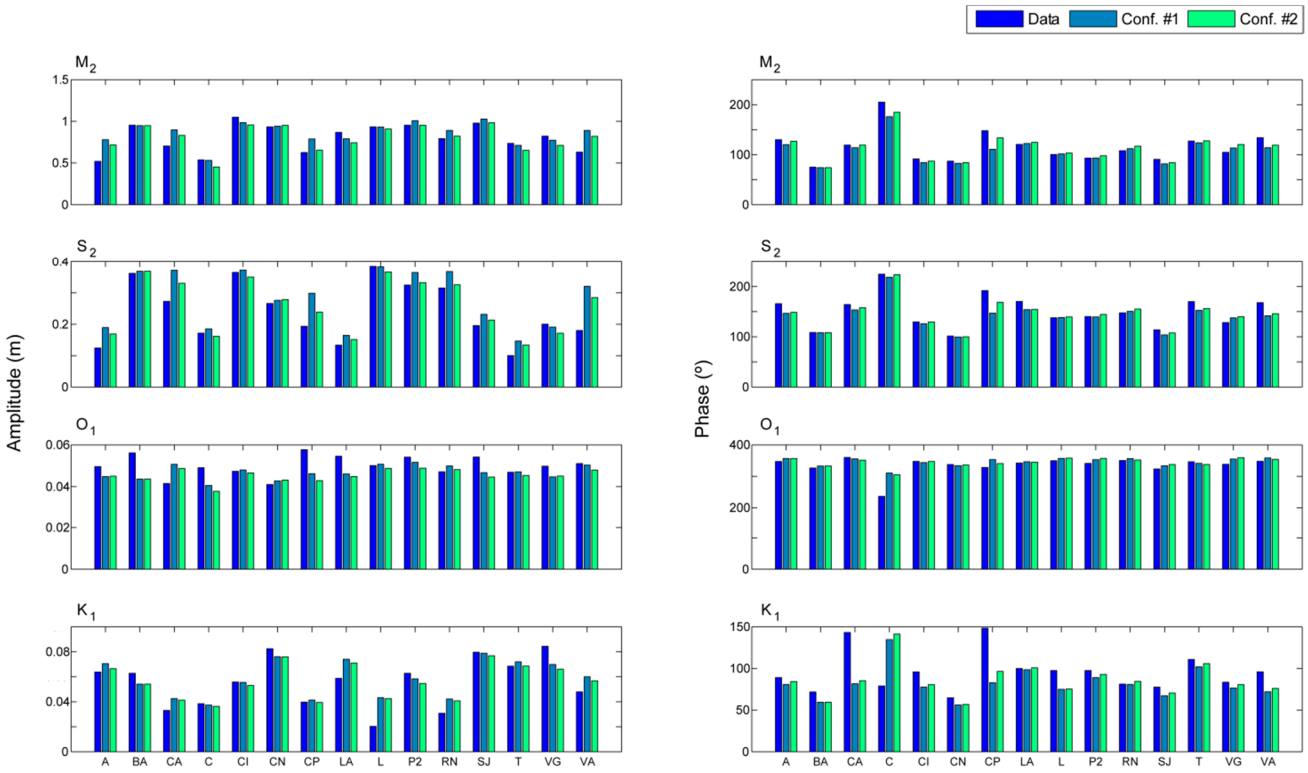

Figure 7.3 Harmonic comparison for the 15 stations spatially distributed in Ria de Aveiro lagoon. At the first column is represented the amplitude of the four tidal constituents M2, S2, O1 and K1, whereas the second represents their phase. Dark blue bars are the observed data, lighter blue the results for Configuration #1 and green bars represent the results of the current configuration (Configuration #2).

The predicted water temperature over the stations 1-9 is strongly consistent with the observations ($skill_{Conf.\#1}$ = 0.97; $skill_{Conf.\#2}$ = 0.97), with differences between predictions and observations ranging between 1.2-1.7 ºC (Figure 7.4). For the station 10, the differences raise up to 2.4 ºC.

The salinity values show the same pattern between predictions and observation data (Figure 7.5), though the agreement between them turned out to be poor ($skill_{Conf.\#1}$ = 0.73; $skill_{Conf.\#2}$ =

0.71), mainly due to constraints in representing the stations nearby river mouths, as already reported for Configuration #1 (LAGOONS, 2014).

The higher discrepancies occurred at station 10 and are mostly due to the closing of a dike (located in Rio Novo do Príncipe) from late spring until the first rains, not contemplated in the model. Moreover, other uncertainties relate with river forcing at discharge points, which is only available from catchment models due to the unavailability of useful measured data for the interfaces between the lagoon and the catchment, and with the assumption of no spatial variability of meteorological inputs. According to these results, the newly configuration satisfactory reproduces the salt and heat transport processes in Ria de Aveiro lagoon.

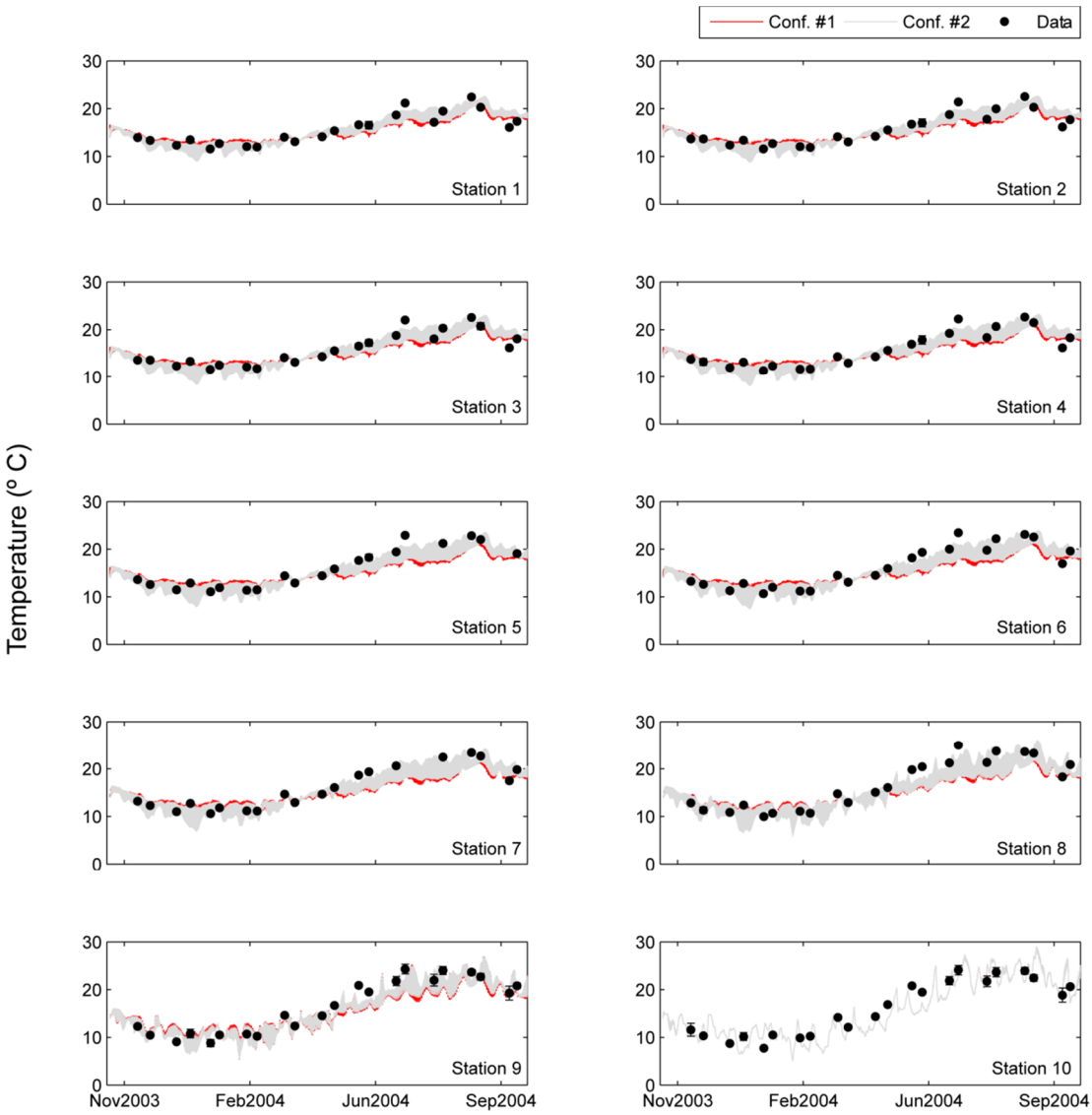

Figure 7.4 Observations (black dots) and model predictions for both Configuration #1 (red line) and Configuration #2 (grey line) for water temperature for the sampling stations 1-10, from November 2003 to September 2004.

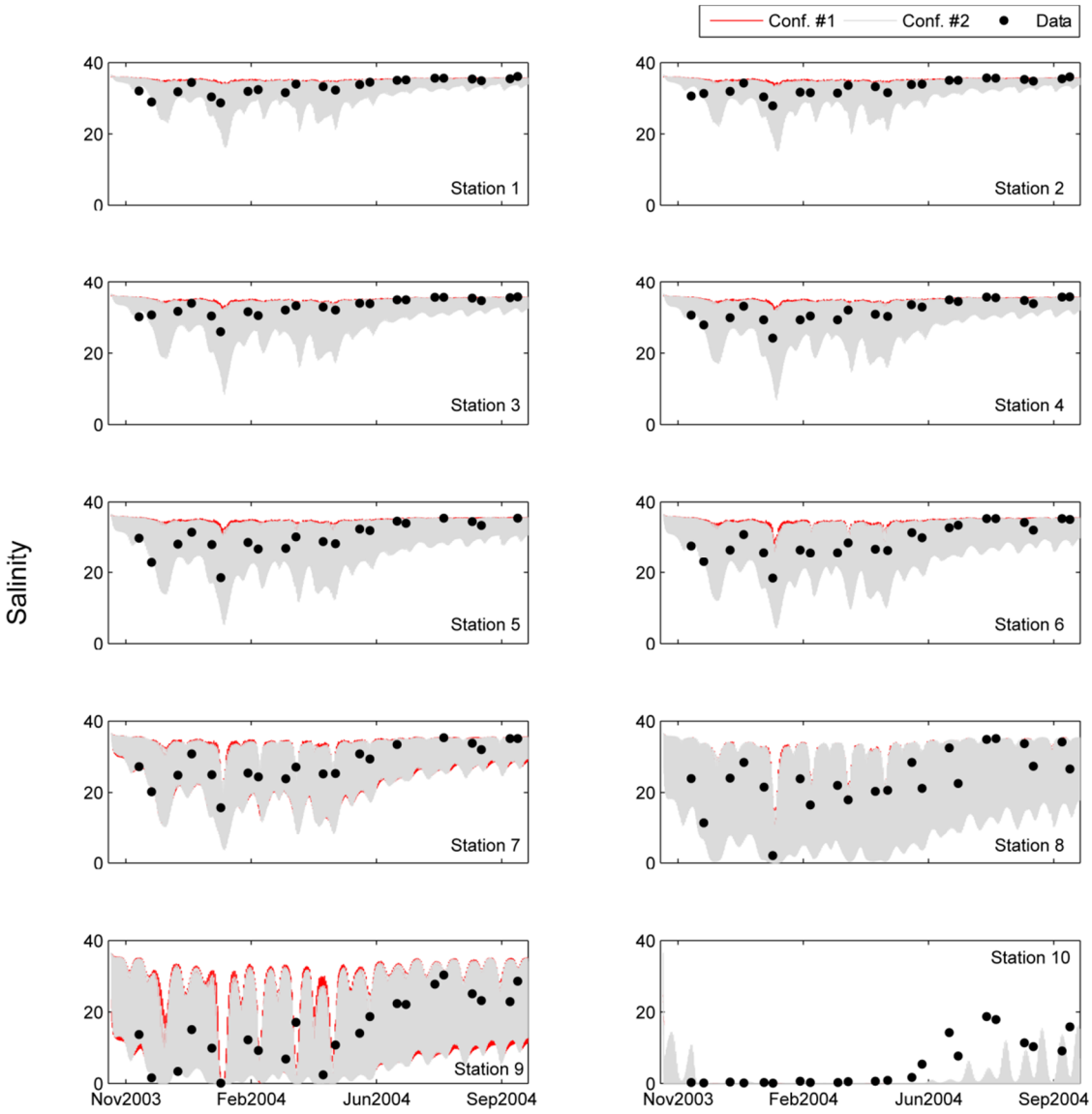

Figure 7.5 Observations (black dots) and model predictions for both Configuration #1 (red line) and Configuration #2 (grey line) for salinity for the sampling stations 1-10, from November 2003 to September 2004.

7.4 MODEL INPUTS

Following the state of the art presented in Chapter 1, the current work considered as major driving factors the tide, wind and freshwater inflow, set as the main forcing mechanisms of water circulation within Aveiro lagoon. These drivers were provided to the model as boundary conditions, using the output of other models available for the scientific community or as time series.

The ecological system is therefore generally controlled by water fluxes, ambient temperature, incident light and nutrient discharges. To validate the hydrodynamic results, the same inputs from the previous configuration were used.

7.4.1 Atmospheric boundary

Meteorological data used to force the atmospheric boundary of the model was obtained from the European Centre for Medium-Range Weather Forecasts (ECMWF, www.ecmwf.int), which provides a global atmospheric reanalysis model, ERA-Interim.

The data assimilation system used to produce ERA-Interim is based on a 2006 release of the IFS (Integrated Forecasting System: Cy31r2). The system includes a 4-dimensional variation analysis (4D-Var) with a 12-hour analysis window. The spatial resolution of the data set is approximately 80 km on 60 vertical levels from the surface up to 0.1 hPa (ECMWF, www.ecmwf.int). Data supplied from ERA-Interim had a chosen temporal resolution of 3 hours and allowed to calculate the heat flux and wind parameters required by Delft3D-FLOW. The heat flux model needs data on relative air humidity (%), air temperature (ºC) and net solar radiation (J m^{-2} s^{-1}), while wind process requires wind velocity (m s^{-1}) and direction (º). Extracted data ranged from January 2012 to January 2014, to comprise the period of experimental surveys of seagrass seasonality, and the spatial domain varied from 40-41 ºN and 7-10ºW. The meteorological data extracted are presented in Figure 7.6.

Air relative humidity concerns to the ratio of the partial pressure of water vapour to the equilibrium vapour pressure of water in air, at a given ambient temperature, and so, less water vapour is needed to reach high air relative humidity at low temperatures, while more water vapour is needed to reach high relative air humidity in warmer air. Though the close dependence with air temperature, air relative humidity (Figure 7.6a) have not presented a clear seasonal trend, as it also depends on the specific provenience and signatures of air masses.

Air temperature presents an expected seasonal trend with higher values registered during summer and lower ones during the winter season (Figure 7.6b). Moreover, the net solar radiation also presents an overall and expected unimodal pattern, with higher values during summer months and lower ones during the winter (Figure 7.6c).

Concerning wind data, the wind regime during the simulation period is presented in Table 7.5, according to the Beaufort wind force scale. The representability of light winds (lower than 3.3 m s^{-1}) ranges between 17.7-22.5%. Gentle, moderate and fresh breezes correspond to the prevailing wind regime, representing 74.7-79.6% of wind intensity. Strong winds (>10.8 m s^{-1}) were the less representative, with only 0.7-10.3%. The distribution of wind vectors throughout the seasons, and illustrated in Figure 7.7, indicates the direction from which the wind blows. In spring (Figure 7.7a), the wind blows mainly from North (along the shore) and Northwest direction.

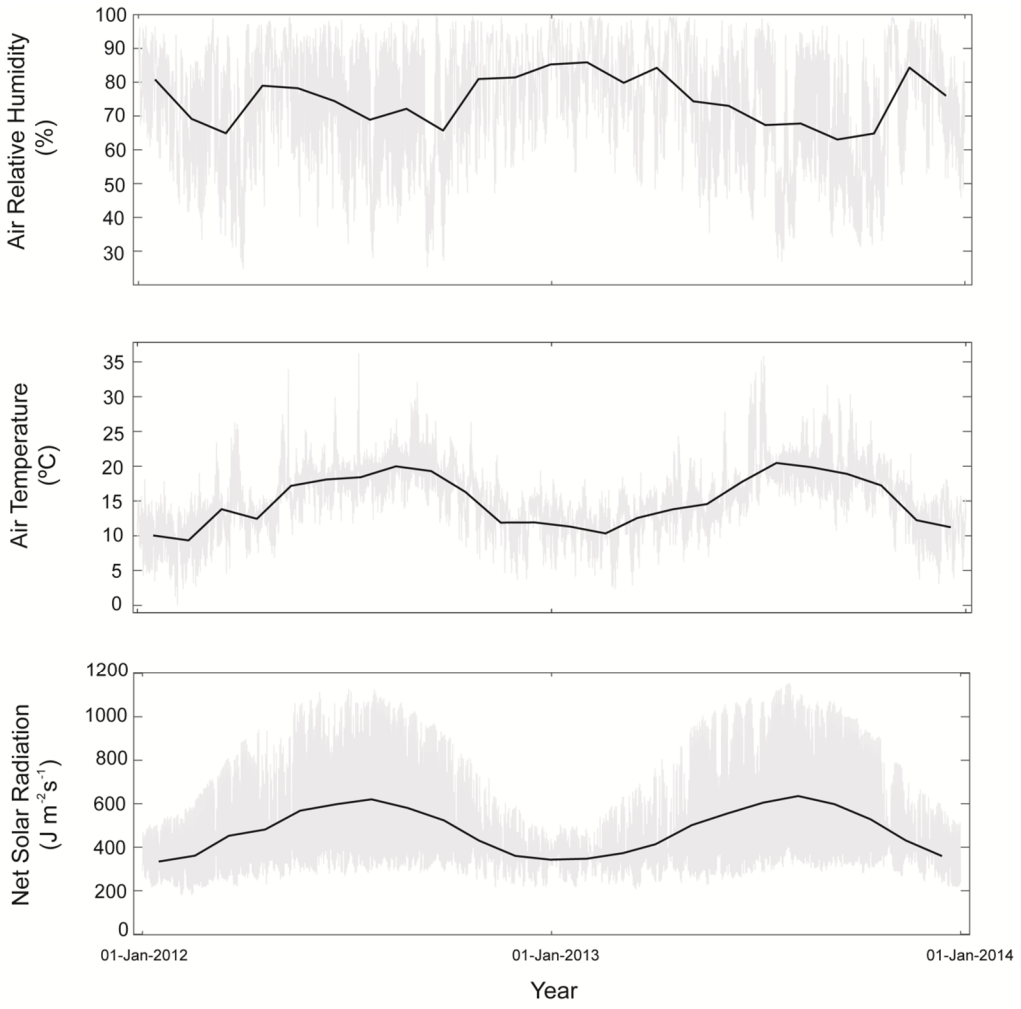

Figure 7.6 Meteorological data used to build the heat flux model (grey line): a) air relative humidity (%), b) air temperature and c) Net solar radiation (J m^{-2} s^{-1}). Monthly average: black line.

Table 7.5 Events (%) for each range of wind speed according to Beaufort scale, for the different seasons and overall occurrence.

Limits of wind speed (m s^{-1})	Wind descriptive terms	Spring (%)	Summer (%)	Autumn (%)	Winter (%)
<1.5	Calm	4.1	4.6	3.7	4.1
1.6 – 3.3	Light breeze	13.6	15.1	16.1	18.4
3.4 – 5.4	Gentle breeze	24.9	30.9	26.2	23.9
5.5 – 7.9	Moderate breeze	26.8	35.6	30.8	27.0
8.0 – 10.7	Fresh breeze	23.0	13.1	17.7	16.3
10.8 – 13.8	Strong breeze	7.1	0.7	5.2	8.6
>13.9	Near gale	0.5	0	0.3	1.7

This pattern is even more noticeable during summer (Figure 7.7b), as expected, clearly showing higher frequencies of winds coming from Northwest direction. During autumn (Figure 7.7c), the prevailing winds blow from the North. In winter (Figure 7.7d), the strongest winds are from Southwest directions, though the most frequent ones blow from North directions.

Solar radiation data was given every 10 minutes to force light conditions of the seagrass model. These data, measured by the automatic meteorological station of university campus (CESAMET), is located nearby the study site (Figure 7.8). As expected, the seasonal trend presents higher daily radiation during late spring and summer, than the winter season.

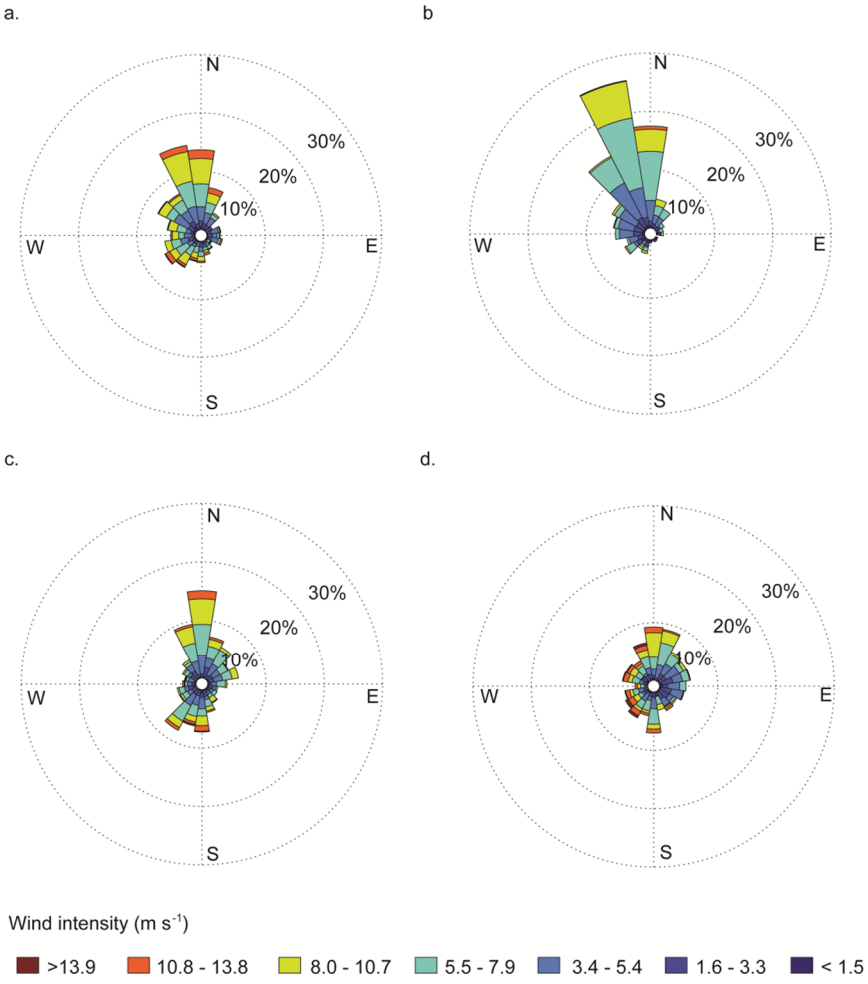

Figure 7.7 Wind rose diagrams (m s^{-1}) calculated for each season between the period of January 2012 and December 2013: a) spring, b) summer, c) autumn and d) winter.

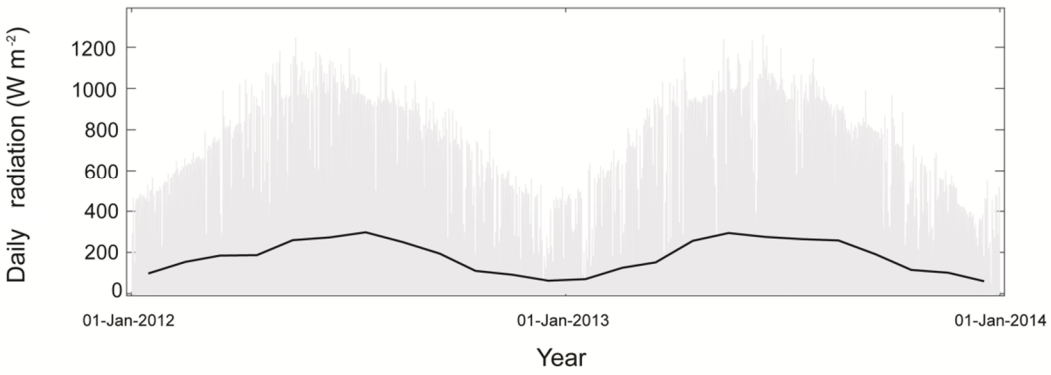

Figure 7.8 Every 10 minute- surface radiation used to force the seagrass model (Data gathered from CESAMET: grey data. Monthly average: black line).

7.4.2 Ocean boundary

The flow conditions at the oceanic open boundary used the same astronomic forcing type as the previous application of Delft3D-FLOW in Ria de Aveiro lagoon, by imposing the main 19 astronomic tidal constituents (LAGOONS, 2012).

The water temperature and salinity conditions at this boundary were calculated using the inputs from Copernicus Marine Environment Monitoring system (CMEMS, marine.copernicus.eu). Within CMEMS, MyOcean project provides reanalysis data on daily water temperature and salinity with 0.083ºx0.083º resolution, for 50 vertical levels, from the surface down to 5500 m depth. The product used was designated by IBI_Reanalysis_Phys_005_002 (Atlantic-Iberian-Biscay-Irish ocean physics reanalysis).

Temporal range of extracted data for water temperature (Figure 7.9a) and salinity (Figure 7.9b) was from January 2012 to January 2014, to comprise the period of experimental surveys performed to assess seagrass seasonality, and the spatial domain varied from 40-41 ºN and 7-10ºW. Afterwards, the nearest point of the grid data extracted was selected, according to the coordinates of the lagoon entrance.

7.4.3 River boundaries

The input of freshwater volume and temperature (cf.Figure 7.10) was taken from the SWIM model (SWIM, Soil and Water Integrated Model, Potsdam Institute for Climate Impact Research, www.pik-potsdam.de), due to the unavailability of useful measured data for the interfaces between the lagoon and the catchment, and as used for the previously application of Delft-3D to Ria de Aveiro lagoon (LAGOONS, 2014).

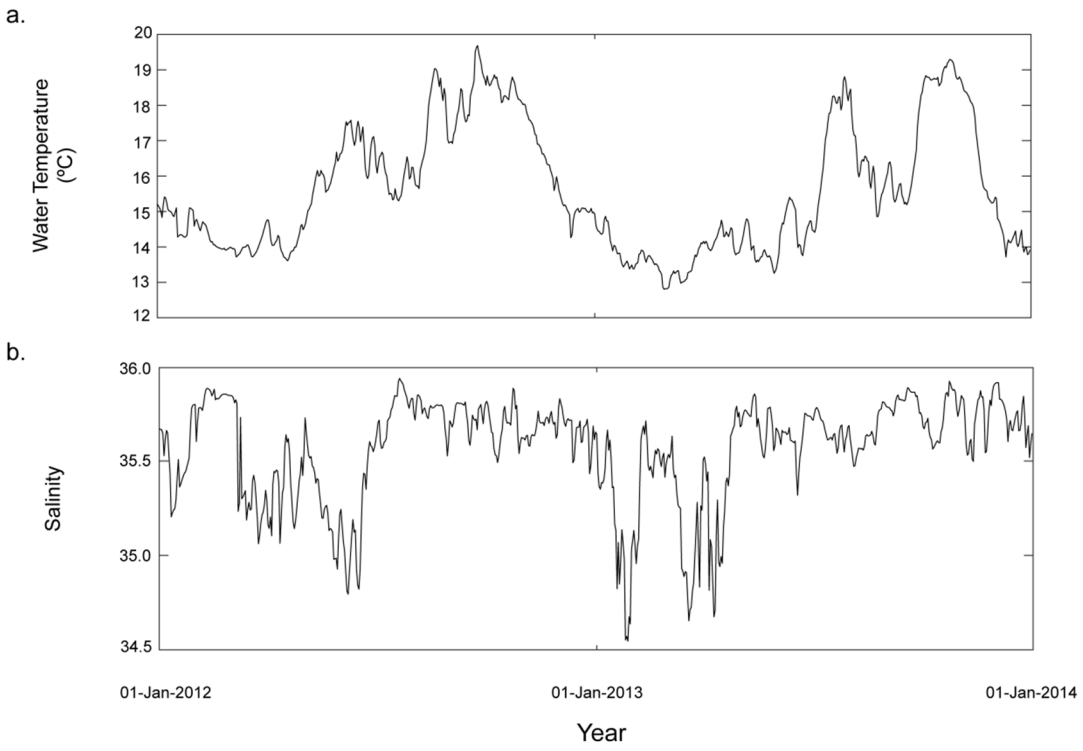

Figure 7.9 Water temperature and salinity conditions at the oceanic boundary: a) water temperature and b) salinity.

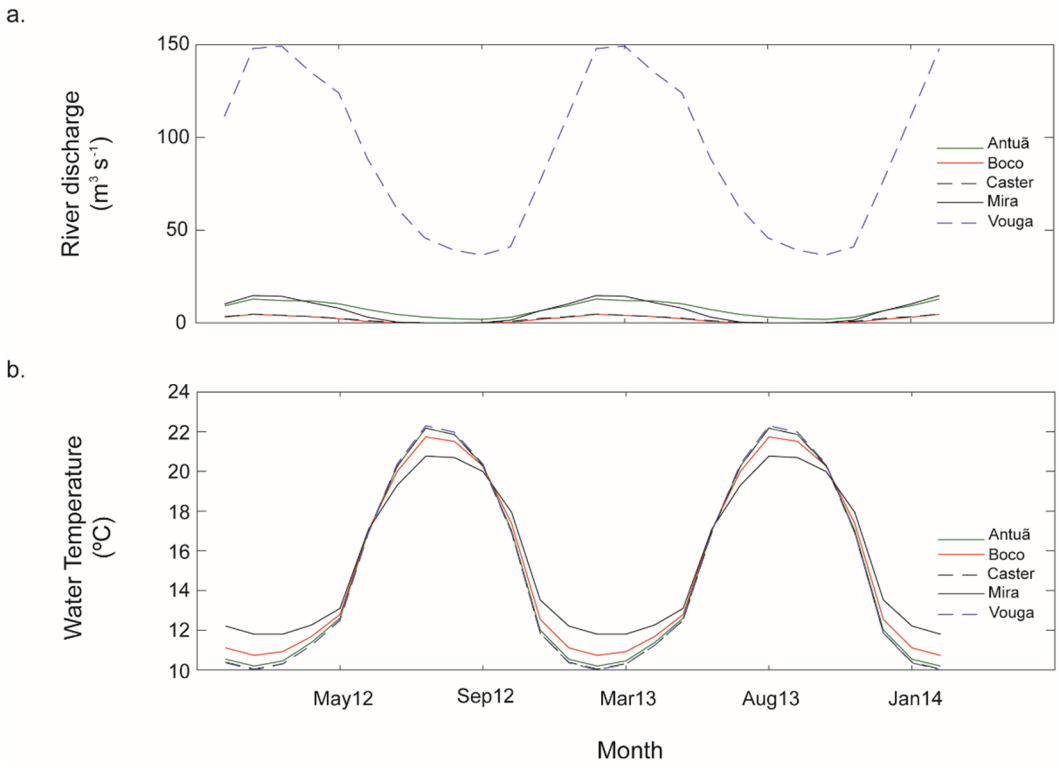

Figure 7.10 Properties imposed at river boundaries to force Delft3D-FLOW and Delft3D-WAQ - a) river discharge ($m^3 s^{-1}$), b) water temperature (ºC).

To obtain typical averaged monthly values of mentioned parameters, a climatological analysis of 30 years, from 1981-2010, was performed (Appendix 5). Concerning monthly averaged river discharges (Figure 7.10a), the results showed higher values during winter and early spring, and lower ones during summer and early autumn, as expected. Highest values clearly occur for Vouga river, representing about 84% of freshwater input in Ria de Aveiro lagoon, followed by Antuã (7%), Mira (6%), Caster (2%) and Boco (2%). This is consistent with river discharge values previously reported for Ria de Aveiro (Génio et al., 2008; Vaz et al., 2016).

The water temperature (Figure 7.10b) presented a general unimodal pattern throughout the year and monthly averaged values ranged from 10-22.3 ºC. The highest variability of this parameter, between rivers, occurs at winter and summer months (about 1.9 ºC), and the lowest at late spring (about 0.2 ºC).

7.5 PRELIMINARY MODEL TESTING FOR CONTINUITY

The Delft3D-WAQ module uses an artificial conservative tracer so-called *Continuity*, which has no physical or chemical meaning, to establish the accuracy and stability of the simulation (Deltares, 2017). Therefore, prior to the simulation of the substances and processes described, a preliminary approach tested the model in terms of continuity and numerical stability. The assignment of the same concentration (1 mg L^{-1} in this study) to all water sources (i.e. initial condition, boundary condition and river discharges) should remain constant during the whole simulation, as no processes are included to dilute or concentrate. One may consider that if the tracer concentration deviates significantly from the assigned concentration, a source of water may be overlooked or the simulation is numerically unstable (Deltares, 2017). Since the tracer concentration never deviated more than 0.03% from the assigned concentration, the model was considered numerically stable, conserving mass and ready to include the chosen substances and processes.

7.6 SEAGRASS MODEL AND DESICCATION ADD-ON ON DELFT3D-WAQ

7.6.1 Seagrass model calibration

Process-based models are simplified representations of natural systems, using sets of equations to express scientifically accepted principles. The purpose of the calibration in the present study is to determine the optimum parameter settings of the Delft3D-WAQ module to compute the seagrass dynamics, in terms of above and belowground biomass, according to the light and ambient temperature variations throughout the seasonal cycle. Many model runs were performed to calibrate the numerical water quality model (only the parameters comprised in the biological seagrass model were adjusted) and therefore reducing the differences between the

available observational data and predictions. Model predictions were compared against ground-surveyed data (presented and discussed in Chapter 3).

The model predictions for seagrass biomass were compared with observed data, collected at a well-established meadow in Mira channel (Ria de Aveiro lagoon), monthly during a year, for both above (Figure 7.11a) and belowground biomass (Figure 7.11b) – state variables.

a.

b.

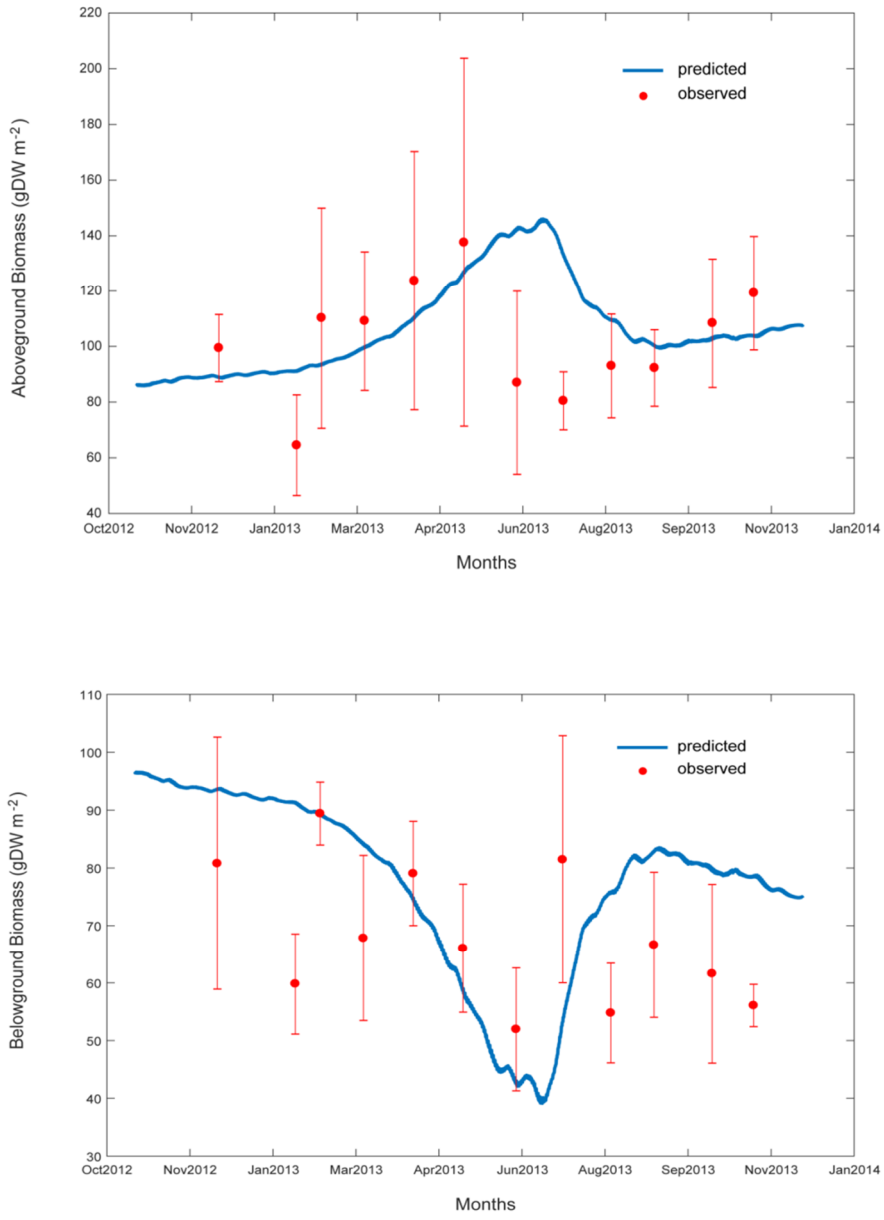

Figure 7.11 Comparison between predicted (blue line) and average per month of observed (red dots) seagrass seasonal biomass: a) Aboveground biomass; b) Belowground biomass. The red bars represent the standard deviation (n=5).

A visual comparison showed a good agreement between the predicted and observed aboveground biomass, with only 3 out of 12 predictions outside the variability range of spatial

variation (Figure 7.11a). Model predictions seem to underestimate the averaged aboveground biomass for the winter, spring and autumn months. For the summer months, the model fails to reproduce the observed aboveground biomass pattern. For the belowground biomass, the visual adjustment seems only fair, with 6 out of 12 predictions outside the variability range of spatial variation (Figure 7.11b). Between late spring and late summer the model appears to underestimate the averaged observed belowground values, while for autumn and winter months, on the contrary, the model overestimated the observations.

The set of model parameters that produced the best fit between predicted and observed values are indicated in Table 7.6. For reference sources please address Table 4.1.

Table 7.6 List and values of parameters used in the model. Reference values from the literature were also given.

Abbreviation	Short description	Reference value (units)	Value
$trns_{AB\_BB}$	Translocation of aboveground to belowground biomass	0.25 (adim.) 0.2 (adim.)	0.25
$g_{\max}$	Maximum growth rate	0.23 (d^{-1}) 0.043	0.126
K_0	Function value at $T = T_0$ (T_0 = 0ºC)	0.01 (adim.)	0.1
K_m	Function value at $T = T_{\max}$	0.00001 (adim.)	0.00001
T_{opt}	Optimal temperature for growth	29 (ºC) 20 (ºC)	20
$T_{\max}$	Maximum temperature for growth	35 (ºC)	35
stt	Control the shape function on $F(T)$	1.8 (adim.) 2 (adim.)	2
HSL	Half-saturation constant for light	24 (W m^{-2})	24
K_w	Extinction coefficient of water	0.4 (m^{-1}) 1.2 (m^{-1})	0.5
K_L	Extinction coefficient of leaf biomass	0.0272 (gDW $^{-1}$ m^2)	0.0272
σ	Maximum aboveground biomass	500 (gDW m^{-2}) 297(gDW m^{-2})	250
LMR_{20}	Maximum aboveground mortality rate at 20 ºC	0.025 (d^{-1}) 0.02-0.06 (d^{-1})	0.0265
RMR_{20}	Maximum belowground mortality rate at 20 ºC	0.025 (d^{-1})	0.025
θ	Mortality increasing rate with temperature	1.1 (adim.)	1.1

adim. – Dimensionless. *if submerged, T = Twater (water temperature); else, T=Tair (air temperature)
For reference values of each parameter, please check Table 4.1

7.6.2 Overview of seagrass model performance

7.6.2.1 Error statistical methods

As modelled parameters may be difficult to measure or not well known, the relevance of its uncertainties in measurement and estimation is highly important for the overall assessment of model performance (Kenov et al., 2013). Therefore, evaluating the confidence of model results must consider the complex combination of both model and observational uncertainties.

The model errors mainly derive from misconceptions in process descriptions, parameterization and forcing functions, whereas the errors in observations principally arise from basic measurement error, inappropriate scales of sample distribution or lack of replication in highly heterogeneous systems (Allen et al., 2007).

In the previous topic, the above and belowground trends were investigated and described, in terms of how well the model reproduces the observed seasonal cycle of the dynamics of the state variables. However, as a well reproduce trend does not necessarily mean small errors in precision, the error statistic was evaluated in terms of model efficiency, bias and cost function, according to the formulation and criteria presented in Allen et al. (2007) and therein references (Table 7.7).

Table 7.7 Statistic methods used to assess the seagrass model performance (from Allen et al. (2007)).

Error statistic method	Formulation	Performance criteria - scale
Model efficiency - Nash Sutcliffe Model Efficiency	$ME = 1 - \frac{\sum_{n=1}^{N}(D_n - M_n)^2}{\sum_{n=1}^{N}(D_n - \overline{D})^2}$	• <0.2 poor • 0.2-0.5 good • 0.5-0.65 very good • >0.65 excellent
Percentage model bias	$Bias(\%) = \frac{\sum_{n=1}^{N}(D_n - M_n)}{\sum_{n=1}^{N} D_n} \cdot 100$	• >40% poor • 20-40% good • 10-20% very good • <10% excellent
Cost function	$CF = \frac{1}{N}\sum_{n=1}^{N}\frac{\lvert D_n - M_n \rvert}{\sigma_D}$	• >3 poor • 2-3 reasonable • 1-2 good • <1 very good

ME – model efficiency; D – ground-surveyed data; M – corresponding model estimate; $\overline{D}$ – mean of dataset for the chosen variable; N – total number of model data matches; n – nth comparison; CF – Cost function; σ_D - standard deviation of the data

The results obtained by the error statistical analysis showed distinct results. The assessment of model efficiency was usually negative, which indicated no model skill at all, but simulations for aboveground biomass were better (-0.7; less negative values) than for the belowground biomass (-1.9).

On the contrary, for percentage model bias, the model performance to simulate the aboveground biomass was scaled as excellent (|bias|=6%), whereas for belowground biomass it was set as very good (|bias|=11%) (Figure 7.12a). Moreover, through the cost function, the model performance was scaled as good for both the above and belowground biomass) (Figure 7.12b).

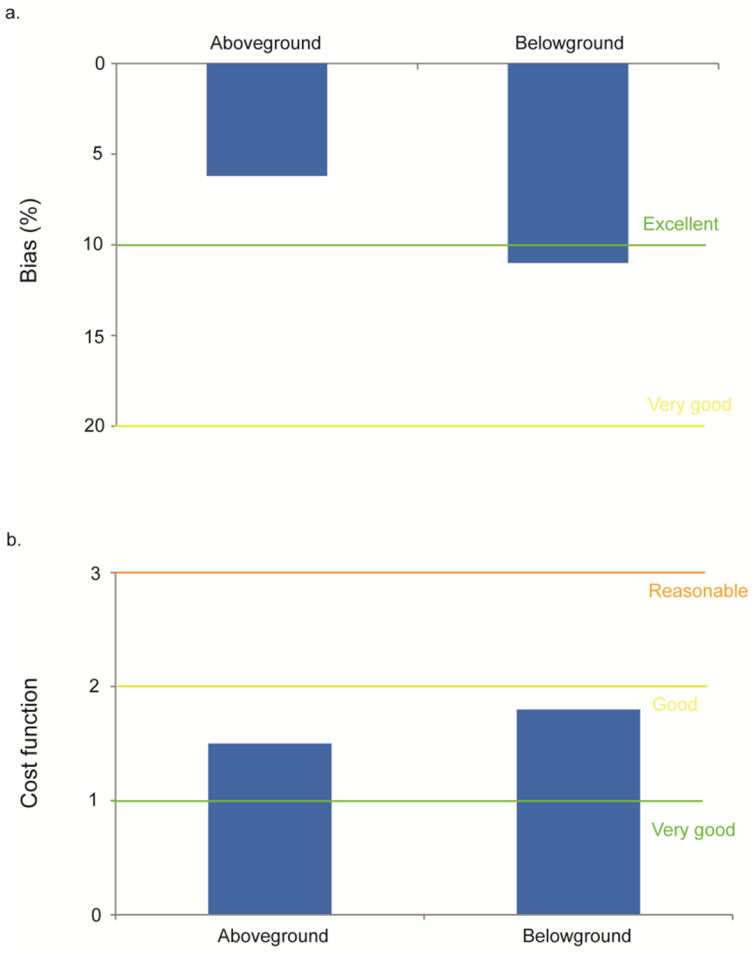

Figure 7.12 Results of computing the model performance assessment by a) percentage model bias and b) cost function.

7.6.2.2 Sensitivity analysis

The sensitivity analysis was carried out to assess the relative influence of model parameters on the overall model results. Different methodologies can be used for this purpose (e.g. Local Sensitivity Analysis – *LSA*; Global Sensitivity Analysis – *GSA*). In the present work, only a *LSA* approach was followed, by evaluating the parameter changes comparing with the reference condition (set as the baseline), and respective variations on model outputs.

A sensitivity analysis has been performed, by changing each parameter of ±10%. The model was re-launched at each variation, and a sensitivity index (*SI*, in %) was computed and averaged on the two simulations (±10%), following the methodology presented by Plus et al. (2003) (Eq. 7.3).

$$SI = \frac{100}{p \cdot n} \cdot \sum_{i=1}^{n} \frac{\left| X_i - X_i^{ref} \right|}{X_i^{ref}} \tag{7.3}$$

Where, p is variation of the parameter (±10%), n is total duration of the simulation (days), X_i is new value of the observed state variable and X_i^{ref} is reference value of the observed state variable.

The results of the LSA showed that above and belowground biomass remained stable regarding parameter variation (Figure 7.13a and b), as changes in model predictions for both state variables were generally small, always below 4%. The highest sensitivity parameter for aboveground biomass was the mortality increasing rate with ambient temperature (θ), with *SI*>3%. Other high sensitivity parameters, such as maximum aboveground mortality rate at 20ºC (LMR_{20}) and aboveground maximum growth rate (g_{max}), presented *SI* values within the range of 1-2%. The belowground biomass seemed, however, to be less stable to parameter variation comparing to the aboveground biomass. The highest sensitivity parameter for belowground biomass was the aboveground maximum growth rate (g_{max}), with *SI*>3%. Other high sensitivity parameters, such as the mortality increasing rate with temperature (θ), maximum below and aboveground mortality rate at 20ºC (RMR_{20} *and* LMR_{20}), belowground maximum growth rate (g_{max_BB}) and translocation of above to belowground biomass ($trns_{AB\_BB}$), presented *SI* values within the range of 1-3%. The remaining parameters showed lower sensitivity (*SI*<1%).

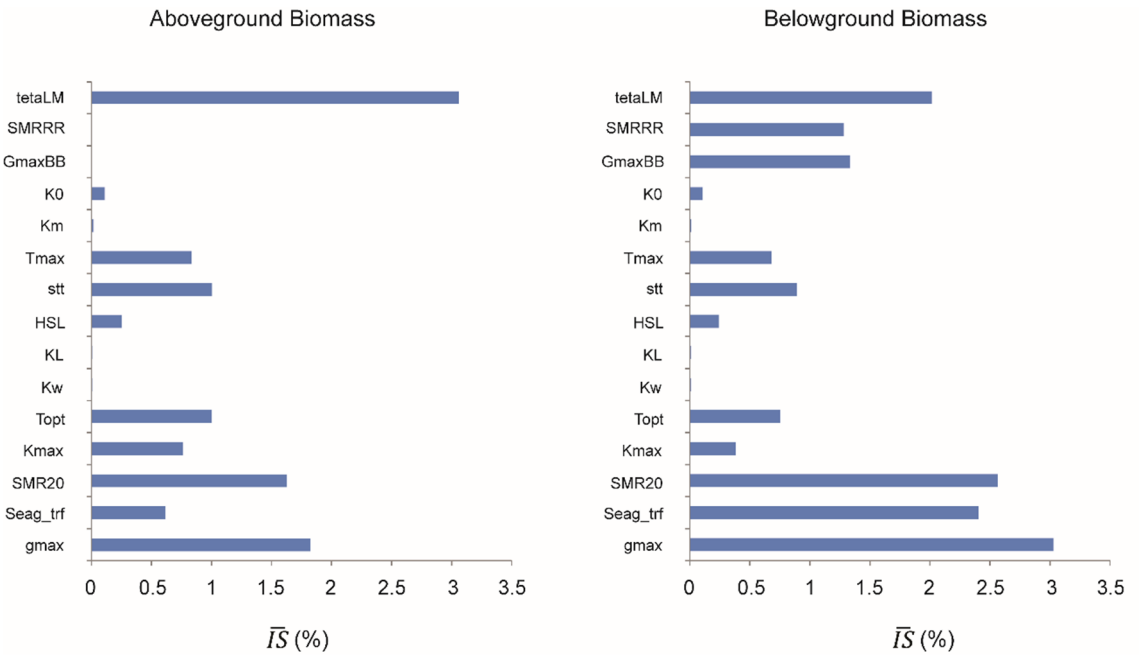

Figure 7.13 Averaged Sensitivity Index (SI) for a) aboveground and b) belowground biomasses.

7.6.3 Desiccation add-on

The desiccation add-on module, developed and implemented in Delft3D-WAQ, within the scope of this work, aimed to address the periodic air-exposure conditions during low tide, occurring at intertidal seagrass meadows. Similar to the seagrass dynamic model, its implementation on Delft3D-WAQ took advantage of the possibility to create new substances and processes, integrating them in the water quality model.

As so, the formulations presented and described in Chapter 5 were transposed to the water quality model of Delft3D suite. The relative water content (*RWC*), defined as a state variable, depends on the air temperature and water height.

The *RWC* obtained with Delft3D-WAQ showed that the air temperature is relatively more important than the intertidal height, as even at neap tides, a higher air temperature results in higher relative water content loss of seagrass leaves, than for lower temperatures at spring tides (Figure 7.14a-c). Moreover, model results slightly overestimated the ground-surveyed results, showing a higher loss on leaves' *RWC* than actually was measured in field surveys (Figure 7.14a – red line; 13th August).

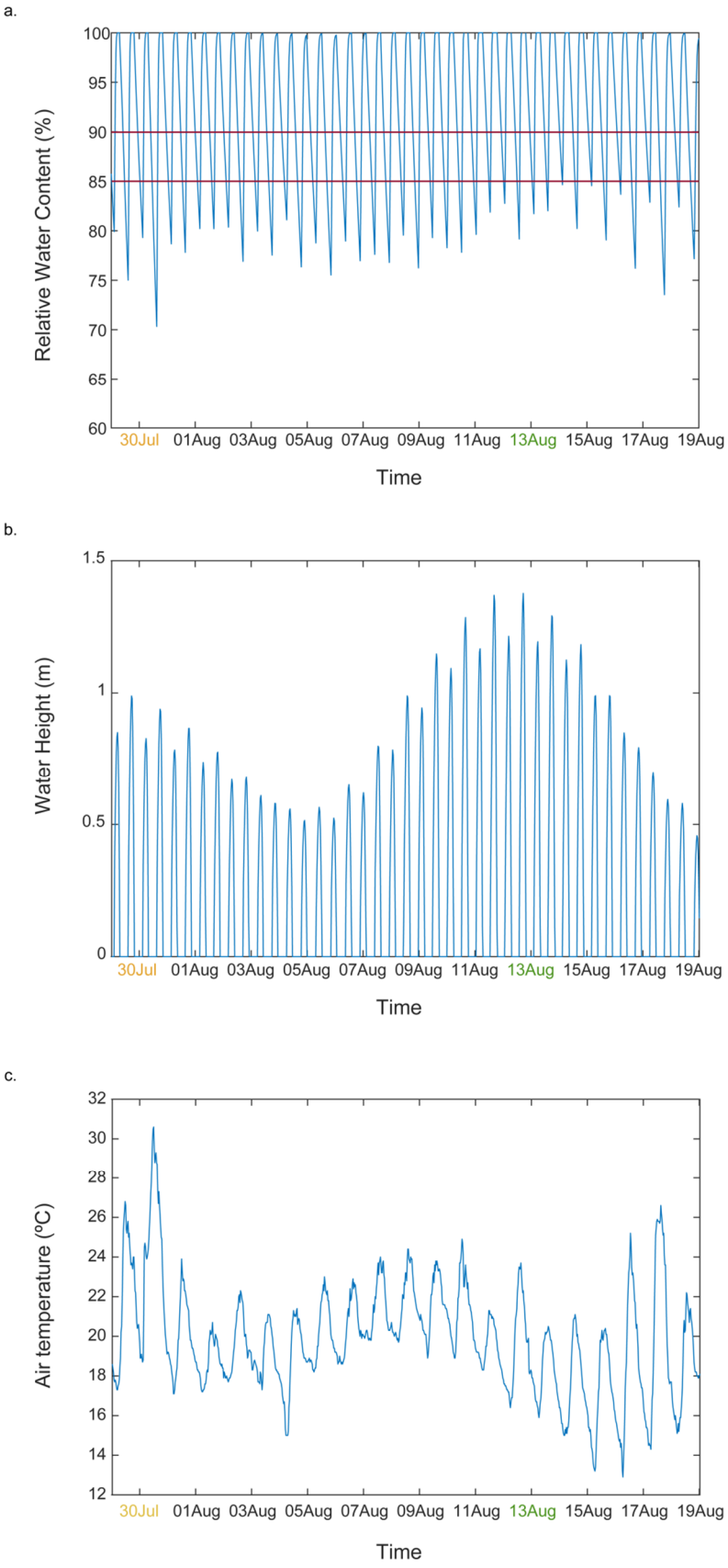

Figure 7.14 Delft3D-WAQ model results for the a) relative water content, and according to the b) water height and c) air temperature. The orange date represents the warmest day of the year, whereas the green one stands for the sampling day. Red lines define the ground-surveyed range of variation for the state variable.

7.7 DISCUSSION AND CONCLUSIONS OF THE CHAPTER

This chapter started by presenting the model inputs for both the hydrodynamic and water quality modules required by Delft3D model suite. The model inputs came from different sources, including other models (e.g. atmospheric model, soil and water-integrated model), as it stands for the best information available since observed data for the study area is scarce.

To provide further detail of the sampling location, the numerical grid was refined. The modifications over the previous configuration showed that the hydrodynamic model (Delft3D-FLOW) is still successfully able to simulate the hydrodynamic features, such as the tidal propagation along Ria de Aveiro main channels, as well as the salt and heat transport. In punctual locations within Ria de Aveiro lagoon, the model results were actually better in terms of root mean squared error and model skill, comparing with the computed differences between model results and the same time-series data from the previous configuration.

After assuring the model performance to simulate the hydrodynamics, testing the model continuity by using a conservative tracer showed that its concentration never deviated significantly from the assigned one. As so, the accuracy and stability of the simulations were guaranteed and pursuit to the water quality modelling.

The major contribution to add to the previous configuration of Delft3D-WAQ for the water quality model of Ria de Aveiro lagoon was going beyond the default substances and processes supplied in the model suite and by the creation and linking of newly developed state variables to describe and formulate seagrass dynamic model plus desiccation add-on.

The coupling of the seagrass dynamic and desiccation models (previously presented and discussed in Chapter 4 and 5, respectively) contributed therefore to address the specificities of intertidal seagrass meadows, periodically exposed to alternate air exposure and submerged periods. As both seagrass dynamics and desiccation experimental data and model features were previously discussed, this section solely highlights the most important model limitations afterwards the coupling procedure with Delft3D-WAQ. As so, although this was a comprehensive effort towards the ability of water quality models to integrate and simulate intertidal seagrass dynamics, since the majority focus on the dynamics of subtidal meadows (permanent submerged), there are several constraints that should be later addressed and fulfilled in future works.

The developed model does not include a comprehensive description of *Z. noltei* physiology, i.e. the internal nutrient dynamics. Although these component would complete the model, it was not prioritised due to the assumption that in Ria de Aveiro *Z. noltei* populations are not limited by nutrients (please see Chapter 2). Different inorganic nutrients, namely nitrogen and phosphorous, are required for seagrass growth. The seagrass morphology, differentiated by above (leaves) and belowground (roots and rhizomes) organs, generally exhibit different temporal N-content patterns, pointing to different strategies of nitrogen storage and use (Kraemer and Mazzella, 1999). Moreover, not only seagrasses optimise the use of nutrients by

different mechanisms, such as nutrient resorption, use of porewater nutrients and storage, but also their requirements are estimated to be 8-50 times less nitrogen and 1.5-100 times less phosphorous for daily growth than macroalgae or phytoplankton, respectively (Duarte, 1995), enhancing its potential adaptation of growing in nutrient-poor environments.

Phosphorous limitation of seagrass growth has been widely demonstrated in carbonate sediments (Perez et al., 1991), but as *Z. noltei* often grows in organic sediments (rich in nutrients due to the mineralization of organic matter), they are seldom limited by nutrients (Greve and Binzer, 2004). Even though some *Z. noltei* models already comprise internal nutrient dynamics (e.g. Kenov, 2014; Kenov et al., 2013; Plus et al., 2003), and therefore the mentioned studies would be valuable starting points for further improvements to the current configuration. This would also enable to prospect the viability of more sandy sediments for seagrass restoration. To do so, the other requirement of the seagrass model developed in this study that entails further developed and to be included is the link of seagrass-sediment interactions. Among other abiotic factors required, a suitable substratum where rhizomes can elongate and roots can fasten is mandatory for seagrass thriving. *Z. noltei* usually grows at soft sediments with higher percentage of fines sediment (Valle et al., 2011). These interactions are however far more complex than exclusively sediment grain size characteristics, but rather involve establishing dynamic exchanges and (positive or negative) feedback relations between sediment and seagrasses.

In one way, sediments can limit or inhibit seagrass colonization and growth if containing toxic materials or have some physical property that reduces growth. However, on the other hand, sediment may also provide the nutrients required to the photosynthetic part of the plant, by the root-rhizome system (Zimmerman et al., 1987).

Conversely, seagrasses are ecosystem engineers and so are able to change the vicinity sediment profiles, through feedbacks that improve abiotic conditions that favour seagrass growth (Hu et al., 2015; van der Heide et al., 2012). In fact, increased lability of seagrass leaf detritus can enhance concentration and quality of organic matter in the sediments, and together with nitrogen content, it may stimulate ammonium production (and nitrogen recycling), through metabolism of the organic matter, part of which may then become available for seagrass growth (Zimmerman et al., 1987). Moreover, the oxygen produced during photosynthesis may be pumped to the root system and consequently to the surrounding sediment, re-oxidizing sulfides and other porewater and solid constituents in seagrass rhizosphere (Eldridge and Morse, 2000).

The described complexity on the dynamics between seagrass-sediment interaction and therein feedback, highly increase the challenges for pursuing process-modelling integration in the context of this study, even if few studies were conducted to address generic geochemical modelling linked to seagrass meadows (Eldridge and Morse, 2000; Zaldívar et al., 2009). Therefore, further work is required to include the influence on and by seagrasses on sediment

environment, in order to improve this feature in the seagrass biological model, and enable a more realistic application, i.e., to reduce constraints and uncertainty.

Regarding the model results, the simulation of the aboveground biomass was overall very good, with the exception of the summer months. The simulation of the belowground biomass was only fair, which points out for some sort of misrepresentation at both process-level and timescale, but also for the need of widening the ground-surveyed dataset to carefully address the spatial and temporal variability of *Z. noltei* biomass in Ria de Aveiro lagoon (previously discussed in Chapter 3).

An initial assessment on model performance used three different methodologies of error statistical methods and sensitivity analysis. One out of the three methodologies used (i.e. model efficiency) pointed out to no skill of model results, for both the above and belowground biomass. As it measures a ratio of the model error to the variability of data, the squaring of the error rewards a good fit and punishes a poor fit (Allen et al., 2007), showing to be highly sensitive to extreme values, which is not desirable due to the greater variability of the ground-surveyed data gathered throughout the present study (Legates and McCabe, 1999).

On the contrary, the other two remaining methods (percentage model bias - sum of model error normalized by the data; cost function - indicative non-dimensional value that quantifies the difference between model results and measurement data), pointed for opposite conclusions, presenting respectively excellent and good model performance for aboveground biomass, and very good and good for belowground biomass. The formulation of these two indices diminishes the influence of extreme values comparing with the model efficiency one (Allen et al., 2007).

As so, to accurately conclude about the model performance, computing additional indices may be valuable to complement the followed approach, such as skewness and receiver operator characteristic curve *(ROC*), although extensive datasets are required for valid results. In fact, to boost the practical application of the model results obtained in the scope of this work, a more effective evaluating and interpreting model performance would provide more accurate information to potential communicate to stakeholders and decision-makers on the model's intended use. Therefore, rather than only evaluating initial model performance, evaluating outliers and extremes in observed values, compute estimations on uncertainties in both observed and predicted values, and re-evaluating model performance considering accuracy, precision and hypothesis testing would certainly comprise an extended and comprehensive approach (Harmel et al., 2014).

The assessment of model sensitivity to controlled variations on each parameter showed that, for both above and belowground biomass, the parameters linked with ambient temperature are overall more sensitive, which may be due to the exponential-type formulations of this factor. This result is in agreement with those found by Plus et al. (2003), although those authors had substantial higher *SI* values and variability range (*SI* of 5-11%) than the ones of the present work (*SI*<4%). Furthermore, the findings of this study partially corroborate those found by Kenov et al. (2013), pointing out the aboveground mortality rate (for both above and belowground

biomass state variables) and translocation of aboveground to belowground biomass (for belowground biomass state variable), as high sensitivity parameters.

Summing up, the sensitivity analysis highlights the need of accuracy for parameters related with the effect of ambient temperature in seagrass mortality, maximum growth rate and translocation coefficient between above and belowground organs.

Regarding the model results for desiccation, expressed in terms of *RWC* (relative water content), the model results slightly overestimated the leaves' water loss, which may be related to not considering the shading effect on the minimization of water evaporation. Moreover, the seagrass relative water content in this work only depends from air temperature and water height, though abiotic factors like air humidity and wind speed are essential to the intertidal seagrass dynamics during the air-exposure periods. As so, more comprehensive field surveys should consider this to improve the desiccation add-on produced in the present study.

As final remarks of this chapter, it is important to highlight that, in spite of the acknowledged limitations, namely in terms of seagrass-sediment interactions and internal nutrient dynamics, the model fairly simulated the seasonal above and belowground dynamics.

Future work may focus on complementing and adding new state variables and respective processes to better describing the dynamics of intertidal seagrass meadows. Furthermore, and considering the outcomes of this work, building a longer dataset on ground-surveyed-data, namely those found to present high sensitivity in the model, would be a major asset to improve the current model application, as well as widening the diversity of suitable model performance assessment techniques to complement the present approach.

Chapter 8

SCENARIOS AND APPLICATIONS

This chapter builds upon the previous established assumptions, i.e. that *Z. noltei* population is not limited by nutrients and intertidal mudflats (minimum of about 21% of fine grain sized sediment) are suitable to maintain a well-established population. It presents an exploratory approach of the model described throughout the previous chapters. It selects a set of modelled descriptors suitable for characterising areas with favourable conditions for the presence of seagrass. Each of these descriptors is then scored from non-favourable to highly favourable according to literature thresholds. An exploratory index is proposed to aggregate these scores and its fitness is validated against ground-surveyed data (not produced in the scope of this work).

The potential effects of extreme events, already recorded in Ria de Aveiro, on intertidal seagrass meadows, such as extreme river flows and heat waves were also simulated in this chapter and presented through changes in water velocity and salinity (for extreme river flows scenario) and alterations in the ambient temperature limiting function of seagrass growth (for heat wave scenario).

Assuming that at Ria de Aveiro *Zostera noltei* population mostly undergo vegetative propagation, i.e. sprouting repeatedly from its rhizome, and therefore with limited genetic variability, a set of simulations to prospect possible effects of climate change addressed different scenarios for the end of the century. This was done by forcing the model with the projections of Representative Concentration Pathways (RCPs), RCP 4.5 and RCP 8.5. The aim was to ultimately assess a relative potential decrease of up-to-date areas colonised with seagrasses, under the viewpoint of multiple stressors scenarios. Therefore, projections to the end of the century are not considering genetic variability and natural selection. Results must be interpreted with caution, as a population with genetic variability is more likely to survive as a species in a changing environment, than a species with limited variability. This means that the worst case scenario, i.e. limited genetic variability, was considered.

8.1 RATIONAL

The general applicability of numerical models allows the investigation of hypothetical scenarios, supported by the abovementioned assumptions. As so, three different research questions supported the followed methodology to explore the features of the model presented throughout this work.

Firstly, *how selected model outputs may explain the current spatial distribution of seagrass meadows in Ria de Aveiro lagoon?* This involved the selection of model outputs that support the description of habitat suitability for the presence of seagrass *Z. noltei* and which outputs are determinant of seagrass growth and distribution, including physical, chemical and biological properties (Table 8.1).

Hydrodynamic regimes highly influence the physical stability of seagrass beds, overall ecology and sedimentation rates (van Keulen, 1998; Lanuru et al., 2018); sediment environment conditions the suitability of benthic habitats for seagrass establishment and growth, namely through grain size of sediment particles and intertidal height (Valle et al., 2011); bottom shear stress, illustrate a complex interaction between water and sediment layers and also contributes to influence seagrass dynamics (Ganthy et al., 2015). Seagrass growth, survivorship and distribution highly depend on salinity regimes (Lirman and Cropper, 2003), light and ambient temperature. For intertidal seagrasses, the *RWC* also performs an important role for its thriving (this work, Chapter 5).

The second research question of this chapter, *what are the expected effects on seagrasses of Ria de Aveiro to extreme events?*, was motivated by the fact that extreme events, such as extreme river flows and heat waves, are expected to occur at short timescales and to become more frequent and to be intensified in the near future, under a climate change context.

The third research question was *what is the decline prospect, assuming the worst case of a population with limited genetic variability, of the areas presently colonised by seagrasses, under distinct climate change projections?* In fact, the current global warming trend is evident through

Table 8.1 Layers of information for mapping potential favourable areas for seagrass restoration.

Layer	Descriptor
Hydrodynamics	• Water velocity (depth averaged – 2D)
Sediment	• Grain size (in terms of fines %)
Water Quality	• Limiting functions of seagrass growth (i.e. light, space, air/water temperature) • Salinity
Other	• Bottom shear stress (*BSS*) • Intertidal height • Relative water content (*RWC*)

an unprecedented global rise of air temperature, mostly driven by increased emissions of carbon dioxide and other anthropogenic-originated greenhouse gases into the atmosphere. As result, much of this increased heat and concentration of greenhouse gases is absorbed by the oceans, contributing to its acidification and warming, which drives to a seawater thermal expansion, glacier melting and ultimately to global mean sea level rise. As so, this panoply of impacts of global climate change is important to address, as it is expected to exacerbate effects of natural and anthropogenic drivers of seagrass decline, through the complex interaction of multiple stressors, such as sea level rise, increase air temperature and radiative forcing (Duarte, 2002). The effects of the climate change on seagrass meadows are prospected by a set of scenarios, with the atmospheric and oceanic forcing built according to the Representative Concentration Pathways (*RCPs*) described in in the *IPCC* 5th Assessment Report.

8.2 METHODOLOGY

For this exercise, the model setup used the parametrisation validated in Chapter 7, including wind forcing, river flow from Vouga, Antuã, Boco, Cáster and Mira rivers, and the same heat flux model (Configuration #2). Moreover, it also considers the same values used in the final calibration run of the seagrass seasonal dynamics, including the same computed model substances and process parameters (Configuration #2).

8.2.1 Suitable areas for *Z. noltei* restoration

To give response to the first research question of this chapter, *how selected model outputs may explain the current spatial distribution of seagrass meadows in Ria de Aveiro lagoon?*, a year-long numerical simulation was run for the correspondent period of the field-surveys and used the model configuration previously summarised for Delft3D-FLOW and Delft3D-WAQ (cf.Table 7.2 and 7.3).

The selection of model outputs included descriptors known to condition seagrass growth and distribution, such as physical, chemical and biological properties (cf. Table 8.2), with the following caveats for the intertidal height and sediment grain size: i) the intertidal height derived from the topo-hydrographic data used to generate the bathymetry and; ii) sediment grain size, exclusively represented by the percentage of fine particles in the sediment matrix, resulted from a linear interpolation of the spatially discrete data coverage gathered by Rodrigues et al. (2011), to obtain a continuous coverage of sediment grain size distribution throughout the lagoon.

As water velocity and bottom shear stress increase, the conditions for potential seagrass establishment become worsen. For the generality of the remaining descriptors however, their increase leads to the improvement of conditions for seagrass growth. Thus, for water velocity

and bottom shear stress, the maximum value at each grid cell along the year-long simulation was taken, while for the remaining descriptors the minimum value was kept. A matrix with the exact grid dimensions was produced for each descriptor with the corresponding year-long estimation.

Furthermore, four different scores were attributed, ranging from non favourable (score: 1) to highly favourable conditions (score: 4), set according to the criteria found in the literature for each factor (Table 8.2). This methodology produced a spatially distributed map for each descriptor according to its suitability for seagrass growth.

To create an aggregated map of all descriptors, the statistic mode of the scores of each descriptor was computed for each grid cell, illustrating the potential holistic habitat suitability for seagrass presence. An initial approach assumed the same relative contribution of each descriptor, without any specific data ponderation. This prospective map was qualitatively validated with remote sensing and aerial photography observations of seagrass distribution presented in previous works (Sousa et al., *submitted*). The qualitative information of

Table 8.2 Criteria used to qualitatively classify the selected descriptors according to the habitat suitability for seagrass presence.

Descriptors	NF	PF	MF	HF	Reference
Water velocity (m s^{-1})	>0.35	0.10-0.35	0.01-0.10	<0.01	Peralta et al. (2006)
Fines (%)	<15	15-30	30-50	>70	This work van Lent et al. (1991)
F(L)	<0.25	0.25-0.50	0.50-0.75	>0.75	Attempt
F(S)	<0.25	0.25-0.50	0.50-0.75	>0.75	Attempt
F(T)	<0.25	0.25-0.50	0.50-0.75	>0.75	Attempt
Salinity	<0.5	0.5-5	5-14	>14	Sousa et al. (2017a) Charpentier et al. (2005)
BSS (N m^{-2})	>2.695	0.949-2.695	0.261-0.949	<0.261	Ganthy et al. (2015)
IH (m)	>3.54 <0.38	0.68-3.54	0.58-0.68	0.38-0.58	This work Valle et al. (2011)
RWC (%)	<40	40-60	60-80	>80	This work Björk et al. (1999)

NF – not favourable; PF – poorly favourable; MF – moderately favourable; HF – highly favourable; *F(L)* – light limiting function; *F(S)* – space limiting function; *F(T)* – air/water temperature limiting function; *BSS* – bottom shear stress; *IH* – intertidal height; *RWC* – relative water content

both the observed (presence vs absence) and prospective suitability (ranging from 1 – not favourable – to 4 – highly favourable) was crossed to validate the habitat suitability by the model, following the criteria of Table 8.3 and mapped. The criteria for cross-validation mapping considered that when the observed data points to seagrass presence and the predicted suitability ranges from moderate to highly favourable, the assigned score is maximum (i.e. score: 4), whereas if the observed data is absent but the predicted suitability is still moderate to high, the assigned score is 3. Where observed data pointed out for seagrass presence but the predictable suitability is not or poorly favourable, the assigned crossed-validation score is 2. For observed areas without seagrasses and where the predicted suitability is nil or low, the minimum cross-validation was assigned (score: 1).

Moreover, an alternative approach explored the possibility of excluding descriptors, i.e. for each factor, not favourable and poor favourable conditions primarily excluded the possibility for seagrass presence. This was discussed in terms of the relative area that actually currently exists but is not prospected by the model using the selected model outputs.

Table 8.3 Criteria for cross-validation mapping.

Observed	Predicted suitability	Cross-validation score to map
Present	moderate to highly favourable	4
Absent	moderate to highly favourable	3
Present	not favourable to poorly favourable	2
Absent	not favourable to poorly favourable	1

8.2.2 Extreme events

To give response to the second research question of this chapter, *what are the expected effects on seagrasses of Ria de Aveiro to extreme events?,* two different scenarios have been explored: the potential changes in the suitability of seagrass habitat to an extreme river flow event and in seagrass growth rate to a heat wave during spring tidal conditions.

8.2.2.1 Extreme river flow

A construction of an extreme river flow scenario for Antuã, Boco, Cáster, Mira and Vouga rivers considered the highest peak discharges, statistically computed by Lopes (2016) for a return period of 100 years, and it is illustrated in Figure 8.1.

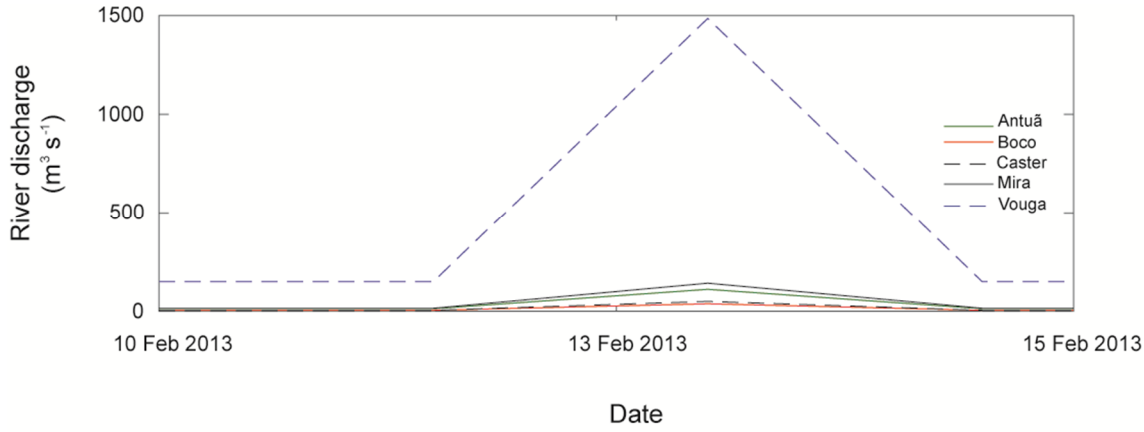

Figure 8.1 Fluvial discharges for the freshwater inputs in Ria de Aveiro lagoon (adapted from (Lopes, 2016)).

The model was run during 5 days from the 10th-15th February 2013, as the climatological analysis for river discharge (Appendix 5) showed that February is generally the rainiest month of the year and this period coincides with neap tides, as it is expected to have less tidal influence.

The river discharge initially was set on the baseline value considering the monthly mean previously computed by the climatological analysis (section 7.4.3 and Annex 5). Afterwards, the river discharge was increased at a constant rate until reaching the peak, followed by a return to the baseline flow (cf. Figure 8.1).

Solely the differences between the water velocity and salinity from the reference run (for the same period of the extreme river flow scenario) and the extreme river flow scenario were computed, as the sediment compartment is not linked yet to the seagrass module developed in this work. The normalised anomaly between the reference and the extreme river flow scenario was computed and mapped for each descriptor. Moreover, the criteria used for score attribution presented in Table 8.2 was also adopted in this section for the water velocity and salinity descriptors. The difference between the scores assigned in reference scenario and extreme river flow scenario was also computed and mapped, to assess potential differences in habitat suitability for seagrass presence during the extreme event.

8.2.2.2 Heat wave

The construction of the heat wave scenario considered the definition of HWDI (heat wave duration index), which describes a heat wave with an annual count of days with at least 6 consecutive days, where the maximum air temperature corresponds to the average maximum plus 5º C (Alexander et al., 2006). As the average warmest temperature in the study area is 25 ºC (Yr, 2018), a hypothetical heat wave scenario was set oscillating around 30 ºC and forced during 6 days (Figure 8.2, red line).

The period under the effect of the heat wave was set between the 25th-31st July 2013, as it verifies different criteria: it includes the warmest day registered in that year (31st July); corresponds to spring tide conditions; and the low tide matches with late morning and early noon (11h30-13h00). Therefore, this period intents to reflect the major harsher conditions met by seagrass meadows exposed to air, during low tide periods. Effects of a heat wave on seagrass meadows have been assessed through changes in ambient temperature limitation function and furthermore in seagrass growth rate.

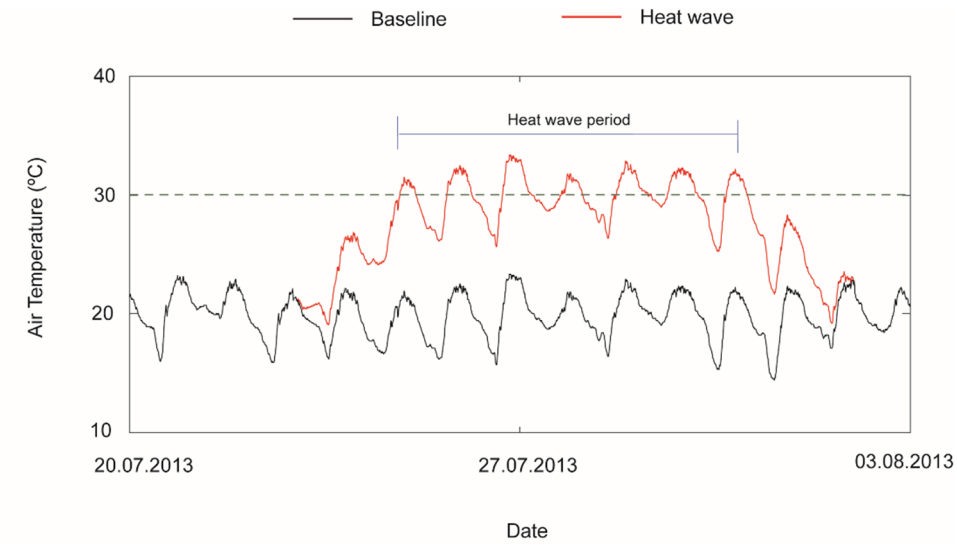

Figure 8.2 Plot of the air temperature used to simulate a hypothetical heat wave scenario.

8.2.3 Prospective effects of climate change in intertidal seagrass meadows of Ria de Aveiro

To address the third research question of this chapter, *what is the prospective decline of up-to-date areas colonised with seagrasses in Ria de Aveiro, under distinct climate change projections and the abovementioned assumptions*, a set of different scenarios were built and run to investigate potential changes on seagrass spatial distribution in Ria de Aveiro lagoon. These scenarios, built according to the projections of the 5th Assessment Report from the IPCC, were based on the projections of Representative Concentration Pathways (*RCP*s), *RCP* 4.5 and *RCP* 8.5, considering sea level rise, air temperature increase and probable changes in radiative forcing.

The results are presented towards a prospective and qualitative analysis on the effect of climate change scenarios on the spatial distribution of *Z. noltei* within Ria de Aveiro lagoon. Discussion of these scenarios and applicability of results, e.g. for management proposes, is restricted to the established assumptions, i.e. mudflats are suitable for well-established *Z. noltei* populations; the population is not limited by nutrients; the population undergo vegetative propagation, having low genetic variability. This means that extrapolations to other conditions require the development of additional model components, as discussed in Chapter 7.

8.2.3.1 Model inputs

This study simulated two different future warming scenarios, according to the projections of the 5th Assessment Report from the *IPCC* for the radiative forcing of 4.5 W·m^{-2} and 8.5 W·m^{-2} (RCP 4.5 and RCP 8.5, respectively), at the end of the 21st century (Appendix 6).

At the oceanic open boundary, the sea surface salinity (*SSS*) and sea surface temperature (*SST*) were forced by *EC-EARTH*, a Global Circulation Model (*GCM*) from CMIP5 project (http://cmip-pcmdi.llnl.gov/cmip5/) (Appendix 6), which was bilinearly interpolated on a 1º x 1º grid, following the methodology used by deCastro et al. (2016).

The aforementioned *GCM* forced a Regional Circulation Model (*RCM*), *RACMO22E*, producing the atmospheric forcing required to run the model. This *RCM* was gathered from the *CORDEX* project (http://www.cordex.org/) and present a horizontal resolution of 12.5 km.

The sea level rise (*SLR*) for both RCP 4.5 and RCP 8.5, derived by Lopes (2016) for the study area, and based on the 5th Assessment Report from the *IPCC*, pointed out for an increase of 0.47 m and 0.63 m, respectively. The increase of air temperature assigned for RCP 4.5 and RCP 8.5 were, respectively, 1.8 and 3.7 ºC.

Similar to the reference scenario, the input of freshwater volume and temperature (Figure 8.3 and Appendix 5) were taken from the SWIM model (SWIM, Soil and Water Integrated Model, Potsdam Institute for Climate Impact Research, www.pik-potsdam.de), obtained in the scope of LAGOONS Project (lagoons.web.ua.net) (Stefanova et al., 2015).

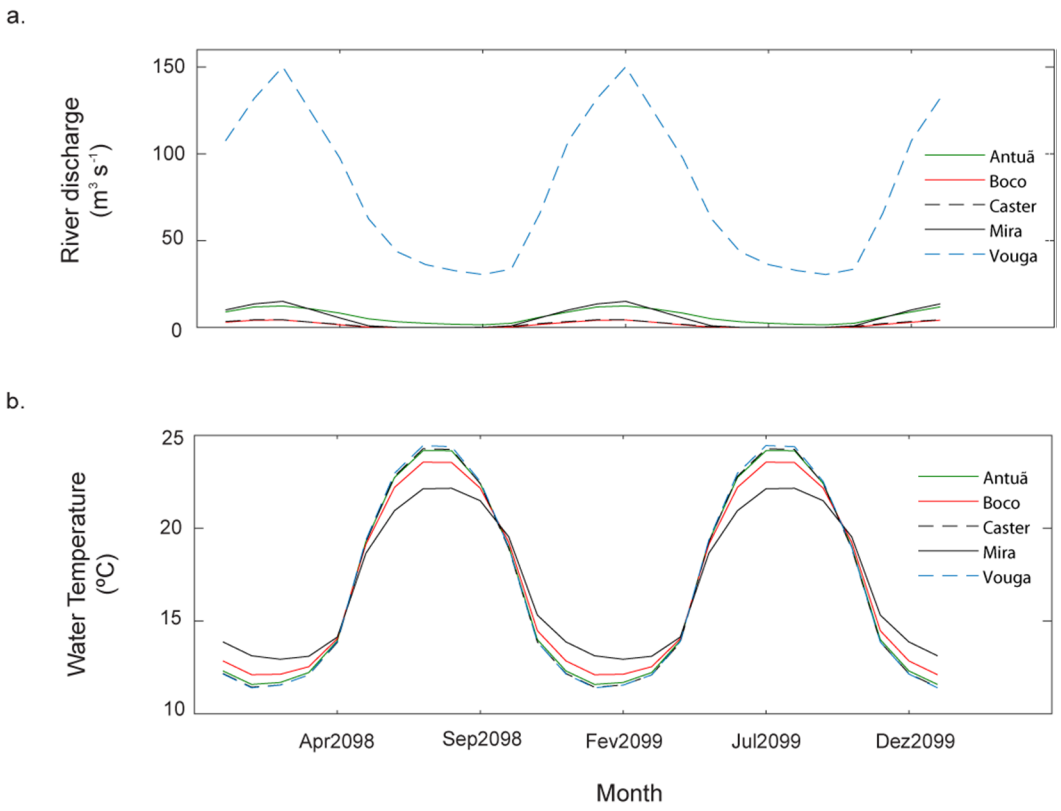

Figure 8.3 Properties imposed at river boundaries to force Delft3D-FLOW and Delft3D-WAQ, at climate change scenarios - a) river discharge (m^3 s^{-1}), b) water temperature (ºC) .

8.2.3.2 Scenarios to prospect potential changes in spatial distribution of Z. noltei in Ria de Aveiro lagoon

An overall of fourteen scenarios have been constructed (Table 8.4), addressing both the projections for a less hazardous scenario (i.e. *RCP* 4.5) and a more pessimistic (i.e. *RCP* 8.5), to ultimately characterise the qualitative effects on seagrass meadows of Ria de Aveiro and conclude about the suitability of present colonised areas to seagrass restoration.

The construction of the scenarios considered an assessment of the isolate effects of sea level rise (Sc1 and Sc2), ambient temperature (Sc3 and Sc4) and light (Sc5 and Sc6), for both *RCP*s. Furthermore, the scenario complexity increased by a combined approach between two stressors, namely SLR+ambient temperature (Sc7 and Sc8), SLR+light (Sc9 and Sc10) and ambient temperature+light (Sc11 and Sc12). Lately, the combined effect of SLR+ambient temperature+light was also assessed (Sc13 and Sc14).

The analysis of these results preliminarily considered solely the changes in seagrass biomass at the present areas colonised by seagrasses and mapped by Sousa et al. (*submitted*).

Table 8.4 Summary of model runs to address the climate change scenarios.

	SLR		**Ambient Temperature**		**Solar radiation**	
RCP	4.5	8.5	4.5	8.5	4.5	8.5
Sc1	x					
Sc2		x				
Sc3			x			
Sc4				x		
Sc5					x	
Sc6						x
Sc7	x		x			
Sc8		x		x		
Sc9	x				x	
Sc10		x				x
Sc11			x		x	
Sc12				x		x
Sc13	x		x		x	
Sc14		x		x		x

SLR – Sea Level Rise; Ambient temperature – concerns both water and air temperature.

The results of the prospective scenarios were then classified and mapped according to areas that prospect to continue to be colonised by seagrasses, areas that only lost biomass for the most pessimistic scenario and areas that were lost for both less and more pessimistic scenarios. For each scenario, the relative percentage of areas that represent a loss of seagrass biomass was determined. By computing the cumulative percentage of lost areas for the combined scenarios and compared it with the sum of the areas lost in the isolated and originated stressor scenarios, the synergy *vs* antagonism among stressors was evaluated.

Furthermore, an additional methodology intended to prospect the overall spatial distribution of the descriptors in terms of increase, decrease and unchanged throughout the lagoon, to assess in what scenarios do they improve or reduce the suitable conditions for seagrass presence within the lagoon.

The anomalies between the reference and each scenario for each descriptor were computed, except for those descriptors previously used but that are not outputs given by the model (i.e. intertidal height and sediment grain size). These anomalies, computed in %, were normalised to the average of each descriptor for the reference condition and the minimum and maximum anomalies plotted. The relative area represented by negative, nil and positive anomalies were systematised in a contingency table, according to each descriptor and scenario.

8.3 RESULTS

8.3.1 Suitable areas for *Z. noltei* restoration

The spatially distributed maps of selected descriptors, illustrated in Figure 8.4, have been based on indicative criteria previously set and ranging between “not favourable” to “highly favourable” of suitability for seagrass growth.

Under the hydrodynamic viewpoint, the water velocity is lower for the central part of the lagoon, northernmost part of Ovar channel and mid-upper part of Mira channel, which points out these areas as the most favourable ones, if exclusively considering this abiotic factor (Figure 8.4a). According to the bottom shear stress (Figure 8.4b), solely the deepest locations of the lagoon, roughly designed as mainly navigation areas, are not suitable for seagrass presence. The uppermost part of Ovar channel presents moderate to highly favourable conditions, as opposite to the middle and southernmost areas of the same channel, it presents poor condition. At central lagoon and mid-upper part of Mira channel, the set classes for bottom shear stress range from moderate to highly favourable for seagrass presence. The salinity is highly favourable for seagrass presence at the west-central lagoon and Ovar channel, getting less favourable as the influence of freshwater sources within the lagoon increases (Figure 8.4c).

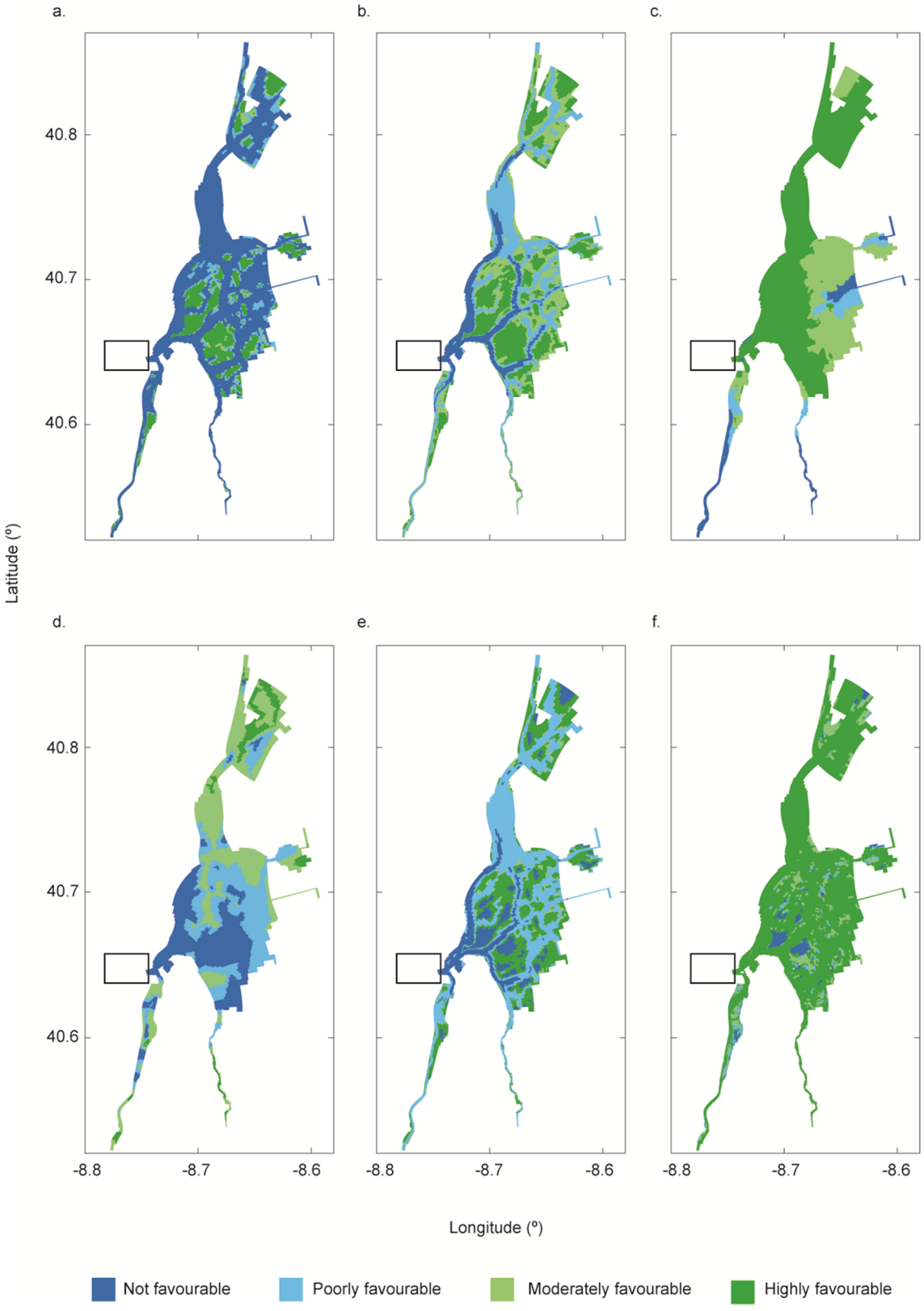

Figure 8.4 Mapping suitable conditions for seagrass presence, according to the selected descriptors: a) water velocity, b) bottom shear stress, c) salinity, d) fines %, e) intertidal height, f) *RWC* (relative water content), g) *F(S)* (space limiting function of growth), h) *F(T)* (ambient temperature function of growth limitation), i) *F(L)* (light limiting function of growth). Black rectangle: assigns the inlet of the lagoon.

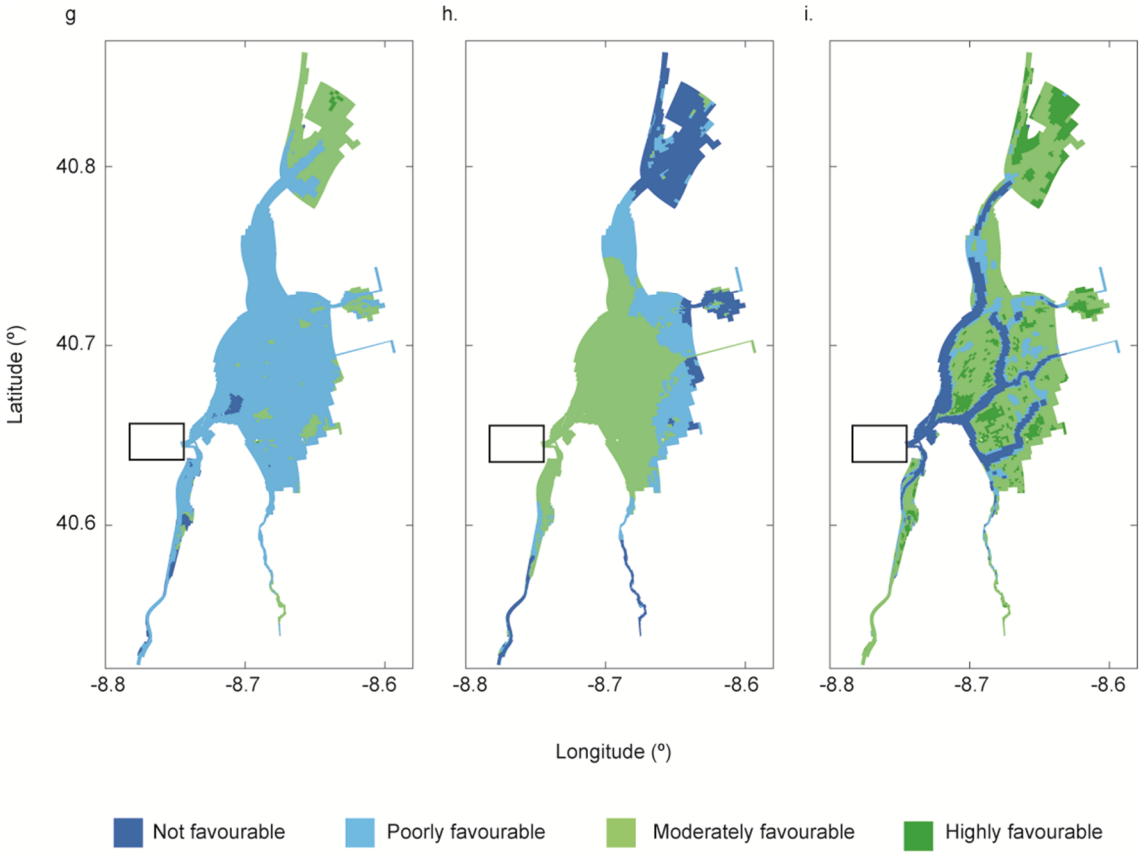

Figure 8.4 (Continued) Mapping suitable conditions for seagrass presence, according to the selected descriptors: a) water velocity, b) bottom shear stress, c) salinity, d) fines %, e) intertidal height, f) *RWC* (relative water content), g) *F(S)* (space limiting function of growth), h) *F(T)* (ambient temperature function of growth limitation), i) *F(L)* (light limiting function of growth). Black rectangle: assigns the inlet of the lagoon.

The sediment descriptor, exclusively represented by the percentage of fine particles in the sediment matrix, shows that the most favourable areas for seagrass presence occur at the head of the main channels, ranging for moderate to highly favourable conditions (Figure 8.4d). At the central lagoon, the sedimentary descriptor reveals not favourable to poor suitable conditions for seagrass presence. As the seagrass meadows of Ria de Aveiro are restricted to intertidal meadows, intertidal height is also considered (Figure 8.4e). The potential most favourable areas, under the point of view of this descriptor, are located at the central lagoon, the uppermost part of Ovar channel and mid Mira channel.

The relative water content is overall highly favourable throughout the entire lagoon, excluding the shallower areas subject to periodic exposure to air during low tide. These areas are mostly located at the central lagoon and mid-upper part of Mira channel (Figure 8.4f).

When concerning to the space limiting function (*F(S)*), the results point out to a tendency of establishment of highly dense meadows which reflects a higher limitation in terms of available space to further growth at the overall lagoon, except punctual locations at central lagoon and head of Ovar channel (Figure 8.4g). Inversely, the ambient temperature function of growth limitation (*F(T)*) shows more favourable conditions at the west-central lagoon and upper Mira channel, contrasting with the lower favourable conditions at the upper-east central lagoon and head of Ovar channel (Figure 8.4h). The light limiting function is consistent with the depth, as main channels and deeper areas present higher light limitation that shallower ones (Figure 8.4i).

A visual validation of model projections to describe habitat suitability of Ria de Aveiro lagoon for thriving of intertidal seagrass meadows with observed data provided by Sousa et al. (*submitted*), is illustrated in Figure 8.5.

The observed patches colonised by seagrasses are mostly distributed over the central areas of the lagoon and east upper-middle areas of Mira channel (Figure 8.5a).

The positive habitat suitability prospected by the model, and ranging from moderately to highly favourable for seagrass growth, overall extends through the same areas as the observed patches (Figure 8.5b). Furthermore, these results and those represented by the cross-validation map (Figure 8.5c) show that model estimations point out for further areas to be potentially fit for seagrass thriving, namely at extra areas of central lagoon and the northernmost part of Ovar channel.

A detail of the cross-validation map (Figure 8.5d), zooming in the presently colonised areas by seagrasses, shows that, of the delimited patches, very few are not simultaneously reproduced by model prospections as moderately to highly favourable conditions for seagrass growth. These areas represent 9% of the total area known to be colonised by seagrasses. When considering the hypothesis of exclusion factors, this percentage differs according to the descriptor, as shown in Figure 8.6. The relative percentage of area colonised by seagrasses during ground-surveys that are not simultaneously targeted by the model as presenting moderate to highly favourable conditions were over 9%, showing no improvements comparing with the previous approach of giving the same weight to all the selected descriptors. However, for the remaining descriptors, this primarily exclusion approach reveals a substantial decreasing in the relative percentage of the areas colonised (observed) but without predicted favourable conditions (model predictions), showing an improvement in the habitat suitability prediction for seagrass potential growth.

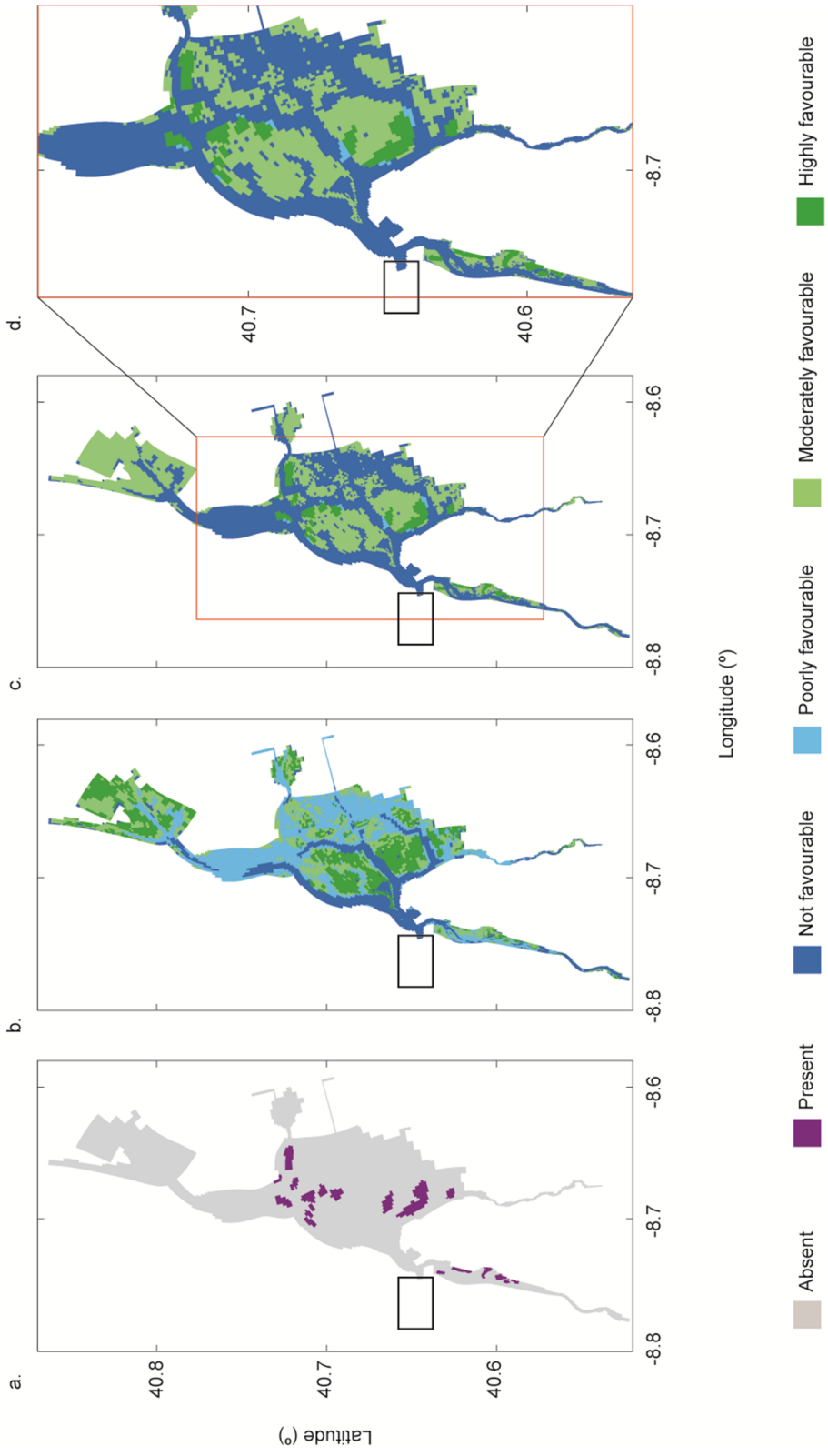

Figure 8.5 Mapping suitable conditions for seagrass presence: a) observed data of spatial distribution of seagrasses in Ria de Aveiro indicative of seagrass presence/absence; b) composite model projections for habitat suitability for seagrass growth; c) crossed-map between observed vs model projections; d) zoom-in of c) to highlight the area of interest. Black rectangle: assigns the inlet of the lagoon. Red rectangle: assigns a detail of the area of interest.

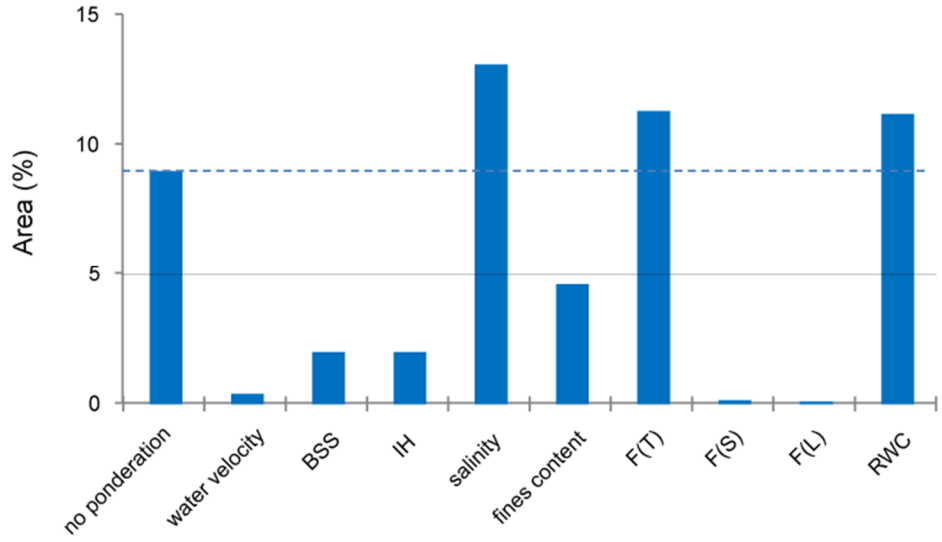

Figure 8.6 Relative areas of presently colonised seagrass meadows that are not simultaneously targeted by the model as favourable areas for seagrass growth, when excluding each descriptor. Dashed line indicates the baseline area without any ponderation of the descriptors. *F(L)* – light limiting function; *F(S)* – space limiting function; *F(T)* – air/water temperature limiting function; *BSS* – bottom shear stress; *IH* – intertidal height; *RWC* – relative water content

8.3.2 Extreme events

8.3.2.1 Extreme river flow scenario

Normalised anomalies between the reference and extreme river flow scenarios for water velocity and salinity are illustrated in Figure 8.7 (a and b), as well as the respective differences between the scores assigned according to the criteria presented on Table 8.2 (Figure 8.7c and d).

The normalised anomaly for water velocity showed more negative values nearby the river inputs, namely for Vouga River, showing that the water velocity of the reference scenario, within the simulated period, is substantially lower than the estimated for the extreme river flow scenario (Figure 8.7a).

As expected, salinity presented an opposite pattern, showing expressive positive anomalies particularly at the central part of the lagoon and north-most part of Mira channel, and therefore presenting overall higher salinity at the reference scenario than the extreme river flow scenario (Figure 8.7b).

The difference between the scores of suitability for seagrass presence, for water velocity, revealed higher values nearby the input of Vouga river (i.e. river with higher discharge within the lagoon). In the vicinity of the remaining freshwater sources considered, the differences between scores show that extreme river flow events reduce the suitability of these areas, in terms of water velocity, in about one unit (Figure 8.7c).

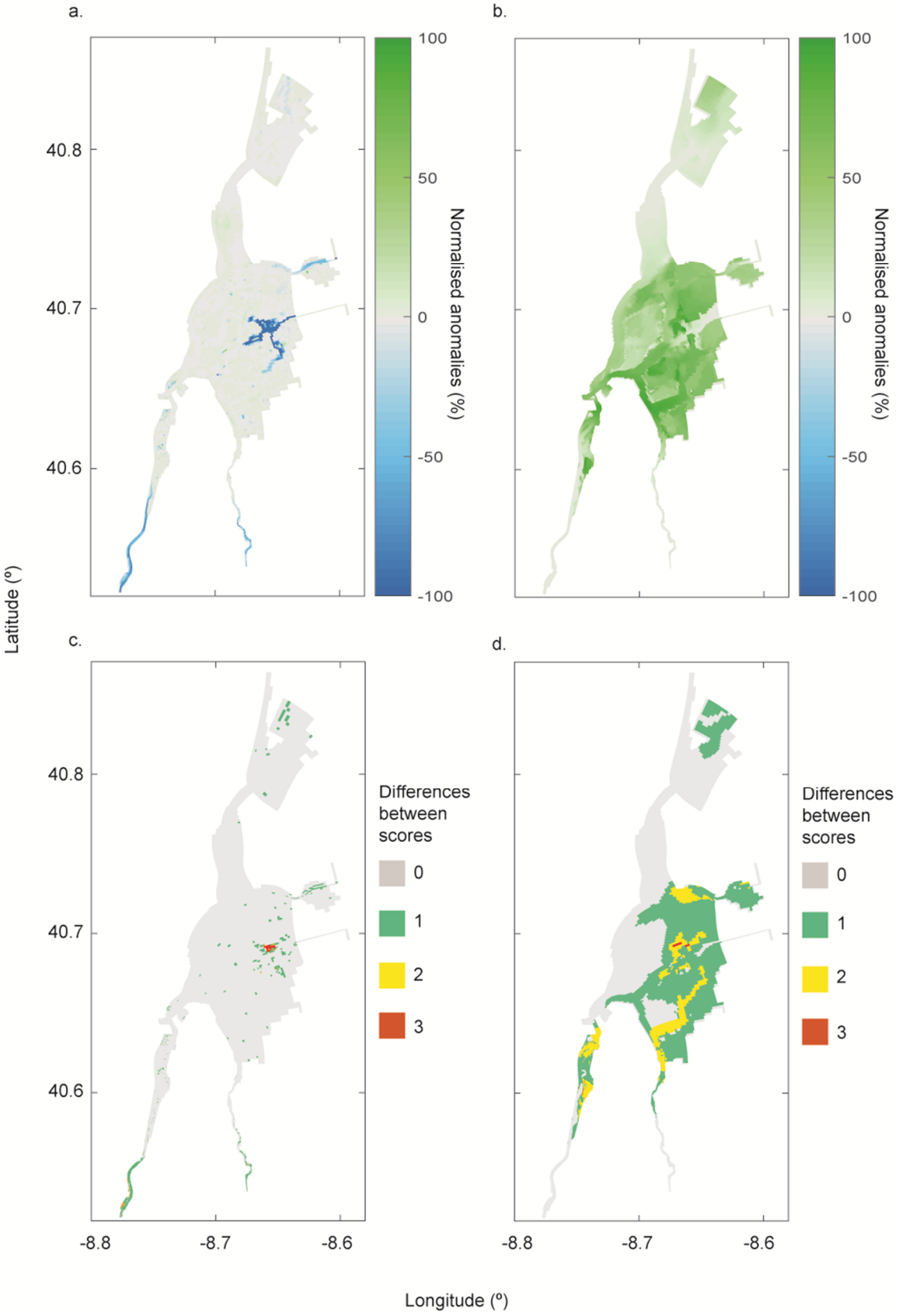

Figure 8.7 Normalised anomalies between the reference and extreme river flow scenarios for a) water velocity and b) salinity and c) and d) respective differences between the scores assigned according to the criteria of Table 8.2.

For salinity, the difference between the scores of suitability for seagrass presence is also higher nearby the Vouga river (three units), probably as a result of its high and representative freshwater discharge (Figure 8.7d).

Changes in the suitability score for seagrass presence shows to be far more notorious for salinity than for water velocity, as the differences between the scenarios are widely distributed throughout the lagoon, predominantly at the eastern-central lagoon, that presents a reduction of the suitability index for seagrass presence between one and two units.

8.3.2.2 Heat-wave scenario

The effects of heat wave, expressed in terms of changes on ambient temperature limiting function of seagrass growth (*F(T)*) and illustrated in Figure 8.8 (red line), showed that during the heat wave period there is a noticeable higher limitation (i.e. lower *F(T)* values) than during the baseline conditions (Figure 8.8, black line). Therefore, seagrass growth during the heat wave period is about 60% lower compared with the baseline situation.

The first days after imposing the heat wave were prominently more limiting than the last two days, as the first ones were closer to the peak of spring tide (22nd July) and coincident with the warmest moment of the day (noon), indicating a longer exposure period of intertidal seagrasses to air. Moreover, and as expected, the results point out that during submersion events the effects of the heat-wave are attenuated.

As the frequency and intensity of heat waves are expected to increase in the future due to climate change, this scenario clearly points out for potential damaging effects on growth of intertidal seagrass meadows, especially by means of an increase limitation due to the increase of ambient temperature.

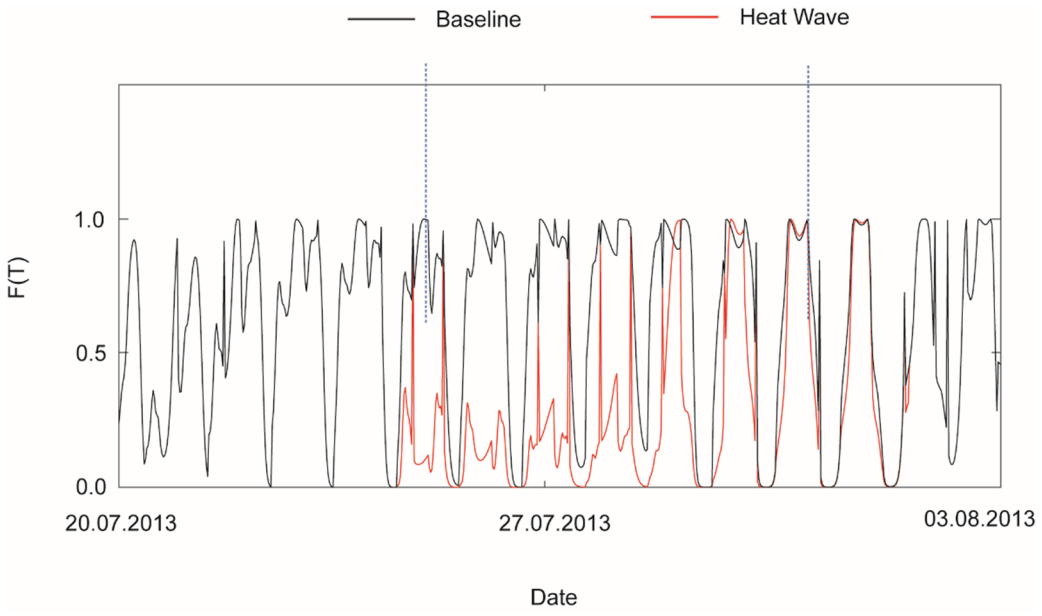

Figure 8.8 Effects of heat wave scenario on the water temperature limiting function of seagrass growth.

8.3.3 Prospective climate change scenarios

The results of prospective climate change scenarios are presented as illustrative maps of potential changes in the present areas colonised by seagrasses (Figure 8.9) and by the quantification of the respective relative loss areas to assess effects of synergy or antagonism between multiple stressors (Figure 8.10a and b).

Considering the modelling results of isolated effects of climate change features, the assessment of the isolated effect of SLR revealed that modelled prospections for both *RCP* 4.5 and *RCP* 8.5 pointed out for unchanging areas presently colonised by seagrass meadows in Ria de Aveiro and therefore the results for these two scenarios were not mapped.

The effects of individual changes on ambient temperature (Figure 8.9a) and light (Figure 8.9b) turned on a relative reduction of the colonised areas by seagrasses under the *RCP* 8.5, on about 16.3% and 12.3% (Figure 8.10a), respectively, whereas for the *RCP* 4.5 the colonised areas remained the same as the present condition. Moreover, a combined effect of light+ambient temperature drove to a remarkable relative decline of 22.7% and 46.5%, for *RCP* 4.5 and *RCP* 8.5, respectively (Figure 8.9c and Figure 8.10a).

On the other combined-effect scenarios, a joint variation of SLR+ambient temperature produced no changes in the contemporary colonised areas for *RCP* 4.5, although for *RCP* 8.5 it led to a relative 3.6% decrease compared with the current area (Figure 8.9d and Figure 8.10a). The collective influence of SLR+light produced noteworthy relative declines of seagrass colonised area (Figure 8.9e), of about 11.8% and 14.3 (Figure 8.10a), for *RCP* 4.5 and *RCP* 8.5, respectively.

At the most complex multiple stressor scenario (SLR+light+ambient temperature), the relative loss areas of seagrass meadows was the highest predicted, varying from 30.4 to 70.3% (Figure 8.9f and Figure 8.10a), for *RCP* 4.5 and *RCP* 8.5, respectively, showing that both scenarios prospect substantial negative effects on the spatial distribution of seagrass biomass.

The cumulative percentages of seagrass lost areas on multiple stressors scenarios showed no regular pattern (Figure 8.10b). For Sc7 (SLR+ambient temperature, *RCP* 4.5), the lost area is nil and equal to the cumulative percentage of respectively individual ones (SLR and ambient temperature for *RCP* 4.5 – Scs1 and 3). Solely for Sc8 (SLR+ambient temperature, *RCP* 8.5), the area lost by the multiple stressor scenario was lower than the cumulative percentage of the individual stressors (SLR and ambient temperature for *RCP* 8.5 – Scs 2 and 4), showing an antagonistic effect of the increasing sea level rise and ambient temperature. For the remaining scenarios, however, the area lost by the combined multiple stressor scenarios was always higher than the cumulative percentage of the individual stressors themselves, showing a synergy effect between the stressors.

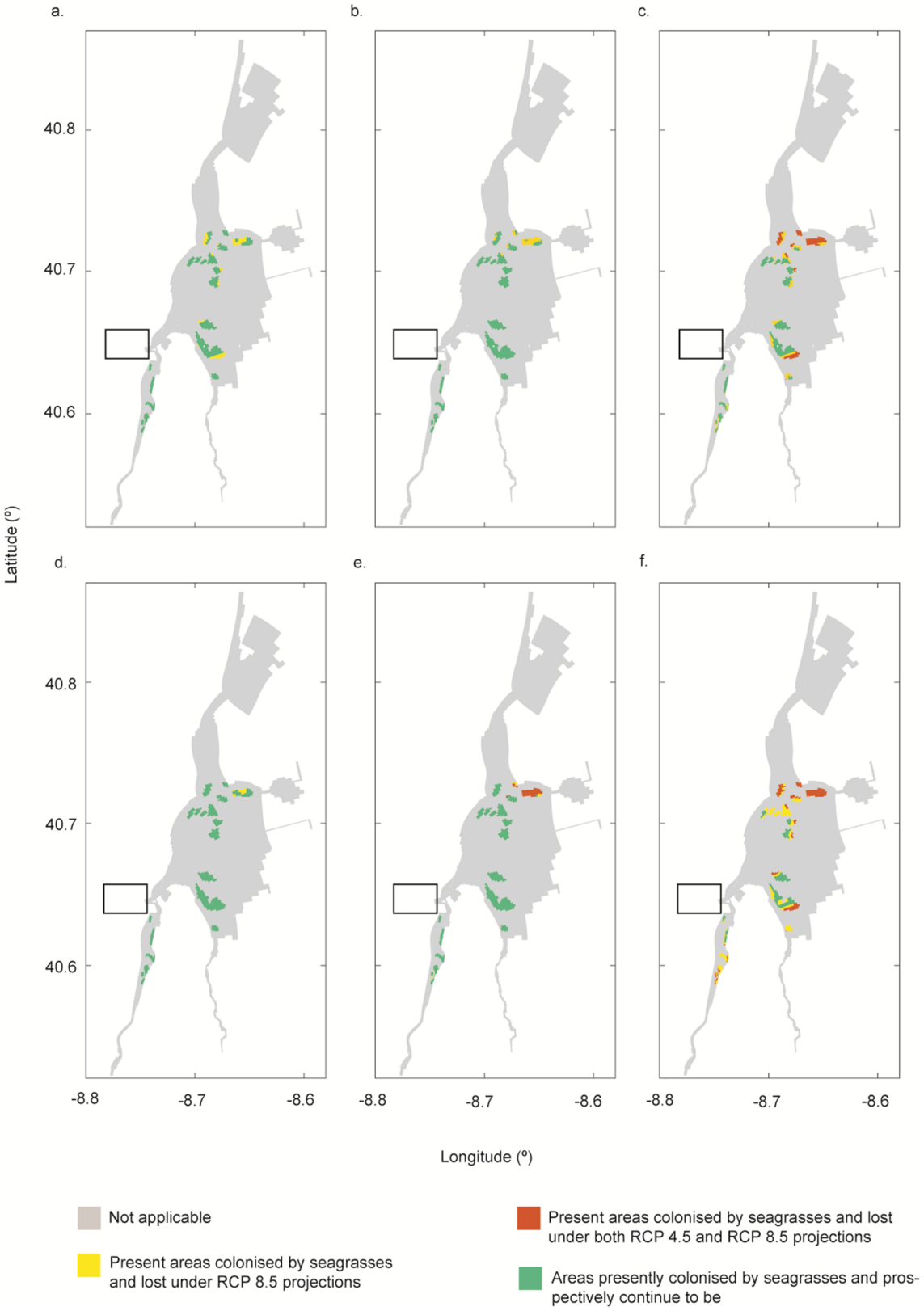

Figure 8.9 Modelled estimations for climate change scenarios - *RCP* 4.5 and *RCP* 8.5. Single parameter scenarios: a) ambient temperature; b) light; and multiple stressors scenarios c) ambient temperature and light d) sea level rise and ambient temperature; e) sea level rise and light; f) ambient temperature, sea level rise and light.

a.

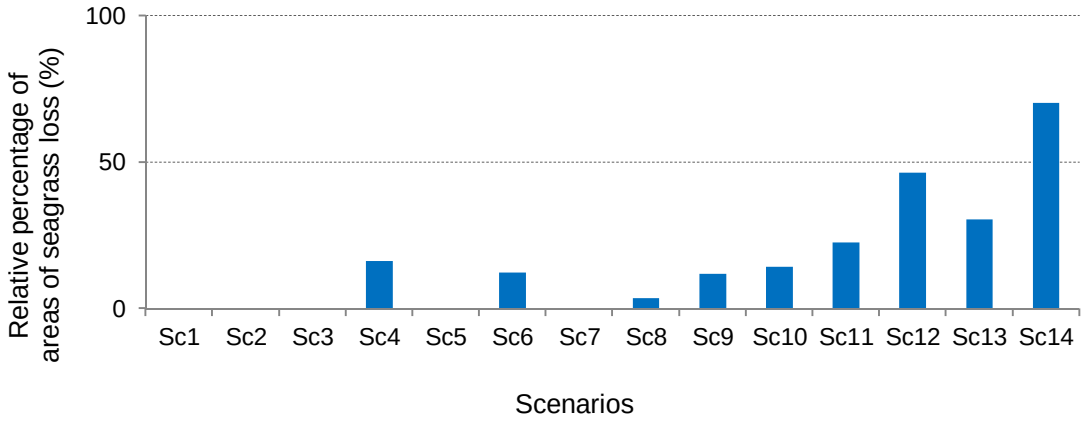

b.

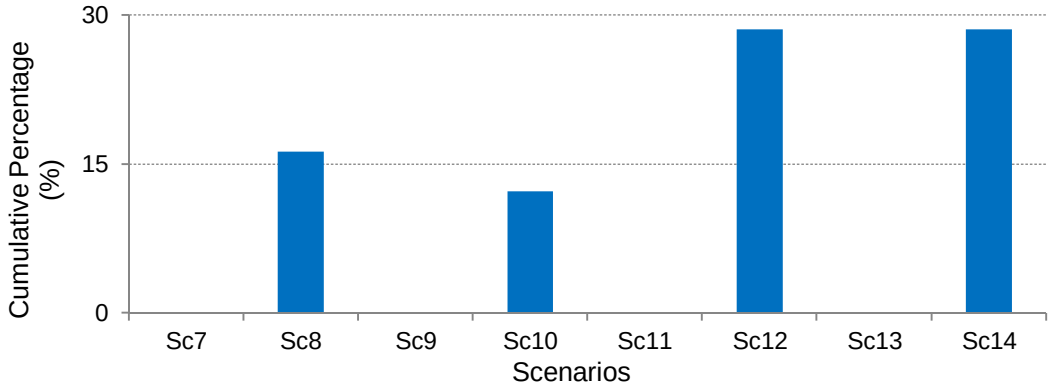

Figure 8.10 Seagrass areas loss relatively to the reference condition for a) each scenario and b) multiple stressors scenarios (combined scenarios), considering cumulative percentages of areas of seagrass loss from isolated scenarios.

The minimum and maximum normalised anomalies for different descriptors and scenarios are illustrated in Figure 8.11, and mapped in Appendix 7.

These results showed that the maximum normalised anomalies for water velocity (above 150%) occured in the scenarios with sea level rise for the *RCP* 8.5 (Scs 2, 8, 10 and 14). Moreover, the minimum normalised anomalies (below -100%) occurred for the scenarios with sea level rise, but for both *RCP* 4.5 (Scs 1, 7, 9 and 13) and *RCP* 8.5 (Figure 8.11a).

Likewise, the maximum and minimum normalised anomalies for bottom shear stress were found in the scenarios with sea level rise for both *RCP* 4.5 and *RCP* 8.5 (Figure 8.11b).

The maximum normalised anomalies (above 100%) for salinity were obtained, similarly to water velocity and bottom shear stress, in the scenarios with sea level rise (Scs 1, 2, 7, 8, 9, 10, 13, 14) for both *RCP* 4.5 and *RCP* 8.5, whereas the minimum anomalies (below -150%) were found to the combined scenarios of ambient temperature+solar radiation, for both *RCP*s (Figure 8.11c).

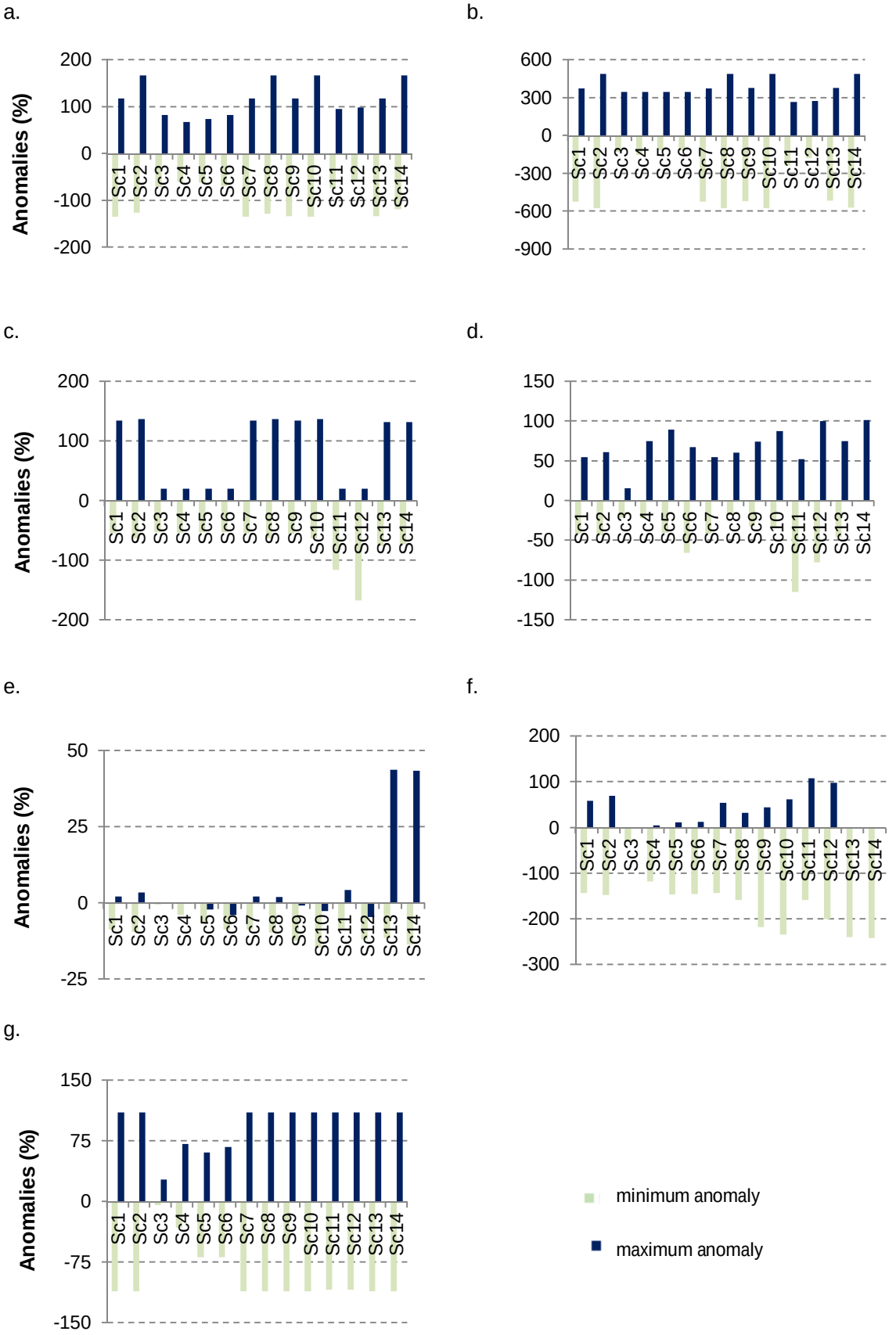

Figure 8.11 Minimum and maximum normalised anomalies (%) for the different scenarios and descriptors: a) water velocity, b) bottom shear stress, c) salinity, d) ambient temperature limiting function, e) light limiting function, f) space limiting function and g) relative water content.

For the ambient temperature limitation function of seagrass growth (*F(T)*), the minimum normalised anomalies (slightly below -100%) were revealed to the combined scenarios of ambient temperature+light (Sc 12) and SLR+ambient temperature+light (Sc 14), namely for *RCP* 8.5 (Figure 8.11d). However, the maximum anomalies (below 100%) occurred in the combined scenarios of ambient temperature+light and SLR+ambient temperature+light, for *RCP* 8.5 (Figure 8.11d).

The light limitation function of seagrass growth (*F(L)*) presented the lowest absolute normalised anomalies of all the considered descriptors. Both the maximum (lower than 50%) and minimum (highest than -25%) anomalies were found in the combined SLR+ambient temperature+light scenarios (Scs 13 and 14), for *RCP* 4.5 and *RCP* 8.5 (Figure 8.11e).

In the case of the space limiting function of seagrass growth (*F(S)*), the minimum anomalies (below -200%) were generally revealed at the combined scenarios of SLR+light for both *RCP*s (Scs 9 and 10) and SLR+ambient temperature+light (Scs 13 and 14). The maximum anomalies (slightly over 100%) were found at the combined scenarios of ambient temperature+light (Scs 11 and 12) (Figure 8.11f).

The relative water content presented both the highest (110%) and lowest (-111%) normalised anomalies for the individual scenarios with sea level rise (Scs 1 and 2) and combined scenarios of SLR+ambient temperature (Scs 7 and 8), SLR+light (Scs 9 and 10), ambient temperature+light (Scs 11 and 12) and SLR+ambient temperature+light (Scs 13 and 14), for both *RCP*s (Figure 8.11).

The relative areas represented by the normalised negative nil and positive normalised anomalies were computed and systematised in contingency table (Table 8.5). As for the descriptors water velocity and bottom shear stress the highest the values, the lowest the suitability for seagrass presence (according to the criteria of Table 8.2), the areas concerning the positive normalised anomalies indicate lower water velocities and bottom shear stress values, and so potential increase of suitable areas for seagrass presence. In this case, the reference condition presents less suitability than the scenario.

Conversely, for the remaining descriptors, however, the areas with positive anomalies indicate less suitable areas for seagrass presence and, as the highest the values the highest the suitability for seagrass presence, the reference condition presents better suitability than the scenario.

The results systematised in Table 8.5 show therefore that in the case of water velocity, salinity and light (*F(L)*) and space (*F(S)*) limiting functions of seagrass growth, the relative areas characterised by negative normalised anomalies were generally more representative over the nil and positive anomalies. The bottom shear stress (*BSS*) and the ambient temperature limiting function of seagrass growth (*F(T)*) presented dominant areas with normalised positive anomalies. The nil normalised anomalies were generally below 8% for all the descriptors and all scenarios, except for the relative water content (*RWC*), which showed that the relative areas characterised by normalised nil anomalies were predominant, and so without differences between the reference and the overall scenarios.

Table 8.5 Relative areas with negative, nil and positive normalised anomalies (in %), according to the descriptor and scenario.

Descriptors	Negative anomalies (% total area)				Nil anomalies (% total area)				Positive anomalies (% total area)			
Water velocity	53.4	52.2	29.9	30.1	6.5	6.3	7.8	7.8	40.1	41.5	62.3	62.1
	30.0	29.9	53.4	52.2	7.8	7.8	6.5	6.3	62.2	62.3	40.1	41.5
	53.6	51.8	30.0	27.7	6.5	6.3	7.7	7.8	39.9	41.9	62.3	64.5
	53.0	52.1			6.5	6.3			40.5	41.6		
BSS	47.2	45.6	30.5	31.6	6.5	6.3	7.8	7.8	46.3	48.1	61.7	60.6
	30.6	31.0	47.2	45.7	7.7	7.8	6.5	6.3	61.7	61.2	46.3	48.0
	47.3	45.4	31.2	29.5	6.5	6.3	7.7	7.8	46.2	48.3	61.1	62.8
	47.4	45.6			6.5	6.3			46.1	48.1		
Salinity	90.7	90.9	49.7	48.9	5.8	5.8	5.8	5.8	3.5	3.3	44.5	45.3
	53.5	53.7	90.7	90.9	5.8	5.8	5.8	5.8	40.7	40.5	3.5	3.3
	90.6	90.9	64.4	57.6	5.8	5.8	5.8	5.8	3.6	3.3	29.8	36.6
	91.3	91.4			5.8	5.8			2.9	2.8		
F(T)	84.7	84.9	48.4	14.9	6.6	6.6	6.6	6.6	8.7	8.5	45.0	78.5
	25.1	18.3	85.0	17.8	6.6	6.6	6.6	6.6	68.3	75.1	8.4	75.6
	35.0	26.9	19.0	0.1	6.6	6.6	6.6	6.7	58.4	66.5	74.4	93.2
	26.6	0.1			6.6	6.6			66.8	93.3		
F(S)	2.6	2.4	76.4	92.3	6.9	6.7	10.8	7.6	90.5	90.9	12.8	0.1
	91.9	91.2	2.8	83.0	7.6	7.6	6.9	6.7	0.5	1.2	90.3	10.3
	88.2	82.5	92.4	92.5	6.7	6.7	7.5	7.4	5.1	10.8	0.1	0.1
	93.3	93.4			6.7	6.6			0.0	0.0		
F(L)	1.3	1.0	67.9	84.1	6.6	6.6	6.6	6.6	92.1	92.4	25.5	9.3
	93.4	93.4	1.3	1.4	6.6	6.6	6.6	6.6	0.0	0.0	92.1	92.0
	93.4	93.4	93.3	93.3	6.6	6.6	6.6	6.7	0.0	0.0	0.1	0.0
	54.0	73.5			6.6	6.6			39.4	19.9		
RWC	17.3	17.3	0.1	0.1	82.4	82.4	82.5	82.5	0.3	0.3	17.4	17.4
	7.9	7.6	17.3	17.3	82.7	82.7	82.4	82.3	9.4	9.7	0.3	0.4
	17.3	17.3	3.6	1.8	82.4	82.3	81.6	81.9	0.3	0.4	14.8	16.3
	17.2	17.2			81.9	82.1			0.9	0.7		

Legend: Sc1 Sc2 Sc3 Sc4 Sc5 Sc6 Sc7 Sc8 Sc9 Sc10 Sc11 Sc12 Sc13 Sc14

F(L) – light limiting function; *F(S)* – space limiting function; *F(T)* – air/water temperature limiting function; *BSS* – bottom shear stress; *IH* – intertidal height; *RWC* – relative water content

For the water velocity, the relative areas dominated with normalised negative anomalies ranged from 52.1-53.6%, respectively for the combined SLR+ambient temperature+light scenario of *RCP* 8.5 (Sc 14) and the combined scenario of SLR+light of *RCP* 4.5 (Sc 9). The remaining scenarios were dominated by relative areas characterised with normalised positive anomalies ranging from 62.1-64.5% for respectively the isolated scenario of ambient temperature and the combined scenario of ambient temperature+light, for *RCP* 8.5, suggesting a reduction of the water velocity in that areas and therefore potentially more favourable areas for seagrass presence (Table 8.5).

In the case of the *BSS*, the scenarios without the sea level rise (Scs 3-6 and Scs 11-12) presented a higher relative area dominated by normalised positive anomalies and ranging from 60.6-62.8%, for respectively the isolated scenario of ambient temperature (Sc 4) and the combined scenario of ambient temperature+light (Sc 12), for *RCP* 8.5. These results point out

for potential improvements on bottom shear stress conditions for the seagrass presence, under the aforementioned circumstances. The remaining scenarios presented a balanced proportion between the relative areas dominated by normalised positive and negative anomalies (Table 8.5).

In the case of the salinity, the relative areas predominantly with negative anomalies were always higher (ranging between 48.9-91.4%), for each scenario, than the positive ones (Table 8.5). This result suggests, that whenever the scenario, there is an increase of the salinity comparing with the reference condition within the lagoon, and therefore an overall improvement of this descriptor for *Z. noltei* presence, particularly in the combined scenarios of SLR+ambient temperature+light for both *RCP*s (Scs 13 and 14). However, this dominance is more remarked at the scenarios with SLR, as for the remaining ones the relative areas with normalised positive anomalies may represent about 29.8-45.3, respectively observed for the combined scenario of ambient temperature+light for *RCP*4.5 (Sc 11) and the isolated scenario of ambient temperature for *RCP* 8.5 (Sc 4).

The ambient temperature limiting function of seagrass growth is suggested to be more limiting in all the scenarios, with relative areas dominated by positive anomalies (58.4-93.3%), comparing to negative ones (Table 8.5). The exceptions of this result concerned the isolated effect of SLR (Scs 1 and 2), isolated effect of ambient temperature (Sc3) and the combined scenario of SLR+ambient temperature (Sc7) for *RCP* 4.5, ranging between 48.4-85.0%.

For the space limiting function of seagrass growth, the areas characterised by negative anomalies are overall higher than the positive ones, ranging between 76.4-93.4%. Moreover, the combined scenarios of SLR+ambient temperature+light, for both *RCP*s, showed nil positive anomalies. Solely the isolated scenarios for SLR (Scs 1 and 2) and combined SLR+ambient temperature (Sc 7) presented a higher percentage of areas with positive anomalies, ranging between 90.3-90.9%. These results suggest a lower limitation by space for seagrass growth in the overall considered scenarios (i.e. *F(S)* values closer to 1) relative to the reference condition, and therefore lower biomass values are expected to occur.

The prospections for light limiting function of seagrass growth are similar to those found for the space limiting function, pointing out for more areas dominated with negative anomalies (54.0-93.4%) than the positive anomalies, except for the isolated scenarios for SLR (Scs 1 and 2) and combined scenario of SLR+ambient temperature (Scs 7 and 8), ranging between 1.0-1.4%. Furthermore, both the combined and isolated scenarios with light (Scs 5-6 and 9-12), presented nil normalised positive anomalies.

In the case of the relative water content, the relative areas characterised by negative anomalies are also higher than the positive ones for scenarios with SLR (Scs 1 and 2) and the combined scenarios with SLR+ambient temperature (Scs 7 and 8), SLR+light (Scs 9 and 10) and SLR+ambient temperature+light (Scs 13 and 14) in both *RCP*s. These areas represent about 17%, suggesting that an increase of sea level rise in these scenarios may limit the exposure of seagrasses to air and therefore reduce its loss of relative water content. The

remaining scenarios presented predominantly areas with positive anomalies, ranging between 14.8-17.8%, suggesting that isolated and combined effects of increases of light and/or ambient temperature may increase the loss of water by intertidal seagrasses, as expected.

8.4 DISCUSSION OF THE CHAPTER

Seagrasses have experienced severe regressions at a worldwide scale, which are expected to be further extended due to a combined effect of anthropogenic factors and climate change impacts, ultimately resulting in crucial ecosystem losses.

Therefore, guidelines for management strategies to enhance the resilience of seagrasses, like those proposed by Björk et al. (2008), are important to ensure seagrass survival to anthropogenic and climate-related events. Following these principles, the first exploratory approach on the model projections aimed to set and map the potentially suitable areas for *Z. noltei* presence, according to a selection of descriptors based on water quality conditions, hydrodynamics and sediment features, including the individual and combined analysis of each descriptor.

From the individual assessment of each descriptor, solely the result of “highly favourable” conditions for the light limitation function of seagrass growth was not expected. In fact, even focusing on intertidal seagrasses, this result was not anticipated as one of the impacts of temporal changes in the state of the lagoon, previously showed by the application of the DPSIR approach (cf. Chapter 2), was actually the reduction of light penetration. Such result remits to the crucial need of further work on the Zostera biological model within the scope of the ecological model for Ria de Aveiro developed in the beforehand mentioned LAGOONS project (lagoons.web.ua.net), highlighting the inclusion of sediment processes to provide a closer-to-truth condition of water column turbidity and better describe the light conditions at the benthic environments.

The validation of the inferred habitat suitability for seagrass presence, considering all the selected descriptors, was performed against data on the presence/absence of seagrass, assessed through ground-surveyed experiments (Sousa et al., submitted). This cross-validation revealed that the areas presently colonised by seagrasses overall strongly matched with moderate to highly favourable areas regarding the habitat suitability for seagrass presence, inferred from model predictions. Furthermore, the areas predicted as nil to poorly suitable were also generally consistent with those pointed out in the observed data as non-colonised ones, and are located along the main navigation channels and east part of the lagoon.

Few differences were found between the observed areas colonised by seagrasses and pointed as not suitable to poorly suitable areas, being mainly restricted to punctual areas within the central lagoon. These differences are however substantially reduced to less than 1% when considering exclusion factors such as water velocity, space and light limiting functions of

seagrass growth. This result suggests that the selected descriptors may have different relative importance for characterising the habitat suitability.

The main differences recorded in the cross-validation were located at the central lagoon at the northernmost part of Ovar channel. In these areas, the observed data pointed out for the absence of seagrasses, in spite of the inferred habitat suitability ranged from moderate to highly favourable areas. Some possible causes rely on the model uncertainties, oversimplification of the model formulation that may not take into account critical processes for seagrass dynamics (e.g. nutrient dynamics; processes occurring at the interface seagrass-sediment), but also in the high natural variability of the system itself.

Beyond the model constraints, there are also important factors as sources of uncertainty and therefore contribute to the differences referred, such as the limitations associated with the observed data. Actually, and as discussed by Sousa et al. (submitted), the current mapping of seagrass meadows in Ria de Aveiro lagoon also presents uncertainties, mostly due to the imagery acquisition procedure and resolution.

The different temporal scales covered by the model and ground-surveyed data are also very distinct. The model was run to simulate changes during a year, according to variations in light, ambient temperature and tide, while the observed data is collected at discrete moments and exposed to previous natural and anthropogenic impacts, most of the times with unknown extension. This is supported by earlier findings from Silva et al. (2004) and Cunha et al. (2013) for the northernmost part of Ovar channel, that confirmed the presence of seagrasses in the area, which is consistent with the inferred moderate to highly favourable habitat suitability, but not with the used ground-surveyed data recently gathered. However, Cunha et al. (2013) verified that seagrass meadows in this area are very prone to disappear during extreme rainfall events, due to mechanical uprooting and reduction in water clarity. The findings of this work for the extreme river flow scenario (short scale event) further confirmed this statement, as it shows a decrease of the suitability index for both descriptors water velocity and salinity for the northernmost part of Ovar channel. Moreover, the used sediment grain size data may not be good enough for the present work, though it is the best information available. The linear interpolation made to the data from Rodrigues et al. (2011) was the methodology chosen to overcome the unavailability of a continuous dataset on the sediment grain size along the lagoon, although it is a raw methodology to the required level of detail in such an important conditioning factor to seagrass growth and thriving.

The results on extreme river flow scenarios were the expected, as they revealed that both water velocity and salinity showed higher differences in the habitat suitability nearby the Vouga river, which has the higher expression of fluvial discharge within the lagoon. Furthermore, changes in habitat suitability seem to be spatially more notorious due to changes in salinity than in the water velocity.

Besides this extreme event, a heat wave was also simulated, as under a global climate change context, extreme events are expected to increase in frequency and intensity. A typical

heat wave was then tested and the results showed an apparent increase in the ambient temperature limitation function of seagrass growth, resulting in a lower seagrass growth rate.

Heat waves may lead to massive seagrass losses, especially at intertidal communities exposed to air during low tide periods and subjected to air temperature extremes (Massa et al., 2009), comprising devastating loss of their ecosystems functions, such as carbon sequestration, as showed by Arias-Ortiz et al. (2018). The underlying molecular response is different according to the seagrass species to heat stress, as reported by Franssen et al. (2014). Whilst *Z. noltei* presents higher thermal tolerance at a 26ºC heat wave, in *Z. marina* heat shock proteins (HSPs) genes were induced under the same conditions, highlighting the importance of stress-related genes on seagrass tolerance to thermal variation (Franssen et al., 2014). Moreover, a study conducted by Marín-Guirao et al. (2017) showed that shallow plants, living in a more unstable thermal environment, optimized phenotype variation in response to warming, presenting a pre-adaptation of genes in anticipation of stress.

Due to this higher phenotypic plasticity of seagrass communities, an adaptation to warm temperatures is expected to reduce sensitivity to heatwaves, though the continued resistance of seagrass to further anthropogenic stresses may be impaired by heat-induced downregulation of genes related to photosynthesis and stress tolerance (Jueterbock et al., 2016) and other physiological strategies to thrive to thermal stress (Duarte et al., 2018).

Through the investigation of the impact of different climate change scenarios on the potential changes of seagrass spatial distribution in Ria de Aveiro lagoon, a qualitative analysis of the isolated and combined effects of sea level rise, ambient temperature and light was achieved and mapped. This approach helped to target the critical areas presently colonised by seagrasses and potentially better positioned to survive to climate change impacts, emphasising its higher priority to restoration actions.

The isolated effect of sea level rise turned into no relative differences between the prospected and presently occupied areas with seagrass, for both projections (*RCP* 4.5 and *RCP* 8.5). The lack of remission on seagrass colonised areas for these scenarios can be related with the conditioned effect of the complex geomorphology of Ria de Aveiro lagoon on tidal height and range, as well as therein factors that regulate the distribution of seagrass meadows. This result was not however the expected, as the changes on the water circulation, tidal amplitude, water current, salinity regimes, coastal erosion and water turbidity, driven by the sea level rise, are likely to negatively impact seagrass growth and functioning, according to Duarte et al. (2004).

On the other hand, the isolated effects of irradiance and ambient temperature drove to a reduction of the relative area of seagrass for the most pessimistic scenario (*RCP* 8.5), as expected. Higher irradiance may increase potential mutagenic and physiological damages in seagrass communities, namely to those colonising the shallow intertidal areas, due to periodic emersion at low tides (Short and Neckles, 1999). The physiological adaptation strategies to overcome this stress are yet to be deeply understood but comprise increases in plant content of phenolic and other secondary compounds, such as flavonoids. Moreover, the harmful effects of

higher irradiance are variable according to the species, ranging from inhibition of photosynthesis to the increased metabolic cost of producing UV-B blocking compounds within plant tissue (Raven, 1991). Furthermore, increasing ambient temperature directly affects the metabolic rates, and thus the seasonal and distribution patterns, varying according to the species and consequent thermal tolerance and optimum temperatures of multiple physiological processes.

Regarding relative loss of seagrass area, the combined effect of stressors showed to be overall synergic to both *RCP*s, comparing with the sum of the isolated stressors. Therefore, a combination in stressors drives to harmful effects, exacerbating their isolated effect. This result is consistent with the findings of Fraser et al. (2014), concluding that where extreme climatic events overlap and cause multiple, synergistic stressors to plant communities, ecological responses are likely to be more extreme, particularly in ecosystems where foundation species exist near upper thermal tolerance limits, as it occurs in the present study for *Zostera noltei* (Borum and Greve, 2004; Cunha et al., 2013).

Additional stressors not considered in the scope of this work may, however, show potential antagonistic effects with light, such as atmospheric carbon dioxide, which increases the carbon supply for secondary metabolism and the ability of higher plants to block UV-B radiation (Caldwell et al., 1989). This is particularly important for intertidal seagrass meadows, as during exposure periods to air the carbon dioxide diffusion is substancially different from that occurring at submersion periods in water, and therefore the extension of this antagonistic effect may also vary during alternating immersion/submersion periods.

As the interactions between stressors were not cumulative and the normalised anomalies presented no clear variation pattern according to the descriptor and scenario, the results suggest an intrinsic complexity on the interaction between the selected descriptors. The only exception, found for descriptor salinity, consistently showed an increase towards potential more suitable conditions (negative anomalies) for seagrass presence in all of the considered scenarios. Moreover, for the remaining descriptors, although some of the areas may present considerable alterations towards less suitable conditions, the results also point out conversely for a potential improvement in other areas elsewhere within the lagoon (Appendix 7).

The results of this chapter, particularly the long-term prospects, should therefore be analysed with some reservations, as the notorious seagrass plasticity, expressed by the high ability for adaptation and acclimatisation to gradual changes may assure seagrass resiliency to climate change (Duarte et al., 2018). In spite of its physiological plasticity, this natural response by the natural system may however not be as effective as seen for long-time scales when exposed to extreme events that potentially occur at shorter timescales, as the changes are more abrupt (Massa et al., 2009).

Foreseeing the potentialities of future complementary work on this chapter, the main suggestions would be widening the application of seagrass biological model into the ecological model of the lagoon by improving the model formulation and the communication protocols between the biological and ecological models, especially to explicitly address sediment-seagrass interactions and internal nutrient dynamics. Therefore, a more holistic viewpoint would

be expected by considering the biotic interactions between seagrasses and algae to different stressors' combination, which is particularly important in the context of management interventions and climate change, due to a potential replacement of high structural complexity seagrass-species by lower complex and even opportunistic ones (Pergent et al., 2014).

Moreover, dredging interventions in Ria de Aveiro comprised relevant pressures in the past that drove to changes in the morphohydrodynamic environment and on the spatial distribution of seagrass meadows in Ria de Aveiro (cf. Chapter 2). Nowadays, these anthropogenic actions still take place to keep the safety of navigable channels and their indirect effects, such as the alteration of the water circulation and sediment dynamics, may increase the erosion on seagrass meadows and sediment resuspension that increases turbidity (Duarte et al., 2004). Although not considered throughout this work, setting dredging scenarios may provide an important view of the continuity of anthropogenic effects on these communities.

8.5 CONCLUSIONS OF THE CHAPTER

This chapter focuses on the exploration of model features and their response to different hypothetic scenarios, from extreme events (e.g., extreme river flow and heat wave) to two prospective climate change scenarios: *RCP* 4.5 and, a more pessimistic one, *RCP* 8.5.

At the present condition, the model predictions targeted the south-central lagoon and northwest central lagoon as the more suitable areas for seagrass presence, considering the simulated conditions. The results were overall satisfactory validated by ground-surveyed data.

The extreme river flow scenarios showed substantial variable alterations in seagrass habitat nearby the rivers, regarding the descriptors considered, water velocity and salinity, pointing out for less suitable conditions for seagrass presence during these events. Moreover, during heat waves, the limitation of seagrass growth by ambient temperature is remarkably higher during air-exposure periods, comparing with the reference scenario, suggesting a reduction in seagrass growth under those conditions.

The climate change scenarios prospected a noticeable seagrass decline throughout the areas presently colonised, with the particular exception at central lagoon which suggests that a number of existent patches remain resilient to climate change and potential existence of genetic variability.

Regarding the extension of these climate change scenarios to the entire lagoon, no clear pattern is overall evident for neither scenarios, nor descriptors. Nevertheless, the modelled prospections were capable and helpful in identifying areas where the habitat suitability for seagrass presence seems to decrease, simultaneously with the apparent improvement of other areas. As so, the overall balance is not possible to determine, as the interactions between descriptors and stressors are rather complex and there is the missing link of the natural response of the system due to the seagrass plasticity. Nevertheless, the exploratory approach

showed important insights of potential variations on the panoply of descriptors considered, which may be reflected in the scope of management actions and strategies to the recovery of seagrass meadows in Ria de Aveiro lagoon.

When acknowledging the assumptions and the required improvements, the present work illustrates that numerical models are indeed important supportive tools for coastal management planning. However, it is disclaimed the need of a critic and careful interpretation of model results, afore their application to real situations, as they are developed with the best available information and are a simplification of natural complex systems.

Chapter 9

FINAL CONCLUSIONS AND FUTURE WORK

Similar to other coastal systems worldwide, Ria de Aveiro lagoon has been experienced an evident decline of seagrass meadows, resulting in the impoverishment of associated key ecosystem services and functions. Suitable management actions require a comprehensive understanding of these drivers of decline, effectively needed to overturn this trend.

The general objective of this work was, therefore, to study the present state of seagrass meadows in Ria de Aveiro, through numerical modelling approaches and supported by collected ground-surveyed data, to ultimately use the best model configuration in evaluating seagrass spatial distribution, within a climate change context. As so, a preliminary biological model of the seasonal dynamics of intertidal seagrass *Zostera noltei* was developed with PowerSim Studio and further incorporated into a water quality model (Delft3D-WAQ).

Hereby, this final chapter presents a wrap-up of the summary conclusions according to the workflow and additional research guidelines that may require further investigation.

In Chapter 2, the temporal variation and current state of seagrass meadows in Ria de Aveiro lagoon were described. The once diverse and abundant seagrass meadows are nowadays restricted to intertidal areas and monospecific meadows of *Z. noltei*, due to changes in hydrodynamic environment and deterioration of water quality of the lagoon. As shown by the DPSIR framework application, the most noticeable changes in both seagrass covered area and biomass, seem however to be majorly correlated and explained itself by alterations in the hydrodynamic regime.

The following chapter continued to address the current state of intertidal meadows but in further detail, by conducting ground-survey experiments. Data from shoot density and above and belowground biomasses presented high spatial variability and heterogeneity along the year, with the last presenting no seasonal pattern.

This one-year sampling, at a healthy patch in Mira channel with monthly periodicity, comprises the best information available, though it does not consider the inter-annual natural variability of the seagrass community. As so, an extended and spatial distributed experimental sampling design should be drawn in future work to overcome this limitation.

A preliminary testing analysis followed the conceptualisation of seagrass biological model to check it regarding units and links between model features, showing consistent patterns and variability ranges within those found in the literature. Seagrass growth was defined regarding above and belowground biomass (state variables), fundamentally controlled by the water temperature, light and space availability.

To prepare the model to the inherent particularities of intertidal seagrass populations, additional field surveys were performed to investigate the *RWC* of *Z. noltei* leaves, according to the air exposure times and sediment descriptors (sediment grain size and organic matter). This work pointed out that relative importance of sediment characteristic was more effective in conditioning the *RWC* of seagrasses over a tidal cycle, than air exposure time. Furthermore, seagrass leaves of colonised finer grain size sediments presented less relative water loss, suggesting a more suitable habitat for *Z. noltei* establishment.

Afterwards, the desiccation model was formulated, based on both literature revision and data analysis from the field-surveyed experiment. This mechanistic model functions according to the tide, air temperature and sediment type, and defines the *RWC* as a dynamic variable, depending on hydration and desiccation of seagrass leaves. The model predictions reproduced well the observed patterns, although slightly overestimating the water loss by intertidal seagrasses at high air temperatures and spring low tides in medium sand sediments.

The versatility of the numerical modelling suite, Delft3D, particularly on the water quality module (Delft3D-WAQ), allows extending the default substances and processes, to meet users' aims. Therefore, this model suite was elected to platform the coupling of dynamic intertidal seagrass biological model with the add-on desiccation model. This methodology also leaves open the possibility of future work on further improvements of model formulations and studies that go beyond the scope of the present study and comprises an ecological perspective of the systems where seagrasses are included. Moreover, in the specific part of the desiccation model, this software feature allows the adaptation of evapotranspiration estimations to seagrasses during air exposure periods, further study of wind effect on desiccation and the prospection to a wider application to other seagrass populations.

The user-friendly interface of the model suite also permitted additional improvements of the numerical grid resolution in Mira channel, to better simulate the hydrodynamics, due to its relevancy for seagrass meadows spatial distribution, previously shown in Chapter 2 through the DPSIR framework.

After coupling the seagrass plus desiccation models to Delft3D-WAQ, a yearly simulation of the aboveground biomass turned out overall very good results, with the exception of the summer months. The simulation results of the belowground biomass, however, were only fair compared to the ground-surveyed data, which points out for some sort of misrepresentation at both process-level and time scale. On the model results for desiccation, expressed in terms of *RWC*, the model results slightly overestimated the leaves' water loss, which may be related to not considering the shading effect on the minimization of water evaporation, as the seagrass

RWC only depends on air temperature and water height. Abiotic factors like air humidity and wind speed are however essential to the intertidal seagrass dynamics during the air-exposure periods.

An initial assessment on model performance used three different methodologies of statistical methods and sensitivity analysis. Different error statistical methods presented different results and an accurate conclusion based on model performance require re-evaluating model performance, by computing additional indices and considering accuracy, precision and hypothesis testing, that would certainly comprise an extended and comprehensive approach. The assessment of model sensitivity to controlled variations on each parameter showed that, for both above and belowground biomass, the parameters linked with ambient temperature are overall more sensitive, which may be due to the exponential-type formulations of this factor, but it converges with results from previous works on the same species. These parameters, together with those to improve the formulation of desiccation add-on (e.g. air humidity and wind effects), should therefore be considered on future field experiments aiming to widen the ground-surveyed dataset for an auxiliary study on the spatial and temporal variability of *Z. noltei* biomass in Ria de Aveiro lagoon and further model tuning.

Though the model presents fair good results simulating the seasonal dynamics of intertidal seagrass meadows in Ria de Aveiro lagoon, the most limiting features stand with the lack of processes to describe the complex and critical interaction between seagrass-sediment, feedback mechanisms and internal nutrient dynamics. These factors condition the potential application to other coastal systems with similar problematics and are therefore suggested as the most priority guidelines to further model improvements.

In spite of the limitations found, some prospective scenarios were studied. As global warming may be a relevant driver of further seagrass regressions, the potential long-term changes on seagrass spatial distribution were therefore investigated under a climate change context viewpoint, using the projections described by two different scenarios: *RCP* 4.5 and *RCP* 8.5 (more pessimistic). This methodology allowed for identifying the most suitable areas for seagrass presence, considering basic water quality conditions, hydrodynamics and sediment features, and helping to target the critical areas presently colonised by seagrasses and potentially positioned to survive to climate change impacts, emphasising its higher priority to restoration actions.

Two hypothetic extreme scenarios of extreme river flow and a typical heat wave were tested, as these events are expecting to increase frequency, and showed, respectively, a decrease in the habitat suitability for seagrass and an increase in the ambient temperature limitation function of seagrass growth, resulting in a lower seagrass growth rate.

In terms of relative loss of seagrass area, the combined effect of multiple stressors projected to be overall synergic to both *RCP*s, comparing with the sum of the isolated stressors. A conjunction in stressors drives to harmful effects, exacerbating their isolated effect, converging to previous studies that state how ecological responses are likely to be extreme, particularly in

ecosystems where foundation species exist near upper thermal tolerance limits, as it occurs in the present study for *Z. noltei*. A remarkable decline seems to potentially occur in the worst-case scenario, and the potential most favourable areas for seagrass presence in the future are located mainly in the south-central lagoon and northwest central lagoon.

The prospected changes throughout the Ria de Aveiro, using the normalised anomalies between reference and scenarios, do not show regular patterns of increase/decrease of habitat suitability for seagrass presence. Nevertheless, this exploratory approach, using the best available information, showed comprehensive insights of potential variations on the considered descriptors, which may be useful to support management actions and strategies for the recovery of seagrass meadows in Ria de Aveiro lagoon. However, the natural response of the seagrasses to the long-term changes was not considered, which suggests a critic and careful interpretation of model prospection of climate change scenarios. Furthermore, in the scope of the Blue Growth, an integrated maritime policy of the European Union to support a holistic and sustainable growth in marine and maritime sectors, the harbour activities in Ria de Aveiro will certainly continue to require maintenance actions that may imply shifts in the baseline condition considered to compare with long-term scenarios.

As future work, and beyond that already mentioned throughout this study, the impact of dredging interventions contemplated in current management plans for the main branches of Ria de Aveiro lagoon may also provide an additional detailed documentation on the anthropogenic effects on seagrass communities and better comprehension on the natural evolution of these communities and mechanical disturbances effects.

As final remarks, this work comprised a multidisciplinary approach, contributing to a better representation of intertidal seagrass through numerical model approaches. The overall initial purposes were achieved although many referred complementary approaches may drive to substantial improvements to the present configuration and consequent representation of the intertidal seagrass meadows at local and global scales.

REFERENCES

Abrantes, I., Dias, J.M., Rocha, F., 2006. Spatial and temporal variability of suspended sediments concentration in Ria de Aveiro lagoon and fluxes between the lagoon and the ocean. *Journal of Coastal Research, SI 39 (Proceeding of the 8th International Coastal Symposium)*, 718-723.

Alexandre, A., Cabaco, S., Santos, R., Serrao, E.A., 2006. Timing and success of reproductive stages in the seagrass *Zostera noltii*. *Aquatic Botany* 85(3), 219-223.

Allen, J.I., Holt, J.T., Blackford, J., Proctor, R., 2007. Error quantification of a high-resolution coupled hydrodynamic-ecosystem coastal-ocean model: Part 2. Chlorophyll-a, nutrients and SPM. *Journal of Marine Systems* 68(3-4), 381-404.

Anderson, M.J., Gorley, R.N., Clarke, K.R., 2008. PERMANOVA+ for PRIMER: Guide to Software and Statistical Methods. PRIMER-E, Plymouth, UK. 214 pp.

Araújo, I.B., Dias, J.M., Pugh, D.T., 2008. Model simulations of tidal changes in a coastal lagoon, the Ria de Aveiro (Portugal). *Continental Shelf Research* 28(8), 1010-1025.

Arias-Ortiz, A., Serrano, O., Masqué, P., Lavery, P.S., Mueller, U., Kendrick, G.A., Rozaimi, M., Esteban, A., Fourqurean, J.W., Marbà, N., Mateo, M.A., Murray, K., Rule, M.J., Duarte, C.M., 2018. A marine heatwave drives massive losses from the world's largest seagrass carbon stocks. *Nature Climate Change* 8(4), 338-344.

Arnaud-Haond, S., Duarte, C.M., Diaz-Almela, E., Marbà, N., Sintes, T., Serrão, E.A., 2012. Implications of Extreme Life Span in Clonal Organisms: Millenary Clones in Meadows of the Threatened Seagrass *Posidonia oceanica*. *Plos One* 7(2).

Auby, I., Labourg, P.J., 1996. Seasonal dynamics of *Zostera noltii* Hornem in the Bay of Arcachon (France). *Journal of Sea Research* 35(4), 269-277.

Aveytua-Alcázar, L., Camacho-Ibar, V.F., Souza, A.J., Allen, J.I., Torres, R., 2008. Modelling *Zostera marina* and *Ulva* spp. in a coastal lagoon. *Ecological Modelling* 218(3-4), 354-366.

Azevedo, A., Sousa, A.I., Lencart e Silva, J.D., Dias, J.M., Lillebø, A.I., 2013. Application of the generic DPSIR framework to seagrass communities of Ria de Aveiro: a better understanding of this coastal lagoon. *Journal of Coastal Research, SI 65 (Proceeding of the International Coastal Symposium)*, 19-24.

Azevedo, A., Dias, J.M., Lillebø, A.I., 2016. Thriving of *Zostera noltei* under intertidal conditions: implications for the modelling of seagrass populations. *Marine Biology* 163:114(5).

Baird, M.E., Adams, M.P., Babcock, R.C., Oubelkheir, K., Mongin, M., Wild-Allen, K.A., Skerratt, J., Robson, B.J., Petrou, K., Ralph, P.J., O'Brien, K.R., Carter, A.B., Jarvis, J.C., Rasheed, M.A., 2016. A biophysical representation of seagrass growth for application in a complex shallow-water biogeochemical model. *Ecological Modelling* 325, 13-27.

Bartleson, R.D., Kemp, W.M., Stevenson, J.C., 2005. Use of a simulation model to examine effects of nutrient loading and grazing on *Potamogeton perfoliatus* L. communities in microcosms. *Ecological Modelling* 185(2-4), 483-512.

Beer, S., Eshel, A., 1983. Photosynthesis of *Ulva* sp. I. Effects of desiccation when exposed to air. *Journal of Experimental Marine Biology and Ecology* 70, 91-97.

Bertelli, C.M., Robinson, M.T., Mendzil, A.F., Pratt, L.R., Unsworth, R.K.F., 2017. Finding some seagrass optimism in Wales, the case of *Zostera noltii*. *Marine Pollution Bulletin* 134, 216-222.

Bianchi, T.S., 2007. *Biogeochemistry of Estuaries*. Oxford University Press, Inc., New York, USA, 706 pp.

Björk, M., Uku, J., Weil, A., Beer, S., 1999. Photosynthetic tolerances to desiccation of tropical intertidal seagrasses. *Marine Ecology Progress Series* 191, 121-126.

Björk, M., Short, F., McLeod, E., Beer, S., 2008. Managing seagrasses for resilience to climate change, IUCN Resilience Science Group Working Paper Series - No 3. IUCN, Gland, Switzerland, 56 pp.

Bocci, M., Coffaro, G., Bendoricchio, G., 1997. Modelling biomass and nutrient dynamics in eelgrass (*Zostera marina* L.): applications to the Lagoon of Venice (Italy) and Oresund (Denmark). *Ecological Modelling* 102(1), 67-80.

Bocci, M., 2000. A mathematical model for studying *Zostera noltii* dynamics in the Venice Lagoon. *Venice Lagoon Ecosystem: Inputs and Interactions between Land and Sea* 25, 455-464.

Borum, J., Greve, T.M., 2004. *The four European seagrass species. in European Seagrasses: an Introduction to Monitoring and Management*. J Borum, CM Duarte, D Krause-Jensen and TM Greve Eds (The M&MS project), 1-7 pp.

Bos, A.R., Bouma, T.J., de Kort, G.L.J., van Katwijk, M.M., 2007. Ecosystem engineering by annual intertidal seagrass beds: Sediment accretion and modification. *Estuarine, Coastal and Shelf Science* 74(1-2), 344-348.

Bueno-Pardo, J., Garcia-Seoane, E., Sousa, A.I., Coelho, J.P., Morgado, M., Frankenbach, S., Ezequiel, J., Vaz, N., Quintino, V., Rodrigues, A.M., Leandro, S., Luis, A., Serôdio, J., Cunha, M.R., Calado, A.J., Lillebø, A., Rebelo, J.E., Queiroga, H., 2018. Trophic web structure and ecosystem attributes of a temperate coastal lagoon (Ria de Aveiro, Portugal). *Ecological Modelling* 378, 13-25.

Burd, A.B., Dunton, K.H., 2001. Field verification of a light-driven model of biomass changes in the seagrass *Halodule wrightii*. *Marine Ecology Progress Series* 209, 85-98.

Buzzelli, C., Robbins, R., Doering, P., Chen, Z., Sun, D., Wan, Y., Welch, B., Schwarzschild, A., 2012. Monitoring and Modeling of *Syringodium filiforme* (Manatee Grass) in Southern Indian River Lagoon. *Estuaries and Coasts* 35(6), 1401-1415.

Cabaço, S., Santos, R., 2007. Effects of burial and erosion on the seagrass *Zostera noltii*. *Journal of Experimental Marine Biology and Ecology* 340(2), 204-212.

Cabaço, S., Machás, R., Vieira, V., Santos, R., 2008. Impacts of urban wastewater discharge on seagrass meadows (*Zostera noltii*). *Estuarine Coastal and Shelf Science* 78(1), 1-13.

Cabaço, S., Machás, R., Santos, R., 2009. Individual and population plasticity of the seagrass *Zostera noltii* along a vertical intertidal gradient. *Estuarine, Coastal and Shelf Science* 82(2), 301-308.

Caldwell, M.M., Teramura, A.H., Tevini, M., 1989. The changing solar ultraviolet climat and the ecological consequences for higher-plants. *Trends in Ecology & Evolution* 4(12), 363-367.

Cardoso, P.G., Pardal, M.A., Lillebø, A.I., Ferreira, S.M., Raffaelli, D., Marques, J.C., 2004. Dynamic changes in seagrass assemblages under eutrophication and implications for recovery. *Journal of Experimental Marine Biology and Ecology* 302(2), 233-248.

Cerco, C.F., Moore, K., 2001. System-wide submerged aquatic vegetation model for Chesapeake Bay. *Estuaries* 24(4), 522-534.

Cerejo, M., Dias, J.M., 2007. Tidal transport and dispersal of marine toxic microalgae in a shallow, temperate coastal lagoon. *Marine Environmental Research* 63(4), 313-340.

Chapelle, A., Ménesguen, A., Deslous-Paoli, J.M., Souchu, P., Mazouni, N., Vaquer, A., Millet, B., 2000. Modelling nitrogen, primary production and oxygen in a Mediterranean lagoon. Impact of oysters farming and inputs from the watershed. *Ecological Modelling* 127(2-3), 161-181.

Charpentier, A., Grillas, P., Lescuyer, F., Coulet, E., Auby, I., 2005. Spatio-temporal dynamics of a *Zostera noltii* dominated community over a period of fluctuating salinity in a shallow lagoon, Southern France. *Estuarine Coastal and Shelf Science* 64(2-3), 307-315.

Chen, Y.Z., Lin, W.Q., Zhu, J.R., Lu, S.Q., 2016. Numerical simulation of an algal bloom in Dianshan Lake. *Chinese Journal of Oceanology and Limnology* 34(1), 231-244.

Clarke, K.R., Gorley, R.N., 2006. *PRIMER v6: User Manual/Tutorial. PRIMER-E, Plymouth, UK.* 190 pp.

Cloern, J.E., Foster, S.Q., Kleckner, A.E., 2014. Phytoplankton primary production in the world's estuarine-coastal ecosystems. *Biogeosciences* 11(9), 2477-2501.

CMEMS, Copernicus Marine Environment Monitoring System, URL: marine.copernicus.eu (last acceded: 30 October 2016).

Coelho, H., Vieira, S., Serôdio, J., 2009. Effects of desiccation on the photosynthetic activity of intertidal microphytobenthos biofilms as studied by optical methods. *Journal of Experimental Marine Biology and Ecology* 381(2), 98-104.

Collier, C.J., Waycott, M., 2014. Temperature extremes reduce seagrass growth and induce mortality. *Marine Pollution Bulletin* 83(2), 483-490.

Costa, S., Oliveira, E., Coelho, C., Lopes, M.P., 2011. Erosion and deposition rates in estuaries - the saltpans area of Aveiro Lagoon, Portugal. *Journal of Coastal Research, SI 64 (Proceeding of the International Coastal Symposium)*, 1472-1476.

Costanza, R., d'Arge, R., deGroot, R., Farber, S., Grasso, M., Hannon, B., Limburg, K., Naeem, S., Oneill, R.V., Paruelo, J., Raskin, R.G., Sutton, P., van den Belt, M., 1997. The value of the world's ecosystem services and natural capital. *Nature* 387(6630), 253-260.

Cunha, A.H., Assis, J.F., Serrão, E.A., 2013. Seagrasses in Portugal: A most endangered marine habitat. *Aquatic Botany* 104, 193-203.

Cunha, M.Â., Dias, J.M., Almeida, M.A., Lopes, J.F., Alcântara, E., 2003. Fluxes of bacterioplankton between a tidal estuary and the sea: returning to the "Outwelling Hypothesis". *Aquatic Ecology* 37(1), 45-54.

da Silva, E.T., Asmus, M.L., 2001. A dynamic simulation model of the widgeon grass *Ruppia maritima* and its epiphytes in the estuary of the Patos Lagoon, RS, Brazil. *Ecological Modelling* 137(2-3), 161-179.

Davison, D.M., Hughes, D.J., 1998. *Zostera biotopes (volume I). An overview of dynamics and sensitivity characteristics for conservation management of marine SACs. Scottish Association for Marine Science, (UK Marine SACs Project).* 95 pp.

de los Santos, C.B., Brun, F.G., Bouma, T.J., Vergara, J.J., Pérez-Lloréns, J.L., 2010. Acclimation of seagrass *Zostera noltii* to co-occurring hydrodynamic and light stresses. *Marine Ecology Progress Series* 398, 127-135.

deCastro, M., Sousa, M.C., Santos, F., Dias, J.M., Gomez-Gesteira, M., 2016. How will Somali coastal upwelling evolve under future warming scenarios? *Scientific Reports* 6

Deltares, 2014a. *Open Process Library. User Manual, version 0.99.33644*. 66 pp.

Deltares, 2014b. *Delft3d-FLOW. Simulation of multi-dimensional hydrodynamic flows and transport phenomena, including sediments. User Manual, version 3.15.34158*. 710 pp.

Deltares, 2017. *D-Water Quality. Versatile water quality modelling in 1D, 2D or 3D systems including physical, (bio)chemical and biological processes. User Manual, version 4.99*. 400 pp.

den Hartog, C., 1970. *The seagrasses of the world.* . North-Holland Publishing Company. 275 pp.

Dias, J.M., Lopes, J.F., Dekeyser, I., 1996a. *Modelling water circulation in Ria de Aveiro, Portugal. in Hydrodynamics: Theory and Applications, Vols 1 and 2. Chwang, A. T., Lee, J. H. W. & Leung, D. Y. C. Editors*, 715-720 pp.

Dias, J.M., Lopes, J.F., Dekeyser, I., 1996b. *Numerical modelling of tidal fluxes and passive pollutants concentration in Ria de Aveiro, Portugal. in Coastal Environment: Environmental Problems in Coastal Regions. Ferrante, A. J. & Brebbia, C. A. Editors*, 285-294 pp.

Dias, J.M., Lopes, J.F., Dekeyser, I., 2000. Tidal propagation in Ria de Aveiro lagoon, Portugal. *Physics and Chemistry of the Earth Part B – Hydrology Oceans and Atmosphere* 25(4), 369-374.

Dias, J.M., Lopes, J.F., Dekeyser, I., 2001. Lagrangian transport of particles in Ria de Aveiro lagoon, Portugal. *Physics and Chemistry of the Earth Part B – Hydrology Oceans and Atmosphere* 26(9), 721-727.

Dias, J.M., Lopes, J.F., Dekeyser, I., 2003. A numerical system to study the transport properties in the Ria de Aveiro lagoon. *Ocean Dynamics* 53(3), 220-231.

Dias, J.M., Lopes, J.F., 2006a. Implementation and assessment of hydrodynamic, salt and heat transport models: The case of Ria de Aveiro lagoon (Portugal). *Environmental Modelling & Software* 21(1), 1-15.

Dias, J.M., Lopes, J.F., 2006b. Calibration and validation of hydrodynamic, salt and heat transport models for Ria de Aveiro lagoon (Portugal). *Journal of Coastal Research, SI 39 (Proceeding of the International Coastal Symposium)*, 1680-1684.

Dias, J.M., Abrantes, I., Rocha, F., 2007. Suspended Particulate Matter Sources and Residence Time in a Mesotidal Lagoon. *Journal of Coastal Research, SI 50 (Proceeding of the International Coastal Symposium)*, 1034-1039.

Dias, J.M., Sousa, M.C., Bertin, X., Fortunato, A.B., Oliveira, A., 2009. Numerical modeling of the impact of the Ancão Inlet relocation (Ria Formosa, Portugal). *Environmental Modelling & Software* 24(6), 711-725.

Dias, J.M., Mariano, S.C., 2011. Numerical Modelling of Hydrodynamic Changes Induced by a Jetty Extension - the Case of Ria de Aveiro (Portugal). *Journal of Coastal Research, SI 64 (Proceeding of the International Coastal Symposium)*, 1008-1012.

Dias, J.M., Picado, A., 2011. Impact of morphologic anthropogenic and natural changes in estuarine tidal dynamics. *Journal of Coastal Research, SI 64 (Proceeding of the International Coastal Symposium)*, 1490-1494.

Duarte, B., Valentim, J.M., Dias, J.M., Silva, H., Marques, J.C., Caçador, I., 2014. Modelling sea level rise (SLR) impacts on salt marsh detrital outwelling C and N exports from an estuarine coastal lagoon to the ocean (Ria de Aveiro, Portugal). *Ecological Modelling* 289, 36-44.

Duarte, B., Martins, I., Rosa, R., Matos, A.R., Roleda, M.Y., Reusch, T.B.H., Engelen, A.H., Serrão, E.A., Pearson, G.A., Marques, J.C., Caçador, I., Duarte, C.M., Jueterbock, A., 2018. Climate Change Impacts on Seagrass Meadows and Macroalgal Forests: An Integrative Perspective on Acclimation and Adaptation Potential. *Frontiers in Marine Science* 5 (190).

Duarte, C.M., 1989. Temporal biomass variability and production biomass relationships of seagrass communities. *Marine Ecology Progress Series* 51(3), 269-276.

Duarte, C.M., Sandjensen, K., 1990. Seagrass colonization - biomass development and shoot demography in *Cymodocea nodosa* patches. *Marine Ecology Progress Series* 67(1), 97-103.

Duarte, C.M., 1991. Allometric scaling of seagrass form and productivity. *Marine Ecology Progress Series* 77(2-3), 289-300.

Duarte, C.M., 1995. Submerged aquatic vegetation in relation to different nutrient regimes. *Ophelia* 41, 87-112.

Duarte, C.M., 2000. Marine biodiversity and ecosystem services: an elusive link. *Journal of Experimental Marine Biology and Ecology* 250(1–2), 117-131.

Duarte, C.M., 2002. The future of seagrass meadows. *Environmental Conservation* 29(2), 192-206.

Duarte, C.M., Marba, N., Santos, R., 2004. *What may cause loss of seagrasses? in European Seagrasses: an Introduction to Monitoring and Management. J Borum, CM Duarte, D Krause-Jensen and TM Greve Eds (The M&MS project)*, 24-32 pp.

ECMWF, European Centre for Medium-Range Weather Forecasts, URL: www.ecmwf.int (last acceded: 30 October 2016).

Edebeatu, C.C., 2015. Comparison of four empirical evapotranspiration models against the penman-montieth in a mangrove zone. *International Journal of Applied Sciences and Engineering Research* 4(4), 580-589.

Eldridge, P.M., Morse, J.W., 2000. A diagenetic model for sediment-seagrass interactions. *Marine Chemistry* 70(1-3), 89-103.

Elkalay, K., Frangoulis, C., Skliris, N., Goffart, A., Gobert, S., Lepoint, G., Hecq, J.H., 2003. A model of the seasonal dynamics of biomass and production of the seagrass *Posidonia oceanica* in the Bay of Calvi (Northwestern Mediterranean). *Ecological Modelling* 167(1-2), 1-18.

European Commission, 2000. Water Framework Directive: Directive 2000/60/EC of the European Parliament and of the Council of 23 October 2000 establishing a framework for the community action in the field of water policy, Official Journal of the European Communities, pp. L327/321-L327/372

Fernández, Á., Arenas, F., Trilla, A., Rodríguez, S., Rueda, L., Martínez, B., 2015. Additive effects of emersion stressors on the ecophysiological performance of two intertidal seaweeds. *Marine Ecology Progress Series* 536, 135-147.

Ferreira, J.G., Simas, T., Nobre, A., Silva, M.C., Shifferegger, K., Lencart e Silva, J., 2003. Identification of sensitive areas and vulnerable zones in transitional and coastal Portuguese systems. *In.* I.N.A.G.-Instituto da Água, IMAR-Instituto do Mar (Eds.), Application of the United States National Estuarine Eutrophication Assessment to the Minho, Lima, Douro, Ria de Aveiro, Mondego, Tagus, Sado, Mira, Ria Formosa and Guadiana systems, pp. 53-65

Flindt, M.R., Pardal, J.A., Lillebø, A.I., Martins, I., Marques, J.C., 1999. Nutrient cycling and plant dynamics in estuaries: A brief review. *Acta Oecologica-International Journal of Ecology* 20(4), 237-248.

Folmer, E.O., van der Geest, M., Jansen, E., Olff, H., Anderson, T.M., Piersma, T., van Gils, J.A., 2012. Seagrass-Sediment Feedback: An Exploration Using a Non-recursive Structural Equation Model. *Ecosystems* 15(8), 1380-1393.

Fortunato, A.B., Rodrigues, M., Dias, J.M., Lopes, C., Oliveira, A., 2013. Generating inundation maps for a coastal lagoon: A case study in the Ria de Aveiro (Portugal). *Ocean Engineering* 64, 60-71.

Franssen, S.U., Gu, J., Winters, G., Huylmans, A.K., Wienpahl, I., Sparwel, M., Coyer, J.A., Olsen, J.L., Reusch, T.B.H., Bornberg-Bauer, E., 2014. Genome-wide transcriptomic responses of the seagrasses *Zostera marina* and *Nanozostera noltii* under a simulated heatwave confirm functional types. *Marine Genomics* 15, 65-73.

Fraser, M.W., Kendrick, G.A., Statton, J., Hovey, R.K., Zavala-Perez, A., Walker, D.I., 2014. Extreme climate events lower resilience of foundation seagrass at edge of biogeographical range. *Journal of Ecology* 102(6), 1528-1536.

Ganju, N.K., Brush, M.J., Rashleigh, B., Aretxabaleta, A.L., del Barrio, P., Grear, J.S., Harris, L.A., Lake, S.J., McCardell, G., O'Donnell, J., Ralston, D.K., Signell, R.P., Testa, J.M., Vaudrey, J.M.P., 2016. Progress and Challenges in Coupled Hydrodynamic-Ecological Estuarine Modeling. *Estuaries and Coasts* 39(2), 311-332.

Ganthy, F., Soissons, L., Sauriau, P.G., Verney, R., Sottolichio, A., 2015. Effects of short flexible seagrass *Zostera noltei* on flow, erosion and deposition processes determined using flume experiments. *Sedimentology* 62(4), 997-1023.

Gao, K.S., Qiu, B.S., Xia, J.R., Yu, A.J., Li, Y.G., 1998. Effect of wind speed on loss of water from *Nostoc flagelliforme* colonies. *Journal of Applied Phycology* 10(1), 55-58.

Génio, L., Sousa, A., Vaz, N., Dias, J.M., Barroso, C., 2008. Effect of low salinity on the survival of recently hatched veliger of *Nassarius reticulatus* (L.) in estuarine habitats: A case study of Ria de Aveiro. *Journal of Sea Research* 59(3), 133-143.

Greve, T.M., Binzer, T., 2004. Which factors regulate seagrass growth and distribution? *in* European Seagrasses: an Introduction to Monitoring and Management. J Borum, CM Duarte, D Krause-Jensen and TM Greve Eds (The M&MS project), pp. 19-23

Hall, L.M., Hanisak, M.D., Virnstein, R.W., 2006. Fragments of the seagrasses *Halodule wrightii* and *Halophila johnsonii* as potential recruits in Indian River Lagoon, Florida. *Marine Ecology Progress Series* 310, 109-117.

Harmel, R.D., Smith, P.K., Migliaccio, K.W., Chaubey, I., Douglas-Mankin, K.R., Benham, B., Shukla, S., Muñoz-Carpena, R., Robson, B.J., 2014. Evaluating, interpreting, and communicating performance of hydrologic/water quality models considering intended use: A review and recommendations. *Environmental Modelling & Software* 57, 40-51.

Helmuth, B., Mieszkowska, N., Moore, P., Hawkins, S.J., 2006. Living on the edge of two changing worlds: Forecasting the responses of rocky intertidal ecosystems to climate change. *Annual Review of Ecology, Evolution and Systematics* 37, 373-404.

Hemminga, M.A., Duarte, C.M., 2000. *Seagrass Ecology*. Cambridge University Press. 298 pp.

Hogarth, P., 2007. *The Biology of Mangroves and Seagrasses. 2nd Edition*. Oxford University Press. 273 pp.

Hu, K.L., Chen, Q., Wang, H.Q., 2015. A numerical study of vegetation impact on reducing storm surge by wetlands in a semi-enclosed estuary. *Coastal Engineering* 95, 66-76.

Huang, J., Zhang, X.F., Chua, V.P., 2016. Spatially-averaged diffusivities for pollutant transport in vegetated flows, in: Wu, J., Shu, C., Zhao, N., Lee, C.B., Zhu, C.L. (Eds.), *Proceedings of the Sixth International Symposium on Physics of Fluids,* 42.

Jiang, T., Skyllberg, U., Bjorn, E., Green, N.W., Tang, J.H., Wang, D.Y., Gao, J., Li, C.X., 2017. Characteristics of dissolved organic matter (DOM) and relationship with dissolved mercury in Xiaoqing River-Laizhou Bay estuary, Bohai Sea, China. *Environmental Pollution* 223, 19-30.

Jiang, Z., Huang, X., Zhang, J., Zhou, C., Lian, Z., Ni, Z., 2014. The effects of air exposure on the desiccation rate and photosynthetic activity of *Thalassia hemprichii* and *Enhalus acoroides*. *Marine Biology* 161(5), 1051-1061.

Jueterbock, A., Franssen, S.U., Bergmann, N., Gu, J., Coyer, J.A., Reusch, T.B.H., Bornberg-Bauer, E., Olsen, J.L., 2016. Phylogeographic differentiation versus transcriptomic adaptation to warm temperatures in *Zostera marina*, a globally important seagrass. *Molecular Ecology* 25(21), 5396-5411.

Kahn, A.E., Durako, M.J., 2009. Photosynthetic tolerances to desiccation of the co-occurring seagrasses *Halophila johnsonii* and *Halophila decipiens*. *Aquatic Botany* 90(2), 195-198.

Kenov, I.A., Deus, R., Alves, C.N., Neves, R., 2013. Modelling Seagrass Biomass and Relative Nutrient Content. *Journal of Coastal Research* 29(6), 1470-1476.

Kenov, I.A., 2014. *Development and application of a process-oriented model for benthic marine systems. PhD Thesis. Instituto Superior Técnico*. 214 pp.

Koch, E.M., 2001. Beyond light: Physical, geological, and geochemical parameters as possible submersed aquatic vegetation habitat requirements. *Estuaries* 24(1), 1-17.

Koch, E.W., Ackerman, J.D., Verduin, J., van Keulen, M., 2006. Fluid Dynamics in Seagrass Ecology - from Molecules to Ecosystems, *in Seagrasses: Biology, Ecology and Conservation*, pp. 193-225.

Kohlmeier, D., Pilditch, C.A., Bornman, J.F., Bischof, K., 2014. Site specific differences in morphometry and photophysiology in intertidal *Zostera muelleri* meadows. *Aquatic Botany* 116, 104-109.

Kraemer, G.P., Mazzella, L., 1999. Nitrogen acquisition, storage, and use by the co-occurring Mediterranean seagrasses *Cymodocea nodosa* and *Zostera noltii*. *Marine Ecology Progress Series* 183, 95-103.

La Nafie, Y.A., de los Santos, C.B., Brun, F.G., van Katwijk, M.M., Bouma, T.J., 2012. Waves and high nutrient loads jointly decrease survival and separately affect morphological and biomechanical properties in the seagrass *Zostera noltii*. *Limnology and Oceanography* 57(6), 1664-1672.

LAGOONS, 2012. Hydrodynamic and Water Quality Models. LAGOONS Report D6.1. 71 pp.

LAGOONS, 2014. Modelling results and recommendations. LAGOONS Report D6.2. 182 pp.

Lamote, M., Johnson, L.E., Lemoine, Y., 2012. Photosynthetic responses of an intertidal alga to emersion: The interplay of intertidal height and meteorological conditions. *Journal of Experimental Marine Biology and Ecology* 428, 16-23.

Laugier, T., Rigollet, V., de Casabianca, M.L., 1999. Seasonal dynamics in mixed eelgrass beds, *Zostera marina* L. and *Z. noltii* Hornem., in a Mediterranean coastal lagoon (Thau lagoon, France). *Aquatic Botany* 63(1), 51-69.

Legates, D.R., McCabe, G.J., 1999. Evaluating the use of "goodness-of-fit" measures in hydrologic and hydroclimatic model validation. *Water Resources Research* 35(1), 233-241.

Lencart e Silva, J.D., Vaz, N., Dias, J.M., 2012. *The Ria de Aveiro Lagoon - Hydrodynamic and Water Quality Models. in Hydrodynamic and Water Quality Models*. LAGOONS Report D6.1. 71 pp.

Lencart e Silva, J.D., Azevedo, A., Lillebø, A.I., Dias, J.M., 2013. Turbidity under changing physical forcing over two contrasting locations of seagrass meadows, Journal of Coastal Research, SI 65 (Proceeding of the International Coastal Symposium), pp. 2023-2028.

Leston, S., Lillebø, A.I., Pardal, M.A., 2008. The response of primary producer assemblages to mitigation measures to reduce eutrophication in a temperate estuary. *Estuarine Coastal and Shelf Science* 77(4), 688-696.

Leuschner, C., Landwehr, S., Mehlig, U., 1998. Limitation of carbon assimilation of intertidal *Zostera noltii* and *Z. marina* by desiccation at low tide. *Aquatic Botany* 62(3), 171-176.

Lillebø, A.I., Neto, J.M., Martins, I., Verdelhos, T., Leston, S., Cardoso, P.G., Ferreira, S.M., Marques, J.C., Pardal, M.A., 2005. Management of a shallow temperate estuary to control eutrophication: The effect of hydrodynamics on the system's nutrient loading. *Estuarine Coastal and Shelf Science* 65(4), 697-707.

Lillebø, A.I., Flindt, M.R., Pardal, M.A., Marques, J.C., 2006. The effect of *Zostera noltii*, *Spartina maritima* and *Scirpus maritimus* on sediment pore-water profiles in a temperate intertidal estuary. *Hydrobiologia* 555, 175-183.

Lillebø, A.I., Teixeira, H., Pardal, M.A., Marques, J.C., 2007. Applying quality status criteria to a temperate estuary before and after the mitigation measures to reduce eutrophication symptoms. *Estuarine, Coastal and Shelf Science* 72, 177-187.

Lillebø, A.I., Flindt, M.R., Cardoso, P., Leston, S., Dolbeth, M., Pereira, M.E., Duarte, A.C., Pardal, M.A., 2011. Restoration of Seagrass Community to Reverse Eutrophication in Estuaries, in: Eric, W., Donald, M. (Eds.), *Treatise on Estuarine and Coastal Science*. Academic Press, Waltham, pp. 151-164.

Lillebø, A.I., Stålnacke, P., Gooch, G.D., 2015. Coastal Lagoons in Europe: Integrated Water Resource Strategies. IWA publishing; International Water Association (IWA), UK, 254pp. UK. ISBN: 9781780406282; eISBN: 9781780406299. URL: http://wio.iwaponline.com/content/ppiwawio/14/9781780406299.full.pdf.

Longo, R.S., Picado, A., Vaz, N., Dias, J.M., 2016. Biological response of a coastal plain estuary to torrential episodes: a modelling study. *Journal of Coastal Research, SI 75 (Proceeding of the International Coastal Symposium)*, 79-83.

Lopes, C.B., Pereira, M.E., Vale, C., Lillebø, A.I., Pardal, M.A., Duarte, A.C., 2007. Assessment of spatial environmental quality status in Ria de Aveiro (Portugal). *Scientia Marina* 71(2), 293-304.

Lopes, C.B., Lillebø, A.I., Pato, P., Dias, J.M., Rodrigues, S.M., Pereira, E., Duarte, A.C., 2008a. Inputs of organic carbon from Ria de Aveiro coastal lagoon to the Atlantic Ocean. *Estuarine Coastal and Shelf Science* 79(4), 751-757.

Lopes, C.L., Silva, P.A., Rocha, A., Dias, J.M., 2011a. Sensitivity analysis of Ria de Aveiro hydro-morphodynamics to the sea level rise integration period. *Journal of Coastal Research, SI 64 (Proceeding of the International Coastal Symposium)*, 230-234.

Lopes, C.L., Silva, P.A., Dias, J.M., Rocha, A., Picado, A., Plecha, S., Fortunato, A.B., 2011b. Local sea level change scenarios for the end of the 21st century and potential physical impacts in the lower Ria de Aveiro (Portugal). *Continental Shelf Research* 31(14), 1515-1526.

Lopes, C.L., Azevedo, A., Dias, J.M., 2013a. Flooding assessment under sea level rise scenarios: Ria de Aveiro case study. *Journal of Coastal Research, SI 65 (Proceeding of the International Coastal Symposium)*, 766-771.

Lopes, C.L., Plecha, S., Silva, P.A., Dias, J.M., 2013b. Influence of morphological changes in a lagoon flooding extension: case study of Ria de Aveiro (Portugal). *Journal of Coastal Research, SI 65 (Proceeding of the International Coastal Symposium)*, 1158-1163.

Lopes, C.L., Dias, J.M., 2014. Influence of mean sea level rise on tidal dynamics of the Ria de Aveiro lagoon, Portugal. *Journal of Coastal Research, SI 70 (Proceeding of the International Coastal Symposium)*, 574-579.

Lopes, C.L., Dias, J.M., 2015. Tidal dynamics in a changing lagoon: Flooding or not flooding the marginal regions. *Estuarine, Coastal and Shelf Science* 167, Part A, 14-24.

Lopes, C.L., 2016. Flood risk assessment in Ria de Aveiro under present and future scenarios. PhD Thesis. Universidade de Aveiro. 224 pp.

Lopes, J.F., Dias, J.M., Dekeyser, I., 2001. Influence of tides and river inputs on suspended sediment transport in the Ria de Aveiro lagoon, Portugal. *Physics and Chemistry of the Earth Part B – Hydrology Oceans and Atmosphere* 26(9), 729-734.

Lopes, J.F., Dias, J.M., Cardoso, A.C., Silva, C.I.V., 2005. The water quality of the Ria de Aveiro lagoon, Portugal: From the observations to the implementation of a numerical model. *Marine Environmental Research* 60(5), 594-628.

Lopes, J.F., Silva, C., 2006. Temporal and spatial distribution of dissolved oxygen in the Ria de Aveiro lagoon. *Ecological Modelling* 197(1-2), 67-88.

Lopes, J.F., Dias, J.M., Dekeyser, I., 2006. Numerical modelling of cohesive sediments transport in the Ria de Aveiro lagoon, Portugal. *Journal of Hydrology* 319(1-4), 176-198.

Lopes, J.F., Dias, J.M., 2007. Residual circulation and sediment distribution in the Ria de Aveiro lagoon, Portugal. *Journal of Marine Systems* 68(3-4), 507-528.

Lopes, J.F., Silva, C.I., Cardoso, A.C., 2008b. Validation of a water quality model for the Ria de Aveiro lagoon, Portugal. *Environmental Modelling & Software* 23(4), 479-494.

Lopes, J.F., Cardoso, A.C., Moita, M.T., Rocha, A.C., Ferreira, J.A., 2009. Modelling the temperature and the phytoplankton distributions at the Aveiro near coastal zone, Portugal. *Ecological Modelling* 220(7), 940-961.

Lopes, J.F., Almeida, M.A., Cunha, M.Â., 2010. Modelling the ecological patterns of a temperate lagoon in a very wet spring season. *Ecological Modelling* 221(19), 2302-2322.

Lopes, J.F., Vaz, N., Vaz, L., Ferreira, J.A., Dias, J.M., 2015. Assessing the state of the lower level of the trophic web of a temperate lagoon, in situations of light or nutrient stress: A modeling study. *Ecological Modelling* 313, 59-76.

Lopes, M.L., Marques, B., Dias, J.M., Soares, A., Lillebø, A.I., 2017. Challenges for the WFD second management cycle after the implementation of a regional multi-municipality sanitation system in a coastal lagoon (Ria de Aveiro, Portugal). *Science of the Total Environment* 586, 215-225.

Madden, C.J., Kemp, W.M., 1996. Ecosystem model of an estuarine submersed plant community: Calibration and simulation of eutrophication responses. *Estuaries* 19(2B), 457-474.

Marbà, N., Cebrián, J., Enríquez, S., Duarte, C.M., 1996. Growth patterns of western Mediterranean seagrasses: Species-specific responses to seasonal forcing. *Marine Ecology Progress Series* 133(1-3), 203-215.

Marín-Guirao, L., Entrambasaguas, L., Dattolo, E., Ruiz, J.M., Procaccini, G., 2017. Molecular Mechanisms behind the Physiological Resistance to Intense Transient Warming in an Iconic Marine Plant. *Frontiers in Plant Science* 8, 1142.

Martínez-Crego, B., Verges, A., Alcoverro, T., Romero, J., 2008. Selection of multiple seagrass indicators for environmental biomonitoring. *Marine Ecology-Progress Series* 361, 93-109.

Massa, S.I., Arnaud-Haond, S., Pearson, G.A., Serrão, E.A., 2009. Temperature tolerance and survival of intertidal populations of the seagrass *Zostera noltii* (Hornemann) in Southern Europe (Ria Formosa, Portugal). *Hydrobiologia* 619, 195-201.

Mateus, M., Mateus, S., Baretta, J.W., 2008. *Basic concepts of estuarine ecology. in Perspectives on Integrated Coastal Zona Management in South America. Neves, R., Baretta, J.W., Mateus, M. (Editors)*. 604 pp.

McLusky, D.S., Elliott, M., 2004. *The Estuarine Ecosystem - Ecology, Threats and Management*, 3rd Edition ed. Oxford University Press. 224 pp.

Mendes, R., Dias, J.M., Pinheiro, L.M., 2009. Numerical Modeling Estimation of the Spread of Maritime Oil Spills in Ria de Aveiro Lagoon. *Journal of Coastal Research, SI 56 (Proceeding of the International Coastal Symposium)*, 1375-1379.

Mendes, R., Vaz, N., Dias, J.M., 2011. Numerical modeling changes induced by the low lying areas adjacent to Ria de Aveiro. *Journal of Coastal Research, SI 64 (Proceeding of the International Coastal Symposium)*, 1125-1129.

Moll, A., 2000. Assessment of three-dimensional physical-biological ECOHAM1 simulations by quantified validation for the North Sea with ICES and ERSEM data. *ICES Journal of Marine Science* 57(4), 1060-1068.

Montefalcone, M., 2009. Ecosystem health assessment using the Mediterranean seagrass *Posidonia oceanica*: A review. *Ecological Indicators* 9(4), 595-604.

Monteith, J.L., 1965. Evaporation and environment. *Symposia of the Society for Experimental Biology* 19, 205–224.

Morais, P., Martins, F., Chicharo, M.A., Lopes, J., Chicharo, L., 2012. Merging anchovy eggs abundance into a hydrodynamic model as an assessment tool for estuarine ecohydrological management. *River Research and Applications* 28(2), 160-176.

Nayar, S., Bott, K., 2015. *Uptake and translocation of ammonium and nitrate by temperate seagrass Zostera nigricaulis in Port Philip Bay. South Australian Research and Development Institute (Aquatic Sciences), Adelaide. SARDI Publication No. F2014/000665-1. SARDI Research Report Series No. 819.* 51 pp.

Newton, A., Harff, J., You, Z.J., Zhang, H., Wolanski, E., 2016. Sustainability of future coasts and estuaries: A synthesis. *Estuarine Coastal and Shelf Science* 183, 271-274.

Novak, A.B., Short, F.T., 2011. UV-B induces leaf reddening and supports photosynthesis in the seagrass *Thalassia testudinum*. *Journal of Experimental Marine Biology and Ecology* 409(1-2), 136-142.

Orth, R.J., Carruthers, T.J.B., Dennison, W.C., Duarte, C.M., Fourqurean, J.W., Heck, K.L., Jr., Hughes, A.R., Kendrick, G.A., Kenworthy, W.J., Olyarnik, S., Short, F.T., Waycott, M., Williams, S.L., 2006. A global crisis for seagrass ecosystems. *Bioscience* 56(12), 987-996.

OSPAR Commission, 2005. *Synergies in Assessment and Monitoring between OSPAR and the European Union*. OSPAR (Protection of the Marine Environment of the North-East Atlantic) publications. 67 pp.

Park, Y., Cho, K.H., Kang, J.H., Lee, S.W., Kim, J.H., 2014. Developing a flow control strategy to reduce nutrient load in a reclaimed multi-reservoir system using a 2D hydrodynamic and water quality model. *Science of the Total Environment* 466, 871-880.

Passarge, J., Hol, S., Escher, M., Huisman, J., 2006. Competition for nutrients and light: Stable coexistence, alternative stable states, or competitive exclusion? *Ecological Monographs* 76(1), 57-72.

Pato, P., Lopes, C.B., Válega, M., Lillebø, A.I., Dias, J.M., Pereira, E., Duarte, A.C., 2008. Mercury fluxes between an impacted coastal lagoon and the Atlantic Ocean. *Estuarine Coastal and Shelf Science* 76(4), 787-796.

Paul, M., Amos, C.L., 2011. Spatial and seasonal variation in wave attenuation over *Zostera noltii*. *Journal of Geophysical Research-Oceans* 116, C08019.

Pawlowicz, R., Beardsley, B., Lentz, S., 2002. Classical tidal harmonic analysis including error estimates in MATLAB using T-TIDE. *Computers & Geosciences* 28(8), 929-937.

Peralta, G., Brun, F.G., Pérez-Lloréns, J.L., Bouma, T.J., 2006. Direct effects of current velocity on the growth, morphometry and architecture of seagrasses: a case study on *Zostera noltii*. *Marine Ecology Progress Series* 327, 135-142.

Pérez-Lloréns, J.L., Niell, F.X., 1993a. Seasonal dynamics of biomass and nutrient content in the intertidal seagrass *Zostera noltii* Hornem. from Palmones River estuary, Spain. *Aquatic Botany* 46(1), 49-66.

Pérez-Lloréns, J.L., Niell, F.X., 1993b. Temperature and emergence effects on the net photosynthesis of two *Zostera noltii* Hornem. morphotypes. *Hydrobiologia* 254(1), 53-64.

Pérez-Lloréns, J.L., Strother, S., Niell, F.X., 1994. Species-Differences in Short-Term Pigment Levels in 4 Australian Seagrasses in Response to Dessication and Rehydration. *Botanica Marina* 37(1), 91-95.

Perez, M., Romero, J., Duarte, C.M., Sandjensen, K., 1991. Phosphorous limitation of *Cymodocea nodosa* growth. *Marine Biology* 109(1), 129-133.

Pergent-Martini, C., Pasqualini, V., Ferratt, L., Pergent, G., Fernandez, C., 2005. Seasonal dynamics of *Zostera noltii* Hornem. in two Mediterranean lagoons. *Hydrobiologia* 543, 233-243.

Pergent, G., Bazairi, H., Bianchi, C.N., Boudouresque, C.F., Buia, M.C., Calvo, S., Clabaut, P., Harmelin-Vivien, M., Mateo, M.A., Montefalcone, M., Morri, C., Orfanidis, S., Pergent-Martini, C., Semroud, R., Serrano, O., Thibaut, T., Tomasello, A., Verlaque, M., 2014. Climate change and Mediterranean seagrass meadows: a synopsis for environmental managers. *Mediterranean marine science* 15(2), 462-473.

Philippart, C.J.M., 1995a. Seasonal variationin growth and biomass of an intertidal *Zostera noltii* stand in the Dutch Wadden Sea. *Netherlands Journal of Sea Research* 33(2), 205-218.

Philippart, C.J.M., 1995b. Effects of shading on growth, biomass and population maintenance of the intertidal seagrass *Zostera noltii* Hornem. in the Dutch Wadden Sea. *Journal of Experimental Marine Biology and Ecology* 188(2), 199-213.

Picado, A., Dias, J.M., Fortunato, A.B., 2009. Effect of flooding the salt pans in the Ria de Aveiro. *Journal of Coastal Research, SI 56 (Proceeding of the International Coastal Symposium)*, 1395-1399.

Picado, A., Dias, J.M., Fortunato, A.B., 2010. Tidal changes in estuarine systems induced by local geomorphologic modifications. *Continental Shelf Research* 30(17), 1854-1864.

Picado, A., Silva, P.A., Fortunato, A.B., Dias, J.M., 2011. Particle tracking-modeling of morphologic changes in the Ria de Aveiro. *Journal of Coastal Research, SI 64 (Proceeding of the International Coastal Symposium)*, 1560-1564.

Picado, A., Lopes, C.L., Mendes, R., Vaz, N., Dias, J.M., 2013. Storm surge impact in the hydrodynamics of a tidal lagoon: the case of Ria de Aveiro. *Journal of Coastal Research, SI 65 (Proceeding of the International Coastal Symposium)*, 796-801.

Pinheiro, J.P.S., 2017. *Numerical modelling of tide-surge interaction and its influence in estuarine inundation patterns. MsC Thesis. Universidade de Aveiro*. 49 pp.

Plecha, S., 2011. *Contribution to the Study of the Ria de Aveiro Inlet Morphodynamics. PhD Thesis. Universidade de Aveiro*. 163 pp.

Plecha, S., Silva, P.A., Oliveira, A., Dias, J.M., 2012. Establishing the wave climate influence on the morphodynamics of a coastal lagoon inlet. *Ocean Dynamics* 62(5), 799-814.

Plus, M., Deslous-Paoli, J.M., Auby, I., Dagault, F., 2001. Factors influencing primary production of seagrass beds (*Zostera noltii* Hornem.) in the Thau lagoon (French Mediterranean coast). *Journal of Experimental Marine Biology and Ecology* 259(1), 63-84.

Plus, M., Chapelle, A., Ménesguen, A., Deslous-Paoli, J.M., Auby, I., 2003. Modelling seasonal dynamics of biomasses and nitrogen contents in a seagrass meadow (*Zostera noltii* Hornem.): application to the Thau lagoon (French Mediterranean coast). *Ecological Modelling* 161(3), 213-238.

Plus, M., Dalloyau, S., Trut, G., Auby, I., de Montaudouin, X., Emery, E., Noel, C., Viala, C., 2010. Long-term evolution (1988-2008) of Zostera spp. meadows in Arcachon Bay (Bay of Biscay). *Estuarine Coastal and Shelf Science* 87(2), 357-366.

Priestley, C.H.B., Taylor, R.J., 1972. On the assessment of surface heat flux and evaporation using large-scale parameters. *Monthly Weather Review* 100, 81-82.

Raven, J.A., 1991. Responses of aquatic photosynthetic organisms to increased solar UVB. *Journal of Photochemistry and Photobiology B: Biology* 9(2), 239-244.

Reusch, T.B.H., Stam, W.T., Olsen, J.L., 1999a. Size and estimated age of genets in eelgrass, *Zostera marina*, assessed with microsatellite markers. *Marine Biology* 133(3), 519-525.

Reusch, T.B.H., Bostrom, C., Stam, W.T., Olsen, J.L., 1999b. An ancient eelgrass clone in the Baltic. *Marine Ecology Progress Series* 183, 301-304.

Ribeiro, A.S., 2015. *Coupled Modelling of the Tagus Estuary to climate change: a modelling study. MsC Thesis. Universidade de Aveiro*. 106 pp.

Rodrigues, A.M., Quintino, V., Sampaio, L., Freitas, R., Neves, R., 2011. Benthic biodiversity patterns in Ria de Aveiro, Western Portugal: Environmental-biological relationships. *Estuarine Coastal and Shelf Science* 95(2-3), 338-348.

Rodrigues, J.G., 2015. *The Tagus estuarine plume variability: impact coastal circulation and hydrography. MsC Thesis. Universidade de Aveiro*. 70 pp.

Rodrigues, M., Oliveira, A., Costa, M., Fortunato, A.B., Zhang, Y., 2009a. Sensitivity Analysis of an Ecological Model applied to the Ria de Aveiro. *Journal of Coastal Research, SI 56 (Proceeding of the International Coastal Symposium)*, 448-452.

Rodrigues, M., Oliveira, A., Queiroga, H., Fortunato, A.B., Zhang, Y.J., 2009b. Three-dimensional modeling of the lower trophic levels in the Ria de Aveiro (Portugal). *Ecological Modelling* 220(9-10), 1274-1290.

Rodrigues, M., 2012. *Effects of the Climatic Factors and Anthropogenic Actions in Ria de Aveiro. PhD Thesis. Universidade de Aveiro.* 270 pp.

Rodrigues, M., Oliveira, A., Queiroga, H., Brotas, V., 2012. Seasonal and diurnal water quality and ecological dynamics along a salinity gradient (Mira channel, Aveiro lagoon, Portugal), in: Yang, Z., Chen, B. (Eds.), *18th Biennial Isem Conference on Ecological Modelling for Global Change and Coupled Human and Natural System*, pp. 899-918.

Rodrigues, M., Oliveira, A., Queiroga, H., Brotas, V., Fortunato, A.B., 2015. Modelling the effects of climate change in estuarine ecosystems with coupled hydrodynamic and biogeochemical models, in: Park, Y.S., Lek, S., Baehr, C., Jorgensen, S.E. (Eds.), *Advanced Modelling Techniques Studying Global Changes in Environmental Sciences*, pp. 271-288.

Sandoval-Gil, J.M., Ruiz, J.M., Marín-Guirao, L., Bernardeau-Esteller, J., Sánchez-Lizaso, J.L., 2014. Ecophysiological plasticity of shallow and deep populations of the Mediterranean seagrasses *Posidonia oceanica* and *Cymodocea nodosa* in response to hypersaline stress. *Marine Environmental Research* 95, 39-61.

Santos, L., Santos, A.L., Coelho, F., Gomes, N.C.M., Dias, J.M., Cunha, Â., Almeida, A., 2011. Relation between bacterial activity in the surface microlayer and estuarine hydrodynamics. *FEMS Microbiology Ecology* 77(3), 636-646.

Santos, L., Vaz, L., Gomes, N.C.M., Vaz, N., Dias, J.M., Cunha, Â., Almeida, A., 2014. Impact of freshwater inflow on bacterial abundance and activity in the estuarine system Ria de Aveiro. *Estuarine Coastal and Shelf Science* 138, 107-120.

Santos, R., Duarte, P., 1991. Marine plant harvest in Portugal. *Journal of Applied Phycology* 3(1), 11-18.

Saraiva, S., Pina, P., Martins, F., Santos, M., Braunschweig, F., Neves, R., 2007. Modelling the influence of nutrient loads on Portuguese estuaries. *Hydrobiologia* 587, 5-18.

Schreiber, U., Bilger, W., Neubauer, C., 1995. Chlorophyll Fluorescence as a Nonintrusive Indicator for Rapid Assessment of *In vivo* Photosynthesis, in: Schulze, E.-D., Caldwell, M. (Eds.), *Ecophysiology of Photosynthesis*. Springer Berlin Heidelberg, pp. 49-70

Seagrass Watch, 2012. Percent Cover Standards - Methods. http://www.seagrasswatch.org/Methods/2012/Percentcover_standards/SW_Estuary_Z.pdf. Accessed 15 January 2016.,

Shafer, D.J., Sherman, T.D., Wyllie-Echeverria, S., 2007. Do desiccation tolerances control the vertical distribution of intertidal seagrasses? *Aquatic Botany* 87(2), 161-166.

Short, F., Carruthers, T., Dennison, W., Waycott, M., 2007. Global seagrass distribution and diversity: A bioregional model. *Journal of Experimental Marine Biology and Ecology* 350(1-2), 3-20.

Short, F.T., 1980. A simulation model of the seagrass production system, in: Phillips, R.C., McRoy, C.P. (Ed.), *Handbook of seagrass biology: an ecosystem perspective*, New York, pp. 277-295.

Short, F.T., Neckles, H.A., 1999. The effects of global climate change on seagrasses. *Aquatic Botany* 63(3-4), 169-196.

Short, F.T., Carruthers, T.J.R., Waycott, M., Kendrick, G.A., Fourqurean, J.W., Callabine, A., Kenworthy, W.J., Dennison, W.C., 2010. *Zostera noltii*. The IUCN Red List of Threatened Species 2010: e.T173361A6999224. http://dx.doi.org/10.2305/IUCN.UK.2010-3.RLTS.T173361A6999224.en. Downloaded on 18 January 2017.

Short, F.T., Polidoro, B., Livingstone, S.R., Carpenter, K.E., Bandeira, S., Bujang, J.S., Calumpong, H.P., Carruthers, T.J.B., Coles, R.G., Dennison, W.C., Erftemeijer, P.L.A., Fortes, M.D., Freeman, A.S., Jagtap, T.G., Kamal, A.H.M., Kendrick, G.A., Kenworthy, W.J., La Nafie, Y.A., Nasution, I.M., Orth, R.J., Prathep, A., Sanciangco, J.C., van Tussenbroek, B., Vergara, S.G., Waycott, M., Zieman, J.C., 2011. Extinction risk assessment of the world's seagrass species. *Biological Conservation* 144(7), 1961-1971.

Silva, H., Dias, J.M., Caçador, I., 2009a. Is the salt marsh vegetation a determining factor in the sedimentation processes? *Hydrobiologia* 621, 33-47.

Silva, J., Santos, R., 2003. Daily variation patterns in seagrass photosynthesis along a vertical gradient. *Marine Ecology Progress Series* 257, 37-44.

Silva, J., Santos, R., Calleja, M.L., Duarte, C.M., 2005a. Submerged versus air-exposed intertidal macrophyte productivity: from physiological to community-level assessments. *Journal of Experimental Marine Biology and Ecology* 317(1), 87-95.

Silva, J.F., Duck, R.W., 2001. Historical changes of bottom topography and tidal amplitude in the Ria de Aveiro, Portugal - trends for future evolution. *Climate Research* 18(1-2), 17-24.

Silva, J.F., Duck, R.W., Catarino, J.B., 2004. Seagrasses and sediment response to changing physical forcing in a coastal lagoon. *Hydrology and Earth System Sciences* 8(2), 151-159.

Silva, J.F., Duck, R.W., Catarino, J.B., 2005b. Changing use of the estuarine of the Ria de Aveiro, Portugal, and resultant impact on tidal flat sediments. *RMZ e Materials and Geoenvironment* 52, 111-114.

Silva, J.F., Duck, R.W., 2007. Identification of the effects of recent tidal regime changes in intertidal areas of the Ria de Aveiro, Portugal, using airborne and surface observations. *Geophysical Research Abstracts* 9.

Silva, J.F., Duck, R.W., Catarino, J.B., 2009b. Nutrient retention in the sediments and the submerged aquatic vegetation of the coastal lagoon of the Ria de Aveiro, Portugal. *Journal of Sea Research* 62(4), 276-285.

Sousa, A.I., Calado, R., Cleary, D.F.R., Nunes, C., Coimbra, M.A., Serôdio, J., Lillebø, A.I., 2017a. Effect of spatio-temporal shifts in salinity combined with other environmental variables on the ecological processes provided by *Zostera noltei* meadows. *Scientific Reports* 7.

Sousa, A.I., Santos, D.B., da Silva, E.F., Sousa, L.P., Cleary, D.F.R., Soares, A., Lillebo, A.I., 2017b. 'Blue Carbon' and Nutrient Stocks of Salt Marshes at a Temperate Coastal Lagoon (Ria de Aveiro, Portugal). *Scientific Reports* 7.

Sousa, A.I., Silva, J.F., Azevedo, A., Lillebø, A.I., *submitted*. Variability of seagrass meadows spatial extent and Blue Carbon over a decade in a coastal lagoon: Ria de Aveiro (Portugal).

Sousa, L.P., Sousa, A.I., Alves, F.L., Lillebo, A.I., 2016. Ecosystem services provided by a complex coastal region: challenges of classification and mapping. *Scientific Reports* 6.

Sousa, M.C., Dias, J.M., 2007. Hydrodynamic Model Calibration for a Mesotidal Lagoon: the Case of Ria de Aveiro (Portugal). *Journal of Coastal Research, SI 50 (Proceeding of the International Coastal Symposium)*, 1075-1080.

Statton, J., Cambridge, M.L., Dixon, K.W., Kendrick, G.A., 2013. Aquaculture of *Posidonia australis* Seedlings for Seagrass Restoration Programs: Effect of Sediment Type and Organic Enrichment on Growth. *Restoration Ecology* 21(2), 250-259.

Stefanova, A., Krysanova, V., Hesse, C., Lillebo, A.I., 2015. Climate change impact assessment on water inflow to a coastal lagoon: the Ria de Aveiro watershed, Portugal. *Hydrological Sciences Journal-Journal Des Sciences Hydrologiques* 60(5), 929-948.

Stow, C.A., Jolliff, J., McGillicuddy, D.J., Doney, S.C., Allen, J.I., Friedrichs, M.A.M., Rose, K.A., Wallheadg, P., 2009. Skill assessment for coupled biological/physical models of marine systems. *Journal of Marine Systems* 76(1-2), 4-15.

Sullivan, B.K., Sherman, T.D., Damare, V.S., Lilje, O., Gleason, F.H., 2013. Potential roles of *Labyrinthula spp.* in global seagrass population declines. *Fungal Ecology* 6(5), 328-338.

Sven, B., Eshel, A., 1983. Photosynthesis of Ulva sp. I. Effects of desiccation when exposed to air. *Journal of Experimental Marine Biology and Ecology* 70(1), 91-97.

SWIM, Soil and Water Integrated Model, Potsdam Institute for Climate Impact Research. URL: www.pik-potsdam.de/research/climate-impacts-and-vulnerabilities/models/swim, (last acceeded on 08 March 2018).

Tanaka, Y., Nakaoka, M., 2004. Emergence stress and morphological constraints affect the species distribution and growth of subtropical intertidal seagrasses. *Marine Ecology Progress Series* 284, 117-131.

Tomás, L.M., Rodrigues, M., Fortunato, A.B., Azevedo, A., Leitão, P.C., Oliveira, A., Rocha, A., Lopes, J.F., Dias, J.M., 2014. Salinity modelling accuracy of a coastal lagoon: a comparative river flow analysis of basin model vs. traditional approaches. *Journal of Coastal Research, SI 70 (Proceeding of the International Coastal Symposium)*, 586-591.

Trancoso, A.R., 2002. *Modeling Macroalgae in Estuaries. MSc Thesis. Instituto Superior Técnico*. 48 pp.

Trancoso, A.R., Saraiva, S., Fernandes, L., Pina, P., Leitão, P., Neves, R., 2005. Modelling macroalgae using a 3D hydrodynamic-ecological model in a shallow, temperate estuary. *Ecological Modelling* 187(2-3), 232-246.

Valentim, J.M., Vaz, N., Silva, H., Duarte, B., Caçador, I., Dias, J.M., 2013. Tagus estuary and Ria de Aveiro salt marsh dynamics and the impact of sea level rise. *Estuarine Coastal and Shelf Science* 130, 138-151.

Valle, M., Borja, Á., Chust, G., Galparsoro, I., Garmendia, J.M., 2011. Modelling suitable estuarine habitats for *Zostera noltii*, using Ecological Niche Factor Analysis and Bathymetric LiDAR. *Estuarine, Coastal and Shelf Science* 94(2), 144-154.

van der Heide, T., Eklof, J.S., van Nes, E.H., van der Zee, E.M., Donadi, S., Weerman, E.J., Olff, H., Eriksson, B.K., 2012. Ecosystem Engineering by Seagrasses Interacts with Grazing to Shape an Intertidal Landscape. *Plos One* 7(8).

van Lent, F., Nienhuis, P.H., Verschuure, J.M., 1991. Production and biomass of the seagrasses *Zostera noltii* Hornem. and *Cymodocea nodosa* (Ucria) Aschers at the Banc-Darguin (Mauritania, NW Africa) - A preliminary approach. *Aquatic Botany* 41(4), 353-367.

Vasconcelos, R.P., Reis-Santos, P., Maia, A., Fonseca, V., França, S., Wouters, N., Costa, M.J., Cabral, H.N., 2010. Nursery use patterns of commercially important marine fish species in estuarine systems along the Portuguese coast. *Estuarine Coastal and Shelf Science* 86(4), 613-624.

Vaz, L., Mateus, M., Serôdio, J., Dias, J.M., Vaz, N., 2016. Primary production of the benthic microalgae in the bottom sediments of Ria de Aveiro lagoon. *Journal of Coastal Research, SI 75 (Proceeding of the International Coastal Symposium)*, 178-182.

Vaz, N., Dias, J.M., Leitão, P., Martins, W., 2005. Horizontal patterns of water temperature and salinity in an estuarine tidal channel: Ria de Aveiro. *Ocean Dynamics* 55(5-6), 416-429.

Vaz, N., Leitão, P.C., Dias, J.M., 2007a. Channel-ocean exchange driven by tides and river flow: Espinheiro Channel (Portugal). *Journal of Coastal Research, SI 50 (Proceeding of the International Coastal Symposium)*, 1000-1004.

Vaz, N., Dias, J.M., Leitão, P.C., Nolasco, R., 2007b. Application of the Mohid-2D model to a mesotidal temperate coastal lagoon. *Computers & Geosciences* 33(9), 1204-1209.

Vaz, N., Dias, J.M., 2008. Hydrographic characterization of an estuarine tidal channel. *Journal of Marine Systems* 70(1-2), 168-181.

Vaz, N., Dias, J.M., Leitão, P.C., 2009. Three-dimensional modelling of a tidal channel: The Espinheiro Channel (Portugal). *Continental Shelf Research* 29(1), 29-41.

Verhagen, J.H.G., Nienhuis, P.H., 1983. A simulation model of production, seasonal changes in biomass and distribution of eelgrass (*Zostera marina*) in Lake Grevelingen. *Marine Ecology Progress Series* 10(2), 187-195.

Vermaat, J.E., Beijer, J.A.J., Gijlstra, R., Hootsmans, M.J.M., Philippart, C.J.M., Vandenbrink, N.W., Vanvierssen, W., 1993. Leaf dynamics and standing stocks of intertidal *Zostera noltii* Hornem. and *Cymodocea nodosa* (Ucria) Ascherson on the Banc-Darguin (Mauritania). *Hydrobiologia* 258, 59-72.

Vermaat, J.E., Verhagen, F.C.A., 1996. Seasonal variation in the intertidal seagrass *Zostera noltii* Hornem.: Coupling demographic and physiological patterns. *Aquatic Botany* 52(4), 259-281.

Vermaat, J.E., Agawin, N.S.R., Fortes, M.D., Uri, J.S., Duarte, C.M., Marbà, N., Enríquez, S., van Vierssen, W., 1996. The capacity of seagrasses to survive increased turbidity and siltation: the significance of growth form and light use. *Ambio* 25, 499-504.

Wang, K.H., 1994. Characterization of circulation and salinity change in Galveston Bay. *Journal of Engineering Mechanics-Asce* 120(3), 557-579.

Wentworth, C.K., 1922. A scale of grade and class terms for clastic sediments. *Journal of Geology* 30, 377–392.

Wetzel, R.L., Neckles, H.A., 1986. A Model of *Zostera marina* L. Photosynthesis and Growth - Simulated Effects of Selected Physical-Chemical Variables and Biological Interactions. *Aquatic Botany* 26(3-4), 307-323.

Wild-Allen, K., Andrewartha, J., 2016. Connectivity between estuaries influences nutrient transport, cycling and water quality. *Marine Chemistry* 185, 12-26.

Williams, B., 2006. *Hydrobiological modelling - processes, numerical methods and applications. University of Newcastle, NSW, Australia*. 708 pp.

Willmott, C.J., 1981. On the validation of models. *Physical Geography* 2(2), 184-194.

Xu, M., Chua, V.P., 2017. A numerical study on land-based pollutant transport in Singapore coastal waters with a coupled hydrologic-hydrodynamic model. *Journal of Hydro-environment Research* 14, 119-142.

Zaldívar, J.M., Bacelar, F.S., Dueri, S., Marinov, D., Viaroli, P., Hernández-Garcia, E., 2009. Modeling approach to regime shifts of primary production in shallow coastal ecosystems. *Ecological Modelling* 220(21), 3100-3110.

Zharova, N., Sfriso, A., Voinov, A., Pavoni, B., 2001. A simulation model for the annual fluctuation of *Zostera marina* biomass in the Venice lagoon. *Aquatic Botany* 70(2), 135-150.

Zharova, N., Sfriso, A., Pavoni, B., Voinov, A., 2008. Analysis of annual fluctuations of *C. nodosa* in the Venice lagoon: Modeling approach. *Ecological Modelling* 216(2), 134-144.

Zimmerman, R.C., Smith, R.D., Alberte, R.S., 1987. Is growth of eelgrass nitrogen limited? A numerical simulation of the effect of light and nitrogen on the growth dynamics of *Zostera marina*. *Marine Ecology Progress Series* 41, 167-176.

Zimmerman, R.C., Cabello-Pasini, A., Alberte, R.S., 1994. Modeling daily production of aquatic macrophytes from irradiance measurements - a comparative analysis. *Marine Ecology Progress Series* 114(1-2), 185-196.

Appendix

Appendix 1

Synthesis of numerical modelling applications to Ria de Aveiro lagoon

Hydrodynamic Models

(text in grey refers to hydrodynamic applications aiming to explain biological patterns)

Numerical model	Application	Reference
Delft3D-FLOW	• General hydrodynamic features (water level, temperature, salinity)	LAGOONS (2014)
	• Physical controls of turbidity (on seagrass)	Lencart e Silva *et al.* (2013)
ELCIRC	• General hydrodynamic features (tidal prism, currents, asymmetry, …)	Picado et al. (2010)
	• Lagoon flooded area	Picado *et al.* (2009), Picado et al. (2010), Lopes et al. (2013b), Lopes and Dias (2015)
	• Sea level rise (estimations, impact)	Lopes et al. (2013a), Lopes and Dias (2014)
	• Sediment transport	Dias and Picado (2011), Picado et al. (2011)
MOHID 2D	• General hydrodynamic features (water level, temperature, salinity)	Vaz et al. (2005), Vaz et al. (2007b) Mendes et al. (2011)
	• Tidal dynamics on biological features (macrobenthic gradients, saltmarsh dynamics)	Rodrigues et al. (2011), Valentim *et al.* (2013), Duarte et al. (2014)
	• Storm surge impact	Picado et al. (2013)
MOHID 3D	• Vertical structure of Espinheiro channel	Vaz et al. (2009)

Numerical model	Application	Reference
SELFE	• Inundation maps	Fortunato et al. (2013)
	• Salinity pattern	Tomás et al. (2014)
SIMSYS2D	• General hydrodynamic features (tidal prism, flow fields, residual circulation, residence time, dispersion, …)	Dias et al. (2000), Dias et al. (2001), Lopes and Dias (2007), Sousa and Dias (2007),Araújo et al. (2008), Dias and Mariano (2011)
	• Tidal dynamics on biological features (microalgae transport and dispersion, bacterioplankton, toxic microalgae)	Cunha et al. (2003), Cerejo and Dias (2007), Santos et al. (2011), Santos et al. (2014)
	• Pollutant/carbon transport, dispersion and fluxes (e.g. mercury, oil spill, organic carbon)	Lopes et al. (2008a), Pato et al. (2008), Mendes et al. (2009)
	• Salt and heat transport	Dias and Lopes (2006b), Dias and Lopes (2006a)
	• Sediment processes, fluxes, distribution and dynamics	Lopes et al. (2001), Dias et al. (2003), Abrantes et al. (2006), Lopes et al. (2006), Dias et al. (2007), Costa et al. (2011)
	• Sedimentation processes (effects of saltmarsh vegetation)	Silva et al. (2009a)

Ecological and Water Quality Models

Numerical model	Application	Reference
MOHID	• Primary production (macroalgae and phytoplankton) • Nitrogen, oxygen and carbon cycles	Trancoso et al. (2005)
	• Nitrogen load scenarios	Saraiva et al. (2007)
	• Primary production (seagrass meadows)	Kenov et al. (2013)
	• Primary production (benthic microalgae)	Vaz et al. (2016)

Numerical model	Application	Reference
Mike21-WQ	• Oxygen budget • Degradation of organic matter • Nitrification processes	Lopes et al. (2005) Lopes et al. (2008b)
	• Inorganic nutrients • Chlorophyll-a • Dissolved oxygen	Lopes and Silva (2006)
Mike3	• Primary production (phytoplankton) • Extreme weather conditions • Climate change impacts on the lower trophic levels	Lopes et al. (2010) Lopes et al. (2015)
ECO-SELFE 3D	• Ecological model • Primary production (phytoplankton) • Primary consumption (zooplankton) • Nutrient dynamics (N, P, Si) • Anthropogenic and climate change impacts on the lower trophic levels	Rodrigues et al. (2009a) Rodrigues et al. (2009b) Rodrigues et al. (2015) Rodrigues (2012)
	• Oxygen cycle	Rodrigues et al. (2012)
Delft3D-WAQ	• Nutrient dynamics • Impact of climate change on long-term nutrient loads	Lencart e Silva et al. (2012) LAGOONS (2014)
	• Primary production (seasonal dynamics of seagrass meadows) • Potential favorable areas for seagrass restoration • Impact of climate change on seagrasses	This work

Appendix 2

Temporal variations on hydrodynamics and seagrass covered area and biomass

Temporal variation in tidal prism

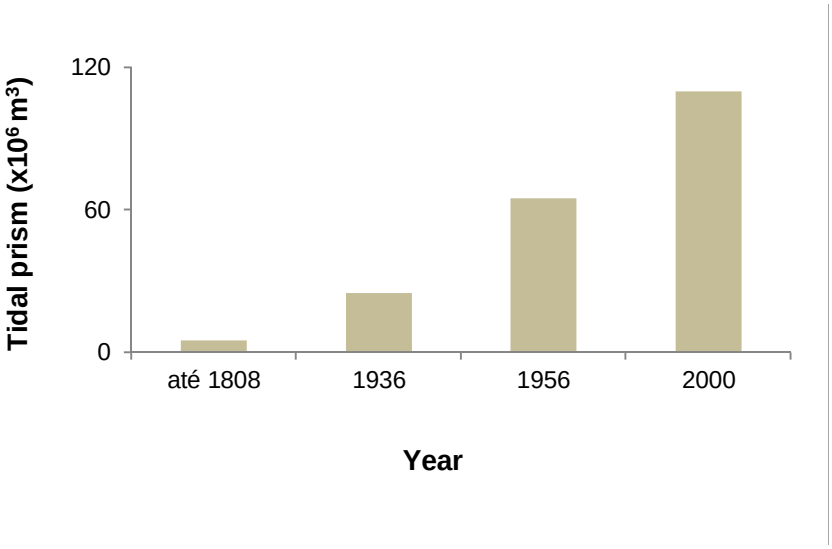

Temporal variation in Seagrass Covered Area (data from Ovar channel)

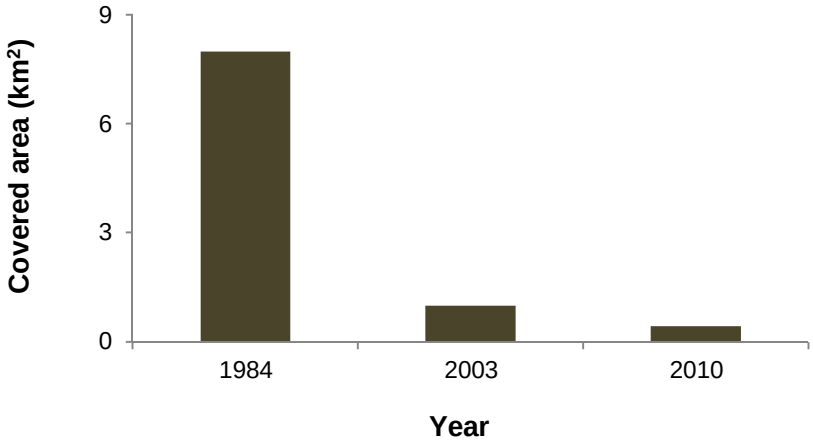

Appendix 3

Temperature limitation function according to Kenov *et al.*, (2003)

Seagrass dependence on temperature, *F(T)*, used by Kenov et al. (2013), retuned a bell-shaped function, ranging between 0 and 1, following the formulation of Trancoso (2002).

$$F(T) = K_A(T) \cdot K_B(T) \tag{A3.1}$$

Where $K_A(T)$ and $K_B(T)$ are respectively determined by equations (A3.2) and (A3.3),

$$K_A(T) = \frac{K_1 e^{\gamma_1 (T - T_{\min})}}{1 + K_1 \left[e^{\gamma_1 (T - T_{\min})} - 1 \right]} \tag{A3.2}$$

$$K_B(T) = \frac{K_4 e^{\gamma_2 (T_{\max} - T)}}{1 + K_4 \left[e^{\gamma_2 (T_{\max} - T)} - 1 \right]} \tag{A3.3}$$

and γ_1 and γ_2 by the equations XX and YY,

$$\gamma_1 = \frac{1}{\left(T_{\min}^{opt} - T_{\min} \right)} \ln \left(\frac{K_2 (1 - K_1)}{K_1 (1 - K_2)} \right) \tag{A3.4}$$

$$\gamma_2 = \frac{1}{\left(T_{\max} - T_{\max}^{opt} \right)} \ln \left(\frac{K_3 (1 - K_4)}{K_4 (1 - K_3)} \right) \tag{A3.5}$$

The parameters correspond to:

$T_{\min}^{opt}$ Minimum temperature for optimal growth interval (13 ºC)

$T_{\max}^{opt}$	Maximum temperature for optimal growth interval (28ºC)
$T_{\min}$	Minimum acceptable temperature (6 ºC)
$T_{\max}$	Maximum acceptable temperature (37 ºC)
K_1, K_2, K_3, K_4	Dimensionless constants to control temperature response (K_1=0.05; K_2=0.98; K_3=0.98; K_4=0.02)

Appendix 4

Evapotranspiration methods

Priestley-Taylor method (1972) – estimation of potential evapotranspiration ET_0

(From **S**olid**W**ater**I**ntegrated**M**odel User Manual. Mathematical Description of the Model Components. Chapter 2. Potential Evapotranspiration. http://www.pik-potsdam.de/~valen/swim_manual/swim-chapter1.pdf, last accessed on 07.12.2016)

Inputs:

Air temperature

Solar radiation

Elevation

Symbol	Unit	Description
ET_0	mm h^{-1}	Potential Evapotranspiration
EP	mm h^{-1}	Plant water transpiration rate - determined according to Ritchie (1972)
RAD	MJ m^{-2} h^{-1}	Solar Radiation
HV	MJ Kg^{-1}	Latent Heat of Vaporization
Δ	kPa $^oC^{-1}$	Slope of Saturation Vapor Pressure Curve
γ	kPa $^oC^{-1}$	Psychrometer Constant
e^o	kPa	Saturation Vapor Pressure
BP	kPa	Barometric Pressure
Elev	m	Elevation : 2.874
AirT	^oC	Air temperature
LAI	mm^2 mm^{-2}	Leaf area index - determined from field data of August 2013: 1.04

Step 1 – Calculation of latent heat of vaporization (HV)

Calculation of latent heat of vaporization (HV) as a function of hourly daily air temperature (AirT)

$$HV = 2.5 - 0.0022 \cdot AirT \tag{A4.1}$$

Step 2 – Calculation of psychrometer constant (γ)

Estimation of barometric pressure (BP) as a function of elevation (Elev),

$$BP = 101 - 0.0115 \cdot Elev + 5.44 \times 10^{-7} \cdot Elev^2 \tag{A4.2}$$

Calculation of psychrometer constant (γ) as a function of barometric pressure (BP),

$$\gamma = 6.6 \times 10^{-4} \cdot BP \tag{A4.3}$$

Step 3 – Calculation of slope of the saturation vapour curve (Δ)

Calculation of saturation vapour pressure as a function of air temperature (AirT)

$$e^0(AirT) = 0.1 \cdot exp\left[54.88 - 5.03 \cdot \ln(AirT + 273) - \frac{6791}{AirT + 273}\right] \tag{A4.4}$$

Calculation of slope of the saturation vapour curve (Δ)

$$\Delta = \left(\frac{e^0(AirT)}{AirT + 273}\right) \cdot \left(\frac{6791}{AirT + 273} - 5.03\right) \tag{A4.5}$$

Step 4 – Estimation of potential evapotranspiration (ET_0)

$$ET_0 = 1.28 \cdot \left(\frac{RAD}{HV}\right) \cdot \left(\frac{\delta}{\delta + \gamma}\right) \tag{A4.6}$$

Step 5 – Estimation of plant transpiration (EP)

As $0 \le LAI \le 3.0$, according to Ritchie (1972),

$$EP = \frac{ET_0 \cdot LAI}{3} \quad \text{(A4.7)}$$

Penman-Monteith method (1965) – estimation of potential evapotranspiration ET_0

(From FAO Corporate Document. Crop evapotranspiration - Guidelines for computing crop water requirements. Chapter 2 - 6. http://www.fao.org/docrep/X0490E/x0490e05.htm#TopOfPage, last accessed on 07.12.2016)

Inputs:

Air temperature

Solar radiation

Air humidity

Wind speed

Elevation

Symbol	Unit	Description
ET_0	mm h^{-1}	Potential evapotranspiration
EP	mm h^{-1}	Plant water transpiration rate - determined according to Ritchie (1972)
R_n	MJ m^{-2} h^{-1}	Net radiation at the grass surface
G_{hr}	MJ m^{-2} h^{-1}	Soil heat flux density
AirT	ºC	Mean hourly air temperature
Δ	kPa $ºC^{-1}$	Saturation slope vapour pressure curve at T_{hr}

Symbol	Unit	Description
γ	kPa $^oC^{-1}$	Psychrometer constant
e^o (AirT)	kPa	Saturation vapour pressure at air temperature AirT
e_a	kPa	Average hourly actual vapour pressure
u_2	m s^{-1}	Average hourly wind speed
RH_{hr}	%	Mean hourly relative humidity
R_S	MJ m^{-2} h^{-1}	Total solar radiation
BP	kPa	Barometric pressure
Elev	m	Elevation : 2.874
φ	radians	Latitude
J	Julian day	Number of the day in the year
d_r	-	Inverse relative distance earth-sun
δ	radians	Solar declination
S_c	h	Seasonal correction for solar time
L_z	^{o}	Set longitude of the centre of the local time zone (0º for Western Europe)
L_m	^{o}	Set longitude of the measurement site
t	h	Standard clock time at the midpoint of the period
t_1	h	Length of the calculation period
ω	radians	Solar time angle at midpoint of the period
R_a	MJ m^{-2} h^{-1}	Extraterrestrial radiation
R_{SO}	MJ m^{-2} h^{-1}	Clear-sky radiation
R_{ns}	MJ m^{-2} h^{-1}	Net shortwave radiation
R_{nl}	MJ m^{-2} h^{-1}	Net longwave radiation
σT_k	MJ m^{-2} h^{-1}	Stefan-Boltzman law
LAI	mm^2 mm^{-2}	Leaf area index - determined from field data of August 2013: 1.04

Step 1 – Calculation of slope of saturation vapour curve (Δ)

$$\Delta = \frac{4098\left[0.6108 exp\left(\frac{17.27 \cdot AirT}{AirT + 273.3}\right)\right]}{\left(AirT + 273.3\right)^2} \quad \text{(A4.8)}$$

Step 2 – Calculation of psychrometer constant (γ)

Estimation of barometric pressure (BP) as a function of elevation (Elev)

$$BP = 101.3\left(\frac{293 - 0.0065 \cdot Elev}{293}\right)^{5.26} \quad \text{(A4.9)}$$

Calculation of psychrometer constant (γ) as a function of barometric pressure (BP),

$$\gamma = 0.665 \times 10^{-3} \cdot BP \quad \text{(A4.10)}$$

Step 3 – Calculation of vapour pressure deficit

Calculation of saturation vapor pressure as a function of air temperature (e^o (AirT))

$$e^0\left(AirT\right) = 0.6108 exp\left[\frac{17.27 AirT}{AirT + 237.3}\right] \quad \text{(A4.11)}$$

Calculation of actual vapor pressure (e_a) as a function of hourly relative humidity (RH_{hr})

$$e_a = e^0\left(AirT\right)\frac{RH_{hr}}{100} \quad \text{(A4.12)}$$

Calculation of vapour pressure deficit (e^o (AirT) – e_a))

$$vapour\ pressure\ deficit = e^0\left(AirT\right) - e_a \quad \text{(A4.13)}$$

Step 4 – Radiation

Set Julian day, J (consult a table with the number of the day in the year)

Set latitude, φ, in radians

$$\varphi = \frac{\pi}{180}\left(latitude\,in\,decimal\,degress\right) \tag{A4.14}$$

Calculation of the inverse relative distance Earth-Sun, d_r

$$d_r = 1 + 0.033\cos\left(\frac{2\pi}{365}J\right) \tag{A4.15}$$

Calculation of solar declination, δ

$$\delta = 0.409\sin\left(\frac{2\pi}{365}J - 1.39\right) \tag{A4.16}$$

Calculation of seasonal correction for solar time (S_c)

$$S_c = 0.1645\sin\left(\frac{4\pi\left(J-81\right)}{364}\right) - 0.1255\cos\left(\frac{2\pi\left(J-81\right)}{364}\right) - 0.025\sin\left(\frac{2\pi\left(J-81\right)}{364}\right) \tag{A4.17}$$

Set longitude of the centre of the local time zone (0º for Western Europe), L_z

Set longitude of the measurement site (L_m)

Set standard clock time at the midpoint of the period (t)

Calculation of the solar time angle at midpoint of the period (ω)

$$\omega = \frac{\pi}{12}\left[t + 0.06667\left(L_z - L_m\right) + S_c - 12\right] \tag{A4.18}$$

Calculation of solar time angles at the beginning and end of the period

$$\omega_1 = \omega - \frac{\pi t_1}{24} \tag{A4.19}$$

$$\omega_2 = \omega + \frac{\pi t_1}{24} \tag{A4.20}$$

Calculation of extraterrestrial radiation in the hour period (R_a)

$$R_a = \frac{59.04}{\pi} \cdot d_r \left[(\omega_2 - \omega_1) \sin(\varphi) \sin(\delta) + \cos(\varphi) \cos(\delta) \left(\sin(\omega_2) - \sin(\omega_1) \right) \right] \quad \text{(A4.21)}$$

Calculation of clear-shy radiation (R_{SO})

$$R_{SO} = \left(0.75 + 2 \times 10^{-5} \cdot Elev \right) \times R_a \quad \text{(A4.22)}$$

Calculation of net shortwave radiation (R_{ns})

$$R_{ns} = 0.77 R_s \quad \text{(A4.23)}$$

Set Stefan-Boltzmann law at different temperatures (σT_k)

Calculation of net longwave radiation (R_{nl})

$$R_{nl} = \sigma T_k \cdot \left(0.34 - 0.14 \sqrt{e_a} \right) \cdot \left(1.35 \frac{R_s}{R_{so}} - 0.35 \right) \quad \text{(A4.24)}$$

Calculation of net radiation (R_n)

$$R_n = R_{ns} - R_{nl} \quad \text{(A4.25)}$$

Calculation of hourly soil heat flux (G_{hr}), for daylight periods

$$G_{hr} = 0.1 \cdot R_n \quad \text{(A4.26)}$$

Step 5 – Calculation of FAO Penman-Monteith equation for hourly timestep

$$ET_0 = \frac{0.408 \cdot \left(R_n - G_{hr} \right) + \gamma \frac{37}{T_{hr} + 273} u_2 \left(e^0 \left(T_{hr} \right) - e_a \right)}{\Delta + \gamma \left(1 + 0.34 u_2 \right)} \quad \text{(A4.27)}$$

Step 6 – Estimation of plant transpiration (EP)

As $0 \leq LAI \leq 3.0$, according to Ritchie (1972),

$$EP = \frac{ET_0 \cdot LAI}{3} \tag{A4.28}$$

Appendix 5

Climatology for river discharge parameters

River Discharge Parameters:

- A. River Flow (m^3 s^{-1})
- B. Water Temperature (ºC)

Useful information for graphic interpretation:

The plots represent the climatology of 1981-2010 and 2071-2100 for river discharge parameters, using SWIM results, for the following rivers: Antuã, Boco, Caster, Mira and Vouga.

The red curve represents the monthly average; line inside box: median; lower and upper box limits: first and third quartiles, respectively; lower and upper whiskers: minimum and maximum river discharges, respectively; dots: outliers.

Appendix 5.1 A. River Flow – Reference Condition

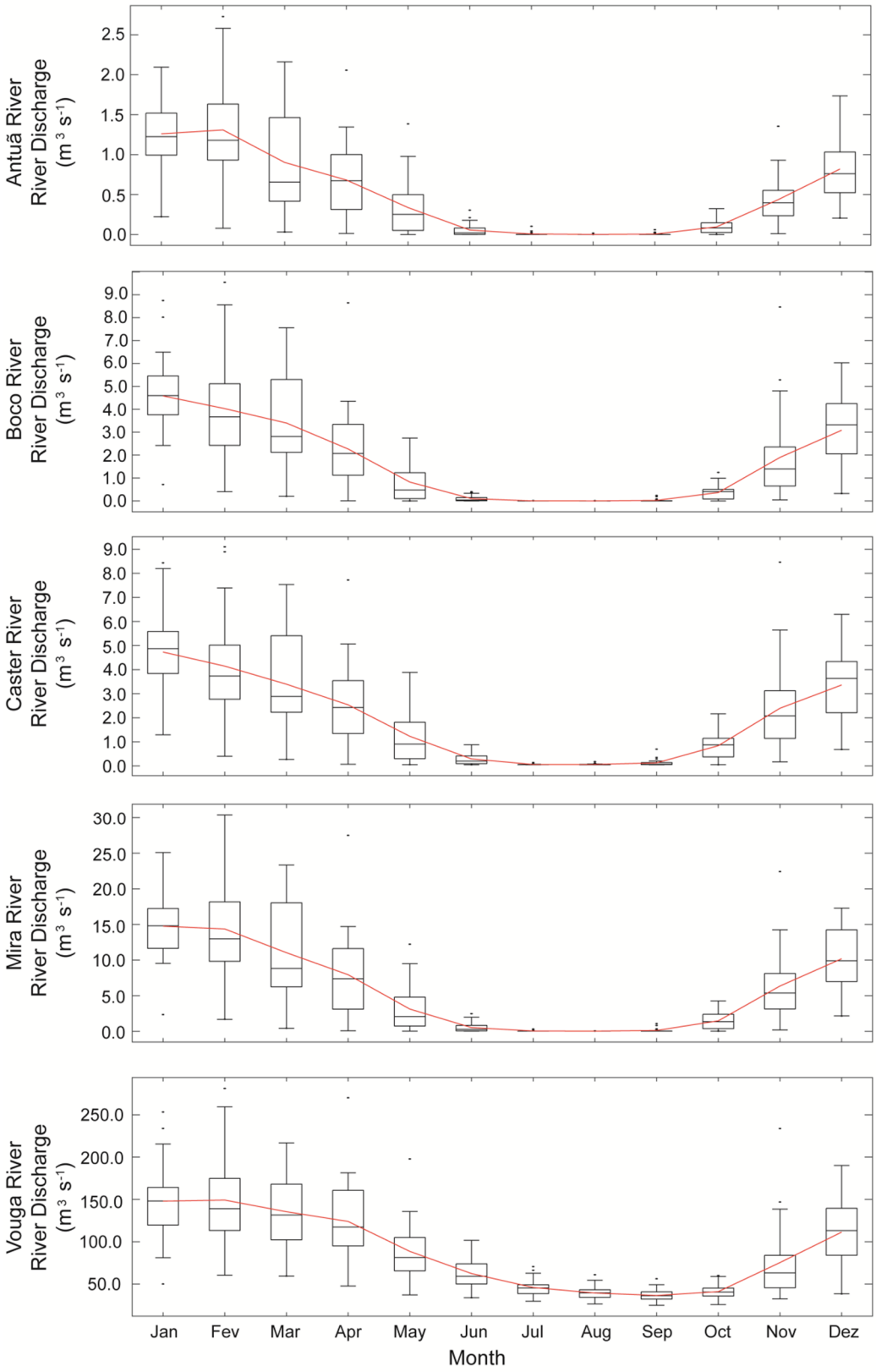

Appendix 5.1 B. Water Temperature – Reference Condition

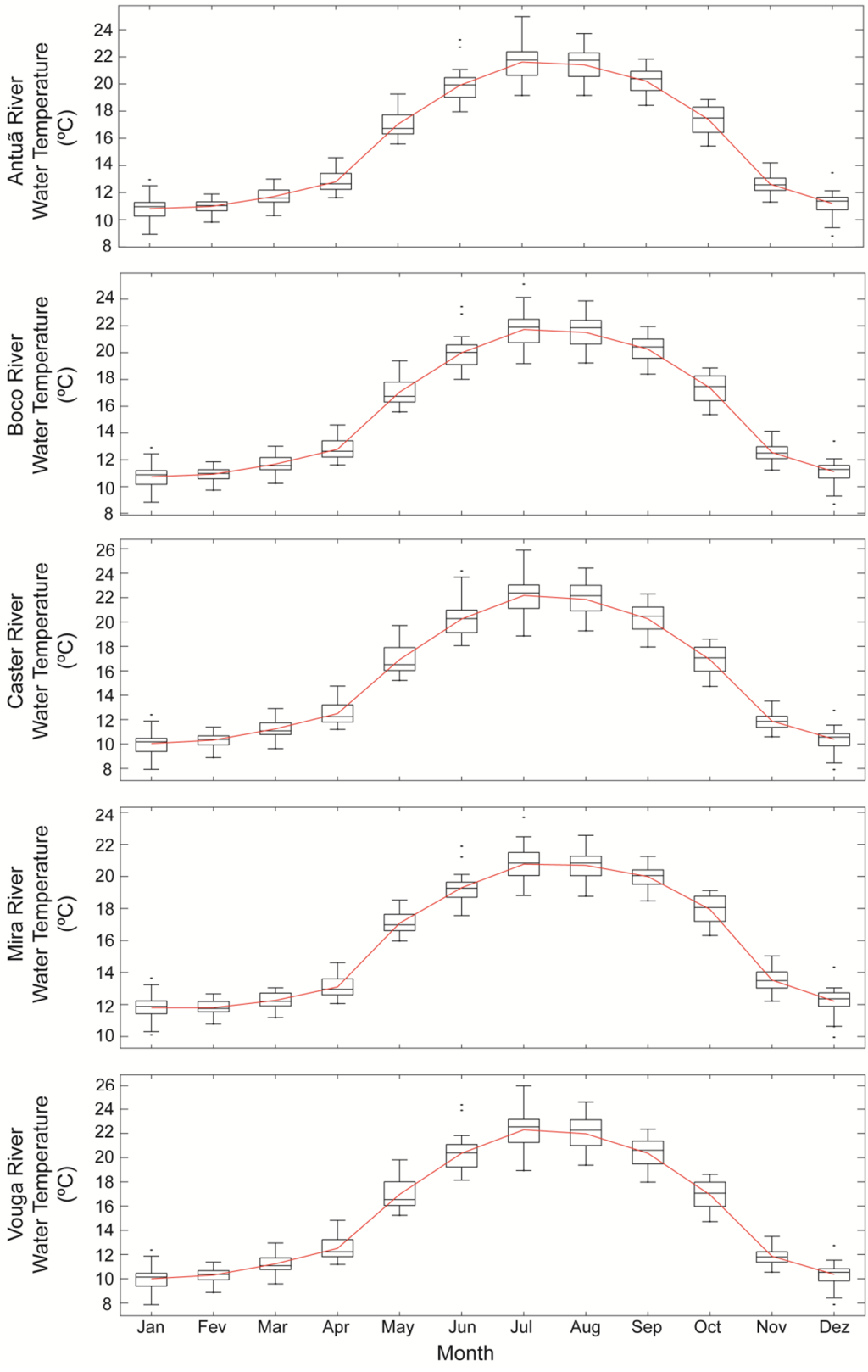

Appendix 5.2 A. River Flow – Future Condition (2071-2100)

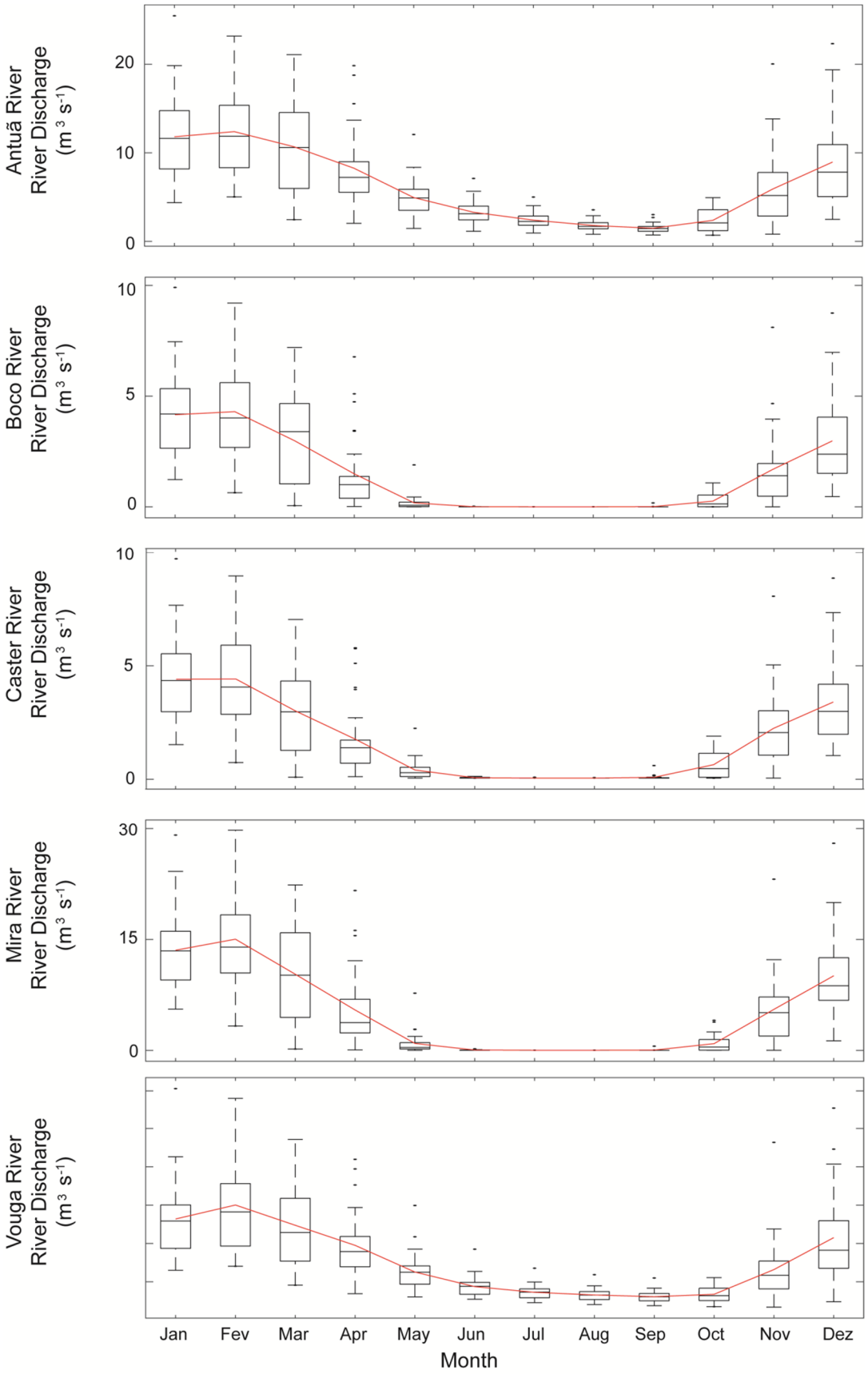

Appendix 5.2 B. Water Temperature – Future Condition (2071-2100)

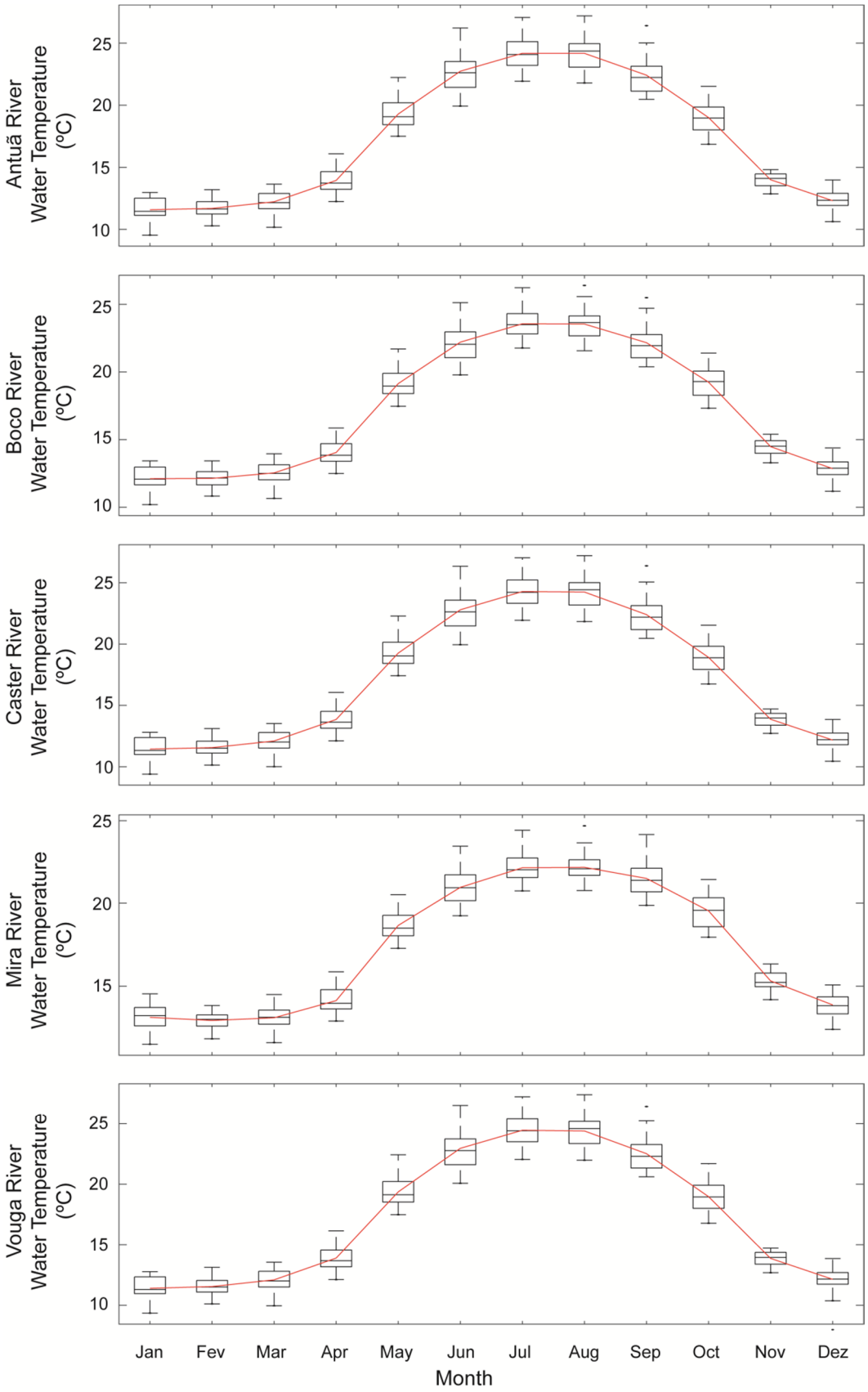

Appendix 6

Model inputs for climate change scenarios

Inputs:

- A. Meteorological data to build the heat flux model
- B. Wind rose diagrams
- C. Surface radiation
- D. Transport conditions at the oceanic boundary

Appendix 6A. Meteorological data to build the heat flux model (grey line), for RCP4.5 and RCP8.5, respectively, for a-b) air relative humidity, c-d) air temperature; d-e) Net solar radiation Monthly average: black line.

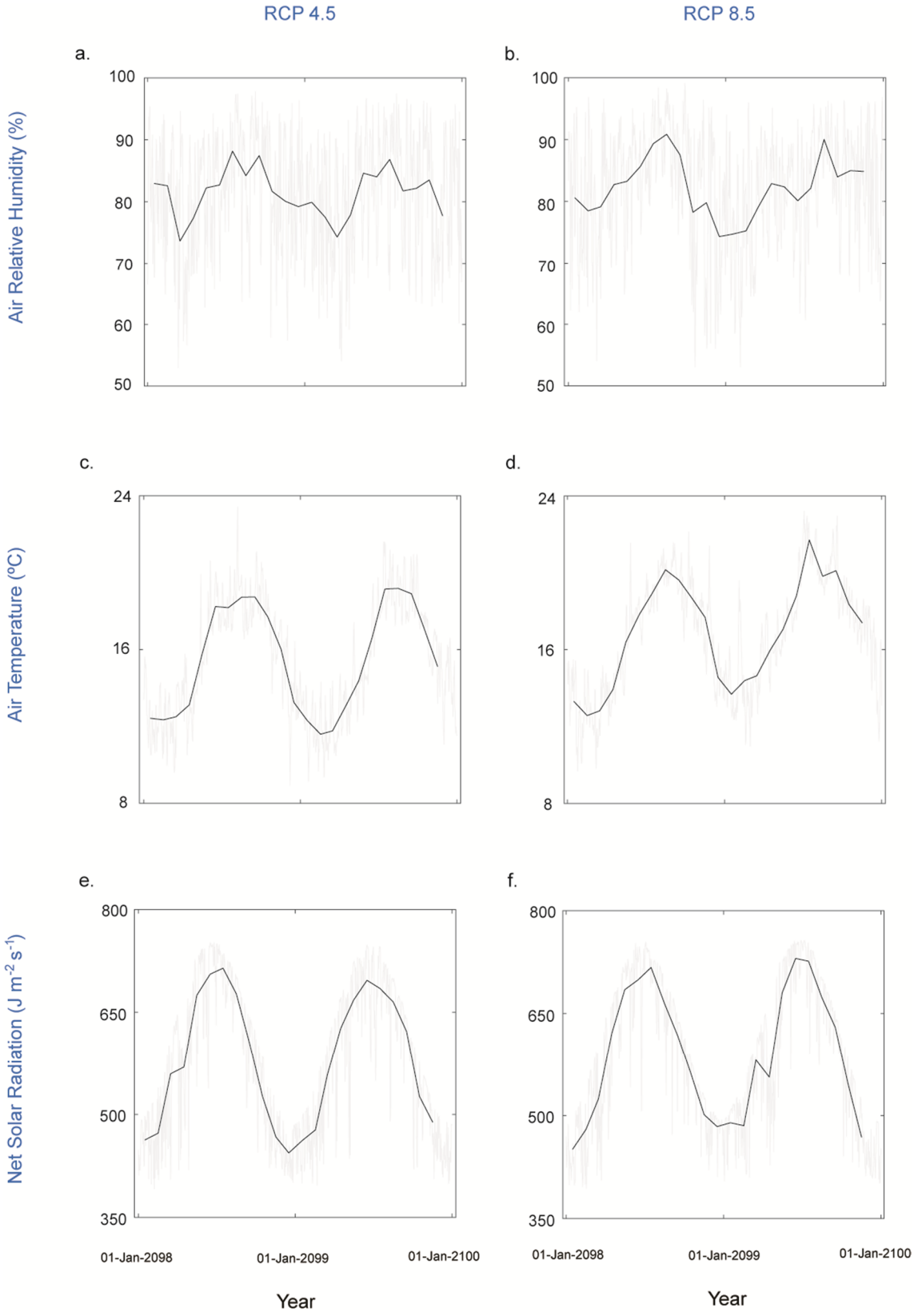

Appendix 6B. Wind rose diagrams (calculated for each season for RCP4.5 and RCP8.5, respectively, for a-b) spring, c-d) summer, e-f) autumn and g-h) winter.

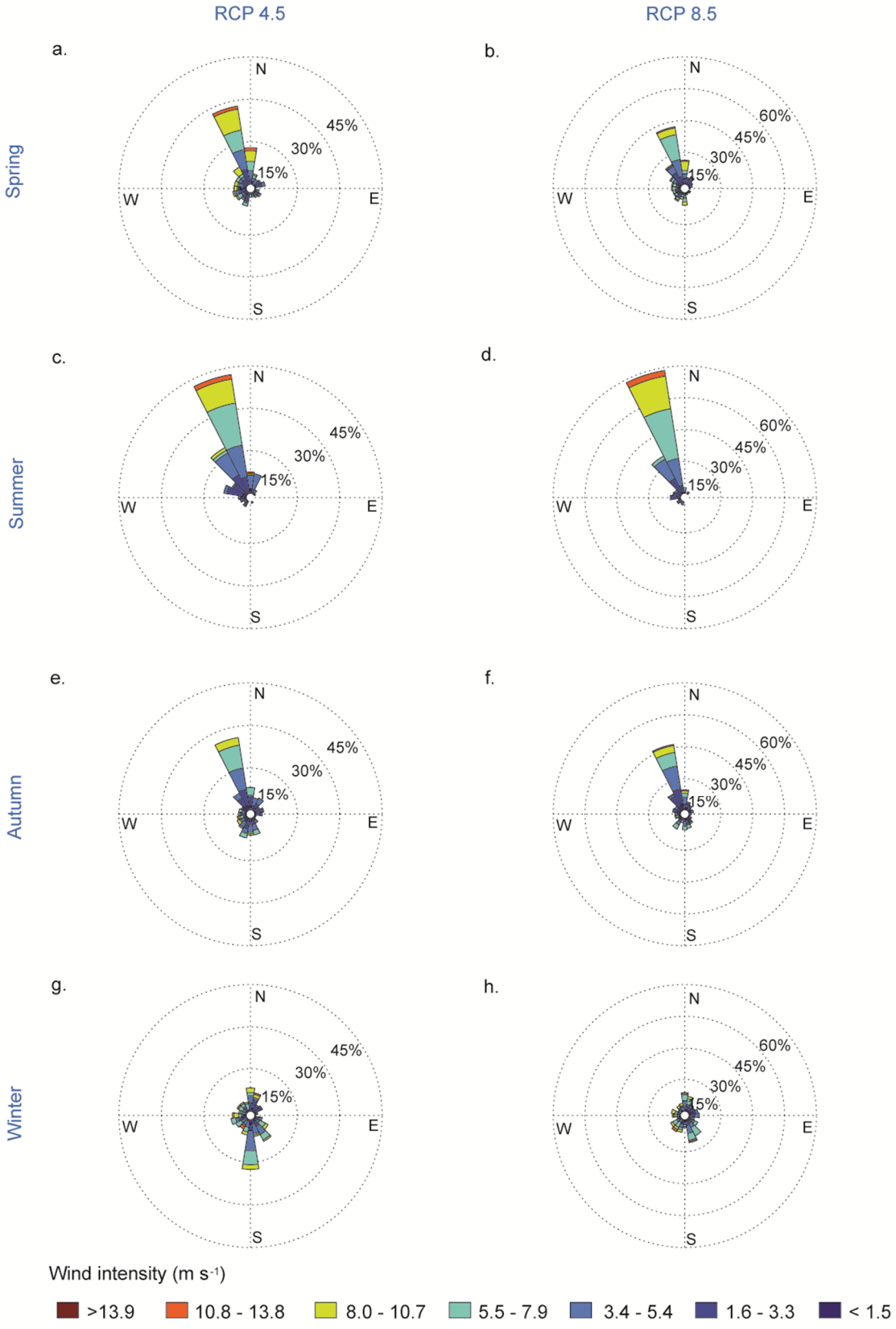

Appendix 6C. Every 10 minute- surface radiation used to force the seagrass model for RCP4.5 (grey line) and RCP8.5 (blue line). Monthly average: black and red lines, respectively

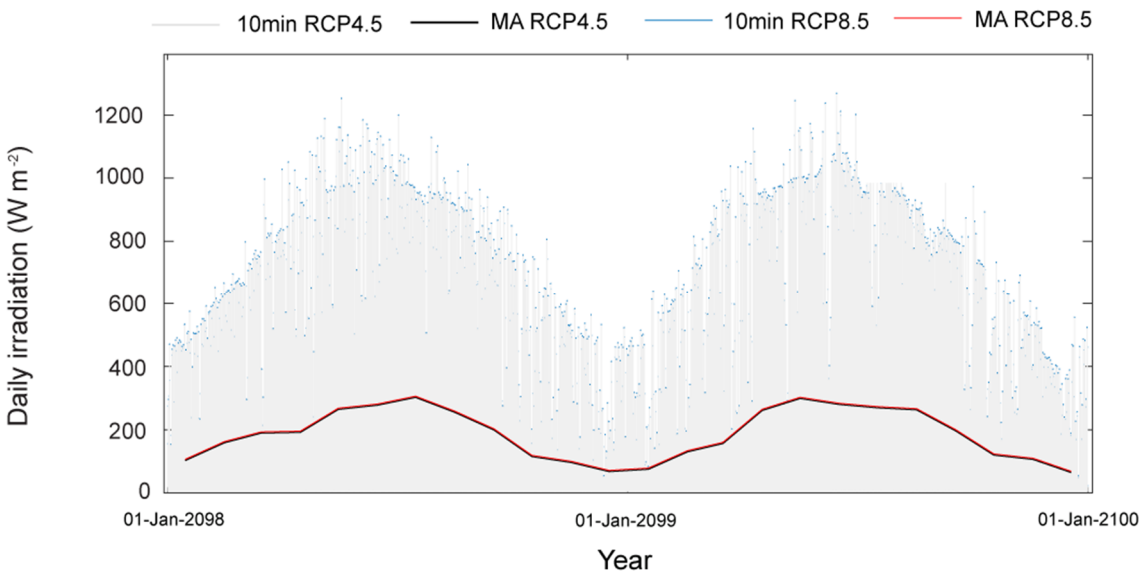

Appendix 6D. Transport conditions at the oceanic boundary, for RCP4.5 and RCP 8.5 for water temperature (red and red dashed lines, respectively) and salinity (blue and dashed blue lines, respectively)

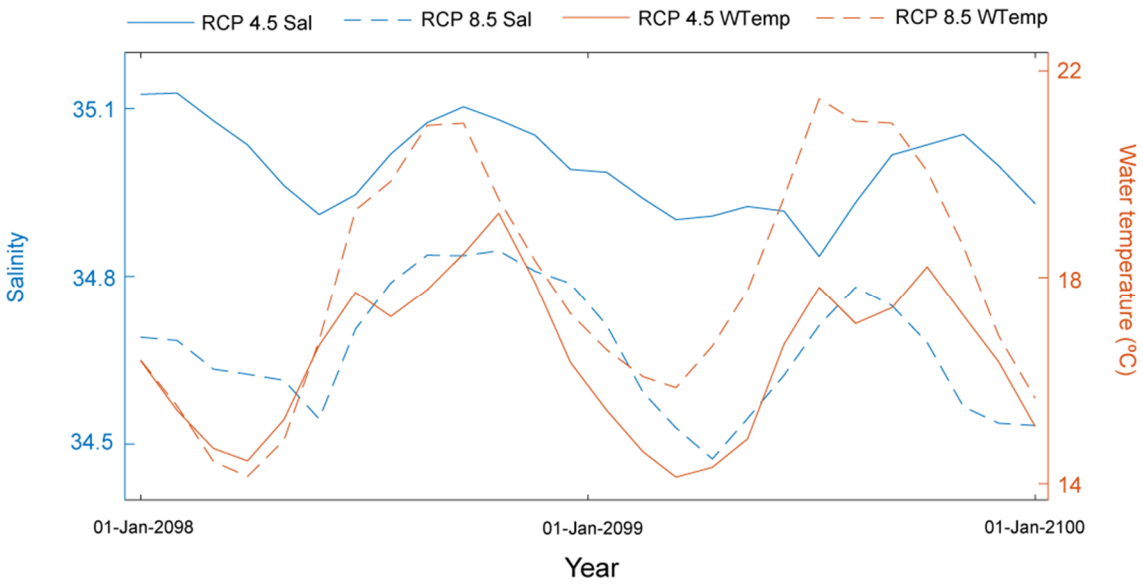

Appendix 7

Spatial distribution of the normalised anomaly for each descriptor and scenario

***Compendium*:**

- A. Water velocity
- B. Bottom shear stress (*BSS*)
- C. Salinity
- D. Ambient temperature limiting function of seagrass growth (*F(T)*)
- E. Space limiting function of seagrass growth (*F(S)*)
- F. Light limiting function of seagrass growth (*F(L)*)
- G. Relative water content (*RWC*)

Appendix 7A. Spatial distribution of normalised anomaly for water velocity descriptor, for each scenario

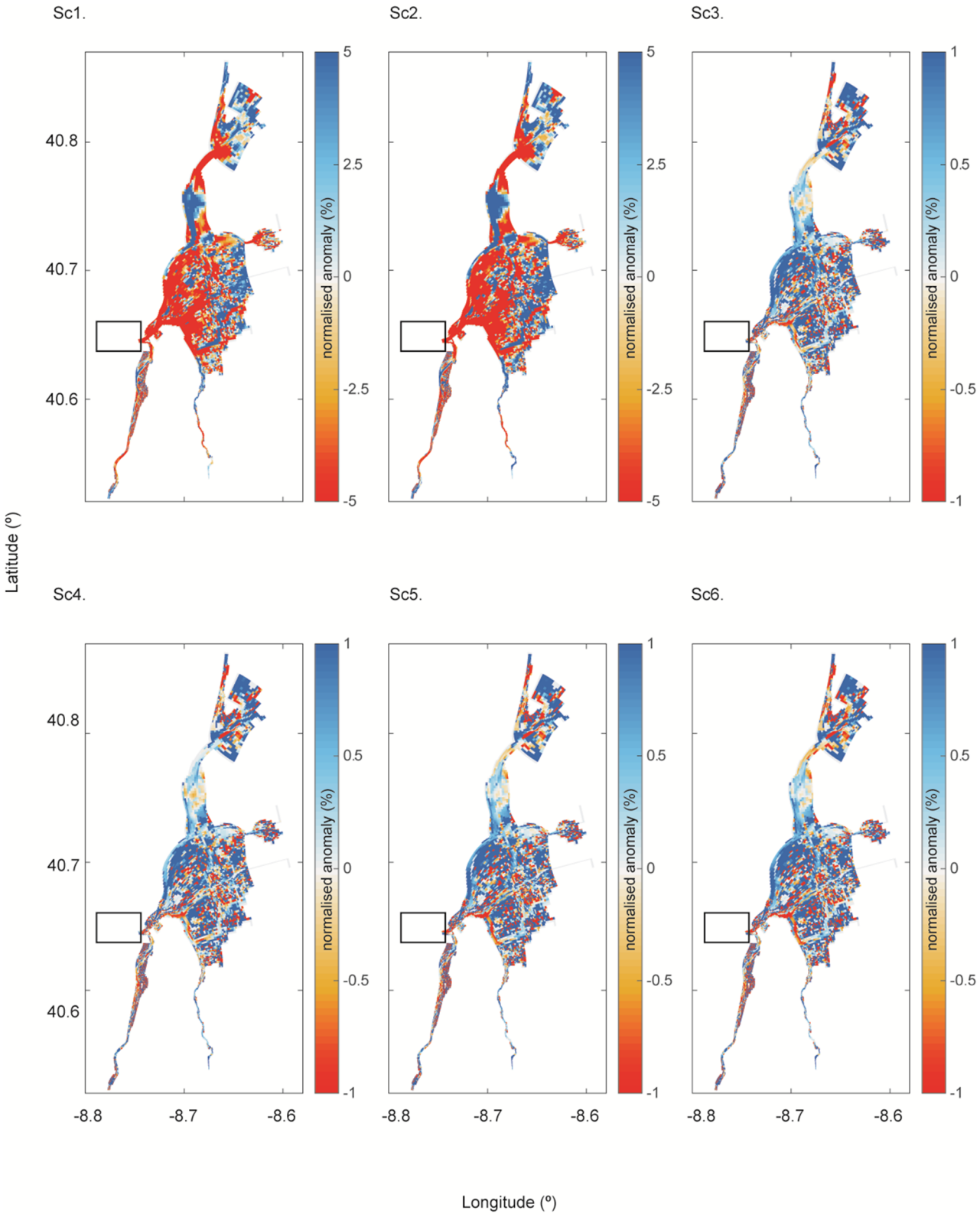

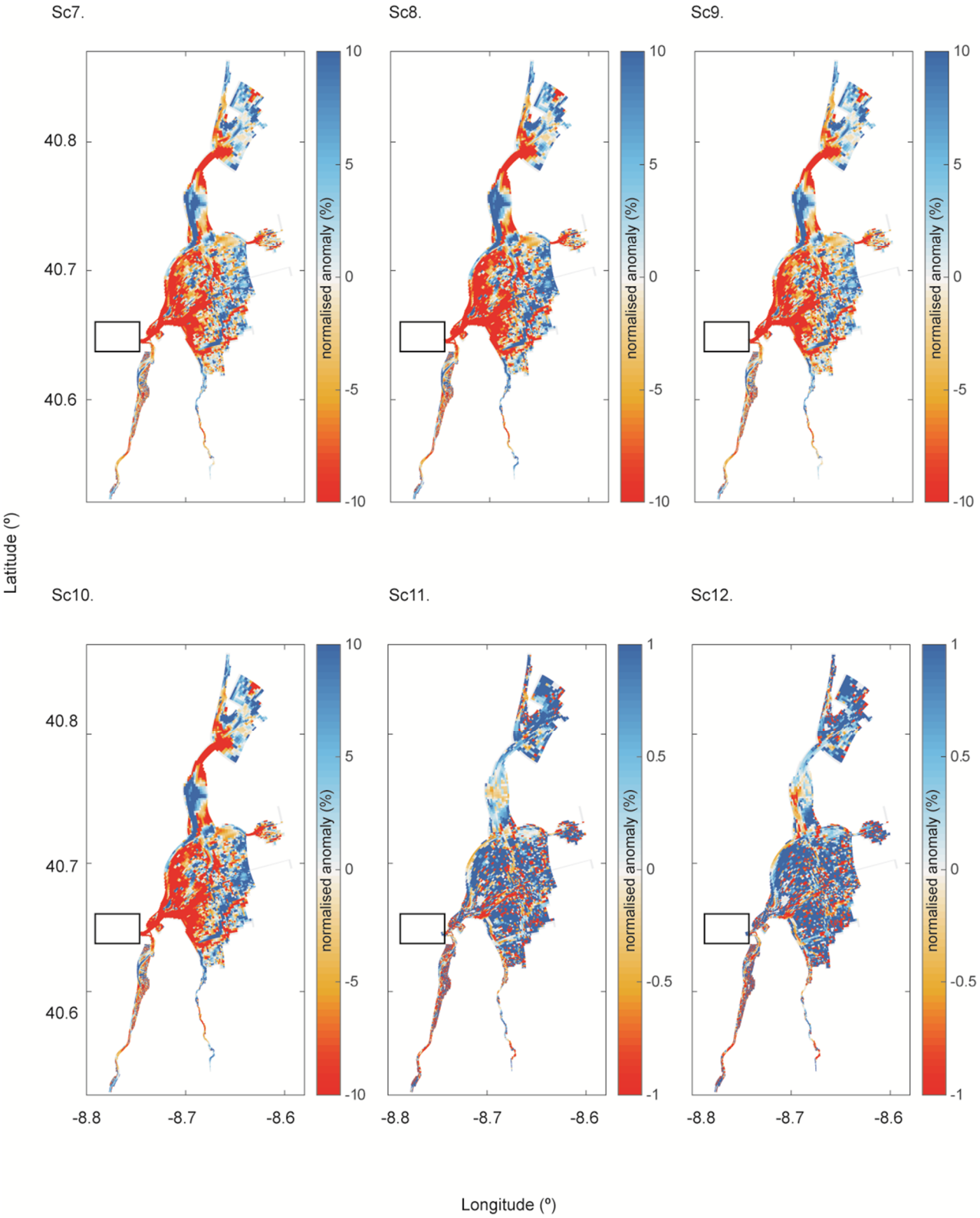
Sc7.
Sc8.
Sc9.
Sc10.
Sc11.
Sc12.
Latitude (°)
Longitude (°)
40.8
40.7
40.6
-8.8
-8.7
-8.6
normalised anomaly (%)
10
5
0
-5
-10
1
0.5
-0.5
-1

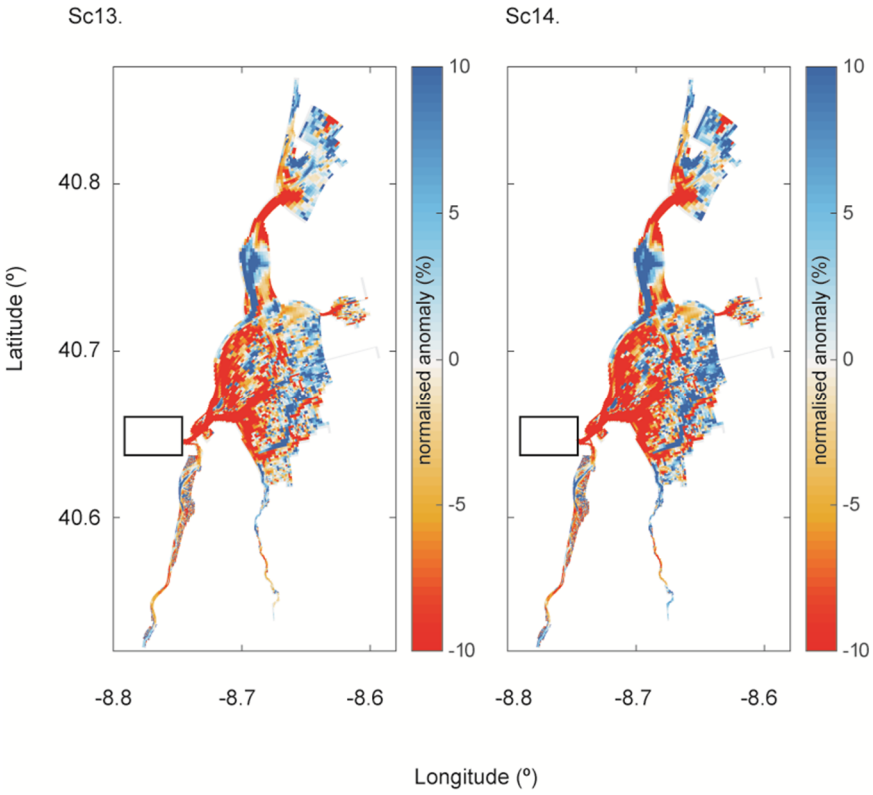

Appendix 7B. Spatial distribution of normalised anomaly for bottom shear stress (*BSS*), for each scenario

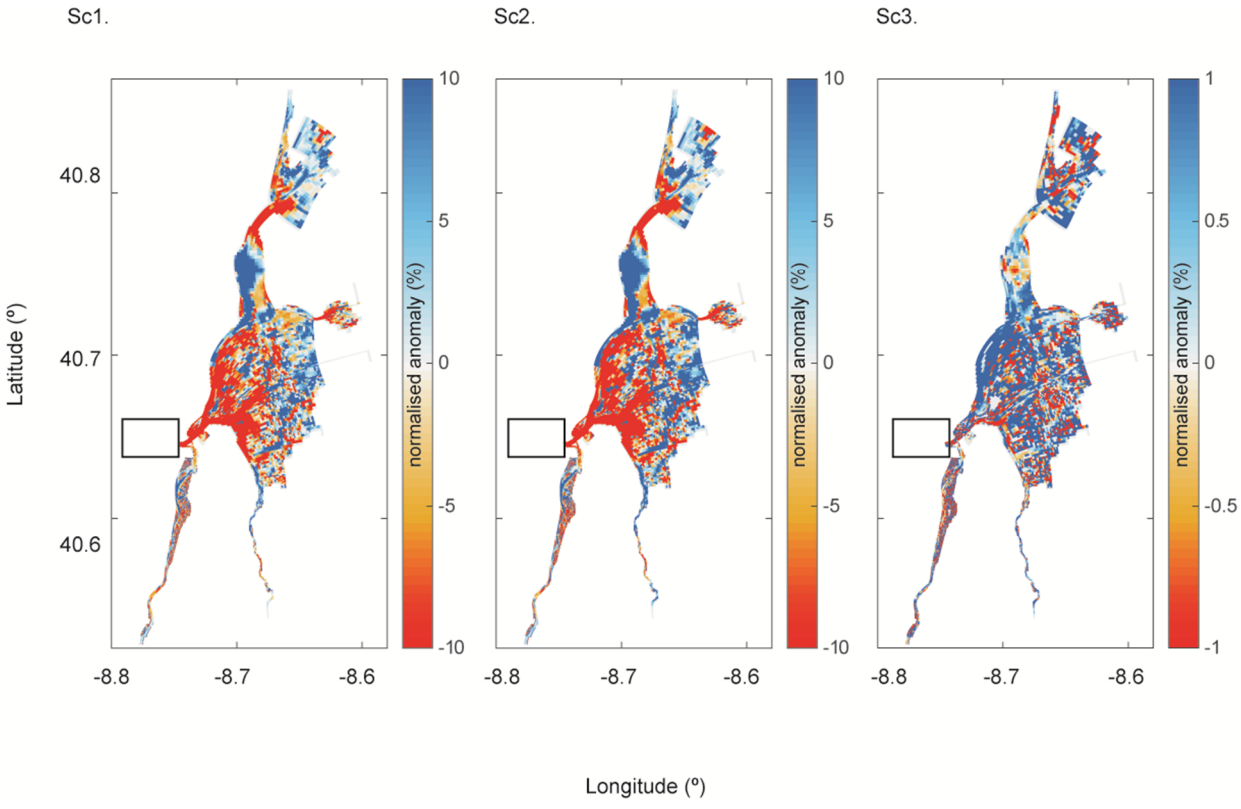

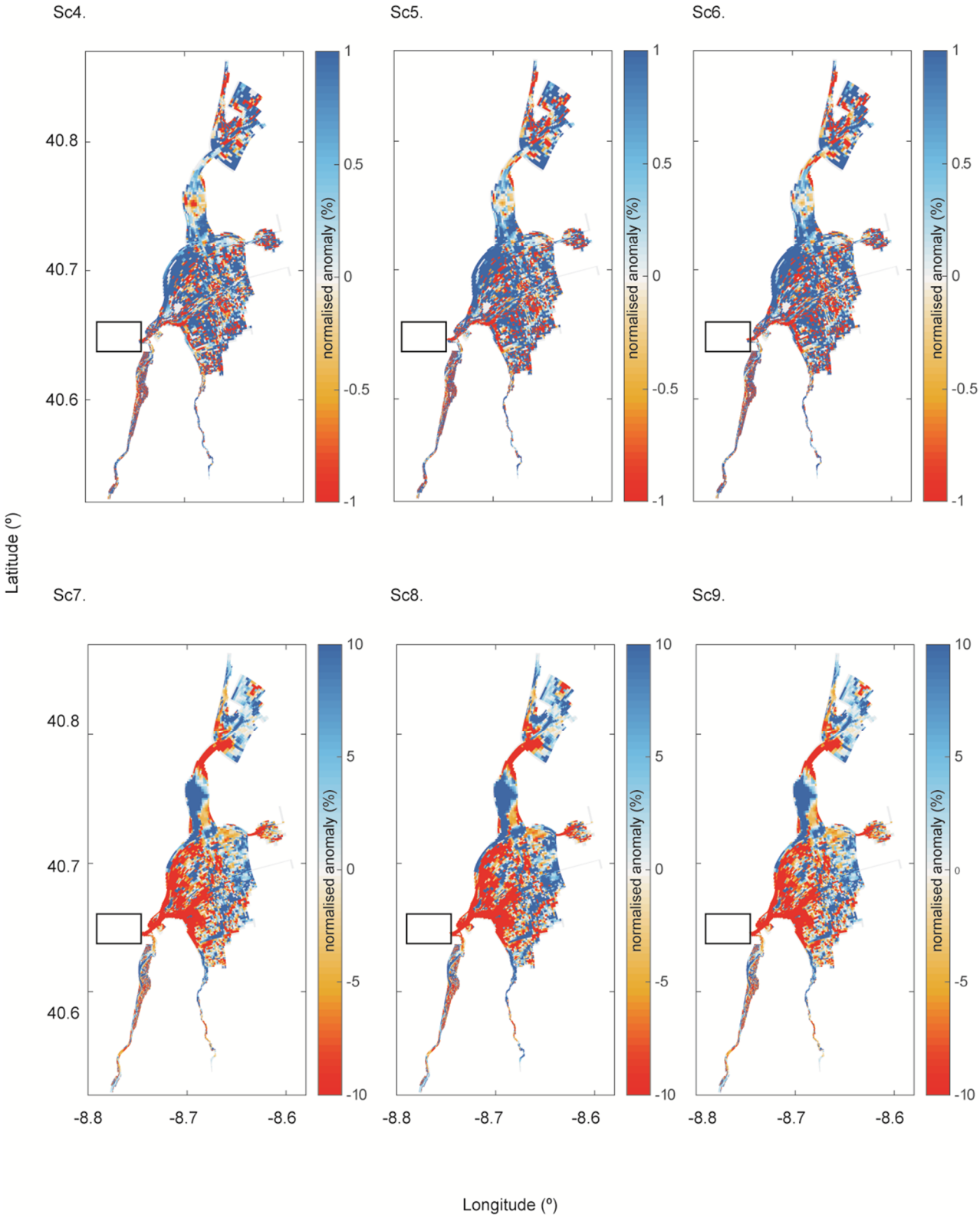
Sc4.
Sc5.
Sc6.
Sc7.
Sc8.
Sc9.
Latitude (°)
Longitude (°)
40.8
40.7
40.6
-8.8
-8.7
-8.6
normalised anomaly (%)
1
0.5
0
-0.5
-1
10
5
0
-5
-10

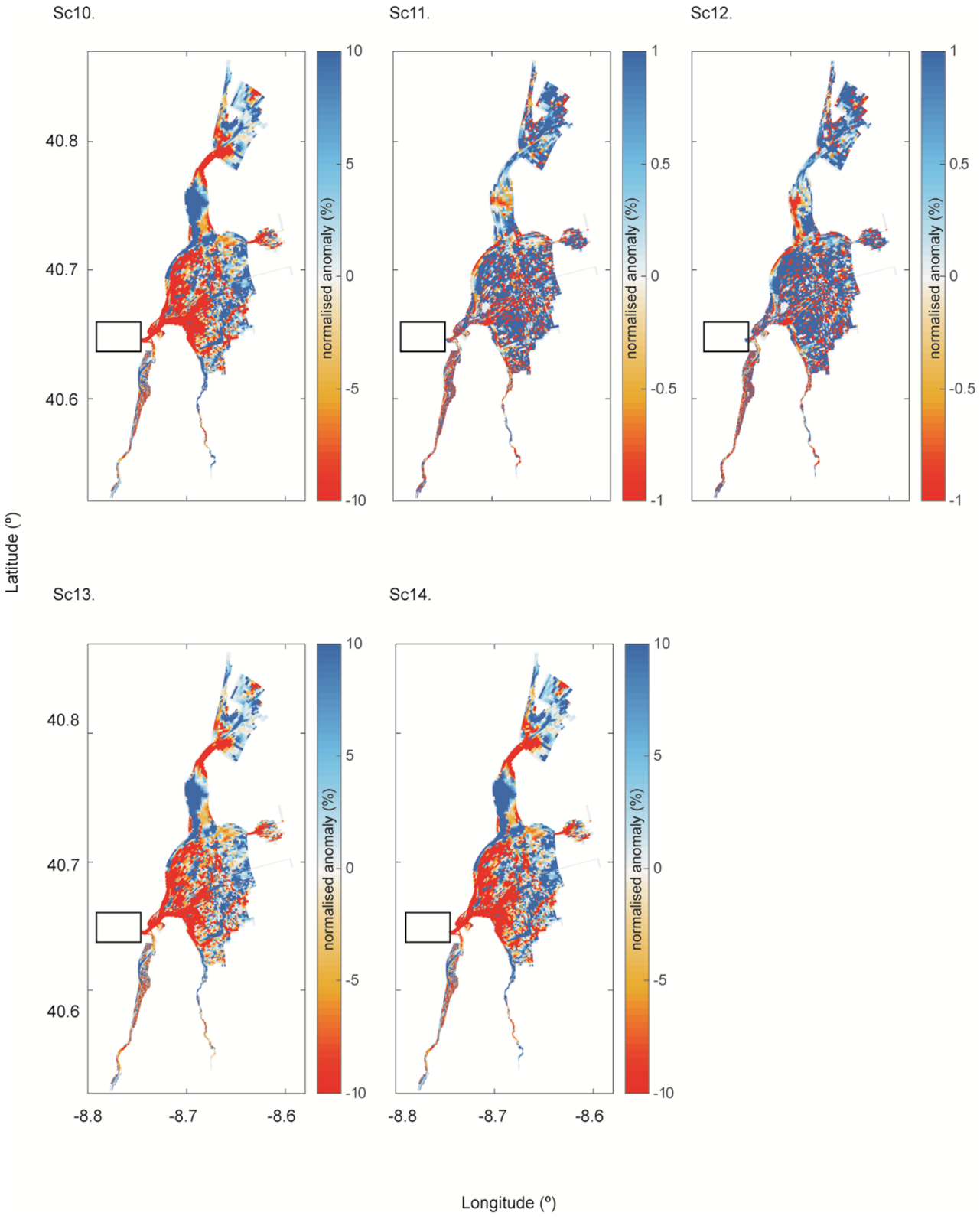
Sc10.
Sc11.
Sc12.
Sc13.
Sc14.
normalised anomaly (%)
10
5
0
-5
-10
1
0.5
0
-0.5
-1
40.8
40.7
40.6
-8.8
-8.7
-8.6
Latitude (°)
Longitude (°)

Appendix 7C. Spatial distribution of normalised anomaly for salinity, for each scenario

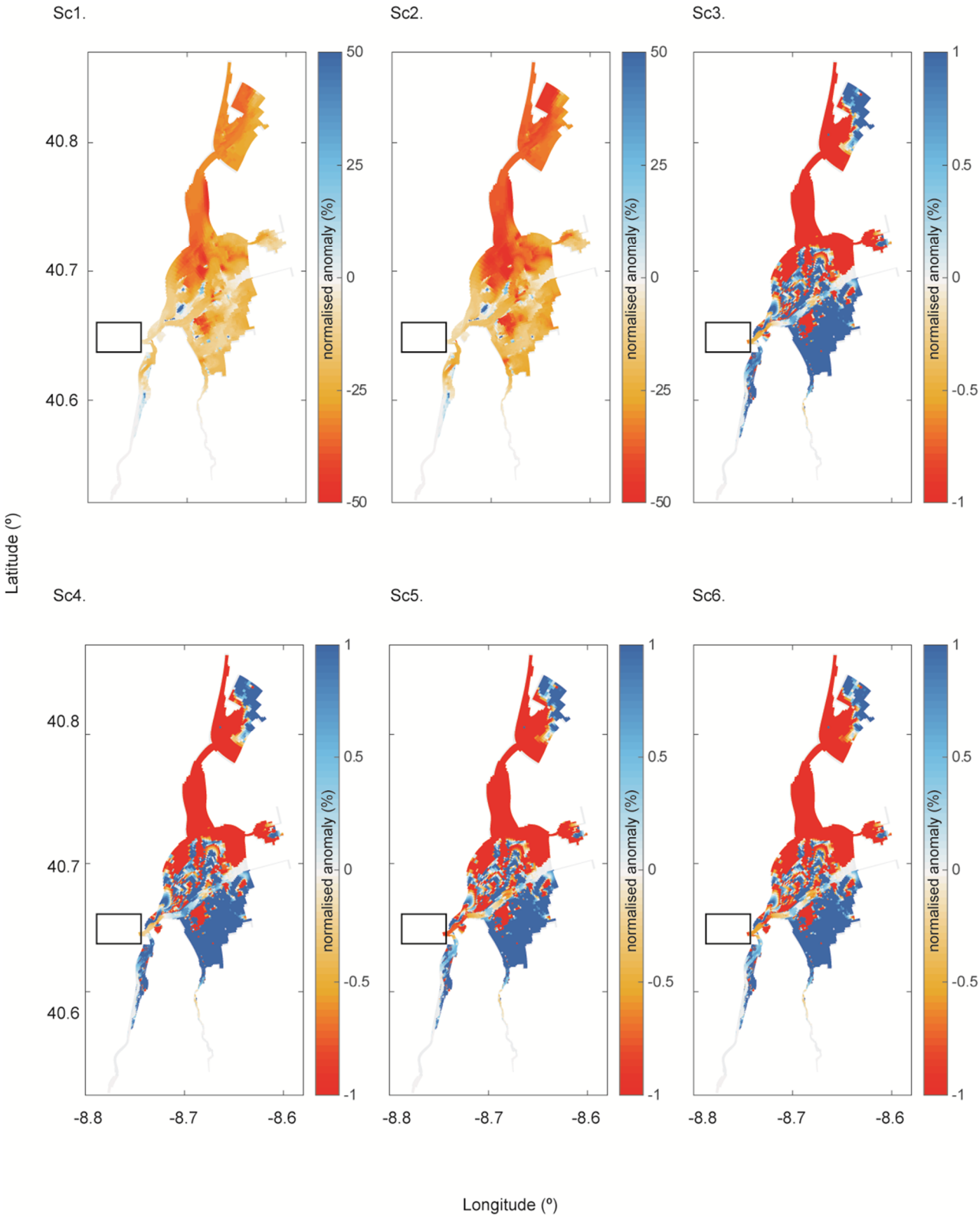

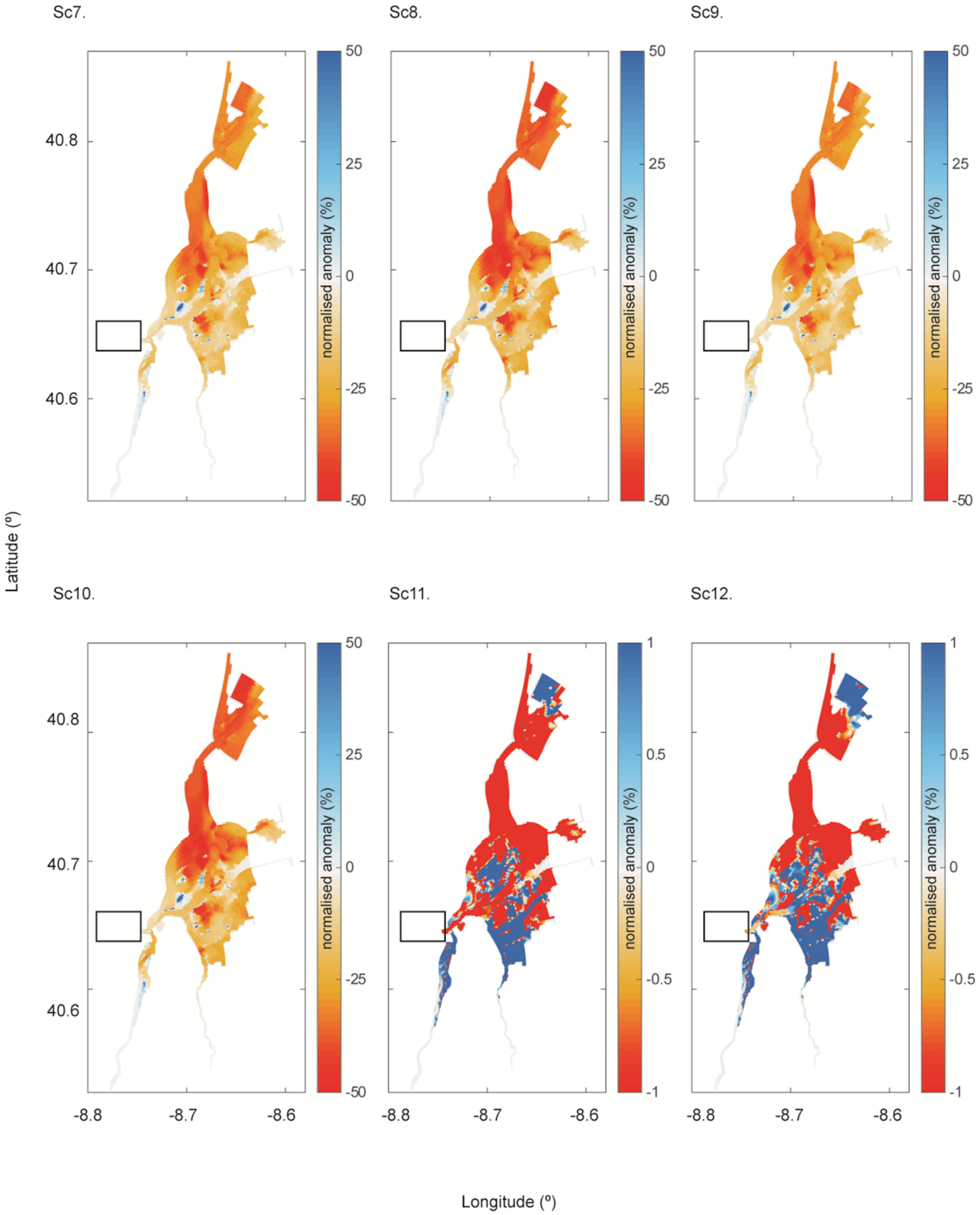
Sc7.
Sc8.
Sc9.
Sc10.
Sc11.
Sc12.
Latitude (°)
Longitude (°)
40.8
40.7
40.6
-8.8
-8.7
-8.6
normalised anomaly (%)
50
25
0
-25
-50
1
0.5
-0.5
-1

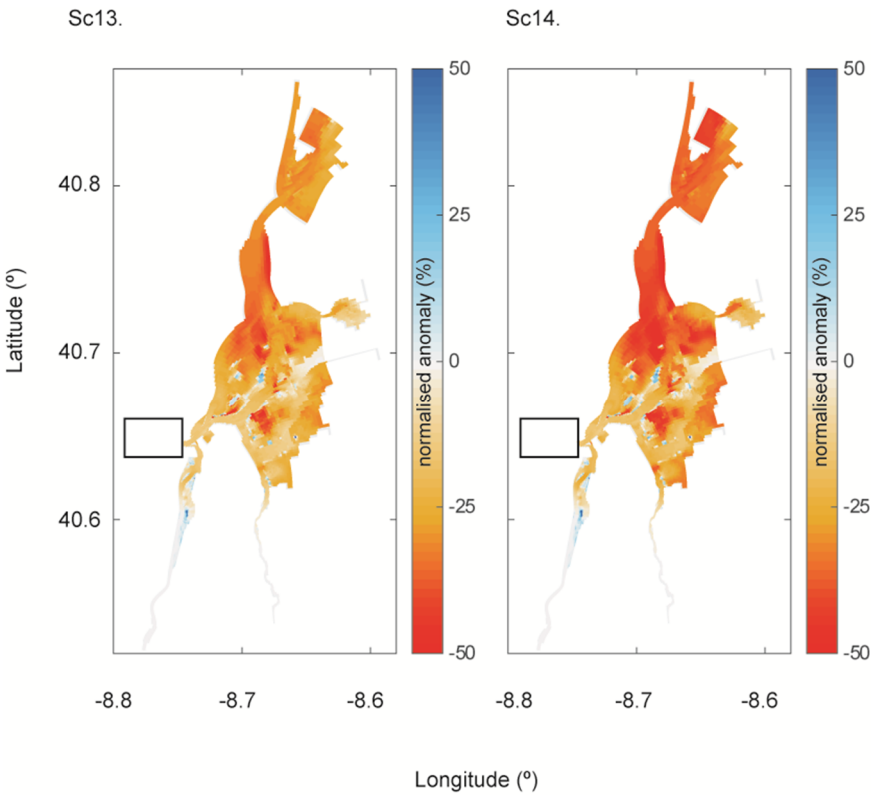

Appendix 7D. Spatial distribution of normalised anomaly for ambient temperature limiting function of seagrass growth (*F(T)*), for each scenario

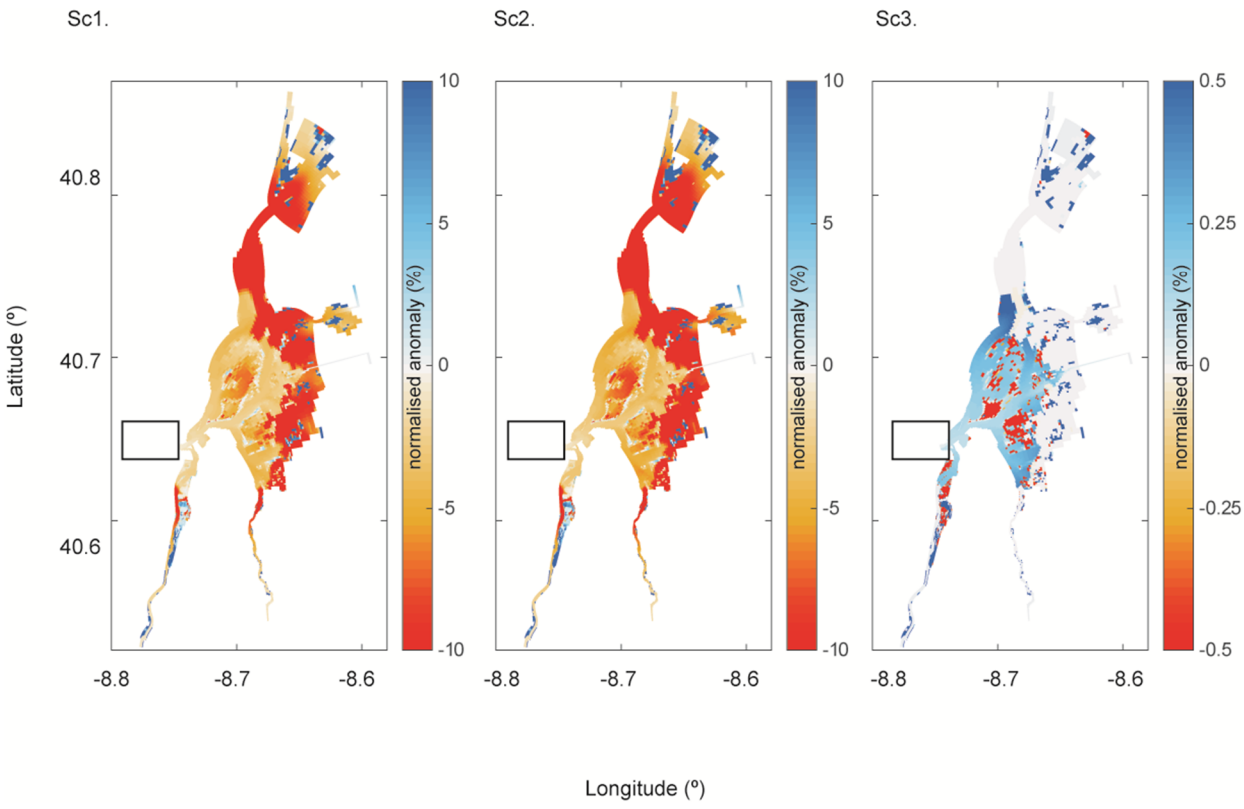

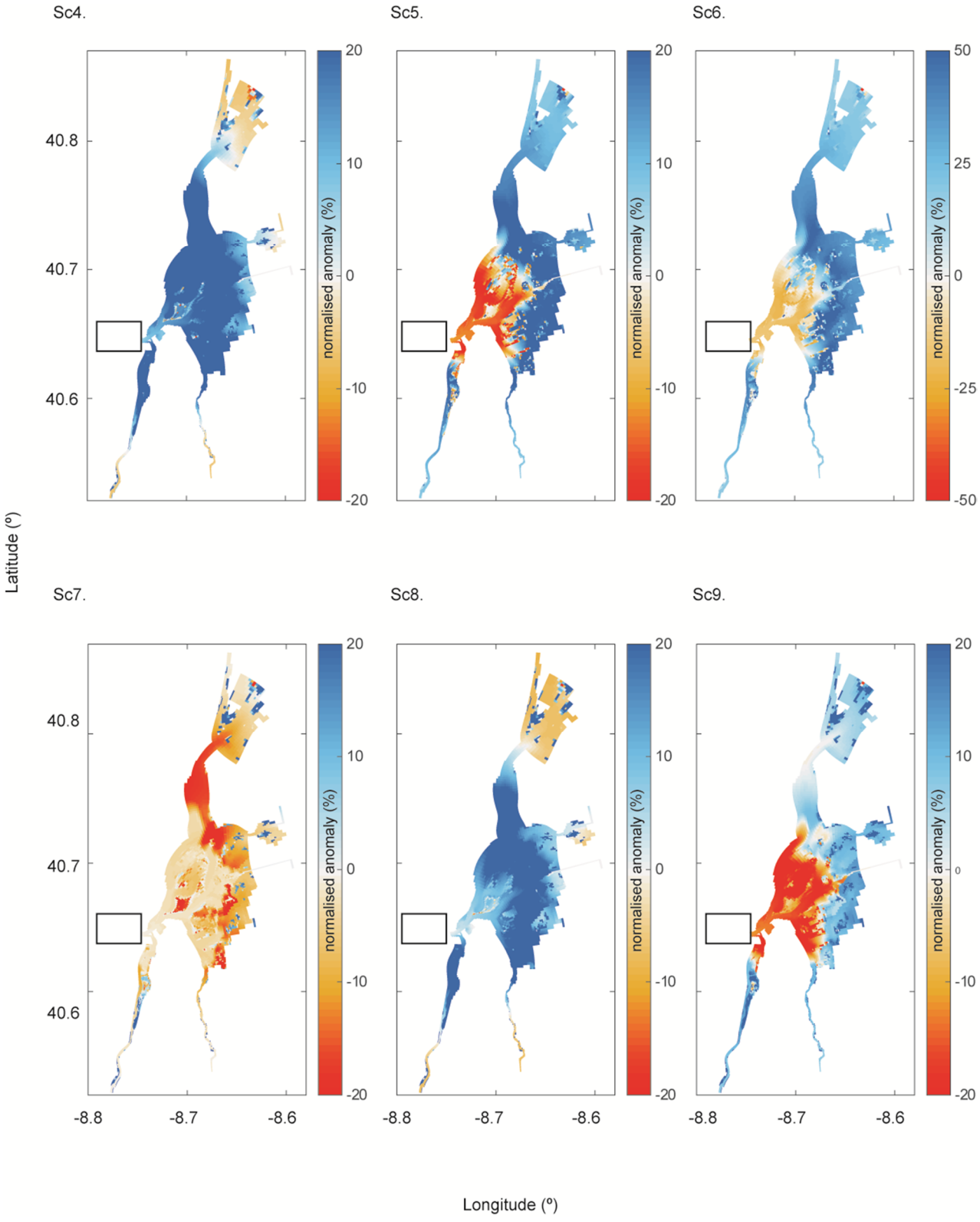
Sc4.
Sc5.
Sc6.
Sc7.
Sc8.
Sc9.
Latitude (°)
Longitude (°)
40.8
40.7
40.6
-8.8
-8.7
-8.6
normalised anomaly (%)
20
10
0
-10
-20
50
25
-25
-50

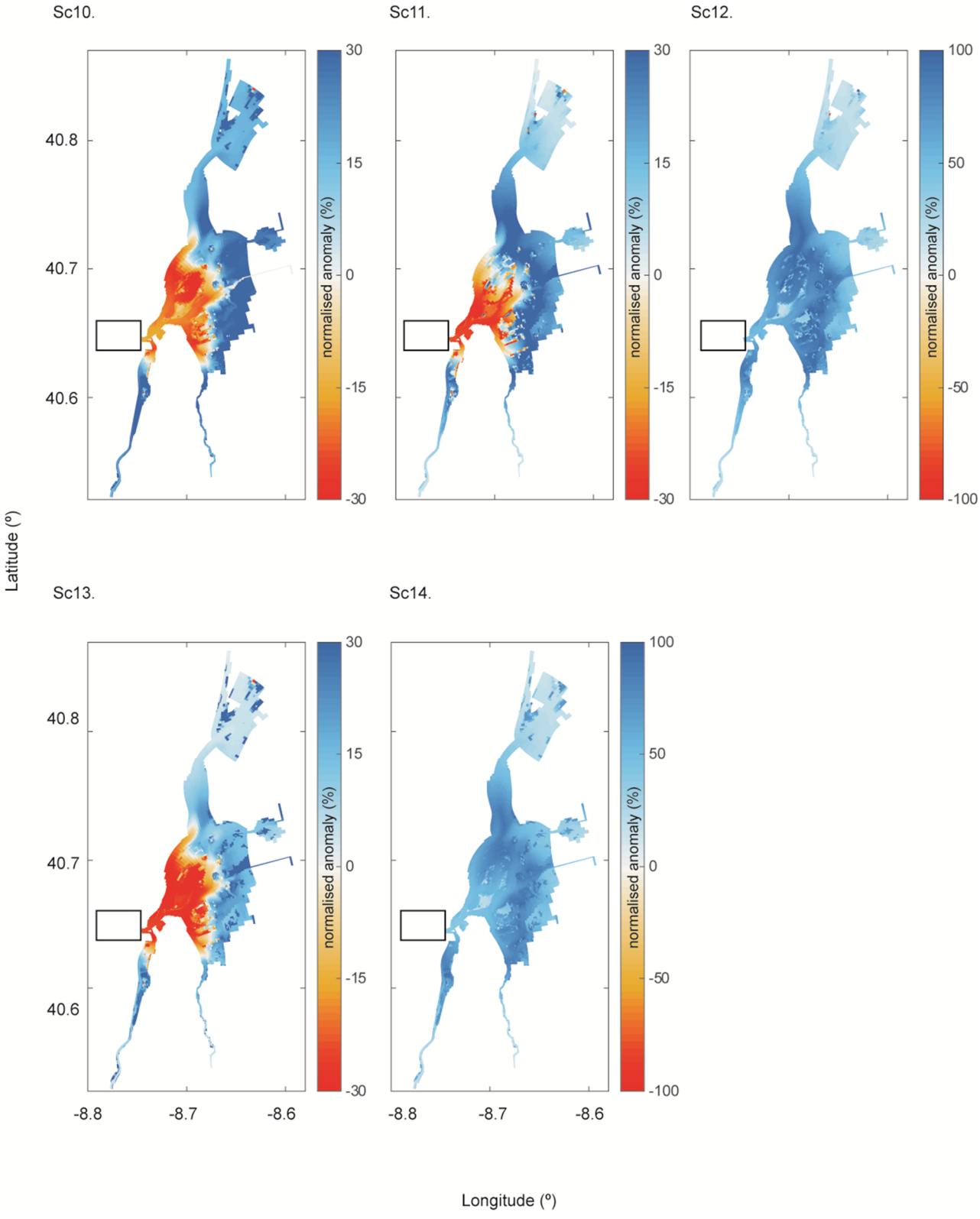
Sc10.
Sc11.
Sc12.
Sc13.
Sc14.
normalised anomaly (%)
30
15
0
-15
-30
100
50
-50
-100
40.8
40.7
40.6
-8.8
-8.7
-8.6
Latitude (°)
Longitude (°)

Appendix 7E. Spatial distribution of normalised anomaly for space limiting function of seagrass growth (*F(S)*), for each scenario

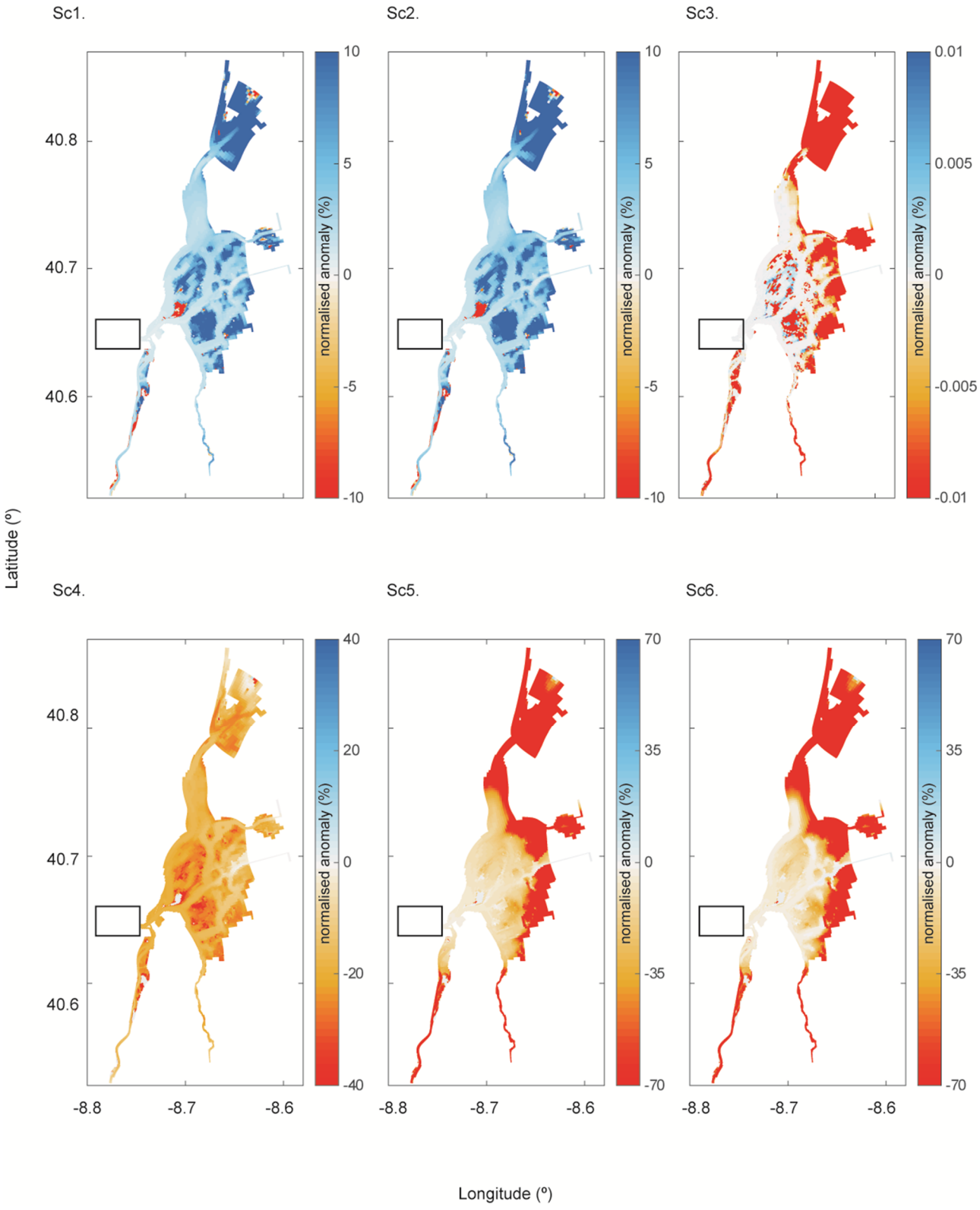

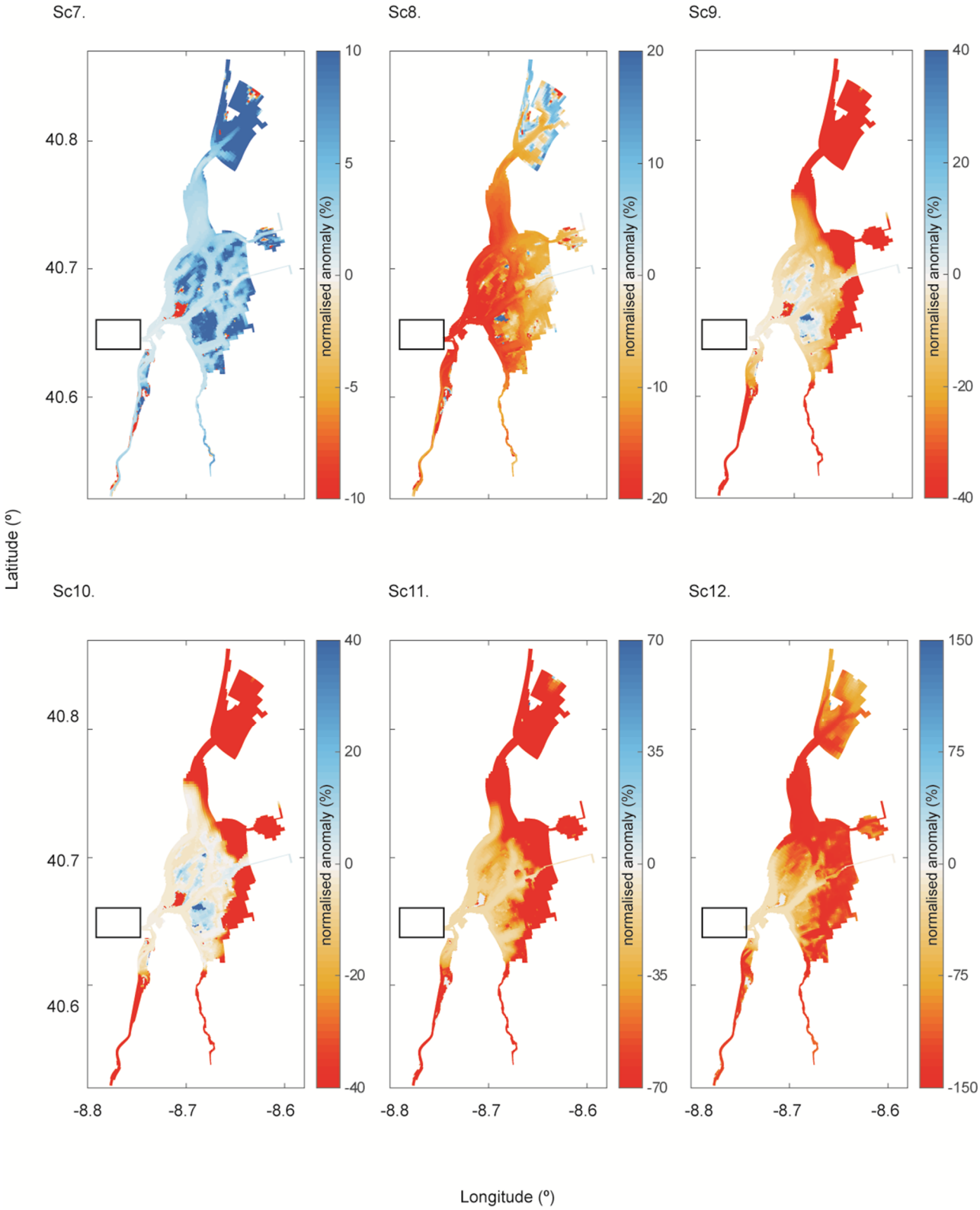
Sc7.
Sc8.
Sc9.
Sc10.
Sc11.
Sc12.
normalised anomaly (%)
Latitude (°)
Longitude (°)
40.8
40.7
40.6
-8.8
-8.7
-8.6
10
5
0
-5
-10
20
-20
40
-40
70
-70
150
75
-75

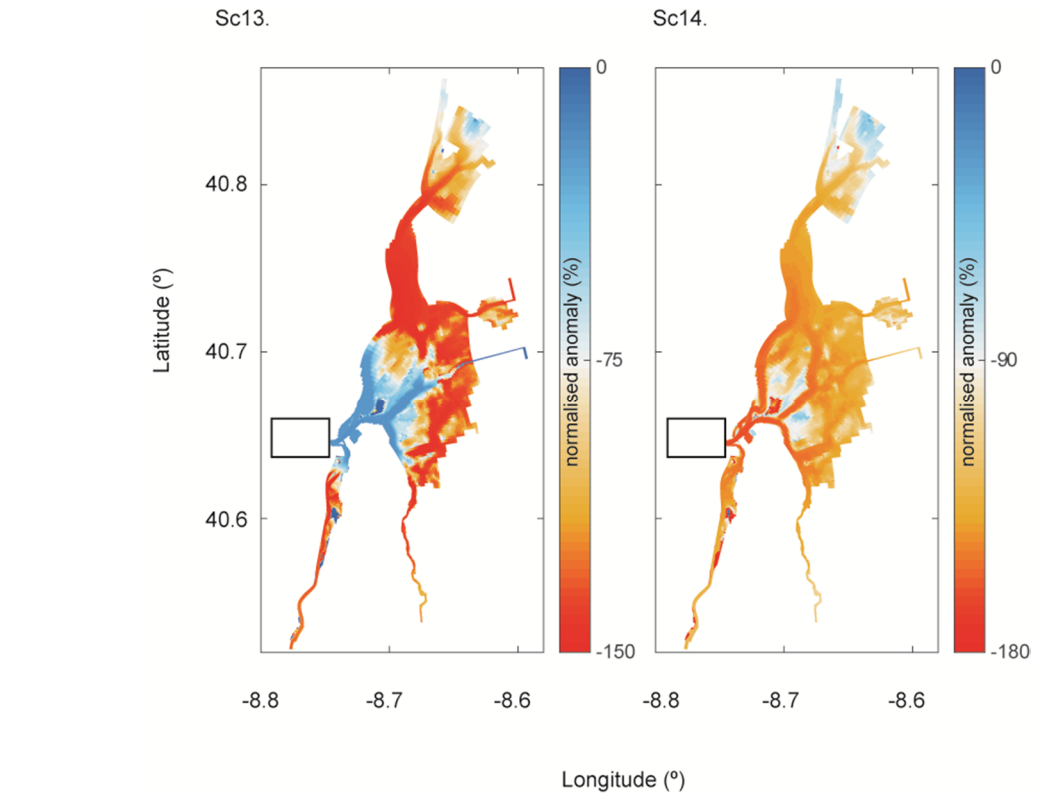

Appendix 7F. Spatial distribution of normalised anomaly for Light limiting function of seagrass growth (*F(L)*), for each scenario

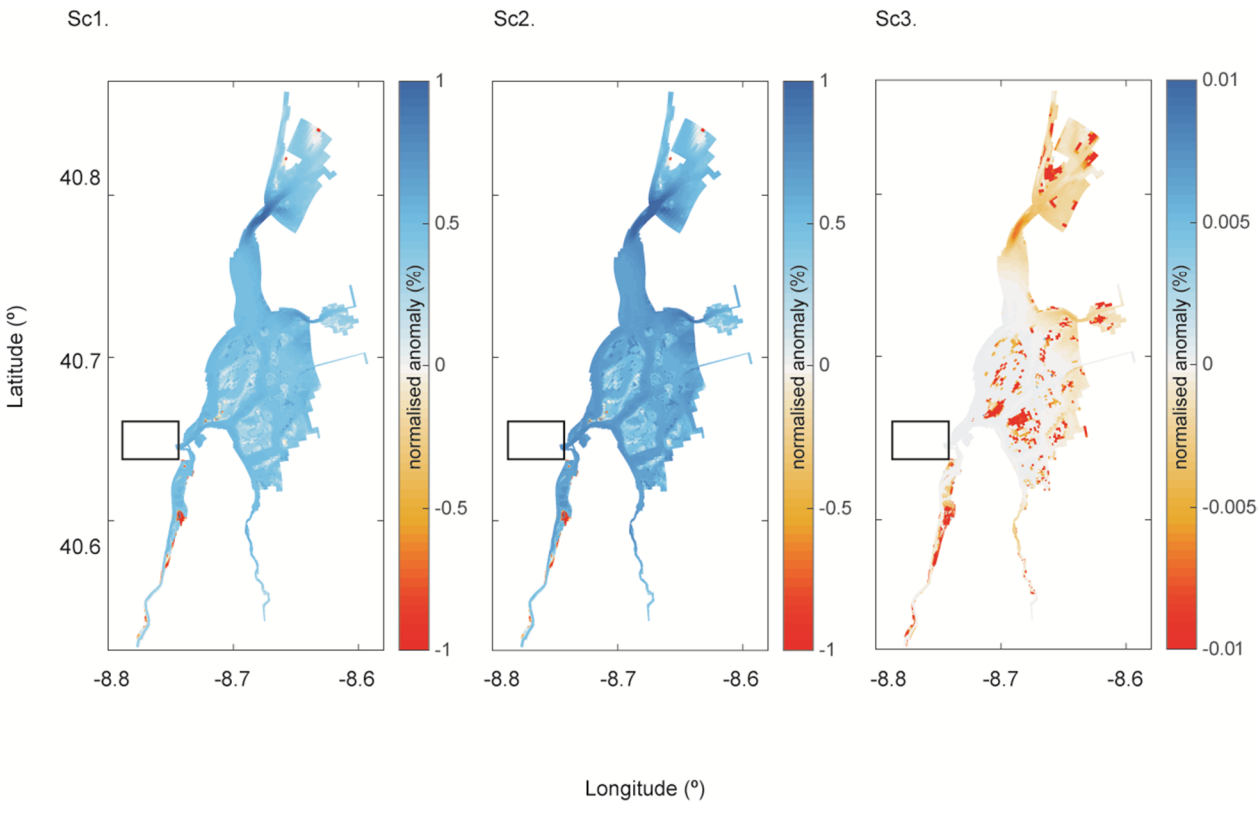

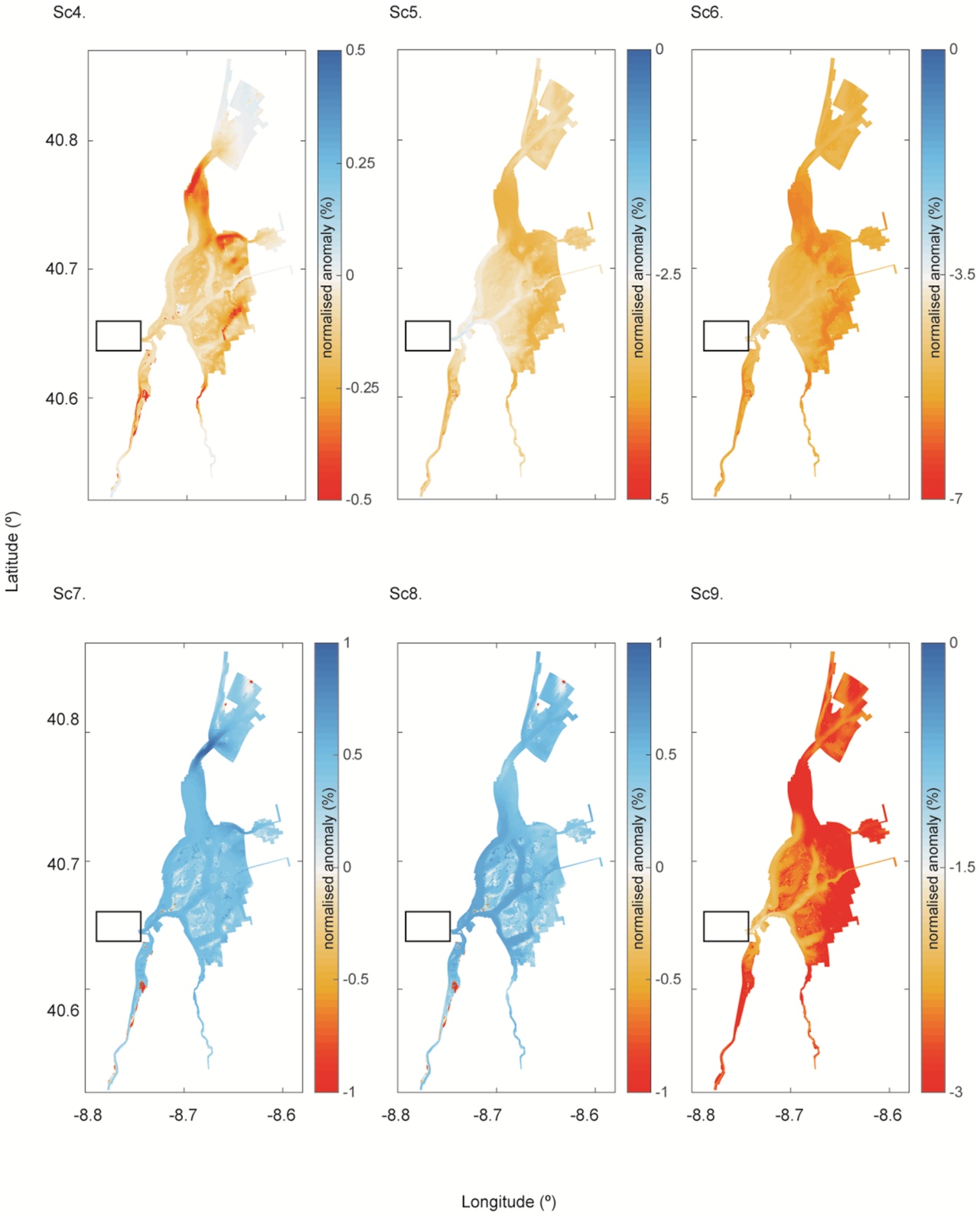
Sc4.
Sc5.
Sc6.
Sc7.
Sc8.
Sc9.
Latitude (°)
Longitude (°)
40.8
40.7
40.6
-8.8
-8.7
-8.6
normalised anomaly (%)
0.5
0.25
0
-0.25
-0.5
-2.5
-5
-3.5
-7
1
-1
-1.5
-3

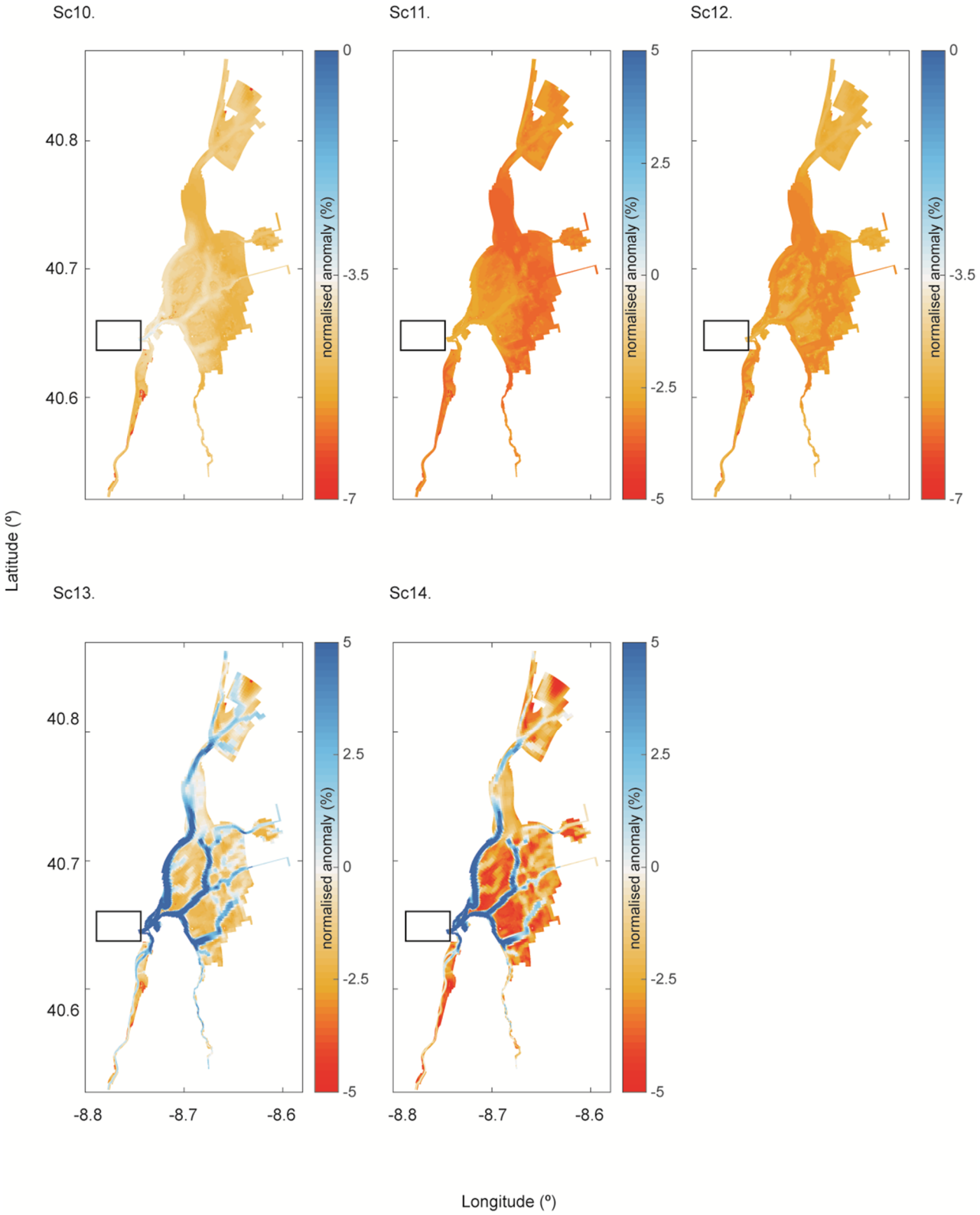
Sc10.
Sc11.
Sc12.
Sc13.
Sc14.
normalised anomaly (%)
0
-3.5
-7
5
2.5
0
-2.5
-5
40.8
40.7
40.6
-8.8
-8.7
-8.6
Latitude (°)
Longitude (°)

Appendix 7G. Spatial distribution of normalised anomaly for Relative water content (*RWC*), for each scenario

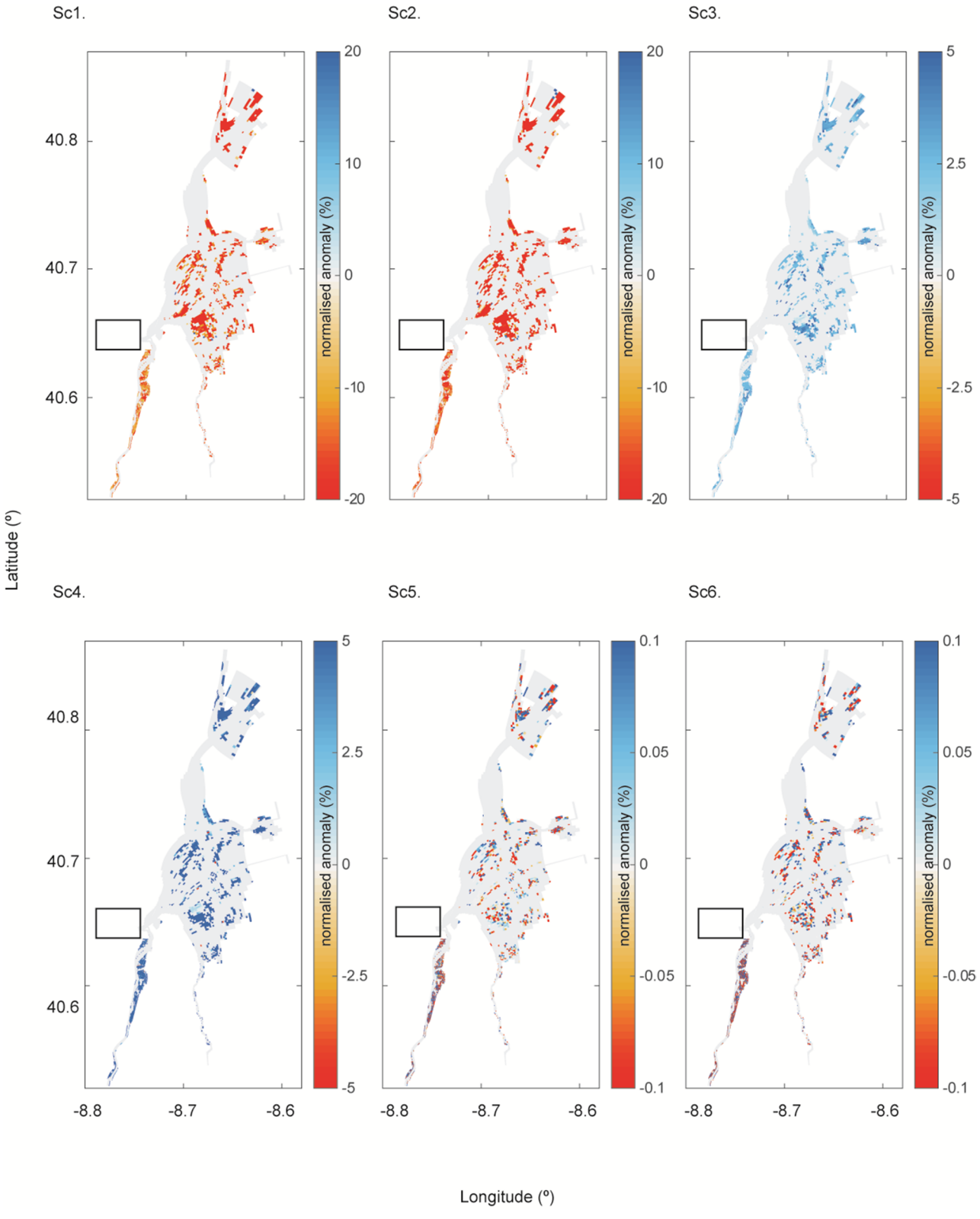

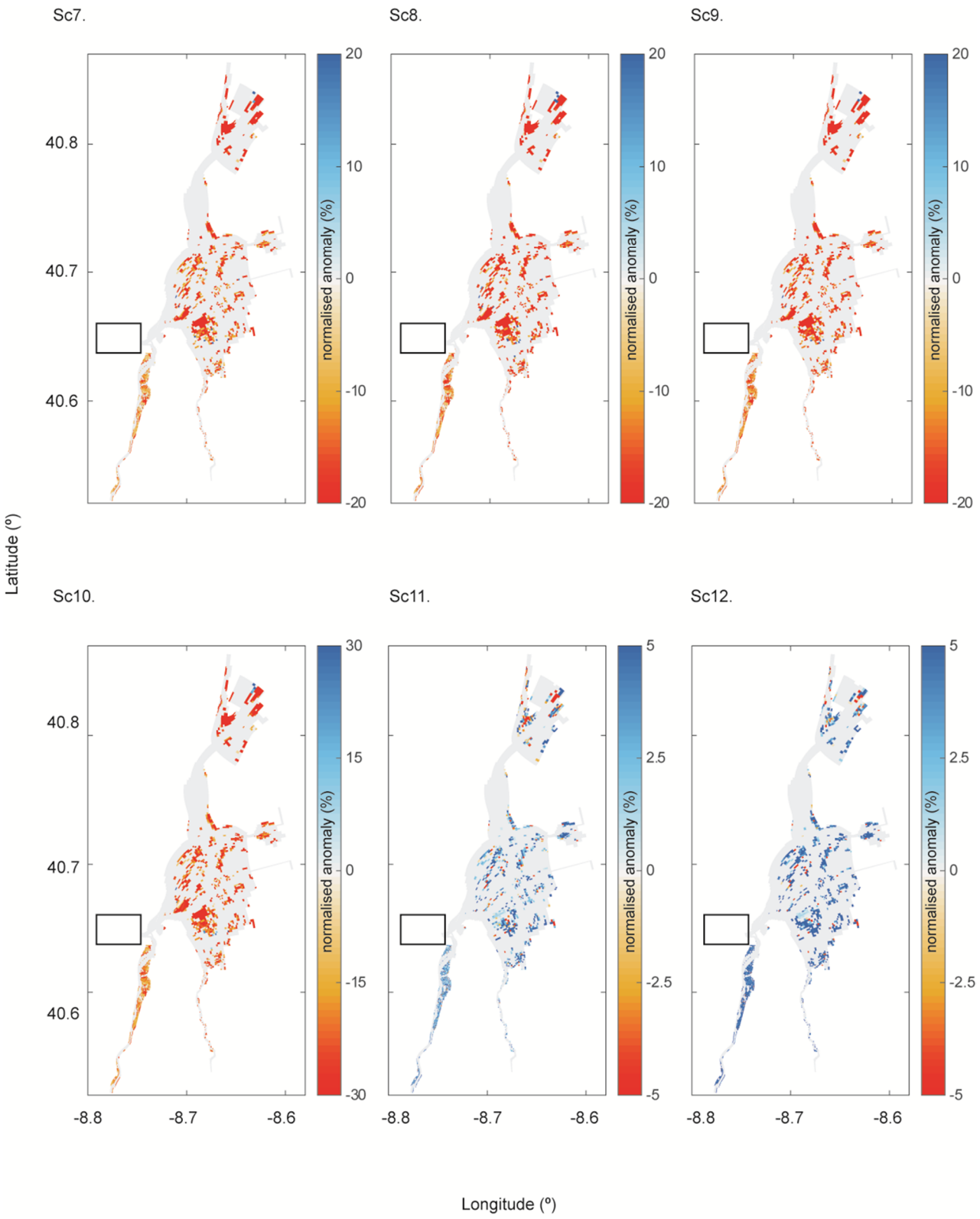
Sc7.
Sc8.
Sc9.
Sc10.
Sc11.
Sc12.
Latitude (°)
Longitude (°)
40.8
40.7
40.6
-8.8
-8.7
-8.6
normalised anomaly (%)
20
10
0
-10
-20
30
15
-15
-30
5
2.5
-2.5
-5

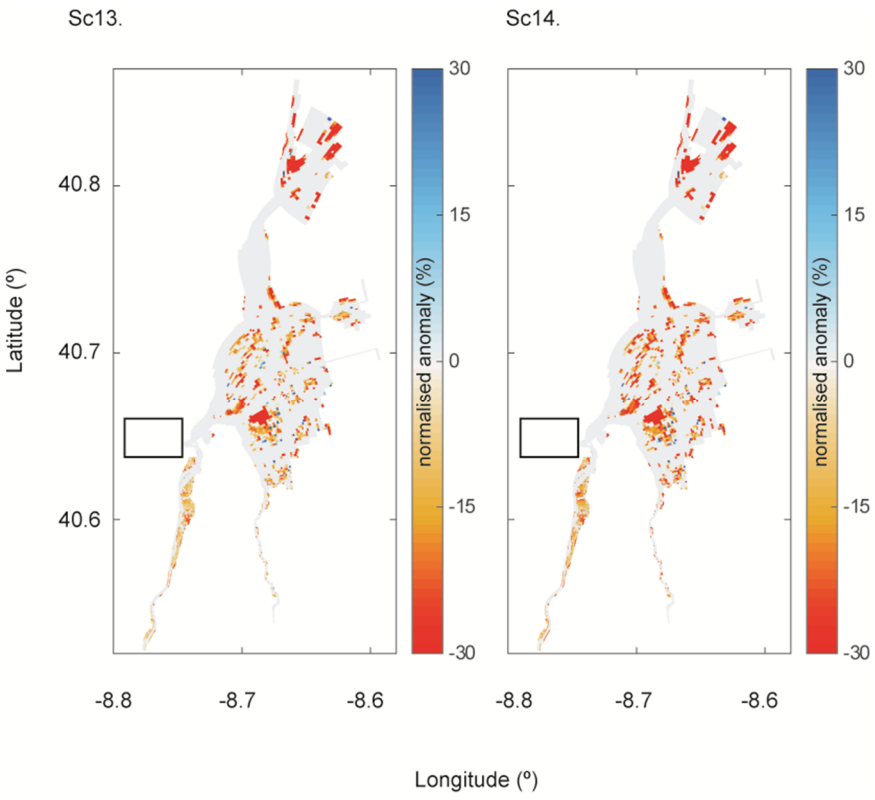
Sc13.
Sc14.
Latitude (°)
40.8
40.7
40.6
-8.8
-8.7
-8.6
Longitude (°)
normalised anomaly (%)
30
15
0
-15
-30